A Contribution to Stress-Displacement Based Mixed Galerkin Finite Elements for Hyperelasticity

Von der Fakultät für Ingenieurwissenschaften,
Abteilung Bauwissenschaften
der Universität Duisburg-Essen
zur Erlangung des akademischen Grades

Doktor-Ingenieur

genehmigte Dissertation

von

Nils Viebahn, M.Sc.

Hauptberichter:	Prof. Dr.-Ing. habil. J. Schröder
Korreferenten:	Prof. Dr.-Ing. habil. Dr. h.c. mult. Dr.-Ing. E.h. Peter Wriggers

Tag der Einreichung:	16. Mai 2019
Tag der mündlichen Prüfung:	02. Oktober 2019

Fakultät für Ingenieurwissenschaften,
Abteilung Bauwissenschaften
der Universität Duisburg-Essen
Institut für Mechanik
Prof. Dr.-Ing. habil. J. Schröder

Berichte des Instituts für Mechanik, Universität Duisburg-Essen

Herausgeber:

Prof. Dr.-Ing. habil. J. Schröder

Organisation und Verwaltung:

Prof. Dr.-Ing. habil. J. Schröder
Institut für Mechanik
Fakultät für Ingenieurwissenschaften
Abteilung Bauwissenschaften
Universität Duisburg-Essen
Universitätsstraße 15
45141 Essen
Tel.: 0201 / 183 - 2682
Fax.: 0201 / 183 - 2680

DOI: 10.17185/duepublico/70593
URN: urn:nbn:de:hbz:464-20191022-150209-6

ISBN-10 3-9818074-9-9
ISBN-13 978-3-9818074-9-3
EAN 9783981807493

Vorwort

Die vorliegende Arbeit entstand während meiner Tätigkeit als wissenschaftlicher Mitarbeiter am Institut für Mechanik (Abteilung Bauwissenschaften, Fakultät für Ingenieurwissenschaften) an der Universität Duisburg-Essen im Rahmen des durch die Deutsche Forschungsgemeinschaft (DFG) finanzierten Projektes SCHR 570/23-1, 570/23-2, WR 19/50-1 und 19/50-2. An dieser Stelle möchte ich der DFG für die finanzielle Unterstützung danken und all jenen meinen persönlichen Dank aussprechen, die zum Gelingen dieser Arbeit beigetragen haben.
An erster Stelle möchte ich meinem geschätzten Doktorvater Professor Jörg Schröder aufrichtig danken, der mir die Möglichkeit gab unter seiner Leitung zu promovieren. Insbesondere mchte ich mich bedanken für die intensive Förderung und das entgegengebrachte Vertrauen in der gesamten Phase meiner Promotion. Mein besonderer dank gilt auch Professor Peter Wriggers, sowohl für die Übernahme des Zweitgutachtens als auch für die erfolgreiche Zusammenarbeit im Rahmen des gemeinsamen DFG Projektes und darüber hinaus. Bei vielen Diskussionen habe ich sein weitreichendes Wissen in der Mechanik zu schätzen gelernt. Weiterhin gilt mein Dank auch Professor Joachim Bluhm, der sich jederzeit gerne für fachliche Ratschläge Zeit nahm. Danken möchte ich auch Professor Daniel Balzani für die gute Zusammenarbeit im Rahmen des gemeinsamen DFG Projektes und seine stets gewissenhaften Korrekturen. Ein herzliches Dankeschön auch an Karl Steeger und Alexander Schwarz, die meine Neugierde an der technischen Mechanik geweckt haben, mich über das gesamte Studium förderten und zu jederzeit ihr umfangreiches Wissen mit mir teilten. Ihr unermüdliches Engagement hat einen großen Anteil an der vorliegenden Arbeit. Ein weiterer Dank geht an Simon Maike für den dauerhaften wissenschaftlichen Austausch und die intensive Korrektur dieser Arbeit. Aufs Herzlichste möchte ich meinen derzeitigen und ehemaligen Kolleginnen und Kollegen, Solveigh Averweg, Julia Bergmann, Dominik Brands, Simon Fausten, Markus von Hoegen, Maximillian Igelbüscher, Simon Kugai, Matthias Labusch, Veronica Lemke, Petra Lindner-Roulle, Sascha Maassen, Simon Maike, Rainer Niekamp, Carina Nisters, Yasemin Özmen, Mangesh Pise, Sabine Ressel, Lisa Scheunemann, Thomas Schmidt, Serdar Serdas und Steffen Specht, für die jederzeit gute Atmosphäre am Institut danken. Meinen Eltern im speziellen und meiner gesamten Familie möchte ich danken für die immerwährende Unterstützung. Abschließend danke ich außerordnetlich meiner Lebensgefährtin Laura, die den langen Weg zur Promotion mit mir gegangen ist. Ihre motivierende Art und immerwährende Unterstützung waren mir stets eine große Hilfe.

Essen, Oktober 2019 Nils Viebahn

Abstract

Mixed Finite Elements (FE) constitute an elegant remedy for the approximation of constrained boundary value problems, where the capability of the classical FE method is limited. This thesis comprises in a first step the mathematical analysis and numerical investigation of different mixed FE approaches in the case of linear elasticity. In a second step novel strategies for the extension of the considered formulations to the nonlinear hyperelastic framework are discussed. Within the main objective of reliable and efficient FE based approximations including large deformations, a focus of the proposed work is set on the construction of elements based on the Hellinger-Reissner variational framework. This family of elements is characterized by a direct discretization of the stresses as well as the displacements and a challenging extension to the large strain regime. The investigation of the efficiency and reliability of the proposed FE schemes is emphasized by a comparison to well established formulations using nontrivial numerical benchmarks. Additionally to the common constraint situations of incompressibility and thin-walled structures, the important case of inextensibility is regarded. This work results in a couple of novel FE discretizations, which are characterized by a notable gain in efficiency and robustness. In addition, further insights considering the reliability and stability of mixed Finite Elements in the hyperelastic framework are gained.

Zusammenfassung

Gemischte Finite Elemente (FE) stellen im Gegensatz zur klassischen FE Methode einen geeigneten Ansatz zur Approximation von Randwertproblemen mit Zwangsbedingungen dar. Die vorliegende Thesis umfasst sowohl die mathematische Analyse als auch die numerische Untersuchung verschiedener gemischter FE Formulierungen für den Fall der linearen Elastizität. Des Weiteren werden neuartige Strategien für die Erweiterung der vorgestellten Formulierungen in den Rahmen der Hyperelastizität entwickelt und diskutiert. Mit dem Ziel der Entwicklung von vertrauenswürdigen und effizienten Finiten Elementen für große Deformationen, liegt ein Fokus der Arbeit auf der Konstruktion von Hellinger-Reissner basierten Elementen. Diese sind im Allgemeinen durch eine Diskretisierung der Spannungen als auch der Verschiebungen sowie einer nicht trivialen Erweiterung für große Verzerrungen charakterisiert. Im weiteren Fokus steht die Untersuchung der Effizienz und Zuverlässigkeit der betrachteten FE Formulierung durch Vergleiche mit bereits etablierten Elementen anhand numerischer Benchmarks. Neben den üblichen Zwangsbedingungen der Inkompressibilität und der Dünnwandigkeit wird zusätzlich auf den wichtigen Fall der Inextensibilität eingegangen. Die vorliegende Arbeit resultiert in einer Reihe neuer FE Diskretisierungen, welche durch einen bedeutenden Zuwachs an Effizienz und Robustheit charakterisiert sind. Zusätzlich werden neue Erkenntnisse bezüglich der Stabilität gemischter Finiter Elemente im Rahmen der Hyperelastizität gewonnen.

Contents

1 Introduction, Motivation and Outline

Many physical problems are mathematically described by a set of Partial Differential Equations (PDEs). These type of equations relate unknown functions of more than one variable with their partial derivatives. For example in the field of solid mechanics, an unknown function for the displacements is solved by the balance of linear momentum, including the divergence of the stress tensor. Therein the stresses are represented by a function including the first order derivative of the displacements. Thus, the related PDE contains derivates of the displacements of second order. In most cases, numerical approaches have to be used to approximate the solution of PDEs since closed form solutions exist only for trivial problems. For the construction of such an approximation, a variety of numerical techniques is available. Their recent achievements are highly connected to the tremendous improvement of the computer performance over the last decades since most complex problems require the management and solution of large systems of equations.

Nowadays, those numerical simulations constitute an essential part in the development of engineering applications. The collective term of Computer Aided Engineering (CAE) comprises their whole range, enclosing e.g. the analysis of structural mechanics, fluid dynamics, multibody systems, and optimization. Due to the fast validation of these numerical approaches, it is possible to incorporate the results of this analysis directly into the design process. Therefore, CAE systems are one of the major providers of information to support the design team and to enable a direct optimization of the considered product. However, the usage of such numerical simulation tools is not restricted to industrial manufacturing but also widely used in fundamental research. A popular example is represented by the Human Brain Project [2019], which has the ambitious goal to unify the knowledge of the human brain and to reconstruct it in a computational model. Another example is the field of material science, where discretization techniques are applied on different length scales in order to couple the material response of the macro scale with the inherent structure of one or more sub-scales. The development of CAE tools combines the knowledge of many different disciplines including engineering, mathematics, physics, material and computer science.

This thesis focuses on the Finite Element Method (FEM) in the framework of isothermal hyperelasticity. Due to its flexibility, the FEM represents one of the most popular discretization techniques for the approximation of PDEs. It is appropriable to a wide range of applications including linear and nonlinear problems, complex shaped domains, varying material coefficients, and different boundary conditions. The basis of the FEM constitutes a variational formulation of a differential equation. In the field of elasticity, the classical variational formulation considers the displacements as the sole unknown quantity and thus is in the following referred to the pure displacement formulation. It represents a suitable approach for the FEM in many different applications. However, if additional constraints are taken into account so-called primal finite element schemes may lead to poor approximations. Common constraints in the framework of solid mechanics are for example the case of (nearly) incompressibility, (nearly) inextensibility of preferred directions or the deterioration of the aspect ratio of the considered domain. They could lead in combination with a pure displacement formulation to so-called locking effects, see i.a. Babuška and Suri [1992], resulting in very poor approximations of the boundary value problems.

The framework of mixed variational formulations constitutes a possible remedy for the suitable incorporation of such constraints and is thus an expedient technique in order to avoid locking effects. First developments in this framework, where additional unknown field quantities are treated in a variational sense, are given in Hellinger [1913], Prange [1916] and Reissner [1950]. Here, an independent stress field is considered as the primary variable and the displacements act in addition as a Lagrangian multiplier. In the following, this two field variational formulation, which is associated to a complementary stored energy, is referred to the Hellinger-Reissner (HR) formulation. Alternatively to the introduction of the complete stresses as an independent field quantity, solely the pressure can be treated as an additional unknown field. This case, where the variational structure is closely related to the framework of the Stokes equations in fluid dynamics, is referred in the following as the displacement-pressure formulation and can be interpreted as a special HR-formulation. A few years later Hu [1955] and Washizu [1955] have proposed independently a variational principle, which treats the displacements, stresses, and strains as independent unknown field quantities. Thus, the Hu-Wahizu principle constitutes the most general framework for the variational treatment of the elasticity problem.

Finite elements based on such mixed variational formulations are denoted as mixed finite elements. A further motivation for these approaches is that in many engineering applications the dual variable (e.g. stress in elasticity) is the main quantity of interest. The calculation of this field via differentiation, as it is usually done in the primal FEM, comes in hand with a loss of accuracy. Thus, it is promising to compute also the dual quantity directly as a fundamental unknown but an increase in accuracy cannot be guaranteed directly due to the choice of a mixed method. In fact, the accuracy highly relies on the chosen finite element discretization spaces. Furthermore, the choice of mixed variational principles can be beneficial in the framework of higher order differential equations, e.g. in the beam theory. Considering in this case the introduction of an additional field circumvents the requirement of a higher order continuity of the unknown field variable. In addition, well-performing ad hoc finite element formulations, for example elements based on selective reduced integration methods, can be transferred into a mixed finite element scheme, see e.g. Malkus and Hughes [1978]. For these ad hoc formulations, which have previously often been diminished as numerical crimes, the method of mixed finite elements provides a suitable mathematical framework, which is capable to establish the required analysis, see i.a. Arnold [1990].

Unfortunately, the method of mixed finite elements comes also in hand with a couple of difficulties. The consideration of further fields as fundamental unknowns leads naturally to an increasing number of degrees of freedom in the discrete system. Also, the saddle point structure, which occurs due to the introduction of a Lagrange multiplier, is associated to an indefinite system matrix, which precludes a couple of efficient solution methods (e.g. Cholesky decomposition, conjugate gradients). In many applications, these difficulties can be overcome by a local elimination of the additional introduced field from the discrete system of equations. In case of a discontinuous approximation, a local static condensation can be utilized on element level at an almost negligible computational cost. If the additional field is approximated by a continuous interpolation, a hybridization procedure may be applied. Therefore, the degrees of freedom associated to the Lagrange multiplier, which are located in the interior of the element or on the edges in 2D or faces in 3D, are eliminated by the introduction of additional degrees of freedom of the primal field. This procedure leads to a nonconforming or hybrid finite element formulation, see

Arnold and Brezzi [1985] and Fraeijs de Veubeke [1965]. Both strategies result in general in a positive definite discrete system with a reduced number of equations. The crucial drawback of mixed methods is the conditional stability, depending on the choice of the finite element discretization spaces. From a mathematical point of view this difficulty is well understood in the framework of linear problems and deduced in the theorem of Babuška [1973] and Brezzi [1974]. The two critical conditions in this theorem are a special condition on coercivity and an inf-sup condition. Together with boundedness, which in the framework of conforming FE approaches is a priori satisfied, they ensure the existence and uniqueness of the solution and thus guarantee the stability of the mixed finite element approximation. Based on this knowledge, stable mixed finite elements can be constructed, yielding optimal convergence rates even in a constrained situation. See in this context the textbooks by Bathe [1996], Braess [2000] and Boffi et al. [2013]. Especially in the framework of elasticity it turned out that the technical proof for the satisfaction of the discrete Babuška-Brezzi conditions is far from being straightforward. In case of mixed finite elements based on the displacement-pressure formulations the pressure can be substituted such that the coercivity condition is a priori fulfilled, as e.g. discussed in Arnold [1990]. Due to this benefit, stable formulations are simply constructed by a suitable enrichment of the displacement related discretization space, such that the inf-sup condition is also satisfied. This has led to the development of a variety of stable mixed finite element formulations, see among others the MINI-element from Arnold et al. [1984b], or the elements of the Taylor-Hood family from Taylor and Hood [1973] and Hood and Taylor [1974]. As recently emphasized by Boffi and Stenberg [2017], the condition on the coercivity is not a priori fulfilled if the approximated pressure is the full hydrostatic pressure, which leads to a deviatoric and volumetric split of the strain energy. In this case, the deviatoric strain energy is not coercive on the entire energy space, and coercivity on the kernel has to be shown explicitly for each constructed element. In the framework of mixed finite elements based on the HR-formulation the coercivity condition remains nontrivial. This situation significantly complicates the construction of stable formulations since the approximation spaces of displacements and stresses have to be carefully balanced. Also, the stress-symmetry condition is not incorporated directly and has to be taken into account. Stable approaches, which consider a strong enforcement of the stress symmetry, have been proposed i.a. by Johnson and Mercier [1978], Arnold et al. [1984c], Arnold and Winther [2002] in 2D, and Adams and Cockburn [2005], Arnold et al. [2008] in 3D. The application of these formulations in engineering problems is not widespread, due to their high polynomial order approximation of the unknown fields and a nontrivial numerical implementation. Some flexibility in the construction of stable elements is given by a weak enforcement of the stress symmetry, see in this context e.g. Boffi et al. [2009]. Well known representatives of such approaches are in this framework Arnold et al. [1984a], Stenberg [1986; 1988], Klaas et al. [1995], Schröder et al. [1997] and Arnold et al. [2007]. A formulation considering a lowest order continuous approximation of the displacements and a normal continuous approximation of the stresses has been proposed by Viebahn et al. [2018b]. Another interesting approach has been introduced by Pechstein and Schöberl [2011], where tangential continuous displacements and normal-normal continuous stresses are taken into account. Alternatively, a mesh dependent parameter can be used for the stabilization of the element formulations as it has been proposed by Franca and Hughes [1988]

and Franca et al. [1988]. The construction of stable finite elements based on the Hu-Washizu principle, which are not equivalent to HR or pure displacement related elements, is rather difficult, as outlined i.a. by Braess [2000]. Remarkable in this field is the family of Enhanced Assumed Strain (EAS) elements, originally introduced for linear elasticity in the pioneering work by Simo and Rifai [1990].

The extension of Babuška and Brezzi's theorem to hyperelasticity is rather difficult since in this framework solutions are not restricted to be unique. Thus, approximation schemes that are proven to be stable and optimal in the linear case could still lead to unphysical and unstable formulations in the large deformation framework, as reported i.a. by Wriggers and Reese [1996] and Auricchio et al. [2005b; 2010]. Despite these well-known uncertainties, mixed formulations are widely used in engineering applications also in the nonlinear framework. Due to its direct extensibility to large deformations, elements based on the displacement-pressure or the Hu-Washizu principle are prevalent. The class of so-called $\boldsymbol{F}$-bar methods, see i.a. Hughes [1980] and Simo et al. [1985], can be interpret as displacement-pressure formulation with an additional interpolation of the volume dilation. It represents one of the most popular formulations in the engineering community. The advantages related to this family of elements are their natural extension to nonlinear theories and their simple implementation such that they can be directly embedded into most FE environments. The common criticism is that many $\boldsymbol{F}$-bar finite elements fail the inf-sup condition already in the linearized setting and thus a physically reasonable solution cannot be guaranteed. However, it became apparent that for most engineering applications those formulations behave very robust and reliable. A related class of finite element approximations, where the minors of the deformation gradient are treated as independent variables, has been introduced by Schröder et al. [2011] and further developed by Bonet et al. [2016] and Kraus et al. [2019]. The extension of EAS formulations to nonlinear problems is also straightforward, which led to numerous different approximations, see i.a. Simo and Armero [1992], Korelc and Wriggers [1996], Glaser and Armero [1997], Korelc et al. [2010] or Krischok and Linder [2016]. Unfortunately, many of the related finite element formulations suffer due to artificial modes, often denoted as hourglassing. These modes appear preferably in case of homogeneous stress states and have been subject of investigations i.a. in de Souza Neto et al. [1995], Wriggers and Reese [1996] and Wall et al. [2000]. In contrast to displacement-pressure and EAS formulations, a nonlinear extension of HR based approaches is nontrivial, since complementary energy functions in terms of stress measures are not available in the general nonlinear case, see Ogden [1984]. However, some effort has been invested in order to extend HR associated finite elements to more general material descriptions, e.g. Atluri [1973], Simo et al. [1989], Wriggers [2009] and Schröder et al. [2017]. A consistent extension to hyperelasticity, which is also part of the proposed thesis, has been suggested in Viebahn et al. [2018a] and Viebahn et al. [2019].

It is worth pointing out that along the already mentioned and predominant approaches, various alternative discretization techniques can be used for the approximation of boundary value problems. A recent promising extension of the classical Galerkin finite element method is the Virtual Element Method (VEM), first introduced in da Veiga et al. [2013]. It is based on a Galerkin projection of the unknown field quantity onto a specific discretization space, leading to a rank-deficient structure. Thus, an additional term for the stabilization of the method is required. The considerable advantage of this method is the permission

of arbitrary polygonal shaped elements which significantly simplifies the mesh construction. Recent publications appropriate to the scope of this thesis are for example the application of VEM to incompressible materials by Wriggers et al. [2017] and to anisotropy with inextensible fibers by Wriggers et al. [2016]. Another concept is the adoption of a least-squares approach, since least-squares finite element formulations a priori guarantee stability of the numerical scheme, due to its inherently minimization structure. We refer in this context to Jiang [1998], Bochev and Gunzburger [2009] and especially in the context of stress-displacement formulations for linear elasticity to Cai and Starke [2003; 2004] and hyperelasticity to **?** and Schwarz et al. [2018]. A further alternative discretization scheme is the Discontinuous Galerkin (DG) approach originally applied in a FE framework by Reed and Hill [1973]. Here, in a first instance the approximation of the variables is discontinuous, and an additional stabilization has to be added in order to achieve the required continuity. Recent developments in the extension of DG to nonlinear elasticity, including problems for nearly incompressibility, have been proposed by Reese et al. [2017] and Bayat et al. [2018]. In the related framework of the Discontinuous Petrov-Galerkin (DPG) method only the test spaces are discontinuous. This leads to the opportunity to design optimal test spaces and thus achieve stable and robust finite element formulations. The DPG method has been introduced by Demkowicz and Gopalakrishnan [2010a;b]. It has been recently extended to the case of linear elasticity by Carstensen and Hellwig [2016] and to simple nonlinear problems by Carstensen et al. [2018].

The objective of this thesis is the construction and investigation of robust and reliable finite element approximations for the hyperelastic framework which are suitable for the incorporation of constraints. Thereby two different constraints will be distinguished in particular, the case of (nearly) incompressibility and (nearly) inextensibility. In order to investigate the stability of the considered element formulations, first an analysis on the well-posedness is carried out in the linear elastic setup. Ensuing the extension to hyperelasticity is carried out, where reliability and robustness are verified by means of numerical investigations. This is followed by the discussion of a suitable finite element formulation, specially constructed for the case of nearly inextensibility in the large deformation setup. In detail, the present work is structured as followed.

The underlying concept of continuum mechanics is introduced briefly in **Chapter 2**. Therein first the kinematics and the concept of stress is discussed and followed by the definition of a boundary value problem based on the balance equations, appropriate constitutive relations, and suitable boundary conditions.

Chapter 3 summarizes the necessary mathematical preliminaries for the analysis of the formulations. Therefore, first suitable function spaces and corresponding norms are introduced, followed by the introduction of abstract variational formulations which are investigated with respect to their well posedness.

Chapter 4 covers a variety of variational formulations for linearized elasticity. In particular, the primal variational formulation and its ill posedness due to incompressibility is discussed in a first step. Subsequently different mixed variational approaches are discussed and analyzed based on the previously introduced conditions on the well posedness of mixed formulations.

Ensuing a prepended discussion on limitation principles and equivalences of mixed finite elements, the finite element method is used for a conforming discretization of the different

discussed variational approaches in **Chapter 5**. The analysis of the well-posedness is retraced for the proposed discrete formulations. This is followed by a numerical verification with the help of significant benchmark problems and their closed form solutions.

Chapter 6 extends the variational framework to the general nonlinear case of elasticity, including large deformations. For each formulation, the weak-variational form and its corresponding consistent linearization is carried out in detail. A special focus is set in this chapter on the Hellinger-Reissner based and displacement-pressure based formulations, because their extension to hyperelasticity is not straightforward.

The discrete counterparts and corresponding system of equations related to the FEM approximation are described in **Chapter 7**. A selection of specific numerical examples is discussed in order to investigate the reliability, robustness and efficiency of the proposed finite elements.

In **Chapter 8** the particular case of transversal isotropic materials, with a nearly inextensible preferred direction, is investigated. This includes the construction of a special variational formulation which accounts for the inherent constraint using a Lagrangian multiplier, its discretization by a suitable and conforming interpolation and numerical verification by means of an academic numerical example and the simulation of a patient specific part of an artery.

Chapter 9 summarizes and concludes the present thesis. In addition a short outlook for possible upcoming projects based on the presented work is given.

2 Continuum Mechanical Foundations

The field of continuum mechanics has a far-reaching history. It's origination as a field of science may be ascribed to Galileo Galilei in the late 16th century. Later, the infinitesimal treatment of the continuum has been developed in the 17th and 18th century based on the beam theories of Jakob Bernoulli and Leonhard Euler. One of the most remarkable keystones approaching modern continuum mechanics has been the introduction of the stress terminology by Augustin Cauchy in the early 19th century. Our contemporary view of continuum mechanics is highly related to the works of Truesdell, Noll and Rivlin from the second half of the 20th century, see e.g. Rivlin [1948], Truesdell and Toupin [1960], Truesdell and Noll [1965] and Noll [1974].
In the following chapter the basic principles of continuum mechanics in the framework of solid mechanics are described. This comprises the introduction of the basic kinematic quantities and the concept of stress. A discussion of the fundamental balance equations is affiliated. The chapter is closed by the derivation of the considered constitutive laws and suitable boundary conditions. Note that the following discussion is reduced to the necessary essentials covering the scope of the present thesis, including the restriction to isothermal and non-dissipative processes. For a comprehensive survey on the continuum mechanics the interested reader is referred to related textbooks as for example Stein and Barthold [1996], Holzapfel [2000] and Malver [1969].

2.1 Kinematics

In continuum mechanics motion, deformation, strain measurements and time derivatives are described by the kinematics. The so-called reference configuration describes the considered body $\mathcal{B}_0 \subset \mathbb{R}^3$ at time t_0 and is parametrized in $\boldsymbol{X}$. We are interested in the movements

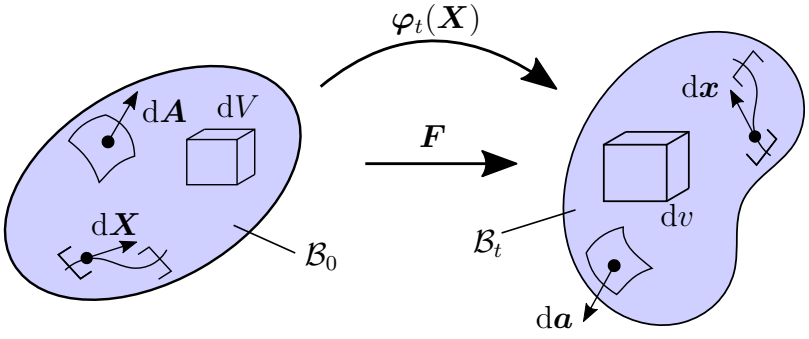

Figure 2.1: Sketch of the body in reference on the left and current configuration on the right.

of this body at time $t > t_0$, including the deformations, translations and rotations. The body at the current configuration at time t is denoted as $\mathcal{B}_t \subset \mathbb{R}^3$ and is parametrized in $\boldsymbol{x}$. The nonlinear, continuous and one-to-one transformation map

$$\varphi_t : \mathcal{B}_0 \to \mathcal{B}_t \tag{2.1}$$

maps points of $\mathcal{B}_0$ onto points of $\mathcal{B}_t$, i.e. $\varphi_t : \boldsymbol{X} \mapsto \boldsymbol{x}$. With the definition of the displacements $\boldsymbol{u}$ as the difference of the position vector of a material point in the reference

configuration and in the current configuration

$$\boldsymbol{u} := \boldsymbol{X} - \boldsymbol{x}\,, \tag{2.2}$$

the transformation map appears as the coordinate vector in the reference configuration plus the displacements

$$\boldsymbol{\varphi}_t = \boldsymbol{X} + \boldsymbol{u}\,. \tag{2.3}$$

The basic kinematical quantity, the deformation gradient $\boldsymbol{F} := \nabla_X \boldsymbol{\varphi}_t(\boldsymbol{X})$, follows as

$$\boldsymbol{F} = \boldsymbol{I} + \nabla_X \boldsymbol{u}\,, \tag{2.4}$$

whereas the operator ∇_X denotes the gradient with respect to $\boldsymbol{X}$ and $\boldsymbol{I}$ the second order identity tensor. These important relations are visualized in Figure 2.1. In order to guarantee $\boldsymbol{\varphi}_t$ to be a one to one transformation map, its inverse mapping has to be uniquely defined. A necessary and sufficient condition for that is a non-zero determinant of the deformation gradient, denoted as the Jacobian. In order to additionally exclude self penetration we restrict the Jacobi determinant to be strictly positive

$$J := \det \boldsymbol{F} > 0\,. \tag{2.5}$$

Material lines, surface and volume elements are mapped from the reference to the current configuration following the fundamental transport equations

$$\begin{aligned} \mathrm{d}\boldsymbol{x} &= \boldsymbol{F}\,\mathrm{d}\boldsymbol{X}\,, \\ \mathrm{d}\boldsymbol{a} &= \mathrm{cof}\boldsymbol{F}\,\mathrm{d}\boldsymbol{A}\,, \\ \mathrm{d}v &= J\,\mathrm{d}V\,, \end{aligned} \tag{2.6}$$

whereas the cofactor of the deformation gradient is defined as $\mathrm{cof}\boldsymbol{F} = \det[\boldsymbol{F}]\boldsymbol{F}^{-T}$. An important quantity in the continuum mechanical description of the deformation is the symmetric and positive definite right Cauchy-Green tensor

$$\boldsymbol{C} := \boldsymbol{F}^T\boldsymbol{F}. \tag{2.7}$$

Its importance emerges with the consideration of the multiplicative decomposition of the deformation gradient into a proper orthogonal tensor of rotation $\boldsymbol{R}$ and a stretch tensor $\boldsymbol{U}$. It demonstrates that the right Cauchy-Green tensor is free of rigid body motions and contains only the stretching part

$$\boldsymbol{C} = \boldsymbol{F}^T\boldsymbol{F} = (\boldsymbol{R}\boldsymbol{U})^T(\boldsymbol{R}\boldsymbol{U}) = \boldsymbol{U}^T\boldsymbol{R}^T\boldsymbol{R}\boldsymbol{U} = \boldsymbol{U}^T\boldsymbol{U}\,. \tag{2.8}$$

Thus, the right Cauchy-Green tensor is suitable for the construction of a strain measure. The requirements for such a strain measure are the independency of rigid body motions, the independency of the direction of deformation and in addition they should vanish in case of a undeformed configuration. Following these principles, many different strain measures have been introduced in the literature. In the scope of this thesis only the nonlinear Green-Lagrange strain tensor $\boldsymbol{E}$ is considered as basic strain measure. It is defined as the difference of the square of an infinitesimal line element in referential and current configuration

$$\frac{1}{2}(\mathrm{d}\boldsymbol{x}\cdot\mathrm{d}\boldsymbol{x} - \mathrm{d}\boldsymbol{X}\cdot\mathrm{d}\boldsymbol{X}) = \Big[\underbrace{\frac{1}{2}(\boldsymbol{C}-\boldsymbol{I})}_{:=\boldsymbol{E}}\,\mathrm{d}\boldsymbol{X}\Big]\cdot\mathrm{d}\boldsymbol{X}\,. \tag{2.9}$$

2.2 Tractions and Stresses

A body which is loaded by external surface or body forces generates an internal state of stress. In order to visualize this, an imaginary cut $\mathcal{S}_t$ of body $\mathcal{B}_t$ into the two parts $\mathcal{B}_{t,1}$ and $\mathcal{B}_{t,2}$ is considered such that the inner forces are released. The resulting traction vector $\boldsymbol{t}$ is then defined by

$$\boldsymbol{t} := \lim_{\Delta a \to 0} \frac{\Delta \boldsymbol{f}}{\Delta a} \,, \tag{2.10}$$

with the area element $\Delta a \subseteq \mathcal{S}_t$ and the associated force vector $\Delta \boldsymbol{f}$. Cauchy's theorem states that a tensor field $\boldsymbol{\sigma}$ exists such that the linear mapping

$$\boldsymbol{t} = \boldsymbol{\sigma} \boldsymbol{n} \tag{2.11}$$

is valid for all unit vectors $\boldsymbol{n}$. Here $\boldsymbol{n}$ denotes the unit vector acting normal to the tangential plane of the cutting surface $\mathcal{S}_t$. The Cauchy stress tensor $\boldsymbol{\sigma}$ is related to the current configuration and often denoted as the true stresses. The stresses related to an imaginary cut in the reference configuration are denoted as the first Piola-Kirchhoff stress tensor $\boldsymbol{P}$ and defined by

$$\boldsymbol{t}_0 = \boldsymbol{P} \boldsymbol{n}_0 \,. \tag{2.12}$$

Here, the traction vector $\boldsymbol{t}_0$ and the normal vector $\boldsymbol{n}_0$ are related to the reference configuration. The kinematic connection between both stress tensors is obtained via the relation $\boldsymbol{t}_0 \, \mathrm{d}A = \boldsymbol{t} \, \mathrm{d}a$ and the transport theorem for area elements $(2.6)_2$ yielding to

$$\boldsymbol{\sigma} = \frac{1}{J} \boldsymbol{P} \boldsymbol{F}^T \,. \tag{2.13}$$

The often used second Piola-Kirchhoff stress tensor is defined as

$$\boldsymbol{S} = \boldsymbol{F}^{-1} \boldsymbol{P} \,. \tag{2.14}$$

It should be noted that, in contrast to the Cauchy and the first Piola-Kirchhoff stresses, the second Piola-Kirchhoff stresses have no physical interpretation, but are widely used because of its inherent symmetry.

2.3 Balance Equations

The set of balance equations constitute the foundation in the description of the mechanical behavior of the considered body. They are based on axioms and have to be fulfilled at each time t for the complete body $\mathcal{B}_t$ and also for each arbitrary partition of the body $\mathcal{P}_t \subseteq \mathcal{B}_t$.

2.3.1 Conservation of Mass

The axiom of mass conservation states that over the process of deformation no mass is lost or produced. With the introduction of the density ρ this can be expressed by the integral statement

$$m := \int_{\mathcal{P}_0} \rho_0 \, \mathrm{d}V = \int_{\mathcal{P}_t} \rho \, \mathrm{d}v = \text{const.} \,, \tag{2.15}$$

where m denotes the mass of the body and ρ_0 the initial density. With the transformation of the volume elements (2.6) the first local statement of the mass conservation is obtained as

$$\rho_0 = \rho\, J\,. \tag{2.16}$$

Furthermore, the time derivative of Equation (2.15) leads to

$$\dot{m} = \int_{\mathcal{P}_0} (\rho_0)^{\cdot}\, \mathrm{d}V = \Big(\int_{\mathcal{P}_t} \rho\, \mathrm{d}v \Big)^{\cdot} = 0\,, \tag{2.17}$$

whereas the notation of the time derivative is defined as $\dot{(\bullet)} = (\bullet)^{\cdot} = \frac{\mathrm{d}(\bullet)}{\mathrm{d}\,t}$. Using the first statement in Equation (2.16) and the time derivative of the Jacobian as $\dot{J} = J \operatorname{div} \dot{\boldsymbol{x}}$ the second statement of the mass conversation follows in global form as

$$\dot{m} \;=\; \int_{\mathcal{P}_t} (\dot{\rho} + \rho\, \operatorname{div} \dot{\boldsymbol{x}})\, \mathrm{d}v = 0\,. \tag{2.18}$$

It constitutes the basis of the fundamental second local statement of mass conservation, which follows as

$$\dot{\rho} + \rho \operatorname{div} \dot{\boldsymbol{x}} = 0\,. \tag{2.19}$$

2.3.2 Balance of Linear Momentum

The balance of linear momentum requires that the time rate of change of the linear momentum of is equal to the resultant force $\boldsymbol{k}$ acting on the body

$$\dot{\boldsymbol{l}} = \boldsymbol{k}\,. \tag{2.20}$$

The linear momentum $\boldsymbol{l}$ of a body moving with the velocity $\dot{\boldsymbol{x}}$ is defined by

$$\boldsymbol{l} := \int_{\mathcal{P}_t} \rho\, \dot{\boldsymbol{x}}\, \mathrm{d}v\,. \tag{2.21}$$

The resultant force can be split into a volume and a surface related term such that

$$\boldsymbol{k} := \int_{\mathcal{P}_t} \rho\, \boldsymbol{b}\; \mathrm{d}v + \int_{\partial\mathcal{P}_t} \boldsymbol{t}\; \mathrm{d}a\,, \tag{2.22}$$

where $\boldsymbol{b}$ is the mass related external acceleration and $\boldsymbol{t}$ the surface traction vector. After some mathematical steps, including the application of the continuity condition (2.19) and the divergence theorem, the axiom of the balance of linear momentum (2.20) can be reformulated with respect to the reference configuration as

$$\int_{\mathcal{P}_0} (\operatorname{Div} \boldsymbol{P} + \rho_0(\boldsymbol{b} - \ddot{\boldsymbol{x}}))\; \mathrm{d}V = \boldsymbol{0}\,. \tag{2.23}$$

This leads to the fundamental local statement as

$$\operatorname{Div} \boldsymbol{P} + \rho_0(\boldsymbol{b} - \ddot{\boldsymbol{x}}) = \boldsymbol{0}\,. \tag{2.24}$$

2.3.3 Balance of Angular Momentum

It is required that the change in time of the angular momentum $\boldsymbol{h}_{(0)}$ related to the fixed point of origin (0) equals to the sum of external moments $\boldsymbol{m}_{(0)}$

$$\dot{\boldsymbol{h}}_{(0)} = \boldsymbol{m}_{(0)} \,. \tag{2.25}$$

The angular momentum is defined via

$$\boldsymbol{h}_{(0)} := \int_{\mathcal{P}_t} \boldsymbol{x} \times (\rho\, \dot{\boldsymbol{x}})\, \mathrm{d}v \tag{2.26}$$

and the sum of external moments as

$$\boldsymbol{m}_{(0)} := \int_{\mathcal{P}_t} \boldsymbol{x} \times (\rho\, \boldsymbol{b})\, \mathrm{d}v + \int_{\partial\mathcal{P}_t} \boldsymbol{x} \times \boldsymbol{t}\, \mathrm{d}a \,. \tag{2.27}$$

The time derivative of the angular momentum is given, with help of the local statement of the balance of mass in Equation (2.19), by

$$\dot{\boldsymbol{h}}_{(0)} = \int_{\mathcal{P}_t} \boldsymbol{x} \times (\rho\, \ddot{\boldsymbol{x}})\, \mathrm{d}v \,. \tag{2.28}$$

Application of the local statement of the balance of linear momentum (2.24) to the axiom (2.25) leads to the global form of the balance of angular momentum as

$$\int_{\mathcal{P}_t} \boldsymbol{I} \times \boldsymbol{\sigma}\, \mathrm{d}v = \boldsymbol{0} \,. \tag{2.29}$$

From the corresponding local form

$$\boldsymbol{I} \times \boldsymbol{\sigma} = \boldsymbol{0} \tag{2.30}$$

the statement on the symmetry of the Cauchy stress tensor is obtained

$$\boldsymbol{\sigma} = \boldsymbol{\sigma}^T \,. \tag{2.31}$$

A reformulation with respect to the reference configuration leads to the related statement for the first Piola-Kirchhoff stress tensor as

$$\boldsymbol{F}\boldsymbol{P}^T = \boldsymbol{P}\boldsymbol{F}^T \,. \tag{2.32}$$

2.3.4 Balance of Energy

The balance equation of energy is often denoted as the first law of thermodynamics and states that the time rate of the sum of kinetic energy K and internal energy E is equal to the sum of the mechanical power W and thermal power Q

$$\dot{E} + \dot{K} = W + Q \,. \tag{2.33}$$

For the internal energy E we assume the existence of an internal energy density $e(\boldsymbol{x})$ such that we may express

$$E := \int_{\mathcal{P}_t} \rho\, e(\boldsymbol{x})\, \mathrm{d}V \,. \tag{2.34}$$

The kinetic energy K is defined as

$$K := \int_{\mathcal{P}_t} \frac{1}{2}\rho\, \dot{\boldsymbol{x}} \cdot \dot{\boldsymbol{x}}\ \mathrm{d}V\,. \tag{2.35}$$

The mechanical and thermal power W and Q follow as

$$\begin{aligned} W &:= \int_{\mathcal{P}_t} \dot{\boldsymbol{x}} \cdot \rho\, \boldsymbol{b}\ \mathrm{d}V + \int_{\partial\mathcal{P}_t} \dot{\boldsymbol{x}} \cdot \boldsymbol{t}\ \mathrm{d}a\,, \\ Q &:= \int_{\mathcal{P}_t} r\,\rho\ \mathrm{d}V - \int_{\partial\mathcal{P}_t} \boldsymbol{q} \cdot \boldsymbol{n}\,\mathrm{d}a\,, \end{aligned} \tag{2.36}$$

where $r := r(\boldsymbol{x}, t)$ denotes an external heat source per unit reference mass and $\boldsymbol{q} := \boldsymbol{q}(\boldsymbol{x}, t)$ the heat flux vector. The local form of the balance of energy can be derived after some mathematical steps from Equation (2.33) as

$$\rho\,\dot{e} = \boldsymbol{\sigma} : \boldsymbol{D} + \rho\, r - \operatorname{div}\boldsymbol{q}\,. \tag{2.37}$$

where $\boldsymbol{D}$ is the spatial strain velocity

$$\boldsymbol{D} := \frac{1}{2}\left(\nabla_x \dot{\boldsymbol{x}} + (\nabla_x \dot{\boldsymbol{x}})^T\right) = \operatorname{sym}[\dot{\boldsymbol{F}}\boldsymbol{F}^{-1}]\,, \tag{2.38}$$

with the gradient operator with respect to the current configuration ∇_x.

2.3.5 Entropy Inequality

The entropy inequality represents the second law of thermodynamics and states that the time rate of the change of total entropy H has to be greater or equal than the sum of the entropy supplied by the body sources and the entropy influx through the surface of the body

$$\dot{H} \geq \int_{\mathcal{P}_t} \frac{1}{\theta} r\ \mathrm{d}v - \int_{\partial\mathcal{P}_t} \frac{1}{\theta}\boldsymbol{q} \cdot \boldsymbol{n}\,\mathrm{d}a\,, \tag{2.39}$$

whereas θ denotes the temperature and the entropy is given by

$$H := \int_{\mathcal{P}_t} \rho\,\eta\ \mathrm{d}v\,, \tag{2.40}$$

with the specific entropy $\eta := \eta(\boldsymbol{x}, t)$ per unit reference mass. Its time derivative follows with aid of the balance of mass (2.19) as

$$\dot{H} = \int_{\mathcal{P}_t} \rho\,\dot{\eta}\ \mathrm{d}v\,. \tag{2.41}$$

The local form appears, with help of the divergence theorem, as

$$\rho\,\dot{\eta} - \frac{r}{\theta}\,\rho + \operatorname{div}\left[\frac{1}{\theta}\boldsymbol{q}\right] \geq 0. \tag{2.42}$$

Inserting the local statement of the balance of energy (2.37) and assuming the existence of a scalar valued free Helmholtz energy $\widetilde{\psi} := e - \theta\eta$, defined per unit reference mass, we obtain

$$-\rho(\dot{\widetilde{\psi}} + \dot{\theta}\eta) + \boldsymbol{\sigma} : \boldsymbol{D} - \frac{1}{\theta}\boldsymbol{q} \cdot \operatorname{grad}\,\theta \geq 0\,. \tag{2.43}$$

Restricting the formulation to isothermal processes and introducing a free energy defined per unit reference volume, i.e. $\psi := \rho_0 \tilde{\psi}$, the local form of the entropy inequality reduces to

$$\boldsymbol{\sigma} : \boldsymbol{D} - \dot{\psi} \geq 0 \,. \tag{2.44}$$

Considering the work conjugated pair $(\boldsymbol{P}, \dot{\boldsymbol{F}})$ and restricting ourselves to hyperelasticity we obtain the equality

$$\boldsymbol{P} : \dot{\boldsymbol{F}} - \partial_F \psi : \dot{\boldsymbol{F}} = 0 \,, \tag{2.45}$$

which directly leads to the constitutive relation for the first Piola-Kirchhoff stress tensor

$$\boldsymbol{P} = \frac{\partial \psi}{\partial \boldsymbol{F}} \,. \tag{2.46}$$

In the framework the work-conjugated pairs related to the reference configuration $(\boldsymbol{S}, \dot{\boldsymbol{E}})$ the local statement in Equation (2.45) can be modified to

$$\boldsymbol{S} : \dot{\boldsymbol{E}} - \partial_E \psi : \dot{\boldsymbol{E}} = 0 \tag{2.47}$$

and thus the constitutive equation is given by

$$\boldsymbol{S} = \frac{\partial \psi}{\partial \boldsymbol{E}} = 2 \frac{\partial \psi}{\partial \boldsymbol{C}} \,. \tag{2.48}$$

2.4 Constitutive Equations

A constitutive law, which relates the stress and strain fields, closes the description of the continuum mechanical model. For the construction of physically reasonable constitutive models several principles have to be incorporated as outlined e.g. in Truesdell and Toupin [1960] and Truesdell [1969]. A detailed discussion of all required principles seems to be too universal for the subject of this thesis. However, the principles of material frame indifference and material symmetry constitute important roles in the description of isotropic and anisotropic material behavior and are briefly recapitulated. In addition the important representation theorem of isotropic tensor functions and the considered hyperelastic material models are discussed briefly.

2.4.1 Principle of Material Frame Indifference

The principle of material frame indifference postulates the invariance of the constitutive quantities to superimposed rigid body motions $\boldsymbol{Q} \in \mathrm{SO}(3)$ onto the current configuration. Therein the special orthogonal group SO(3) describes any orthogonal transformation with $\det \boldsymbol{Q} = 1$ and $\boldsymbol{Q}^T = \boldsymbol{Q}^{-1}$. The corresponding transformed deformation gradient is obtained by

$$\boldsymbol{x}^+ = \boldsymbol{Q}\boldsymbol{x} \quad \rightarrow \quad \boldsymbol{F}^+ = \frac{\partial \boldsymbol{x}^+}{\partial \boldsymbol{X}} = \frac{\partial \boldsymbol{x}^+}{\partial \boldsymbol{x}} \frac{\partial \boldsymbol{x}}{\partial \boldsymbol{X}} = \boldsymbol{Q}\boldsymbol{F} \,. \tag{2.49}$$

For example a strain energy satisfies the requirement of material frame indifference if

$$\psi(\boldsymbol{F}) = \psi(\boldsymbol{F}^+) \quad \forall \, \boldsymbol{Q} \in \mathrm{SO}(3) \,. \tag{2.50}$$

It is a simple task to show that any constitutive description based on the right Cauchy-Green tensor $\boldsymbol{C}$ inherently satisfies the principle of material frame indifference

$$\psi(\boldsymbol{C}) = \psi(\boldsymbol{C}^+) \quad \forall \, \boldsymbol{Q} \in \mathrm{SO}(3) \tag{2.51}$$

since $\boldsymbol{C}^{+} = \boldsymbol{F}^{+^T}\boldsymbol{F} = \boldsymbol{F}^T\boldsymbol{Q}^T\boldsymbol{Q}\boldsymbol{F} = \boldsymbol{C}$. Therefore, the considered hyperelastic material descriptions are restricted to constitutive equations based on the right Cauchy Green tensor.

2.4.2 Principle of Material Symmetry

The principle of material symmetry postulates that no rotation $\boldsymbol{Q} \in \mathcal{G}^k$ on the reference configuration effects the constitutive quantities. Here, $\mathcal{G}^k$ constitutes the symmetry group of the considered material, which incorporates the information of the material symmetry. The restrictions of this principle require exemplary for the free energy function that

$$\psi(\boldsymbol{F}) = \psi(\boldsymbol{F}^*) \quad \forall\, \boldsymbol{Q} \in \mathcal{G}^k\,, \tag{2.52}$$

with the rotated deformation gradient obtained from

$$\boldsymbol{X}^* = \boldsymbol{Q}\boldsymbol{X} \quad \rightarrow \quad \boldsymbol{F}^* = \frac{\partial \boldsymbol{x}}{\partial \boldsymbol{X}^*} = \frac{\partial \boldsymbol{x}}{\partial \boldsymbol{X}}\frac{\partial \boldsymbol{X}}{\partial \boldsymbol{X}^*} = \boldsymbol{F}\boldsymbol{Q}^T\,. \tag{2.53}$$

In the case of isotropic materials the symmetry group is represented by the special orthogonal group $\mathcal{G}^k = \mathrm{SO}(3)$. Otherwise the corresponding subgroups $\mathcal{G}^k \subset \mathrm{O}(3)$ are characterized by the set of crystal classes. It has been shown in Equation (2.51), that the principle of material frame indifference is a priori fulfilled, if the right Cauchy-Green tensor $\boldsymbol{C}$ is used for the description of the constitutive relation. This proposition is not the case for the principle of material symmetry. This can be noticed considering $\boldsymbol{C}^* = \boldsymbol{F}^{*^T}\boldsymbol{F}^* = \boldsymbol{Q}\boldsymbol{F}^T\boldsymbol{F}\boldsymbol{Q}^T = \boldsymbol{Q}\boldsymbol{C}\boldsymbol{Q}^T$ and thus in general we obtain

$$\psi(\boldsymbol{C}) \neq \psi(\boldsymbol{C}^*) \quad \forall\, \boldsymbol{Q} \in \mathrm{SO}(3)\,. \tag{2.54}$$

In order to fulfill the principle of material symmetry in a coordinate invariant setting, the free energy function can be formulated in terms of an extended list of invariants, which are constructed based on the representation theorems for isotropic functions.

2.4.3 Remark on the Representation of Isotropic Tensor Functions

The constitutive description of nonlinear material behavior is mainly constructed by scalar- and tensor-valued tensor functions. The representation theory states that isotropic tensor functions can be represented in terms of scalar valued coordinate independent quantities, denoted as invariants I_s, and tensor generators. In this context the reader is referred to Smith [1970; 1971] and Wang [1969a;b; 1970; 1971]. The existence of an irreducible number of invariants is ensured by *Hilbert's theorem*, see e.g. Spencer [1971]. It can be shown, with the aid of the characteristic polynomial that, the set of principal invariants of the right Cauchy-Green tensor $\boldsymbol{C}$ are given by

$$I_1 := \mathrm{tr}[\boldsymbol{C}]\,, \quad I_2 := \mathrm{tr}[\mathrm{cof}\boldsymbol{C}]\,, \quad I_3 := \det[\boldsymbol{C}]\,. \tag{2.55}$$

The so-called main invariants constitute an alternative representation, which may be beneficial for some applications, where the expression appears in terms of the power of the traces

$$J_1 := \mathrm{tr}[\boldsymbol{C}]\,, \quad J_2 := \mathrm{tr}[\boldsymbol{C}^2]\,, \quad J_3 := \mathrm{tr}[\boldsymbol{C}^3]\,. \tag{2.56}$$

The principal and main invariants are connected by the relation

$$I_1 = J_1\,, \quad I_2 = \frac{1}{2}(J_1^2 - J_2)\,, \quad I_3 = \frac{1}{3}\left(J_3 - \frac{3}{2}J_1J_2 + \frac{1}{2}J_1^3\right)\,. \tag{2.57}$$

In order to extend the representation theory to the framework of anisotropic material descriptions, the related strain energies have to be formulated in form of an isotropic tensor functions. For this purpose the concept of structural tensors is applied, which was first introduced in an attractive way with important applications by Boehler [1978; 1979; 1987], although some similar ideas might have been touched on earlier. The structural tensor is defined as $\boldsymbol{M} = \boldsymbol{a}_0 \otimes \boldsymbol{a}_0$ with the preferred direction vector $\boldsymbol{a}_0$ of unit length. Let $\boldsymbol{Q}(\alpha, \boldsymbol{a}_0)$ characterize all rotations about the $\boldsymbol{a}_0$-axis, then the associated material symmetry group is defined by

$$\mathcal{G}^{\mathrm{ti}} := \{\pm\mathbf{1};\ \boldsymbol{Q}(\alpha, \boldsymbol{a}_0) \mid 0 \leq \alpha < 2\,\pi\}\,. \tag{2.58}$$

The invariance group of the structural tensor preserves the material symmetry group $\mathcal{G}^{\mathrm{ti}}$,

$$\boldsymbol{M} = \boldsymbol{Q}\boldsymbol{M}\boldsymbol{Q}^T \;\forall\; \boldsymbol{Q} \in \mathcal{G}^{\mathrm{ti}}\,. \tag{2.59}$$

Therefore the strain energy can be formulated as an isotropic tensor function with respect to the arguments $\{\boldsymbol{C}, \boldsymbol{M}\}$. Exploiting the fact, that the powers of the structural tensor are the structural tensor itself and restricting ourselves to transversal isotropy, two additional mixed invariants of the two symmetric tensors $\boldsymbol{C}$ and $\boldsymbol{M}$ can be introduced

$$J_4 := \mathrm{tr}[\boldsymbol{C}\boldsymbol{M}] \quad \text{and} \quad J_5 := \mathrm{tr}[\boldsymbol{C}^2\boldsymbol{M}]\,. \tag{2.60}$$

In case of materials, which are characterized by two or more families of fibers additional preferred direction vectors are introduced leading to additional invariants per family of fibers.

Summarizing, constitutive relations for isotropic and transversal isotropic material based on strain energy functions automatically satisfy the crucial requirements of material frame indifference and material symmetry if they are solely defined as a function of the invariants given in Equations (2.56) and (2.60). In this context see i.a. Schröder [2014].

2.4.4 Saint Venant-Kirchhoff Elasticity

A linear relation between the stresses and strains is assumed in the framework of Saint Venant-Kirchhoff elasticity. The constitutive relation between the second Piola-Kirchhoff stresses and the Green-Lagrangian strains is defined as

$$\boldsymbol{S} = \Lambda(\mathrm{tr}\,\boldsymbol{E})\,\boldsymbol{I} + 2\mu\,\boldsymbol{E}\,, \tag{2.61}$$

where $\Lambda \geq 0$ and $\mu > 0$ are the first and second Lamé constants. The corresponding strain energy function is constructed by

$$\psi^{\mathrm{SVK}}(\boldsymbol{E}) := \mu\,\boldsymbol{E} : \boldsymbol{E} + \frac{\Lambda}{2}(\mathrm{tr}\,\boldsymbol{E})^2\,. \tag{2.62}$$

Due to the linear dependency of stresses and strains in Equation (2.61), an explicit complementary form, which describes the Green-Lagrange strains as a function of the second Piola-Kirchhoff stresses, exists as

$$\boldsymbol{E} = \frac{1}{4\mu}\boldsymbol{S} - \frac{\Lambda}{4\mu(3\Lambda + 2\mu)}(\mathrm{tr}\,\boldsymbol{S})\boldsymbol{I}\,. \tag{2.63}$$

The appropriate complementary strain energy χ follows by

$$\chi^{\mathrm{SVK}}(\boldsymbol{S}) := \frac{1}{2\mu}\boldsymbol{S} : \boldsymbol{S} - \frac{\Lambda}{2\mu(3\Lambda + 2\mu)}(\operatorname{tr}\boldsymbol{S})^2 \,. \tag{2.64}$$

Note that the Saint Venant-Kirchhoff material model fulfills the principle of material frame indifference and material symmetry, since it a simple task to express ψ^{SVK} in terms of invariants of $\boldsymbol{C}$. In contrast it does not fulfill the concept of polyconvexity and should be treated with care, especially in the large strain regime, see e.g. Schröder and Neff [2003].

2.4.5 Isotropic Neo-Hookean Material Model

Isotropic Neo-Hookean free energy functions are formulated in terms of the first and third principal invariants of the right Cauchy-Green tensor defined in Equation (2.55), whereas we make use of the identity $I_3 = J^2$. Thus the principles of material frame indifference and material symmetry are satisfied a priori for this family of constitutive relations. In this thesis we consider in detail Neo-Hookean free energies of the form

$$\psi^{\mathrm{NH}}(I_1, I_3) := \frac{\mu}{2}(I_1 - 3) - \mu \ln J + \frac{\Lambda}{2}\vartheta(J)^2 \,, \tag{2.65}$$

whereas the scalar valued function $\vartheta(J)$ is related to the energy due to volumetric deformation and has to satisfy

$$\begin{aligned} &\vartheta(J) = 0 \ \text{ if and only if } J = 1 \text{ and} \\ &\partial_J \vartheta(J)\big|_{J=1} \neq 0 \,. \end{aligned} \tag{2.66}$$

From a mathematical point of view, the first Lamé constant Λ acts in this model as a penalty parameter enforcing $\vartheta(J) \approx 0$. It becomes clear, that the limit $\Lambda \to \infty$ describes the incompressible case. In accordance to Auricchio et al. [2013] two different forms of $\vartheta(J)$ will be considered throughout the numerical examples

$$\begin{aligned} &\text{case 1:} \quad \vartheta(J) = J - 1 \\ &\text{case 2:} \quad \vartheta(J) = \ln J \,. \end{aligned} \tag{2.67}$$

Note that the second choice violates the polyconvexity condition, which is a sufficient condition for ellipticity, ensuing material stability and the existence of minimizers if some further growth conditions are taken into account.

2.4.6 Transverse Isotropic Material Models

The considered strain energies representing fiber reinforced materials are additively decoupled into a function related to the isotropic behavior of the bulk material ψ^{iso} and a function related to the stored energy of the fiber material ψ^{fib} such that

$$\psi^{\mathrm{ti}} = \psi^{\mathrm{iso}} + \psi^{\mathrm{fib}} \,. \tag{2.68}$$

Two different transverse isotropic material models will be considered in the scope of the present thesis.

Simple benchmark model In the first transverse isotropic material model the fiber related strain energy is connected solely to the fiber stretch and thus only depends on the mixed invariant J_4. The corresponding polyconvex strain energy reads as

$$\psi^{\text{fib},1} := \alpha_1 \langle J_4 - 1 \rangle^{\alpha_2} \,, \tag{2.69}$$

where $\alpha_1 > 0$ and $\alpha_2 \geq 2$ are material parameter and the Macaulay brackets $\langle \bullet \rangle = \frac{1}{2}(\bullet + |\bullet|)$ ensure the assumption that the fibers can only carry tensile stresses. The isotropic part of the energy is represented by the Neo-Hookean type function

$$\psi^{\text{iso},1} := \frac{\Lambda}{4}(I_3 - 1) - \left(\frac{\Lambda}{2} + \mu \right) \ln J + \frac{\mu}{2}(I_1 - 3) \,. \tag{2.70}$$

Transverse isotropic material model for the simulation of soft biological tissues The material modeling of soft biological tissues is a large scientific field and many different approaches have been considered. However, since the modeling approach itself is not in the scope of the current work, we will not go into a detailed discussion and the interested reader is referred to the relevant literature, e.g. Holzapfel et al. [2000] and the references therein. The considered constitutive model for soft biological tissues is based on the approach proposed by Balzani et al. [2006]. The isotropic part is represented by a decoupled Neo-Hookean free energy

$$\psi^{\text{iso},2} = c_1 \left(\frac{I_1}{I_1^{1/3}} - 3 \right) + \epsilon_1 \left(I_3^{\epsilon_2} + I_3^{-\epsilon_2} - 2 \right) \,, \tag{2.71}$$

with the material parameter $c_1 > 0$, $\epsilon_1 > 0$ and $\epsilon_2 \geq 1$. Note that the first term is solely related to isochoric deformation and the second term to the volumetric deformation. The transverse isotropic part of the strain energy is given by

$$\psi^{\text{fib},2} = \sum_{a=1}^{n_{\text{fiber}}} \alpha_1 \langle I_1 J_4^{(a)} - J_5^{(a)} - 2 \rangle^{\alpha_2} \,, \tag{2.72}$$

with the number of fibers n_{fiber} and the material parameter $\alpha_1 > 0$ and $\alpha_2 \geq 1$. The polyconvexity of both functions have been proven by Schröder and Neff [2003].

2.5 Boundary Conditions

Suitable conditions for the displacements or stresses have to be specified on the boundary of the body to obtain a complete description of the physical problem. This is especially of importance to exclude rigid body motions such that the resulting state of deformation can be unique. The boundary of the body $\partial\mathcal{B}_0$ is decomposed into a nontrivial Dirichlet part $\partial\mathcal{B}_{0,u}$ and a Neumann part $\partial\mathcal{B}_{0,\sigma}$ such that it holds

$$\begin{aligned} \partial\mathcal{B}_{0,u} \cup \partial\mathcal{B}_{0,\sigma} &= \partial\mathcal{B}_0 \,, \\ \partial\mathcal{B}_{0,u} \cap \partial\mathcal{B}_{0,\sigma} &= \emptyset \,. \end{aligned} \tag{2.73}$$

On the Dirichlet part the displacement vector is fixed to

$$\boldsymbol{u} = \overline{\boldsymbol{u}} \quad \text{on } \partial\mathcal{B}_{0,u} \,, \tag{2.74}$$

whereas $\overline{\boldsymbol{u}}$ represents the values of the prescribed displacements. On the remaining Neumann part the traction vector is prescribed such that

$$\boldsymbol{P}\boldsymbol{n}_0 = \bar{\boldsymbol{t}}_0 \quad \text{on } \partial\mathcal{B}_{0,\sigma}\,, \tag{2.75}$$

where $\bar{\boldsymbol{t}}_0$ contains the prescribed values. Note that technically also a specification of a linear combination of displacements and traction vector is possible. This type of boundary conditions is denoted as Robin boundary condition.

3 Mathematical Preliminaries

The boundary value problem, consisting of the partial differential equation, the constitutive relation and the boundary conditions has been consistently derived in the previous chapter based on the principles of continuum mechanics. A suitable mathematical framework for the analysis of such a problem is represented by the field of functional analysis, which gives a sophisticated insight into the structure of the equations and the characteristics of the solutions. Therefore the development of efficient discretization schemes should be based on the gained knowledge of the functional analysis which examines, in a linearized setting, existence and uniqueness of solutions. In the following chapter some mathematical tools are introduced, which are necessary in order to discuss the problem of elasticity from a functional analysis point of view. In a first step, appropriate function spaces and their corresponding norms are defined. This is followed by the introduction of an abstract primal variational formulation based on the theorem of Lax and Milgram [1954]. This theorem ensures existence and uniqueness of coercive variational problems. In addition an abstract mixed variational formulation is introduced. In this framework the theorem of Lax and Milgram is not applicable and therefore existence and uniqueness of the mixed variational problem is shown by the theorem of Babuška [1973] and Brezzi [1974].

3.1 Function Spaces and Norms

In the following we use Sobolev and Hilbert spaces in order to define suitable function spaces for the unknown field variables. They are based on the space of p-integrable functions on $\mathcal{B}_t$, denoted as the Lebesgue spaces

$$\mathcal{L}^p(\mathcal{B}_t) := \{v : \|v\|_{\mathcal{L}^p} < +\infty\} \quad \text{for } 0 < p < \infty. \tag{3.1}$$

with the associated norm defined as

$$\|v\|_{\mathcal{L}^p} := \left(\int_{\mathcal{B}_t} |v|^p \, \mathrm{d}V \right)^{1/p} \tag{3.2}$$

The norms for vector-valued functions $\boldsymbol{v} \in [\mathcal{L}^p(\mathcal{B}_t)]^n$ and matrix-valued functions $\boldsymbol{A} \in [\mathcal{L}^p(\mathcal{B}_t)]^{n\times m}$ are defined such that each component is in $\mathcal{L}^p(\mathcal{B}_t)$

$$\|\boldsymbol{u}\|_{\mathcal{L}^p} := \left(\sum_{i=1}^{n} \|u_i\|_{\mathcal{L}^p}^p \right)^{1/p}, \quad \|\boldsymbol{A}\|_{\mathcal{L}^p} := \left(\sum_{i=1}^{n} \sum_{j=1}^{m} \|A_{ij}\|_{\mathcal{L}^p}^p \right)^{1/p}. \tag{3.3}$$

The definition of the Lebesgue spaces acts only on the function itself and does not involve statements on their derivatives. Therefore it also includes functions containing local discontinuities. In contrast, Sobolev spaces comprise restrictions for the derivatives of the function and are therefore of special interest if continuity, or even higher order continuity, is required. The standard notation for a Sobolev space is $\mathcal{W}^{s,p}(\mathcal{B}_t)$, whereas $s \geq 0$ is a real number. For $s = 0$ the space $\mathcal{W}^{0,p}(\mathcal{B}_t)$ represents the Lebesgue space $\mathcal{L}^p(\mathcal{B}_t)$ of all p-integrable functions

$$\mathcal{W}^{0,p}(\mathcal{B}_t) := \mathcal{L}^p(\mathcal{B}_t)\,. \tag{3.4}$$

In the framework of the finite element method, the case of s being a positive integer is of main interest. In this case, the space $\mathcal{W}^{s,p}(\mathcal{B}_t)$ consist of all p-integrable functions whose

weak derivatives up to the order s are also p-integrable, i.e.

$$\mathcal{W}^{s,p}(\mathcal{B}_t) := \left\{ v + \sum_{\alpha=1}^{s} \mathrm{D}^\alpha v \in \mathcal{L}^p(\mathcal{B}_t) \right\} \quad \text{for } 1 \leq p < \infty, \tag{3.5}$$

with D^α as the α-st weak differential operator. The associated norm is defined by

$$\|v\|_{\mathcal{W}^{s,p}(\mathcal{B}_t)} := \left(\|v\|^p_{\mathcal{L}^p} + \sum_{\alpha=1}^{s} \|\mathrm{D}^\alpha v\|^p_{\mathcal{L}^p} \right)^{1/p}. \tag{3.6}$$

Thus the often used spaces $\mathcal{W}^{1,p}(\mathcal{B}_t)$ and $\mathcal{W}^{1,p}_0(\mathcal{B}_t)$ are defined by

$$\mathcal{W}^{1,p}(\mathcal{B}_t) := \left\{ v + \mathrm{D}^1 v \in \mathcal{L}^p(\mathcal{B}_t) \right\}, \tag{3.7}$$

and

$$\mathcal{W}^{1,p}_0(\mathcal{B}_t) := \left\{ v \in \mathcal{W}^{1,p}(\mathcal{B}_t) \ : \ v = 0 \ \text{ on } \ \partial\mathcal{B}_{t,u} \right\}, \tag{3.8}$$

whereas the latter is especially important in context of the incorporation of essential boundary conditions. Roughly speaking, $\mathcal{W}^{1,p}(\mathcal{B}_t)$ contains all C^0 continuous p-integrable functions and constitutes therefore the main approximation space for the classical continuous primal FEM for solid mechanics. In addition to these classical Sobolev spaces, which consider the required weak derivatives in each component, the space related to the weak divergence is of special interest in the framework of elasticity. The corresponding space is defined for the three dimensional case by

$$\mathcal{W}^p(\mathrm{div}; \mathcal{B}_t) := \left\{ \boldsymbol{v} \in [\mathcal{L}^p(\mathcal{B}_t)]^3 \ : \ \mathrm{div}\, \boldsymbol{v} \in \mathcal{L}^p(\mathcal{B}_t) \right\} \quad \text{for } 1 \leq p < \infty, \tag{3.9}$$

with the associated norm as

$$\|\boldsymbol{v}\|_{\mathcal{W}^p(\mathrm{div})} := \left(\|\boldsymbol{v}\|^p_{\mathcal{L}^p} + \|\,\mathrm{div}\, \boldsymbol{v}\|^p_{\mathcal{L}^p} \right)^{1/p}. \tag{3.10}$$

In the framework of linear elasticity the case of $p = 2$ is prevalent and denoted as the family of Hilbert spaces

$$\mathcal{H}^s(\mathcal{B}_t) := \mathcal{W}^{s,2}(\mathcal{B}_t) \quad \textit{and} \quad \mathcal{H}^s_0(\mathcal{B}_t) := \mathcal{W}^{s,2}_0(\mathcal{B}_t). \tag{3.11}$$

The definitions of the norms are similar as above $\|v\|_{\mathcal{H}^s} = \|v\|_{\mathcal{W}^{s,2}}$. In case of $s = 0$ and $p = 2$ it obviously holds $\mathcal{L}^2(\mathcal{B}_t) = \mathcal{H}^0(\mathcal{B}_t) = \mathcal{W}^{0,2}(\mathcal{B}_t)$ and $\|v\|_{\mathcal{L}^2} = \|v\|_{\mathcal{H}^0} = \|v\|_{\mathcal{W}^{0,2}}$.

3.2 Abstract Primal Variational Formulation

An abstract variational problem for a primal formulation where v denotes the unknown field quantity is given by: find $v \in V$ such that

$$a(v, \widetilde{v}) = F(\widetilde{v}) \quad \forall\, \widetilde{v} \in V \tag{3.12}$$

with V being a Hilbert space, $F(\widetilde{v})$ a linear form and $a(\bullet, \bullet)$ a bilinear form. The theorem of Lax and Milgram [1954] states, that such a system has a unique solution if the bilinear form $a(\bullet, \bullet)$ is bounded and coercive, i.e.

$$\begin{aligned} &\text{boundedness:} \quad |a(v, \widetilde{v})| \ \leq c_{a,2}\, \|v\|_V\, \|\widetilde{v}\|_V \quad \forall\, v, \widetilde{v} \in V, \\ &\text{coercivity:} \qquad a(\widetilde{v}, \widetilde{v}) \ \geq c_{a,1} \|\widetilde{v}\|^2_V \qquad\quad \forall\, \widetilde{v} \in V, \end{aligned} \tag{3.13}$$

whereas $c_{a,1}$ and $c_{a,2}$ are strictly positive parameter. The Lemma of Lax and Milgram is a fundamental statement in the framework of functional analysis. Its nontrivial proof can be found in many mathematical related finite element textbooks as e.g. Brenner and Scott [1994] or Braess [2000].

3.3 Abstract Mixed Variational Formulation

In a mixed setup more than a single field quantity is unknown. Nonetheless, a corresponding mixed variational problem can also be given in the style of Equation (3.12), assuming v and w as the unknown fields, by: find $(v, w) \in V \times W$ such that

$$\widehat{a}((v, w), (\widetilde{v}, \widetilde{w})) = \widehat{F}((\widetilde{v}, \widetilde{w})) \quad \forall\, (\widetilde{v}, \widetilde{w}) \in V \times W\,, \tag{3.14}$$

whereas V and W are suitable Hilbert spaces, $\widehat{a}(\bullet, \bullet)$ a bilinear and $\widehat{F}(\bullet)$ a linear form. Unfortunately, for the type of problems that we are aiming for, such a mixed bilinear form $\widehat{a}((v, w), (\widetilde{v}, \widetilde{w}))$ is never coercive, as discussed in detail i.a. in Arnold [1990]. Thus, for the mixed problems the theorem of Lax and Milgram alone is no longer helpful in order to proof existence and uniqueness of a solution. In the following an abstract mixed variational formulation is discussed based the theorems of Babuška [1973], Brezzi [1974] and Brezzi and Fortin [1991]. It incorporates the essential and sufficient conditions for the existence and uniqueness of a solution of such a problem as well as stability for the corresponding formulation. For that purpose the underlying problem in Equation (3.14) is reformulated into an equivalent mixed variational form: find $(v, w) \in V \times W$ such that

$$\begin{aligned} a(v, \widetilde{v}) + b(\widetilde{v}, w) &= F_v(\widetilde{v}) \quad \forall\, \widetilde{v} \in V \\ b(v, \widetilde{w}) &= F_w(\widetilde{w}) \quad \forall\, \widetilde{w} \in W \end{aligned} \tag{3.15}$$

with V and W being suitable Hilbert spaces, $F_v(\widetilde{v})$ and $F_w(\widetilde{w})$ linear forms and $a(\bullet, \bullet)$ and $b(\bullet, \bullet)$ bilinear forms. It can be recognized by the structure of the system of Equations (3.15), that the variable w incorporates the role of a Lagrange multiplier. Therefore, in the following the variables associated to v are denoted as the *primary variables* whereas variables associated to w are denoted as *constraining variables*. The first requirement, in order to show existence and uniqueness of the solution of problem (3.15), is the boundedness of both bilinear forms $a(\bullet, \bullet)$ and $b(\bullet, \bullet)$, which demands the existence of the strictly positive constants $c_{a,2} > 0$ and $c_{b,2} > 0$ such that

$$\begin{aligned} |a(v, \widetilde{v})| &\leq c_{a,2} \|v\|_V \|\widetilde{v}\|_V \quad \forall\, v, \widetilde{v} \in V\,, \\ |b(v, \widetilde{w})| &\leq c_{b,2} \|v\|_V \|\widetilde{w}\|_W \quad \forall\, v \in V,\, \widetilde{w} \in W\,. \end{aligned} \tag{3.16}$$

Considering in the following the case of $F_w(\widetilde{w}) = 0$, which is the significant case since the problem can always be reduced into this form (as shown e.g. in Brenner and Scott [1994]), then v in problem (3.15) is determined by: find $v \in Z$ such that

$$a(v, \widetilde{v}) = F_v(\widetilde{v}) \quad \forall\, \widetilde{v} \in Z\,, \tag{3.17}$$

whereas Z represents the so-called kernel space of V defined as

$$Z := \{\widetilde{v} \in V :\, b(\widetilde{v}, \widetilde{w}) = 0 \quad \forall\, \widetilde{w} \in W\}. \tag{3.18}$$

Following the theorem of Lax-Milgram the problem (3.17) is well posed (i.e. there exists a unique solution for $v \in Z$) if $a(\bullet, \bullet)$ is coercive on Z. This means, there exists a positive constant $c_{a,1} > 0$ such that

$$a(\widetilde{v}, \widetilde{v}) \geq c_{a,1} \|\widetilde{v}\|_V^2 \quad \forall\, \widetilde{v} \in Z. \tag{3.19}$$

With the satisfaction of the requirements of Equations $(3.16)_1$ and (3.19) v is well posed and w in problem (3.15) is determined by: find $w \in W$ such that

$$b(\widetilde{v}, w) = F_v(\widetilde{v}) - a(v, \widetilde{v}) \quad \forall\, \widetilde{v} \in V\,. \tag{3.20}$$

It can be shown, that existence and uniqueness of $w \in W$ is ensured if there exists a positive constant $c_{b,1} > 0$ such that

$$\sup_{\widetilde{v} \in V} \frac{|b(\widetilde{v}, \widetilde{w})|}{\|\widetilde{v}\|_V} \geq c_{b,1} \|\widetilde{w}\| \quad \forall\, \widetilde{w} \in W\,. \tag{3.21}$$

This condition is in the literature often referred as the Ladyzhenskaya-Babuska-Brezzi (LBB) or inf-sup condition (since it can be expressed in an equivalent inf-sup form) and has been introduced independently by Ladyzhenskaya [1969], Babuška [1973] and Brezzi [1974]. Summarizing, it has been shown that a mixed variational problem of the form of (3.15) is well posed if the following conditions are satisfied:

- the bilinear forms $a(\bullet, \bullet)$ and $b(\bullet, \bullet)$ are bounded, Equation (3.16)
- the bilinear form $a(\bullet, \bullet)$ is coercive on the kernel of $b(\bullet, \bullet)$, Equation (3.19)
- the inf-sup condition holds, Equation (3.21)

These three conditions are the result of Brezzi's theorem (Brezzi and Fortin [1991], Theorem 1.1) for mixed variational problems and therefore are denoted in the following as *Brezzi's conditions*.

4 Isotropic Linear Elasticity

The goal of the present thesis is the construction and investigation of finite element formulations, suitable for the large deformation case. However, a prior investigation of the elements in the linearized framework enables the opportunity to evolve a deep insight into the characteristics of the formulations using the knowledge of functional analysis. In this chapter, first the linearized problem of elasticity is presented followed by the introduction of suitable primal and mixed variational formulations. The considered variational treatments, which constitute the basis for the subsequent finite element discretizations in the following Chapter 5, are investigated by means of the previously introduced abstract variational formulations in Chapter 3.2 and 3.3. In order to avoid a non-necessarily increase of the notational formalism, we focus on the special case of isotropy.

4.1 Linearization of the Elasticity Problem

In the theory of linearized elasticity infinitesimal deformations and rotations are assumed, which simplifies the underlying continuum mechanical equations significantly. It is assumed that the displacements and also its gradient are small, i.e., $\|\boldsymbol{u}\| \ll 1$ and $\|\nabla \boldsymbol{u}\| \ll 1$. Due to this simplification a distinction between reference and current configuration is not necessary and thus the body of interest is denoted by $\mathcal{B}$. The linearized strain tensor $\boldsymbol{\varepsilon}$, which measures the strain in the theory of linear elasticity, is obtained by the Gateaux-derivative of the Green-Lagrange strain tensor evaluated at the reference configuration

$$\boldsymbol{\varepsilon} := \mathrm{Lin}\boldsymbol{E} = \boldsymbol{E}|_{\boldsymbol{X}} + \frac{\mathrm{d}}{\mathrm{d}\epsilon}[\boldsymbol{E}(\boldsymbol{X} + \epsilon \boldsymbol{u})]|_{\epsilon=0} = \frac{1}{2}\left(\nabla \boldsymbol{u} + (\nabla \boldsymbol{u})^T\right) =: \nabla^s \boldsymbol{u}. \tag{4.1}$$

Furthermore, it can be shown that the linearization at a stress free reference configuration lead to the relations

$$\mathrm{Lin}\boldsymbol{\sigma} = \mathrm{Lin}\boldsymbol{P} = \mathrm{Lin}\boldsymbol{S}\,, \tag{4.2}$$

whereas the notation of $\boldsymbol{\sigma}$ as the linear elastic stress measure has been established in the literature. The second assumption is a linear relation between stresses and strains, represented in case of isotropic material by the well known Hooke's law

$$\boldsymbol{\sigma} = 2\mu\,\boldsymbol{\varepsilon} + \Lambda(\mathrm{tr}\,\boldsymbol{\varepsilon})\,\boldsymbol{I} = \mathbb{C} : \boldsymbol{\varepsilon}\,, \tag{4.3}$$

whereas $\mathbb{C}$ is the fourth order elasticity tensor

$$\mathbb{C} := \Lambda\,\boldsymbol{I} \otimes \boldsymbol{I} + 2\mu\,\mathbb{I} \qquad \text{with} \qquad \mathbb{I}_{ijkl} := \frac{1}{2}(\delta_{ik}\delta_{jl} + \delta_{il}\delta_{jk}) \tag{4.4}$$

and δ as the Kronecker delta. The complete boundary value problem for linear elasticity is given by: find $\boldsymbol{u}$, $\boldsymbol{\varepsilon}$, $\boldsymbol{\sigma}$ such that

$$\begin{aligned} \operatorname{Div}\boldsymbol{\sigma} + \boldsymbol{f} &= \boldsymbol{0} && \text{on } \mathcal{B}, \\ \boldsymbol{\sigma} &= \mathbb{C} : \boldsymbol{\varepsilon} && \text{on } \mathcal{B}, \\ \boldsymbol{\varepsilon} &= \nabla_s \boldsymbol{u} && \text{on } \mathcal{B}, \\ \boldsymbol{\sigma} &= \boldsymbol{\sigma}^T && \text{on } \mathcal{B}, \\ \boldsymbol{\sigma}\boldsymbol{n} &= \bar{\boldsymbol{t}}_0 && \text{on } \partial\mathcal{B}_\sigma, \\ \boldsymbol{u} &= \overline{\boldsymbol{u}} && \text{on } \partial\mathcal{B}_u, \end{aligned} \tag{4.5}$$

which are the balance of linear momentum, constitutive equation, compatibility equation, balance of angular momentum and boundary conditions, respectively. In the following, several variational treatments for the problem of linear elasticity are introduced and investigated based on the abstract variational problems discussed in Chapters 3.2 and 3.3. Since it can be shown that any problem with inhomogeneous Dirichlet boundary conditions can be converted into a problem with homogeneous Dirichlet boundary conditions by a homogenization, only the case of homogeneous Dirichlet boundary conditions is considered without loss of generality. This has the advantage that the same function space for test and solution functions can be used, which reduces the necessary amount of formalism.

4.2 Pure Displacement Formulation

Considering the boundary value problem for linear elastostatics in Equation (4.5) we may insert the compatibility and constitutive condition into the balance of linear momentum. In this case the balance of angular momentum is a priori fulfilled due to the constitutive condition and the inherent symmetry of the strain tensor. This leads to a formulation where the displacements remain as the sole unknown field and the boundary value problem reduces to: find $\boldsymbol{u}$ such that

$$\begin{aligned} \operatorname{Div}[\mathbb{C} : \boldsymbol{\varepsilon}(\boldsymbol{u})] + \boldsymbol{f} &= \boldsymbol{0} && \text{on } \mathcal{B}, \\ (\mathbb{C} : \boldsymbol{\varepsilon}(\boldsymbol{u}))\,\boldsymbol{n} &= \bar{\boldsymbol{t}}_0 && \text{on } \partial\mathcal{B}_\sigma, \\ \boldsymbol{u} &= \boldsymbol{0} && \text{on } \partial\mathcal{B}_u, \end{aligned} \tag{4.6}$$

where $\boldsymbol{\varepsilon}(\bullet) = \nabla^s(\bullet)$ represents the symmetric gradient operator. In order to be able to solve this problem with aid of a variational approach the boundary condition for the displacements $(4.6)_3$ have to be fulfilled by a suitable restriction of the solution space (in the sense of an essential boundary condition). In contrast, the traction boundary condition $(4.6)_2$ will appear as a natural condition directly in the resulting weak form. Multiplication of the balance of linear momentum with a test function $\delta\boldsymbol{u}$ and integration over the domain $\mathcal{B}$ leads to the problem: find $\boldsymbol{u} \in [\mathcal{H}_0^2(\mathcal{B})]^3$ such that

$$\int_{\mathcal{B}} \operatorname{Div}[\mathbb{C} : \boldsymbol{\varepsilon}(\boldsymbol{u})] \cdot \delta\boldsymbol{u}\,\mathrm{d}V = -\int_{\mathcal{B}} \delta\boldsymbol{u} \cdot \boldsymbol{f}\mathrm{d}V \qquad \forall\, \delta\boldsymbol{u} \in [\mathcal{L}_0^2(\mathcal{B})]^3. \tag{4.7}$$

The divergence theorem and integration by parts are utilized, such that the order of the derivatives on the displacements and the corresponding test function are balanced and the traction boundary condition can be incorporated naturally. This yields the weak form: find $\boldsymbol{u} \in [\mathcal{H}_0^1(\mathcal{B})]^3$ such that

$$\int_{\mathcal{B}} (\boldsymbol{\varepsilon}(\boldsymbol{u}) : \mathbb{C} : \boldsymbol{\varepsilon}(\delta\boldsymbol{u}))\,\mathrm{d}V = \int_{\partial\mathcal{B}} \boldsymbol{t}_0 \cdot \delta\boldsymbol{u}\,\mathrm{d}A + \int_{\mathcal{B}} \boldsymbol{f} \cdot \delta\boldsymbol{u}\mathrm{d}V \qquad \forall\, \delta\boldsymbol{u} \in [\mathcal{H}_0^1(\mathcal{B})]^3\,. \tag{4.8}$$

In a next step the boundary integral is decomposed into the displacement and traction part and the traction boundary conditions $(4.6)_2$ are inserted. Therein we make use of the compatibility condition of the test function $\delta\boldsymbol{u} = \boldsymbol{0}$ on $\partial\mathcal{B}_u\, \forall\, \delta\boldsymbol{u} \in [\mathcal{H}_0^1(\mathcal{B})]^3$. This leads to the final weak form G of the pure displacement based linear elasticity problem as: find $\boldsymbol{u} \in [\mathcal{H}_0^1(\mathcal{B})]^3$ such that

$$G := \int_{\mathcal{B}} (\boldsymbol{\varepsilon}(\boldsymbol{u}) : \mathbb{C} : \boldsymbol{\varepsilon}(\delta\boldsymbol{u}))\,\mathrm{d}V - \int_{\partial\mathcal{B}_\sigma} \bar{\boldsymbol{t}}_0 \cdot \delta\boldsymbol{u}\,\mathrm{d}A - \int_{\mathcal{B}} \boldsymbol{f} \cdot \delta\boldsymbol{u}\mathrm{d}V = 0 \qquad \forall\, \delta\boldsymbol{u} \in [\mathcal{H}_0^1(\mathcal{B})]^3\,. \tag{4.9}$$

The solution for the displacements of the weak form is equivalent to the minimizer of the potential energy defined as

$$\Pi^{\mathrm{LE}}(\boldsymbol{u}) = \int_{\mathcal{B}} \psi^{\mathrm{LE}}(\boldsymbol{u})\,\mathrm{d}V + \Pi^{\mathrm{ext}}(\boldsymbol{u}) \qquad \forall\, \boldsymbol{u} \in [\mathcal{H}_0^1(\mathcal{B})]^3\,, \tag{4.10}$$

whereas the strain energy of linear elasticity is given by

$$\psi^{\mathrm{LE}}(\boldsymbol{u}) = \tfrac{1}{2}\,\boldsymbol{\varepsilon}(\boldsymbol{u}) : \mathbb{C} : \boldsymbol{\varepsilon}(\boldsymbol{u}) \tag{4.11}$$

and the definition of the external potential as

$$\Pi^{\mathrm{ext}}(\boldsymbol{u}) = -\int_{\mathcal{B}} \boldsymbol{u} \cdot \boldsymbol{f}\,\mathrm{d}V - \int_{\partial\mathcal{B}_\sigma} \boldsymbol{u} \cdot \bar{\boldsymbol{t}}_0\,\mathrm{d}A. \tag{4.12}$$

The weak form in Equation (4.9) fits into the structure of the abstract primal variational form of Equation (3.12) with $V = [\mathcal{H}_0^1(\mathcal{B})]^3$ and

$$\begin{aligned} a(\boldsymbol{u}, \delta\boldsymbol{u}) &= \int_{\mathcal{B}} \boldsymbol{\varepsilon}(\boldsymbol{u}) : \mathbb{C} : \boldsymbol{\varepsilon}(\delta\boldsymbol{u})\,\mathrm{d}V \text{ and} \\ F(\delta\boldsymbol{u}) &= \int_{\partial\mathcal{B}_\sigma} \bar{\boldsymbol{t}}_0 \cdot \delta\boldsymbol{u}\,\mathrm{d}A + \int_{\mathcal{B}} \boldsymbol{f} \cdot \delta\boldsymbol{u}\,\mathrm{d}V\,. \end{aligned} \tag{4.13}$$

Thus, following the theorem of Lax and Milgram, the analysis on the well posedness of this formulation reduces to the investigation of the inequalities for boundedness and coercivity as discussed in Chapter 3.2. They appear after the application of some mathematical inequalities as

$$\begin{aligned} a(\boldsymbol{u}, \delta\boldsymbol{u}) &\leq \lambda^{\max}(\mathbb{C})\,\|\boldsymbol{u}\|_{\mathcal{H}^1}\,\|\delta\boldsymbol{u}\|_{\mathcal{H}^1} \quad \forall\, \boldsymbol{u}, \delta\boldsymbol{u} \in [\mathcal{H}_0^1(\mathcal{B})]^3\,, \\ a(\delta\boldsymbol{u}, \delta\boldsymbol{u}) &\geq \lambda^{\min}(\mathbb{C})\,c_k\,c_f^{-1}\,\|\delta\boldsymbol{u}\|_{\mathcal{H}^1}^2 \quad \forall\, \delta\boldsymbol{u} \in [\mathcal{H}_0^1(\mathcal{B})]^3\,, \end{aligned} \tag{4.14}$$

where c_k and c_f are positive constants depending on the shape of the considered domain, appearing due to the use of Korn's and Friedrich's inequalities. A detailed analysis of the underlying mathematical steps and the proofs of the used inequalities are found i.a. in

Brenner and Scott [1994]. $\lambda^{\max}(\mathbb{C})$ and $\lambda^{\min}(\mathbb{C})$ denote the maximum and minimum eigenvalues of the elasticity tensor. Taking into account physical meaningful values for the Lamé constants in case of isotropic material, which satisfy

$$\infty > \mu > 0\,, \qquad \Lambda \geq 0\,, \tag{4.15}$$

the minimal and maximal eigenvalues of the constitutive tensor in the three dimensional case are obtained as

$$\lambda^{\max}(\mathbb{C}) = 3\Lambda + 2\mu \quad \text{and} \quad \lambda^{\min}(\mathbb{C}) = \mu\,. \tag{4.16}$$

The well known ill-posedness of the primal displacement method in linear elasticity can be recognized here. Considering the case where Λ tends to be large, the constant in the boundedness inequality $(4.14)_1$ deteriorates. Thus in the framework of incompressibility, which is represented by $\Lambda \to \infty$, existence and uniqueness of the solution cannot be guaranteed. In contrast to Λ the Lamé parameter μ is uncritical, since the length scales of the boundary value problem can always be modified such that the numerical value of μ is in a well posed regime. Nonetheless, the method is well suited for the case of compressible materials assuming a well posed Korn's constant which is the case for domains with non-deteriorated aspect ratios.

4.3 Mixed Variational Formulations

Mixed variational formulations represent suitable approaches in situations where the pure displacement formulation is not well posed, e.g. as previously shown for the framework of incompressibility. In this chapter three different mixed approaches are distinguished. First, the Hellinger-Reissner variational method is investigated. It is constructed as a two field formulation, namely the stresses and displacements and goes back to the work of Hellinger [1913] and Reissner [1950]. This is followed by the introduction of the more general Hu-Washizu method where the strains, displacements and stresses are taken into account as the unknown field quantities. This framework is based on the works of Hu [1955] and Washizu [1955]. In addition the displacement-pressure formulation is considered. This variational form is based on the substitution of the stress part resulting due to volumetric deformation and thus especially suitable for the framework of (nearly) incompressibility.

4.3.1 Hellinger-Reissner Formulation

The associated strong form of the Hellinger-Reissner formulation is obtained by the insertion of the compatibility condition $(4.5)_3$ into to the constitutive Equation $(4.5)_2$ and an ensuing multiplication of the inverted elasticity tensor from the left. This reduces the general boundary value problem for linear elasticity (4.5) into the two-field boundary value

problem as: find $\boldsymbol{\sigma}$, $\boldsymbol{u}$ such that

$$\begin{aligned} &\operatorname{Div}\boldsymbol{\sigma} + \boldsymbol{f} = \boldsymbol{0} && \text{on } \mathcal{B}, \\ &\mathbb{C}^{-1} : \boldsymbol{\sigma} = \boldsymbol{\varepsilon}(\boldsymbol{u}) && \text{on } \mathcal{B}, \\ &\boldsymbol{\sigma} = \boldsymbol{\sigma}^T && \text{on } \mathcal{B}, \\ &\boldsymbol{\sigma}\boldsymbol{n} = \bar{\boldsymbol{t}}_0 && \text{on } \partial\mathcal{B}_\sigma, \\ &\boldsymbol{u} = \boldsymbol{0} && \text{on } \partial\mathcal{B}_u. \end{aligned} \tag{4.17}$$

In contrast to the pure displacement problem, the balance of angular momentum $(4.17)_3$ is not naturally incorporated and has to be additionally taken into account. In the proposed variational approach it is included, similar to the displacement boundary conditions $(4.17)_5$, in form of a direct restriction of the corresponding solution spaces. Note that it is also possible to involve the balance of angular momentum in a variational sense, which would result in an additional weak form. This approach is often applied especially from the mathematical community. The weak forms G_σ and G_u of the Hellinger-Reissner principle follow after the multiplication of $(4.17)_1$ and $(4.17)_2$ with test functions $\delta\boldsymbol{u}$, $\delta\boldsymbol{\sigma}$ and the equivalent mathematical steps as in Chapter 4.2 by: find $\boldsymbol{\sigma} \in [\mathcal{L}^2(\mathcal{B})]^{3\times3}_{\text{sym}}$ and $\boldsymbol{u} \in [\mathcal{H}^1_0(\mathcal{B})]^3$ such that

$$\begin{aligned} G_\sigma &:= \int_{\mathcal{B}} \left(\boldsymbol{\varepsilon}(\boldsymbol{u}) - \mathbb{C}^{-1} : \boldsymbol{\sigma}\right) : \delta\boldsymbol{\sigma} \, \mathrm{d}V = 0 && \forall\, \delta\boldsymbol{\sigma} \in [\mathcal{L}^2(\mathcal{B})]^{3\times3}_{\text{sym}}, \\ G_u &:= \int_{\mathcal{B}} (\boldsymbol{\sigma} : \boldsymbol{\varepsilon}(\delta\boldsymbol{u})) \, \mathrm{d}V - \int_{\partial\mathcal{B}_\sigma} \bar{\boldsymbol{t}}_0 \cdot \delta\boldsymbol{u} \, \mathrm{d}A - \int_{\mathcal{B}} \boldsymbol{f} \cdot \delta\boldsymbol{u} \, \mathrm{d}V = 0 && \forall\, \delta\boldsymbol{u} \in [\mathcal{H}^1_0(\mathcal{B})]^3, \end{aligned} \tag{4.18}$$

whereas the space for the stresses is strictly restricted to symmetric second order tensors such that the balance of angular momentum is fulfilled in a strong form. The solution of the weak forms for the stresses and displacements is equivalent to the saddle point for $\boldsymbol{\sigma} \in [\mathcal{L}^2(\mathcal{B})]^{3\times3}_{\text{sym}}$ and $\boldsymbol{u} \in [\mathcal{H}^1_0(\mathcal{B})]^3$ of the Hellinger-Reissner potential

$$\Pi^{\text{HR}}(\boldsymbol{\sigma}, \boldsymbol{u}) = \int_{\mathcal{B}} \left(-\frac{1}{2}\boldsymbol{\sigma} : \mathbb{C}^{-1} : \boldsymbol{\sigma} + \boldsymbol{\sigma} : \boldsymbol{\varepsilon}(\boldsymbol{u}) \right) \mathrm{d}V + \Pi^{\text{ext}}. \tag{4.19}$$

The two weak forms in Equation (4.18) can be embedded into the mixed abstract variational problem of Equation (3.15) with $V = [\mathcal{L}^2(\mathcal{B})]^{3\times3}_{\text{sym}}$, $W = [\mathcal{H}^1_0(\mathcal{B})]^3$ and

$$\begin{aligned} a(\boldsymbol{\sigma}, \delta\boldsymbol{\sigma}) &:= \int_{\mathcal{B}} \boldsymbol{\sigma} : \mathbb{C}^{-1} : \delta\boldsymbol{\sigma} \, \mathrm{d}V, \\ b(\delta\boldsymbol{\sigma}, \boldsymbol{u}) &:= -\int_{\mathcal{B}} \delta\boldsymbol{\sigma} : \boldsymbol{\varepsilon}(\boldsymbol{u}) \, \mathrm{d}V, \\ F_v(\delta\boldsymbol{\sigma}) &:= 0, \\ b(\boldsymbol{\sigma}, \delta\boldsymbol{u}) &:= -\int_{\mathcal{B}} \boldsymbol{\sigma} : \boldsymbol{\varepsilon}(\delta\boldsymbol{u}) \, \mathrm{d}V, \\ F_w(\delta\boldsymbol{u}) &:= -\int_{\partial\mathcal{B}_t} \bar{\boldsymbol{t}}_0 \cdot \delta\boldsymbol{u} \, \mathrm{d}A - \int_{\mathcal{B}} \boldsymbol{f} \cdot \delta\boldsymbol{u} \, \mathrm{d}V. \end{aligned} \tag{4.20}$$

In this format it can be recognized that the stresses appear as the primary variable in the Hellinger-Reissner framework and the displacements take the role of the constraining variable. Well posedness of the problem can be shown by *Brezzi's conditions* as discussed in Chapter 3.2. Boundedness of the bilinear forms follows trivially as

$$\begin{aligned} |a(\boldsymbol{\sigma}, \delta\boldsymbol{\sigma})| &\leq \lambda^{\max}(\mathbb{C}^{-1}) \, \|\boldsymbol{\sigma}\|_{\mathcal{L}^2} \, \|\delta\boldsymbol{\sigma}\|_{\mathcal{L}^2} \quad \forall \, \boldsymbol{\sigma}, \delta\boldsymbol{\sigma} \in [\mathcal{L}^2(\mathcal{B})]^{3\times 3}_{\mathrm{sym}} \,, \\ |b(\delta\boldsymbol{\sigma}, \delta\boldsymbol{u})| &\leq \|\delta\boldsymbol{\sigma}\|_{\mathcal{L}^2} \|\delta\boldsymbol{u}\|_{\mathcal{H}^1} \qquad\qquad \forall \, \delta\boldsymbol{\sigma}, \delta\boldsymbol{u} \in [\mathcal{L}^2(\mathcal{B})]^{3\times 3}_{\mathrm{sym}} \times [\mathcal{H}^1_0(\mathcal{B})]^3 \,. \end{aligned} \tag{4.21}$$

The maximal eigenvalue of the complementary constitutive tensor $\mathbb{C}^{-1}$ follows by $\lambda^{\max}(\mathbb{C}^{-1}) = \frac{1}{\mu}$, which is again uncritical due to the length scale scalability of μ. For a reasonable small Lamé parameter Λ coercivity of $a(\delta\boldsymbol{\sigma}, \delta\boldsymbol{\sigma})$ on the kernel of $b(\delta\boldsymbol{\sigma}, \delta\boldsymbol{u})$ is automatically involved by the coercivity on the complete space of $\mathcal{H}^1_0(\mathcal{B})^3$ as shown by

$$a(\delta\boldsymbol{\sigma}, \delta\boldsymbol{\sigma}) \geq \lambda^{\min}(\mathbb{C}^{-1}) \, \|\delta\boldsymbol{\sigma}\|^2_{\mathcal{L}^2} \quad \forall \, \delta\boldsymbol{\sigma} \in [\mathcal{L}^2(\mathcal{B})]^{3\times 3}_{\mathrm{sym}} \,, \tag{4.22}$$

with $\lambda^{\min}(\mathbb{C}^{-1}) = \frac{1}{3\Lambda+2\mu}$. But for $\Lambda \to \infty$ the complete coercivity of $a(\delta\boldsymbol{\sigma}, \delta\boldsymbol{\sigma})$ is lost. However it is possible to show, see e.g. Yu et al. [2011], that coercivity on the kernel still holds in the incompressible limit. For the proof of the inf-sup stability of the problem, we make use of the fact that the supremum of a function in the $\mathcal{L}^2(\mathcal{B})$ space is always greater or equal than any gradient of a function in the $\mathcal{H}^1(\mathcal{B})$ space, since the we have $\mathcal{L}^2(\mathcal{B}) \supseteq \mathcal{H}^1(\mathcal{B})$. Thus the constant of the inf-sup condition is clearly bounded from below by the inequality

$$\sup_{\delta\boldsymbol{\sigma}\in\mathcal{L}^2} \frac{\int_{\mathcal{B}} \delta\boldsymbol{\sigma} : \boldsymbol{\varepsilon}(\delta\boldsymbol{u}) \, \mathrm{d}V}{\|\delta\boldsymbol{\sigma}\|_{\mathcal{L}^2}} \geq \frac{\int_{\mathcal{B}} \boldsymbol{\varepsilon}(\delta\boldsymbol{u}) : \boldsymbol{\varepsilon}(\delta\boldsymbol{u}) \, \mathrm{d}V}{\|\boldsymbol{\varepsilon}(\delta\boldsymbol{u})\|_{\mathcal{L}^2}} = \|\boldsymbol{\varepsilon}(\delta\boldsymbol{u})\|_{\mathcal{L}^2} \geq c_f^{-1} c_k \|\delta\boldsymbol{u}\| \ldots$$
$$\ldots \forall \, \delta\boldsymbol{u} \in [\mathcal{H}^1_0(\mathcal{B})]^3 \,, \tag{4.23}$$

where c_k and c_f are again the constants following from the Korn and Friedrich inequalities. It can be summarized, that this variational approach is well suited for the whole range of isotropic materials, including the incompressible limit.

In the prior formulation, the derivatives have been applied to the displacements in form of a symmetric gradient. This approach is in the literature often denoted as the primal Hellinger-Reissner formulation. It is possible to construct an alternative variational approach based on the strong from (4.17), which is denoted as the dual Hellinger-Reissner formulation. Therein the derivatives are applied to the stresses in form of a divergence, using integration by parts for the term related to the balance of linear momentum. This leads to the weak forms G_σ and G_u as: find $\boldsymbol{\sigma} \in [\mathcal{H}_\sigma(\mathrm{Div}, \mathcal{B})]^3_{\mathrm{sym}}$ and $\boldsymbol{u} \in \mathcal{L}^2(\mathcal{B})^3$ such that:

$$\begin{aligned} G_\sigma &:= \int_{\mathcal{B}} \left(\boldsymbol{\sigma} : \mathbb{C}^{-1} : \delta\boldsymbol{\sigma} + \boldsymbol{u} \cdot \mathrm{Div}[\delta\boldsymbol{\sigma}] \right) \mathrm{d}V - \int_{\partial\mathcal{B}_u} \overline{\boldsymbol{u}} \cdot \delta\boldsymbol{\sigma}\boldsymbol{n} \, \mathrm{d}A = 0 \;\; \forall \, \delta\boldsymbol{\sigma} \in [\mathcal{H}_0(\mathrm{Div}, \mathcal{B})]^3_{\mathrm{sym}} \,, \\ G_u &:= \int_{\mathcal{B}} (\mathrm{Div}\, \boldsymbol{\sigma} + \boldsymbol{f}) \cdot \delta\boldsymbol{u} \, \mathrm{d}V = 0 \qquad\qquad \forall \, \delta\boldsymbol{u} \in [\mathcal{L}^2(\mathcal{B})]^3 \,. \end{aligned} \tag{4.24}$$

It is interesting to note, that in this formulation the Neumann boundary conditions are no longer involved in a natural way. They have to be incorporated by a suitable reduction of the stress space

$$[\mathcal{H}_\sigma(\mathrm{Div}, \mathcal{B})]^3_{\mathrm{sym}} = \{ \boldsymbol{\tau}^{3\times 3} \in [\mathcal{H}(\mathrm{Div}, \mathcal{B}_0)]^3_{\mathrm{sym}} : \boldsymbol{\tau}\boldsymbol{n} = \overline{\boldsymbol{t}}_0 \text{ on } \partial\mathcal{B}_\sigma \} \,. \tag{4.25}$$

In contrast now the Dirichlet conditions are naturally imposed in Equation $(4.24)_1$. The solutions of the weak forms for the displacements and stresses are equivalent to the saddle point for $\boldsymbol{u} \in [\mathcal{L}^2(\mathcal{B})]^3$ and $\boldsymbol{\sigma} \in [\mathcal{H}_\sigma(\mathrm{Div}, \mathcal{B})]^3_{\mathrm{sym}}$ of the modified Hellinger-Reissner functional

$$\Pi^{HR^*}(\boldsymbol{\sigma}, \boldsymbol{u}) = \int_{\mathcal{B}} \left(\frac{1}{2} \boldsymbol{\sigma} : \mathbb{C}^{-1} : \boldsymbol{\sigma} + (\mathrm{Div}\, \boldsymbol{\sigma} + \boldsymbol{f}) \cdot \boldsymbol{u} \right) \mathrm{d}V \,. \tag{4.26}$$

The variational approach can be embedded into the abstract mixed variational problem (3.15) with $V = [\mathcal{H}_0(\mathrm{Div}, \mathcal{B})]^3_{\mathrm{sym}}$, $W := [\mathcal{L}^2(\mathcal{B})]^3$ and

$$\begin{aligned} a(\boldsymbol{\sigma}, \delta\boldsymbol{\sigma}) &= \int_{\mathcal{B}} \boldsymbol{\sigma} : \mathbb{C}^{-1} : \delta\boldsymbol{\sigma} \, \mathrm{d}V \,, \\ b(\delta\boldsymbol{\sigma}, \boldsymbol{u}) &= \int_{\mathcal{B}} \mathrm{Div}[\delta\boldsymbol{\sigma}] \cdot \boldsymbol{u} \, \mathrm{d}V \,, \\ F_v(\delta\boldsymbol{\sigma}) &= \int_{\partial\mathcal{B}_u} \overline{\boldsymbol{u}} \cdot \delta\boldsymbol{\sigma}\boldsymbol{n} \, \mathrm{d}A \,, \\ b(\boldsymbol{\sigma}, \delta\boldsymbol{u}) &= \int_{\mathcal{B}} \mathrm{Div}[\boldsymbol{\sigma}] \cdot \delta\boldsymbol{u} \, \mathrm{d}V \,, \\ F_w(\delta\boldsymbol{u}) &= -\int_{\mathcal{B}} \boldsymbol{f} \cdot \delta\boldsymbol{u} \, \mathrm{d}V \,. \end{aligned} \tag{4.27}$$

As in the primal Hellinger-Reissner type formulation boundedness of the bilinear forms follows trivially by

$$\begin{aligned} |a(\boldsymbol{\sigma}, \delta\boldsymbol{\sigma})| &\leq \lambda^{\max}(\mathbb{C}^{-1}) \, \|\boldsymbol{\sigma}\|_{\mathcal{L}^2} \, \|\delta\boldsymbol{\sigma}\|_{\mathcal{L}^2} \quad \forall\, \boldsymbol{\sigma}, \delta\boldsymbol{\sigma} \in [\mathcal{L}^2(\mathcal{B})]^{3\times 3} \,, \\ |b(\delta\boldsymbol{\sigma}, \delta\boldsymbol{u})| &\leq \|\delta\boldsymbol{\sigma}\|_{\mathcal{H}(\mathrm{Div})} \|\delta\boldsymbol{u}\|_{\mathcal{L}^2} \qquad \forall\, \delta\boldsymbol{\sigma}, \delta\boldsymbol{u} \in [\mathcal{H}_0(\mathrm{Div}, \mathcal{B})]^3_{\mathrm{sym}} \times [\mathcal{L}^2(\mathcal{B})]^3 \,. \end{aligned} \tag{4.28}$$

Coercivity on the kernel and the inf-sup condition are sophisticated and not given in detail for sake of brevity. They can be found in many mathematical textbooks dealing with the finite element method, e.g. Boffi et al. [2013] and Braess [2000]. Following their proofs, it turns out that this formulation also satisfies *Brezzi's conditions* and thus is well posed also in the framework of incompressibility. Note that in case of a pure Dirichlet problem, i.e. $\partial\mathcal{B}_\sigma = \emptyset$, the space of the stresses has to be restricted to

$$\boldsymbol{\sigma} \in V = \left\{ \boldsymbol{\sigma} \in [\mathcal{H}(\mathrm{Div})]^3_{\mathrm{sym}} : \int_{\mathcal{B}} \mathrm{tr}\, \boldsymbol{\sigma} \, \mathrm{d}V = 0 \right\}, \tag{4.29}$$

in order to guarantee uniqueness of the solution.

4.3.2 Hu-Washizu Formulation

The most general variational form is constructed such that all essential variables of the elasticity problem enter the formulation as unknown fields, leading to the boundary value

problem equivalent to (4.5): find $\boldsymbol{u}$, $\boldsymbol{\varepsilon}$, $\boldsymbol{\sigma}$ such that

$$\begin{aligned}
\operatorname{Div}\boldsymbol{\sigma} + \boldsymbol{f} &= \boldsymbol{0} && \text{on } \mathcal{B},\\
\boldsymbol{\sigma} &= \mathbb{C} : \boldsymbol{\varepsilon} && \text{on } \mathcal{B},\\
\boldsymbol{\varepsilon} &= \nabla_s \boldsymbol{u} && \text{on } \mathcal{B},\\
\boldsymbol{\sigma} &= \boldsymbol{\sigma}^T && \text{on } \mathcal{B},\\
\boldsymbol{\sigma}\boldsymbol{n} &= \bar{\boldsymbol{t}}_0 && \text{on } \partial\mathcal{B}_\sigma,\\
\boldsymbol{u} &= \overline{\boldsymbol{u}} && \text{on } \partial\mathcal{B}_u.
\end{aligned} \tag{4.30}$$

The balance of angular momentum $(4.30)_4$ and the displacement boundary conditions $(4.30)_6$ are again incorporated in a strong form by a suitable restriction of the solution spaces for the displacements and stresses. It remains to solve Equations $(4.30)_{1-3,5}$ in a weak sense, which leads after the introduction of suitable test-functions $\delta\boldsymbol{\varepsilon}$, $\delta\boldsymbol{u}$, $\delta\boldsymbol{\sigma}$ and some mathematical transformations to the variational problem: find $(\boldsymbol{\varepsilon}, \boldsymbol{u}) \in [\mathcal{L}^2(\mathcal{B})]^{3\times3}_{\text{sym}} \times [\mathcal{H}^1_0(\mathcal{B})]^3$ and $\boldsymbol{\sigma} \in [\mathcal{L}^2(\mathcal{B})]^{3\times3}_{\text{sym}}$ such that

$$\begin{aligned}
G_\varepsilon &:= \int_{\mathcal{B}} (\mathbb{C} : \boldsymbol{\varepsilon} - \boldsymbol{\sigma}) : \delta\boldsymbol{\varepsilon}\, \mathrm{d}V = 0 && \forall\, \delta\boldsymbol{\varepsilon} \in [\mathcal{L}^2(\mathcal{B})]^{3\times3}_{\text{sym}}\\
G_u &:= \int_{\mathcal{B}} (\boldsymbol{\sigma} : \nabla_s \delta\boldsymbol{u} - \boldsymbol{f}\cdot\delta\boldsymbol{u})\, \mathrm{d}V - \int_{\partial\mathcal{B}_\sigma} \bar{\boldsymbol{t}}_0 \cdot \delta\boldsymbol{u}\, \mathrm{d}A = 0 && \forall\, \delta\boldsymbol{u} \in [\mathcal{H}^1_0(\mathcal{B})]^3\\
G_\sigma &:= \int_{\mathcal{B}} (\nabla_s \boldsymbol{u} - \boldsymbol{\varepsilon}) : \delta\boldsymbol{\sigma}\, \mathrm{d}V = 0 && \forall\, \delta\boldsymbol{\sigma} \in [\mathcal{L}^2(\mathcal{B})]^{3\times3}_{\text{sym}}\,.
\end{aligned} \tag{4.31}$$

An equivalent solution is described by the saddle point of the potential given by

$$\Pi^{HW}(\boldsymbol{u}, \boldsymbol{\varepsilon}, \boldsymbol{\sigma}) = \int_{\mathcal{B}} \left(\frac{1}{2}\boldsymbol{\varepsilon} : \mathbb{C} : \boldsymbol{\varepsilon} - \boldsymbol{\sigma} : (\nabla_s \boldsymbol{u} - \boldsymbol{\varepsilon}) \right) \mathrm{d}V + \Pi^{\text{ext}}\,. \tag{4.32}$$

The weak form can be embedded into the abstract mixed variational problem of Equation (3.15) with $V = ([\mathcal{L}^2(\mathcal{B})]^{3\times3}_{\text{sym}} \times [\mathcal{H}^1_0(\mathcal{B})]^3)$, $W = [\mathcal{L}^2(\mathcal{B})]^{3\times3}_{\text{sym}}$ and

$$\begin{aligned}
a((\boldsymbol{\varepsilon}, \boldsymbol{u}), (\delta\boldsymbol{\varepsilon}, \delta\boldsymbol{u})) &:= \int_{\mathcal{B}} \boldsymbol{\varepsilon} : \mathbb{C} : \delta\boldsymbol{\varepsilon}\ \mathrm{d}V\,,\\
b((\delta\boldsymbol{\varepsilon}, \delta\boldsymbol{u}), \boldsymbol{\sigma}) &:= \int_{\mathcal{B}} (\nabla_s \delta\boldsymbol{u} - \delta\boldsymbol{\varepsilon}) : \boldsymbol{\sigma}\ \mathrm{d}V\,,\\
F_v((\delta\boldsymbol{\varepsilon}, \delta\boldsymbol{u})) &:= \int_{\mathcal{B}} \boldsymbol{f}\cdot\delta\boldsymbol{u}\, \mathrm{d}V - \int_{\partial\mathcal{B}_\sigma} \bar{\boldsymbol{t}}_0 \cdot \delta\boldsymbol{u}\, \mathrm{d}V,\\
b((\boldsymbol{\varepsilon}, \boldsymbol{u}), \delta\boldsymbol{\sigma}) &:= \int_{\mathcal{B}} (\nabla_s \boldsymbol{u} - \boldsymbol{\varepsilon}) : \delta\boldsymbol{\sigma}\ \mathrm{d}V\,,\\
F_w(\delta\boldsymbol{\sigma}) &:= 0.
\end{aligned} \tag{4.33}$$

A proof for the coercivity of $a(\bullet, \bullet)$ on the kernel of $b(\bullet, \bullet)$ and the inf-sup condition can be found in Braess [2000]. Boundedness for the bilinear forms is again trivially, whereas the constants depend on the Lamé parameter Λ. Therefore volumetric locking is expected for formulations based on the Hu-Washizu approach. An extension of the Hu-Washizu variational formulation, which leads to a well posed formulation in the incompressible limit has been proposed by Djoko and Reddy [2006].

4.3.3 Displacement-Pressure Formulation

A basic idea, in order to overcome the ill-posedness of the pure displacement formulation for the incompressible case where $\Lambda \to \infty$ or the nearly incompressible case where $\Lambda \gg \mu$ is a substitution with the pressure like-variable

$$p = \Lambda \operatorname{Div} \boldsymbol{u} \,. \tag{4.34}$$

Following this approach, the stresses appear as a function of the strains and the pressure, such that constitutive relation results into

$$\boldsymbol{\sigma}(\boldsymbol{u}, p) = 2\mu\, \boldsymbol{\varepsilon}(\boldsymbol{u}) + p\, \boldsymbol{I} \,. \tag{4.35}$$

The related strong form of the boundary value boundary value problem for the displacement pressure formulation is given by: find $\boldsymbol{u}$, p such that

$$\begin{aligned} &\operatorname{Div}[2\mu\, \boldsymbol{\varepsilon}(\boldsymbol{u}) + p\, \boldsymbol{I}] + \boldsymbol{f} = \boldsymbol{0} && \text{on } \mathcal{B}, \\ &\operatorname{Div} \boldsymbol{u} - \frac{1}{\Lambda}\, p = 0 && \text{on } \mathcal{B}, \\ &\boldsymbol{\sigma}\boldsymbol{n} = \bar{\boldsymbol{t}}_0 && \text{on } \partial\mathcal{B}_\sigma, \\ &\boldsymbol{u} = \overline{\boldsymbol{u}} && \text{on } \partial\mathcal{B}_u \,. \end{aligned} \tag{4.36}$$

The related weak variational form, constructed with the usual mathematical steps, reads: find $\boldsymbol{u} \in [\mathcal{H}_0^1(\mathcal{B})]^3$ and $p \in \mathcal{L}^2(\mathcal{B})$ such that

$$\begin{aligned} G_u := \int_{\mathcal{B}} (2\mu\, \boldsymbol{\varepsilon}(\boldsymbol{u}) : \boldsymbol{\varepsilon}(\delta\boldsymbol{u}) + p \operatorname{Div}[\delta\boldsymbol{u}])\, \mathrm{d}V \ldots \\ \cdots - \int_{\partial\mathcal{B}_t} \bar{\boldsymbol{t}}_0 \cdot \delta\boldsymbol{u}\, \mathrm{d}A - \int_{\mathcal{B}} \boldsymbol{f} \cdot \delta\boldsymbol{u}\, \mathrm{d}V = 0 \quad \forall\, \delta\boldsymbol{u} \in [\mathcal{H}_0^1(\mathcal{B})]^3 \,, \end{aligned} \tag{4.37}$$

$$G_p := \int_{\mathcal{B}} \left(\operatorname{Div}[\boldsymbol{u}] - \frac{1}{\Lambda}\, p \right) \delta p \, \mathrm{d}V = 0 \qquad \forall\, \delta p \in \mathcal{L}^2(\mathcal{B}) \,.$$

An equivalent solution for $\boldsymbol{u}$ and p are described by the stationary point of the potential

$$\Pi^{\mathrm{DP}}(\boldsymbol{u}, p) = \int_{\mathcal{B}} \left(\mu\, \boldsymbol{\varepsilon}(\boldsymbol{u}) : \boldsymbol{\varepsilon}(\boldsymbol{u}) + \operatorname{Div}[\boldsymbol{u}]\, p - \frac{1}{2\Lambda} p^2 \right) \mathrm{d}V + \Pi^{\mathrm{ext}} \,. \tag{4.38}$$

In the incompressible limit $\frac{1}{\Lambda} = 0$ this formulation fits into the mixed abstract variational problem of Equation (3.15) with $V = [\mathcal{H}_0^1(\mathcal{B})]^3$, $W = \mathcal{L}^2(\mathcal{B})$ and

$$\begin{aligned} a(\boldsymbol{u}, \delta\boldsymbol{u}) &:= \int_{\mathcal{B}} 2\mu\, \boldsymbol{\varepsilon}(\boldsymbol{u}) : \boldsymbol{\varepsilon}(\delta\boldsymbol{u})\, \mathrm{d}V \,, \\ b(\delta\boldsymbol{u}, p) &:= \int_{\mathcal{B}} \operatorname{Div}[\delta\boldsymbol{u}]\, p\, \mathrm{d}V \,, \\ F_v(\delta\boldsymbol{u}) &:= \int_{\partial\mathcal{B}_\sigma} \delta\boldsymbol{u} \cdot \bar{\boldsymbol{t}}_0\, \mathrm{d}A + \int_{\mathcal{B}} \delta\boldsymbol{u} \cdot \boldsymbol{f}\, \mathrm{d}V \,, \\ b(\boldsymbol{u}, \delta p) &:= \int_{\mathcal{B}} \operatorname{Div}[\boldsymbol{u}]\, \delta p\, \mathrm{d}V \,, \\ F_w(\delta p) &:= 0. \end{aligned} \tag{4.39}$$

It is a simple task to show boundedness of $a(\bullet,\bullet)$ and $b(\bullet,\bullet)$ and coercivity of $a(\bullet,\bullet)$ on $[\mathcal{H}_0^1(\mathcal{B})]^3$. It should be mentioned that if instead of Equation (4.34) the hydrostatic pressure $p = -\frac{1}{3}\mathrm{tr}[\mathbb{C} : \boldsymbol{\varepsilon}]$ is introduced as an independent quantity, which is sometimes preferred in the engineering community, then only coercivity on the kernel can be shown. This demands caution in the choice of suitable discrete spaces for displacements and pressure, see Boffi and Stenberg [2017] for additional information. However, in both cases the proof of the inf-sup condition is more involved, but can be found in many mathematical based FEM textbooks, e.g. Boffi et al. [2013] and Braess [2000]. Note that in case of a pure Dirichlet problem, i.e. $\partial\mathcal{B}_\sigma = \emptyset$, the space of the pressure has to be restricted to

$$p \in W = \left\{ p \in \mathcal{L}^2(\mathcal{B}) : \int_{\mathcal{B}} p \, \mathrm{d}V = 0 \right\}, \tag{4.40}$$

in order to guarantee uniqueness of the solution.

5 Finite Element Method for Linear Elasticity

In the following chapter different low order finite element approximations of the previously introduced variational forms for linear elasticity are introduced and investigated. After some preposed comments on the basic concept of the Finite Element Method and the discussion of important equivalences between different approaches, the characteristics of the proposed finite elements based on the pure displacement and mixed variational formulations are discussed. The analysis of the element formulation is in particular of importance since even if the variational formulation is well posed on the continuous level there is by no means any guarantee that the discrete counterpart is also well posed.
This analysis is again carried out by the application of the Lax-Milgram theorem in case of coercive problems or Brezzi's conditions in case of mixed approaches, as discussed in detail in Chapters 3.2 and 3.3. The considered finite element formulations are restricted to the framework of conforming approximations. This signifies the restriction of the discrete approximation spaces to closed subspaces of their continuous counterparts, i.e.

$$\boldsymbol{V}_h \subseteq \boldsymbol{V} \quad \text{for all Hilbert spaces } \boldsymbol{V} \tag{5.1}$$

whereas the subscript h indicates the approximation. In the framework of conforming finite element discretizations, boundedness of the discrete bilinear form follows trivially the result obtained by its continuous counterpart since the considered discrete space is always a strict subspace of its continuous counterpart. The same statement holds for the condition on coercivity because also this condition acts only on a single space. However, this inference is not true for the coercivity condition on the kernel or the inf-sup condition. The problem is related to the point that a discrete kernel space is not, in general, a strict subspace of the continuous kernel space as excelently discussed in Boffi et al. [2013]. Thus, the remaining crucial requirements for the well posedness of the mixed finite elements constitute the discrete complements of conditions (3.19) and (3.21). It can be shown that elements which are well posed result in a quasi optimal convergence. In this sense, optimal implies that the approximation error is proportional to the best possible solution related to the discrete space. This is the famous outcome of Cea's lemma proposed in Cea [1964] and its extension to mixed problems by Brezzi [1974]. In contrast, problems which do not satisfy the mentioned conditions may either lead to singular systems of equations or to non optimal convergence, denoted as locking.

5.1 Triangulation and Finite Element Approximations

The basic idea of the FEM is to calculate an approximative solution of the boundary value problem on a shape-regular triangulation of the considered body $\Omega = \bigcup_e \Omega^e \approx \mathcal{B}$, subdivided into a finite number of elements Ω^e. The unknown field quantities are discretized with the aid of shape functions on each element and globally assembled to a system of algebraic equations. The term shape regularity implies in this framework the exclusion of overlapping elements and hanging nodes. The parameter h is introduced associated to the element size, such that if $h \to 0$, the continuous formulation is recovered. In addition the triangulation is assumed to be quasi-uniform, omitting huge differences of the element size between neighboring elements. A typical element Ω^e is generated in the three dimensional case by an isoparametric mapping from reference elements $\widehat{\Omega}^e$ parameterized in $\boldsymbol{\xi} = \{\xi, \eta, \zeta\}$, whereas the reference element is usually either a unit tetrahedron $\widehat{\Omega}^e = (0,1)^3$

or a hexahedron $\widehat{\Omega}^e = (-1,1)^3$. The unknown field quantities are approximated on the reference element using polynomial based shape functions. For tetrahedra T_k is introduced as the space of polynomials of degree less than or equal to k. In case of hexahedrons Q_k refers to the space of polynomials of degree less than or equal to k in each variable (e.g. Q_1 is the set of trilinear functions). In this work only low order approximation spaces are considered, such that we focus on the polynomials T_1, T_2 and Q_1. The special case of a constant approximation on the reference element is denoted by T_0. In addition, further reduced polynomial spaces are considered, which are combinations of the following polynomial spaces:

$$
\begin{aligned}
Id &:= \operatorname{span}\begin{bmatrix} 1 & 0 & 0 \\ 0 & 1 & 0 \\ 0 & 0 & 1 \end{bmatrix}, \qquad A_0 := \operatorname{span}\begin{bmatrix} \xi & 0 & 0 \\ 0 & \eta & 0 \\ 0 & 0 & \zeta \end{bmatrix}, \\
A_1 &:= \operatorname{span}\begin{bmatrix} \eta & 0 & 0 \\ 0 & \zeta & 0 \\ 0 & 0 & \xi \end{bmatrix}, \qquad A_2 := \operatorname{span}\begin{bmatrix} \zeta & 0 & 0 \\ 0 & \xi & 0 \\ 0 & 0 & \eta \end{bmatrix}, \\
B_0 &:= \operatorname{span}\begin{bmatrix} \eta\zeta & 0 & 0 \\ 0 & \zeta\xi & 0 \\ 0 & 0 & \xi\eta \end{bmatrix}, \quad B_1 := \operatorname{span}\begin{bmatrix} \zeta\xi & 0 & 0 \\ 0 & \xi\eta & 0 \\ 0 & 0 & \eta\zeta \end{bmatrix}, \\
B_2 &:= \operatorname{span}\begin{bmatrix} \xi\eta & 0 & 0 \\ 0 & \eta\zeta & 0 \\ 0 & 0 & \zeta\xi \end{bmatrix}, \quad C := \operatorname{span}\begin{bmatrix} \xi\eta\zeta & 0 & 0 \\ 0 & \xi\eta\zeta & 0 \\ 0 & 0 & \xi\eta\zeta \end{bmatrix}, \\
D &:= \operatorname{span}\begin{bmatrix} \xi^2 & 0 & 0 & \eta^2 & 0 & 0 & \zeta^2 & 0 & 0 \\ 0 & \xi^2 & 0 & 0 & \eta^2 & 0 & 0 & \zeta^2 & 0 \\ 0 & 0 & \xi^2 & 0 & 0 & \eta^2 & 0 & 0 & \zeta^2 \end{bmatrix}.
\end{aligned}
\tag{5.2}
$$

It is worthwhile to mention that the prior introduced polynomial spaces can be simply constructed by direct sums of these spaces as

$$
\begin{aligned}
T_0 &:= Id \\
T_1 &:= Id \oplus A_0 \oplus A_1 \oplus A_2 \\
T_2 &:= Id \oplus A_0 \oplus A_1 \oplus A_2 \oplus B_0 \oplus B_1 \oplus B_2 \oplus D \\
Q_1 &:= Id \oplus A_0 \oplus A_1 \oplus A_2 \oplus B_0 \oplus B_1 \oplus B_2 \oplus C\,.
\end{aligned}
\tag{5.3}
$$

5.2 Limitation Principles and Equivalence of Mixed Finite Elements

The construction of stable mixed finite elements is nontrivial. The discrete counterparts of Brezzi's conditions determine conclusively the well posedness of the element formulation, but their analytical proof is in most cases quite complex. An engineering motivated guideline for the construction of mixed elements is given by the concepts of limitation principles, the count condition and the equivalence of mixed finite elements, which is discussed in the following. However it should always kept in mind, that these principles do

not constitute sufficient conditions for the construction of well posed element formulations. Their results can be interpreted as necessary conditions which already decrease the possible combinations of suitable discretization spaces.

5.2.1 Principle of Limitation

A simple increase of the polynomial order for the approximation of the stresses seems to be a promising approach for enhancement of the stress accuracy in mixed methods in a first glance. However, it can be shown that such an approach is in most cases not expedient, which is related to the *limitation principle*. The pioneering discovery that primal finite elements have equivalent mixed element complements has been made by Fraeijs de Veubeke [1965]. Such an equivalence occurs whenever the additional introduced variable is capable of reproducing precisely the same approximation as its associated variable in the non-mixed formulation. In particular, he has shown that, Hellinger-Reissner based elements which are able to reproduce the same approximation of displacements and stresses as a displacement based element, lead in fact always to equivalent results as the corresponding displacement based approach. In detail, denoting the discrete space of the displacements V_h^{D} in the non-mixed formulation and V_h^{HR} in the Hellinger-Reissner formulation and Σ_h^{HR} the corresponding stress space, both formulations are equivalent if

$$V_h^{\mathrm{HR}} = V_h^{\mathrm{D}} \quad \text{and} \quad \Sigma_h^{\mathrm{HR}} \supseteq \Sigma(V_h^{\mathrm{D}})\,, \tag{5.4}$$

whereas $\Sigma(V_h^{\mathrm{D}})$ is the associated stress space in the displacement based formulation. Stolarski and Belytschko [1987] have extended the *limitation principle* to mixed finite elements based on the Hu-Washizu variational formulation. According to that, the Hu-Washizu based element is equivalent to a Hellinger-Reissner based element if

$$V_h^{\mathrm{HW}} = V_h^{\mathrm{HR}}\,, \quad \Sigma_h^{\mathrm{HW}} = \Sigma_h^{\mathrm{HR}} \quad \text{and} \quad \mathcal{E}_h^{\mathrm{HW}} \supseteq \mathcal{E}(\Sigma_h^{\mathrm{HR}})\,, \tag{5.5}$$

whereas V_h^{HW}, Σ_h^{HW} and $\mathcal{E}_h^{HW}$ denote the discrete spaces of the displacements, stresses and strains of the Hu-Washizu based element.

5.2.2 Count Condition

The priori discussed *principle of limitations* restricts the extension of the discrete spaces of the additional field variables. On the other side, these spaces can also not be arbitrarily reduced. From an algebraic point of view, it has to be ensured that for each patch of elements, including all possible sets of boundary conditions, the number of unknowns according to the primary variable has to be greater or equal to the number of unknowns according to the constraining variable. In case of the Hellinger-Reissner based elements this means that number of degrees of freedom related to the stresses (denoted as n_σ) has to be greater or equal to the number of unknowns related to the displacement (n_u), i.e.

$$n_\sigma \geq n_u\,. \tag{5.6}$$

This statement, known as the *count condition*, goes back to the work of Zienkiewicz et al. [1986] and a contradiction leads to a singular system matrix. In this framework, the *count condition* has been extended to Hu-Washizu formulations by

$$n_\epsilon + n_u \geq n_\sigma \quad \text{and} \quad n_\sigma \geq n_u\,, \tag{5.7}$$

where n_ϵ denotes the number of degrees of freedom associated to the strains.

Even if the limitation principles and the count conditions seem to be quite non-restrictive in first glance, they highly reduce the possible combinations of suitable discrete spaces. For example it is not trivial to construct finite elements which are based on the Hu-Washizu variational framework and are not equivalent to Hellinger-Reissner or displacement based elements. In addition, especially for tetrahedral elements, the construction of novel elements based on the primal Hellinger-Reissner formulation is sophisticated. A possible approach is discussed in Chapter 5.4.2. In contrast, the trilinear term in the approximation of hexahedral shaped elements leads to some flexibility in the construction resulting in the family of assumed stress and enhanced assumed strain finite elements.

5.2.3 Equivalence of Enhanced Assumed Strains and Assumed Stresses

It has been shown by the *principle of limitation* that Hu-Washizu based formulations and Hellinger-Reissner based formulation may lead to equivalent elements. The family of enhanced assumed strains, which can be attributed to the pioneering works of Simo and Rifai [1990] and Pantuso and Bathe [1995], represents a special case of Hu-Washizu based elements. This family of elements has an equivalent counterpart based on the primal Hellinger-Reissner framework, denoted as assumed stress elements. The equivalence between both families has been observed first by Andelfinger and Ramm [1993] and later analyzed by Yeo and Lee [1996], Bischoff et al. [1999] and Djoko et al. [2006]. Therein, it has been shown that if the following three conditions are fulfilled the corresponding enhanced assumed strain and the assumed stress element formulations are equivalent

$$\begin{aligned} &\text{Condition 1:} && \Sigma_h^{\mathrm{HR}} \cap \widehat{E}_h^{\mathrm{EAS}} = \emptyset \\ &\text{Condition 2:} && \Sigma(V_h^{\mathrm{D}}) \subseteq \Sigma_h^{\mathrm{HR}} \oplus \widehat{E}_h^{\mathrm{EAS}} \\ &\text{Condition 3:} && \text{a piecewise constant Jacobian,} \end{aligned} \tag{5.8}$$

whereas $\widehat{E}_h^{\mathrm{EAS}}$ denotes the discrete space of the enhanced strain field. It should be noted that a violation of the third conditions still leads to a socalled *weak* equivalence.

5.3 Pure Displacement Finite Elements

In case of the pure displacement formulation a conforming finite dimensional subspace $U_h \subset [\mathcal{H}_0^1(\Omega)]^3$ is chosen and an approximate solution $\boldsymbol{u}_h \in U_h$ is computed by

$$a(\boldsymbol{u}_h, \delta\boldsymbol{u}_h) = F(\delta\boldsymbol{u}_h) \quad \forall\, \delta\boldsymbol{u}_h \in U_h\,, \tag{5.9}$$

where $a(\bullet,\bullet)$ and $F(\bullet)$ are the discrete counterparts of Equation (4.13) such that

$$\begin{aligned} a(\boldsymbol{u}_h, \delta\boldsymbol{u}_h) &= \int_\Omega \boldsymbol{\varepsilon}(\boldsymbol{u}_h) : \mathbb{C} : \boldsymbol{\varepsilon}(\delta\boldsymbol{u}_h)\ \mathrm{d}V \text{ and} \\ F(\delta\boldsymbol{u}_h) &= \int_{\partial\Omega_\sigma} \bar{\boldsymbol{t}}_0 \cdot \delta\boldsymbol{u}_h\ \mathrm{d}A + \int_\Omega \boldsymbol{f} \cdot \delta\boldsymbol{u}_h\ \mathrm{d}V\,. \end{aligned} \tag{5.10}$$

Suitable finite dimensional subspaces are given by globally C^0-continuous functions which are polynomials on the reference element $\widehat{\Omega}^e$

$$U_h := \{\boldsymbol{u}_h \in [\mathcal{H}_0^1(\Omega)]^3,\ \boldsymbol{u}_h \text{ cont. on } \Omega, \boldsymbol{u}_h|_{\widehat{\Omega}^e} \in P_k \,\forall\, \Omega^e \in \Omega\}\,, \tag{5.11}$$

whereas P_k corresponds to T_k in case of tetrahedral shaped elements or Q_k in case of hexahedral shaped elements and are explicitly given in Equation (5.3). It is clear that, due to the isoparametric mapping from the reference element to the element in the physical space, $\boldsymbol{u}_h$ is only a piecewise polynomial function on Ω^e if the mapping from $\widehat{\Omega}^e$ to Ω^e is affine. Due to the conforming discretization scheme the Lax-Milgram theorem leads for the discrete problem to the same statements as for the continuous problem. The constant for the boundedness condition depends on Λ, such that the formulation is only well posed if the material is in the compressible regime. In case of (nearly) incompressibility volumetric locking is expected and the limit case of perfect incompressibility is excluded from the formulation, see e.g. Bathe [1996] for detailed analysis.

5.3.1 Finite Elements for Tetrahedral

In case of tetrahedral shaped elements, the displacements on the reference tetrahedron $\widehat{\Omega}^e$ are approximated by the polynomial space of order k for each element $\Omega^e \in \Omega$. The corresponding finite dimensional subspace U_h is defined as

$$U_h := \{\boldsymbol{u}_h \in [\mathcal{H}_0^1(\Omega)]^3,\ \boldsymbol{u}_h \text{ cont. on } \Omega : \boldsymbol{u}_h|_{\widehat{\Omega}^e} \in T_k \,\forall\, \Omega^e \in \Omega\}\,. \tag{5.12}$$

In order to be able to adopt the *principle of limitation*, the corresponding spaces for the related discrete strains and stresses are explicitly needed. In case of tetrahedral shaped finite element those spaces follow trivially by

$$\boldsymbol{\varepsilon}(U_h) := \left\{u_h \in U_h;\ \boldsymbol{\varepsilon}(\boldsymbol{u}_h)|_{\widehat{\Omega}^e} \in [T_{k-1}]^3 \,\forall\, \Omega^e \in \Omega\right\} \tag{5.13}$$

for the space of strains and equivalently for the space of stresses as

$$\Sigma(U_h) := \left\{u_h \in U_h;\ \boldsymbol{\sigma}(\boldsymbol{u}_h)|_{\widehat{\Omega}^e} \in [T_{k-1}]^3 \,\forall\, \Omega^e \in \Omega\right\}\,. \tag{5.14}$$

The corresponding finite elements are denoted as T_1 and T_2 and depicted in Figure 5.1.

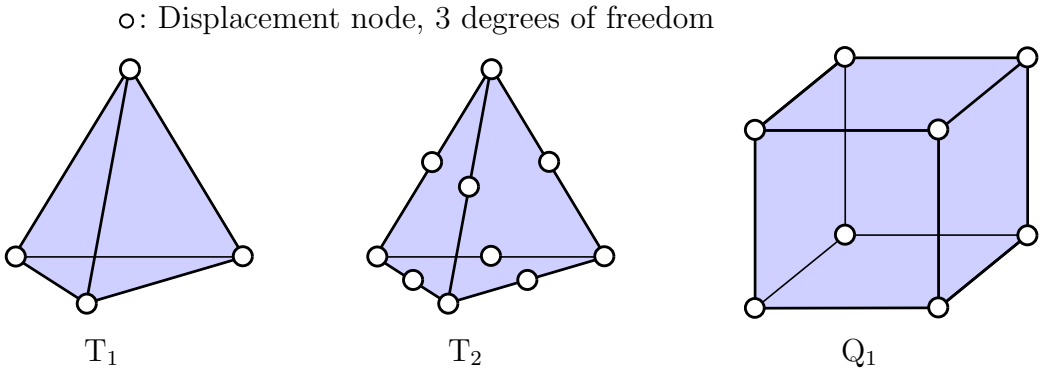

Figure 5.1: Sketch of the T_1, T_2 and Q_1 displacement based elements.

5.3.2 Finite Elements for Hexahedral

The finite dimensional subspace for the displacements of hexahedral shaped elements with a trilinear interpolation on the reference element is defined as

$$U_h := \{\boldsymbol{u}_h \in [\mathcal{H}_0^1(\Omega)]^3,\ \boldsymbol{u}_h \text{ cont. on } \Omega : \boldsymbol{u}_h|_{\widehat{\Omega}^e} \in Q_1 \,\forall\, \Omega^e \in \Omega\}\,. \tag{5.15}$$

In contrast to the tetrahedral elements, the space of the strain and stress tensor is not trivial due to the trilinear term of Q_1. The space of the strains follows by

$$\begin{aligned}\boldsymbol{\varepsilon}(U_h) := \Bigg\{ \boldsymbol{u}_h \in U_h;\ & \begin{pmatrix} \varepsilon(\boldsymbol{u}_h)_{11} \\ \varepsilon(\boldsymbol{u}_h)_{22} \\ \varepsilon(\boldsymbol{u}_h)_{33} \end{pmatrix} \Bigg|_{\widehat{\Omega}^e} \in Id \oplus A_1 \oplus A_2 \oplus B_0 \,\forall\, \Omega^e \in \Omega,\ \ldots \\ & \ldots \begin{pmatrix} \varepsilon(\boldsymbol{u}_h)_{23} \\ \varepsilon(\boldsymbol{u}_h)_{13} \\ \varepsilon(\boldsymbol{u}_h)_{12} \end{pmatrix} \Bigg|_{\widehat{\Omega}^e} \in Id \oplus A_0 \oplus A_1 \oplus A_2 \oplus B_1 \oplus B_2 \,\forall\, \Omega^e \in \Omega \Bigg\}. \end{aligned} \tag{5.16}$$

and the space of the stresses follows due to the assumption of isotropic elasticity as

$$\begin{aligned}\boldsymbol{\Sigma}(U_h) := \Bigg\{ & \boldsymbol{u}_h \in U_h; \ldots \\ & \ldots \begin{pmatrix} \sigma(\boldsymbol{u}_h)_{11} \\ \sigma(\boldsymbol{u}_h)_{22} \\ \sigma(\boldsymbol{u}_h)_{33} \end{pmatrix} \Bigg|_{\widehat{\Omega}^e} \in Id \oplus A_0 \oplus A_1 \oplus A_2 \oplus B_0 \oplus B_1 \oplus B_2 \,\forall\, \Omega^e \in \Omega, \ldots \\ & \ldots \begin{pmatrix} \sigma(\boldsymbol{u}_h)_{23} \\ \sigma(\boldsymbol{u}_h)_{13} \\ \sigma(\boldsymbol{u}_h)_{12} \end{pmatrix} \Bigg|_{\widehat{\Omega}^e} \in Id \oplus A_0 \oplus A_1 \oplus A_2 \oplus B_1 \oplus B_2 \,\forall\, \Omega^e \in \Omega \Bigg\}. \end{aligned} \tag{5.17}$$

The corresponding finite element is denoted as Q_1 and depicted in Figure 5.1,.

Implementation The geometry, displacements and the virtual displacements are approximated by the interpolation

$$\begin{aligned} \boldsymbol{X}_h &= \sum_{I=1}^{n_{\text{u-nodes}}} N^I(\boldsymbol{\xi})\, \hat{\boldsymbol{X}}^I &&= \mathbb{N}\, \hat{\boldsymbol{X}}\,, \\ \boldsymbol{u}_h &= \sum_{I=1}^{n_{\text{u-nodes}}} N^I(\boldsymbol{\xi})\, \boldsymbol{d}^I &&= \mathbb{N}\, \boldsymbol{d}\,, \\ \delta\boldsymbol{u}_h &= \sum_{I=1}^{n_{\text{u-nodes}}} N^I(\boldsymbol{\xi})\, \delta\boldsymbol{d}^I &&= \mathbb{N}\, \delta\boldsymbol{d}, \end{aligned} \tag{5.18}$$

whereas $N^I(\boldsymbol{\xi})$ denote classical shape functions of Lagrange type, defined in the parametric space of the reference element $\boldsymbol{\xi} = \{\xi, \eta, \zeta\}$ and $n_{\text{u-nodes}}$ the number of displacement related nodes per element. In addition $\hat{\boldsymbol{X}}^I$, $\boldsymbol{d}^I$ and $\delta\boldsymbol{d}^I$ represent the global coordinate, displacements and virtual displacements of node I. The alternative representation corresponds to the element nodal coordinate vector $\hat{\boldsymbol{X}}$, element nodal displacement vector $\boldsymbol{d}$ and its virtual counterpart $\delta\boldsymbol{d}$. The nodal wise ordered nested set of all coordinates and displacements of

all element nodes are given by

$$\begin{aligned} \hat{\boldsymbol{X}} &:= \{X_1^I,\, X_2^I,\, X_3^I, \dots\}^T \quad \text{for } I = 1, \dots, n_{\text{nodes}}\,, \\ \boldsymbol{d} &:= \{d_1^I,\, d_2^I,\, d_3^I, \dots\}^T \quad \text{for } I = 1, \dots, n_{\text{nodes}}\,, \\ \delta\boldsymbol{d} &:= \{\delta d_1^I,\, \delta d_2^I,\, \delta d_3^I, \dots\}^T \quad \text{for } I = 1, \dots, n_{\text{nodes}}\,. \end{aligned} \tag{5.19}$$

Therefore $\mathbb{N}$ represents a suitable matrix containing the ansatz functions in appropriate order. The approximation of the displacement gradient is computed with help of the inverse of the Jacobian $\boldsymbol{J}$ as

$$\nabla \boldsymbol{u}_h = \frac{\partial \boldsymbol{u}_h}{\partial \boldsymbol{X}_h} = \frac{\partial \boldsymbol{u}_h}{\partial \boldsymbol{\xi}} \boldsymbol{J}^{-1} \quad \text{with } \boldsymbol{J} = \frac{\partial \boldsymbol{X}_h}{\partial \boldsymbol{\xi}}\,. \tag{5.20}$$

With this in hands it is a straightforward task to calculate the approximation of the strain energy

$$\psi^{\text{LE}}(\boldsymbol{u}_h) = \frac{1}{2}\boldsymbol{\varepsilon}(\boldsymbol{u}_h) : \mathbb{C} : \boldsymbol{\varepsilon}(\boldsymbol{u}_h) \quad \text{with } \boldsymbol{\varepsilon}(\boldsymbol{u}_h) = \frac{1}{2}\left(\nabla \boldsymbol{u}_h + (\nabla \boldsymbol{u}_h)^T\right)\,. \tag{5.21}$$

The discrete weak form in Equation (5.10) follows for a typical element e as

$$\Bigg(\underbrace{\left(\int_{\Omega^e} \frac{\partial^2 \psi(\boldsymbol{\varepsilon}(\boldsymbol{u}_h))}{\partial \boldsymbol{d}\, \partial \boldsymbol{d}} \,\mathrm{d}V \right)}_{\boldsymbol{k}^e} \boldsymbol{d} \underbrace{- \int_{\Omega^e} \frac{\partial (\boldsymbol{f} \cdot \boldsymbol{u}_h)}{\partial \boldsymbol{d}} \,\mathrm{d}V - \int_{\partial\Omega^e} \frac{\partial (\boldsymbol{t}_0 \cdot \boldsymbol{u}_h)}{\partial \boldsymbol{d}} \,\mathrm{d}A}_{\boldsymbol{r}^e} \Bigg) \cdot \delta\boldsymbol{d} = 0\,, \tag{5.22}$$

whereas $\boldsymbol{k}^e$ and $\boldsymbol{r}^e$ denote the element stiffness matrix and element residual vector. Assembling over all elements yield the global stiffness matrix $\boldsymbol{K}$ and residual vector $\boldsymbol{R}$ as

$$\boldsymbol{K} = \mathop{\mathsf{A}}_{e=1}^{num_{ele}} \boldsymbol{k}^e\,, \quad \boldsymbol{R} = \mathop{\mathsf{A}}_{e=1}^{num_{ele}} \boldsymbol{r}^e\,. \tag{5.23}$$

The global discrete system of equations is given by

$$\delta \boldsymbol{D}^T \left(\boldsymbol{K}\, \boldsymbol{D} + \boldsymbol{R}\right) = 0 \quad \forall\, \delta\boldsymbol{D} \neq \boldsymbol{0}\,, \tag{5.24}$$

whereas $\boldsymbol{D}$, $\delta\boldsymbol{D}$ denote the vectors of all nodal displacements and virtual counterparts. Thus, the the nodal displacements can be computed by $\boldsymbol{D} = -\boldsymbol{K}^{-1}\boldsymbol{R}$.

5.4 Elements Based on the Primal Hellinger-Reissner Formulation

In case of mixed elements based on the primal Hellinger-Reissner principle conforming finite dimensional subspaces $\Sigma_h \subset [\mathcal{L}^2(\Omega)]^3$ and $U_h \subset [\mathcal{H}_0^1(\Omega)]^{3\times 3}_{\text{sym}}$ are introduced and an approximate solution $\boldsymbol{\sigma}_h \in \Sigma_h$ and $\boldsymbol{u}_h \in U_h$ is computed by

$$\begin{aligned} a(\boldsymbol{\sigma}_h, \delta\boldsymbol{\sigma}_h) + b(\delta\boldsymbol{\sigma}_h, \boldsymbol{u}_h) &= F_v(\delta\boldsymbol{\sigma}_h) \quad \forall\, \delta\boldsymbol{\sigma}_h \in \Sigma_h \\ b(\boldsymbol{\sigma}_h, \delta\boldsymbol{u}_h) &= F_w(\delta\boldsymbol{u}_h) \quad \forall\, \delta\boldsymbol{u}_h \in U_h\,. \end{aligned} \tag{5.25}$$

The discrete counterparts of Equation (4.20) are given by

$$\begin{aligned} a(\boldsymbol{\sigma}_h, \delta\boldsymbol{\sigma}_h) &:= \int_\Omega \boldsymbol{\sigma}_h : \mathbb{C}^{-1} : \delta\boldsymbol{\sigma}_h \, \mathrm{d}V \,, \\ b(\delta\boldsymbol{\sigma}_h, \boldsymbol{u}_h) &:= -\int_\Omega \delta\boldsymbol{\sigma}_h : \boldsymbol{\varepsilon}(\boldsymbol{u}_h) \, \mathrm{d}V \,, \\ F_v(\delta\boldsymbol{\sigma}_h) &:= 0, \\ b(\boldsymbol{\sigma}_h, \delta\boldsymbol{u}_h) &:= -\int_\Omega \boldsymbol{\sigma}_h : \boldsymbol{\varepsilon}(\delta\boldsymbol{u}_h) \, \mathrm{d}V \,, \\ F_w(\delta\boldsymbol{u}_h) &:= -\int_{\partial\Omega_t} \bar{\boldsymbol{t}}_0 \cdot \delta\boldsymbol{u}_h \, \mathrm{d}A - \int_\Omega \boldsymbol{f} \cdot \delta\boldsymbol{u}_h \, \mathrm{d}V \,. \end{aligned} \tag{5.26}$$

In the scope of the present thesis two different element approaches based on the variational primal Hellinger-Reissner formulation are discussed. First, the well known family of assumed stresses is introduced. Their main characteristics are continuous Lagrangian shape functions for the displacements and a discontinuous discretization of the stresses. The limitation principle and the count condition highly restrict the choice of suitable approximations in this framework. For example a classical fully polynomial displacement ansatz on triangular or tetrahedral shaped elements inherently violates on of these conditions. In contrast the trilinear term, which occurs in the displacement approximation for hexahedral shaped elements, leads to some flexibility in the construction of suitable stress approximations. Thus in the following, the considered assumed stress elements are restricted to a hexahedral reference shape with a trilinear interpolation of the displacements and a reduced, piecewise-continuous stress approximation. In detail, four different stress discretizations are considered, ranging from a minimal number of stress related degrees of freedom up to a stress discretization which accomplishes equivalence to a pure displacement based element. The second approach is based on a tetrahedral reference geometry and also provides a lowest order conforming displacement approximation. In contrast to the discontinuous stress approximation related to the assumed stress approach, the stresses are restricted to a $\mathcal{H}(\mathrm{Div}, \Omega)$ conforming discretization, which leads to a continuous approximation of the traction vector. This interpolation automatically fulfills the limitation principle and leads to an element which is not equivalent to a displacement based approach.

5.4.1 A Family of Assumed Stress Finite Elements for Hexahedral

The first considered family of primal Hellinger-Reissner based elements is denoted in the literature as assumed stress approach. It is based on a hexahedral element geometry and a lowest order, continuous approximation of the displacements. The pioneering works in this framework are Pian [1964] and Pian and Chen [1982], where the derivation of element stiffness matrices based on the Hellinger-Reissner principle are depicted. The most famous representative of assumed stress elements has been derived through a rational choice of stress terms by Pian and Sumihara [1984], representing a minimal number of stress unknowns in the plane strain setup. This formulation has been extended to the three dimensional case by Pian and Tong [1986]. Four different approximation schemes for the stresses are considered in the scope of this thesis. The corresponding interpolation

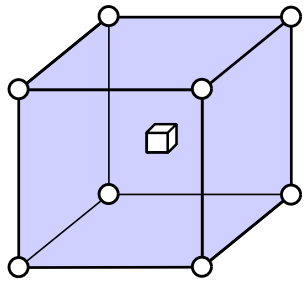

Figure 5.2: Sketch of the AS_n Hellinger-Reissner based elements.

spaces for the displacements and stresses are given in detail by

$$\begin{aligned} U_h &:= \{\boldsymbol{u}_h \in [\mathcal{H}^1_0(\Omega)]^3,\, \boldsymbol{u}_h \text{ cont. on } \Omega : \boldsymbol{u}_h|_{\widehat{\Omega}^e} \in Q_1 \,\forall\, \Omega^e \in \Omega\}\,, \\ \Sigma_h &:= \{\boldsymbol{\tau}_h \in [\mathcal{L}^2(\Omega)]^{3\times 3} : \boldsymbol{\tau}_h|_{\widehat{\Omega}^e} \in S^{\square} \,\forall\, \Omega^e \in \Omega\}\,. \end{aligned} \tag{5.27}$$

The different considered polynomial approximation spaces $S^{\square} \subseteq Q_1$ are constructed by direct sums of the polynomial bases given in Equation (5.2). The representative reference geometry with corresponding degrees of freedom is depicted in Figure 5.2, whereas the utilized combinations are explicitly summarized in Table 5.1. The number of stress

	$(\tau_{11}, \tau_{22}, \tau_{33})^T|_{\widehat{\Omega}^e} \in$	$(\tau_{23}, \tau_{13}, \tau_{12})^T|_{\widehat{\Omega}^e} \in$
AS_{39}	$Id \oplus A_0 \oplus A_1 \oplus A_2 \oplus B_0 \oplus B_1 \oplus B_2$	$Id \oplus A_0 \oplus A_1 \oplus A_2 \oplus B_1 \oplus B_2$
AS_{30}	$Id \oplus A_1 \oplus A_2 \oplus B_0$	$Id \oplus A_0 \oplus A_1 \oplus A_2 \oplus B_1 \oplus B_2$
AS_{24}	$Id \oplus A_1 \oplus A_2 \oplus B_0$	$Id \oplus A_0 \oplus B_1 \oplus B_2$
AS_{18}	$Id \oplus A_1 \oplus A_2 \oplus B_0$	$Id \oplus A_0$

Table 5.1: Considered polynomial bases for the stresses $S^{\square}$ of the assumed stress finite elements.

unknowns per element is given in the abbreviation of the element. Note that, due to the *principle of limitation* in Equation (5.4), the AS_{39} is equivalent to the Q_1 displacement based element, which is obtained by the comparison with the stress space given in Equation (5.17). In contrast the AS_{18}, which corresponds to the well known element proposed by Pian and Tong [1986], constitutes the approximation with a minimal number of stress unknowns regarding to the *count condition* given in Equation (5.6).

Due to the conforming approximation of displacements and stresses the discrete boundedness condition remains trivial. A Λ-dependent coercivity condition can be shown for the complete family of assumed stress elements by

$$a(\delta\boldsymbol{\sigma}_h, \delta\boldsymbol{\sigma}_h) \geq \lambda^{\min}(\mathbb{C}^{-1})\, \|\boldsymbol{\sigma}\|^2_{\Sigma} \quad \forall\, \delta\boldsymbol{\sigma}_h \in \Sigma_h\,. \tag{5.28}$$

Based on this condition, volumetric locking cannot be generally precluded for these elements due to the Λ dependency, which is clear since it is possible to achieve formulations

equivalent to the pure displacement approach. However, in sense of *Brezzi's conditions* coercivity on the kernel suffices to obtain well posed element formulations. This condition highly depends on the relation of the discrete stress and displacement spaces. Yu et al. [2011] have shown a material parameter independent kernel coercivity for the element formulation by Pian and Sumihara [1984]. These results have been extended recently by Li et al. [2017]. The key point in this proof is the balance of the spaces for the trace of the stresses and the displacements. This approach seems to be a promising guideline in order to show Λ-independent kernel coercivity for the AS_{30}, AS_{24} and AS_{18}, since their stress-trace related approximation space is equivalent, compare Table 5.1. Furthermore, Λ dependency of the element formulations is also investigated by meaningful numerical tests in Chapter 5.7.

It is trivial to show that a Hellinger-Reissner element formulation satisfies the discrete inf-sup condition if

$$\boldsymbol{\varepsilon}(\delta \boldsymbol{u}_h) \subseteq \Sigma_h \quad \forall\, \delta \boldsymbol{u}_h \in U_h\,, \tag{5.29}$$

following the same arguments as in Equation (4.23). Due to the trilinear interpolation of the displacements, the space of the strains is obtained in detail by

$$\begin{aligned} \boldsymbol{\varepsilon}(U_h) := \Bigg\{ \boldsymbol{u}_h \in U_h;\, \begin{pmatrix} \varepsilon(\boldsymbol{u}_h)_{11} \\ \varepsilon(\boldsymbol{u}_h)_{22} \\ \varepsilon(\boldsymbol{u}_h)_{33} \end{pmatrix} \Bigg|_{\widehat{\Omega}^e} \in Id \oplus A_1 \oplus A_2 \oplus B_0 \,\forall\, \Omega^e \in \Omega,\, \dots \\ \dots \begin{pmatrix} \varepsilon(\boldsymbol{u}_h)_{23} \\ \varepsilon(\boldsymbol{u}_h)_{13} \\ \varepsilon(\boldsymbol{u}_h)_{12} \end{pmatrix} \Bigg|_{\widehat{\Omega}^e} \in Id \oplus A_0 \oplus A_1 \oplus A_2 \oplus B_1 \oplus B_2 \,\forall\, \Omega^e \in \Omega \Bigg\}. \end{aligned} \tag{5.30}$$

Therefore, the elements AS_{39} and AS_{30} satisfy the discrete inf-sup condition. In case of the AS_{24} and AS_{18} elements, the aforementioned property in Equation (5.29) is not fulfilled, but the inf-sup stability will be validated by means of a numerical inf-sup test in Chapter 5.7.1. In this framework, the works by Yu et al. [2011] and Li et al. [2017] seem to be adequate guidelines in order to proof inf-sup stability also for the latter elements.

Implementation The approximation of the geometry, displacements, its gradient and virtual counterparts follow Equation (5.18) and (5.20). Note that for this formulation N^I is restricted to trilinear Lagrangian interpolation functions. In addition, the stress field in the parametric space is approximated in Voigt type vector notation accordingly to

$$\underline{\boldsymbol{\sigma}}_\xi = (\sigma_{\xi\xi}, \sigma_{\eta\eta}, \sigma_{\zeta\zeta}, \sigma_{\xi\eta}, \sigma_{\eta\zeta}, \sigma_{\xi\zeta})^T = \mathbb{L}_\xi\, \boldsymbol{\beta} \tag{5.31}$$

where due to the strong incorporation of the stress symmetry condition only the six independent stress components are considered and $\boldsymbol{\beta}$ denotes the vector of element wise unknowns related to the stresses. The interpolation matrix $\mathbb{L}_\xi$ has the general structure

$$\mathbb{L}_\xi = \mathrm{diag}(\mathbb{L}_{\xi\xi}, \mathbb{L}_{\eta\eta}, \mathbb{L}_{\zeta\zeta}, \mathbb{L}_{\xi\eta}, \mathbb{L}_{\eta\zeta}, \mathbb{L}_{\xi\zeta}) \tag{5.32}$$

and contains the corresponding interpolation functions. Their explicit polynomial forms are summarized in the following subchapter. The transformation from the isoparametric domain to the physical space for the stresses is described by

$$\boldsymbol{\sigma}_h = \boldsymbol{J}_0\, \boldsymbol{\sigma}_\xi\, \boldsymbol{J}_0^T \quad \text{with } \boldsymbol{\sigma}_\xi = \begin{pmatrix} \sigma_{\xi\xi} & \sigma_{\xi\eta} & \sigma_{\xi\zeta} \\ \sigma_{\xi\eta} & \sigma_{\eta\eta} & \sigma_{\eta\zeta} \\ \sigma_{\xi\zeta} & \sigma_{\eta\zeta} & \sigma_{\zeta\zeta} \end{pmatrix} \tag{5.33}$$

where the mapping between the isoparametric coordinates $\boldsymbol{\xi}$ and the reference coordinates $\boldsymbol{X}$ follows by the special Jacobian as

$$\boldsymbol{J}_0 = \left.\frac{\partial \boldsymbol{X}(\boldsymbol{\xi})}{\partial \boldsymbol{\xi}}\right|_{\boldsymbol{\xi}=0} . \tag{5.34}$$

In order to pass the patch test, it is necessary to use the values of the Jacobian at the origin $\boldsymbol{\xi} = \{\xi, \eta, \zeta\} = \{0, 0, 0\}$ as it is discussed in Pian and Sumihara [1984] and Pian and Tong [1986]. With this in hand the discretized weak form in Equation (5.25) follows for a typical element e as

$$\begin{aligned}
&\Bigg(\underbrace{\int_{\Omega^e} \frac{\partial^2(\frac{1}{2}\boldsymbol{\sigma}_h : \mathbb{C}^{-1} : \boldsymbol{\sigma}_h)}{\partial \boldsymbol{\beta}\, \partial \boldsymbol{\beta}} \, \mathrm{d}V}_{\boldsymbol{k}^e_{\sigma\sigma}} \boldsymbol{\beta} \underbrace{- \int_{\Omega^e} \frac{\partial^2(\boldsymbol{\sigma}_h : \boldsymbol{\varepsilon}(\boldsymbol{u}_h))}{\partial \boldsymbol{\beta}\, \partial \boldsymbol{d}} \, \mathrm{d}V}_{\boldsymbol{k}^e_{\sigma u}} \boldsymbol{d} \Bigg) \cdot \delta\boldsymbol{\beta} = 0 \,, \\
&\Bigg(\underbrace{- \int_{\Omega^e} \frac{\partial^2(\boldsymbol{\sigma}_h : \boldsymbol{\varepsilon}(\boldsymbol{u}_h))}{\partial \boldsymbol{d}\, \partial \boldsymbol{\beta}} \, \mathrm{d}V}_{\boldsymbol{k}^e_{u\sigma}} \boldsymbol{\beta} + \underbrace{\int_{\Omega^e} \frac{\partial(\boldsymbol{f} \cdot \boldsymbol{u}_h)}{\partial \boldsymbol{d}} \, \mathrm{d}V + \int_{\partial\Omega^e} \frac{\partial(\boldsymbol{t}_0 \cdot \boldsymbol{u}_h)}{\partial \boldsymbol{d}} \, \mathrm{d}A}_{\boldsymbol{r}^e_u} \Bigg) \cdot \delta\boldsymbol{d} = 0 \,.
\end{aligned} \tag{5.35}$$

Therefore, the global system of equations is given by

$$\mathop{\mathsf{A}}_{\mathrm{e}=1}^{num_{ele}} \begin{bmatrix} \delta\boldsymbol{\beta} \\ \delta\boldsymbol{d} \end{bmatrix}^T \left(\begin{bmatrix} \boldsymbol{k}^e_{\sigma\sigma} & \boldsymbol{k}^e_{\sigma u} \\ \boldsymbol{k}^e_{u\sigma} & \boldsymbol{0} \end{bmatrix} \begin{bmatrix} \boldsymbol{\beta} \\ \boldsymbol{d} \end{bmatrix} + \begin{bmatrix} \boldsymbol{0} \\ \boldsymbol{r}^e_u \end{bmatrix} \right) = 0 \,, \tag{5.36}$$

which displays the typical saddle point structure associated to the zero entries on the main diagonal of the tangent matrix. As it can be noticed, such a system is remarkable larger compared to the system of equations obtained by a primal finite element given in Equation (5.24). But, since the stresses are interpolated element-wise and no continuity over element patches have to be satisfied, a static condensation can be applied already on element level. In this sense, the degrees of freedom associated to the stresses are solved on the individual element with respect to the displacements. This leads to a reduced global system of equations where only the degrees of freedom associated to the displacements are the remaining unknowns. The condensed form is given for a typical element e by

$$\delta\boldsymbol{d}^T (\underbrace{-\boldsymbol{k}^e_{u\sigma} \, (\boldsymbol{k}^e_{\sigma\sigma})^{-1} \, \boldsymbol{k}^e_{\sigma u}}_{\boldsymbol{k}^e_{\mathrm{red}}} \boldsymbol{d} + \boldsymbol{r}^e_u) = 0 \,. \tag{5.37}$$

Assembling of all element stiffness matrices and element residual vectors yields the global reduced stiffness matrix $\boldsymbol{K}_{\mathrm{red}}$ and residual vector $\boldsymbol{R}_{\mathrm{red}}$ as

$$\boldsymbol{K}_{\mathrm{red}} = \mathop{\mathsf{A}}_{\mathrm{e}=1}^{num_{ele}} \boldsymbol{k}^e_{\mathrm{red}} \,, \quad \boldsymbol{R}_{\mathrm{red}} = \mathop{\mathsf{A}}_{\mathrm{e}=1}^{num_{ele}} \boldsymbol{r}^e_u \,. \tag{5.38}$$

Thus, the nodal displacements are computed by $\boldsymbol{D} = -\boldsymbol{K}^{-1}_{\mathrm{red}} \boldsymbol{R}_{\mathrm{red}}$. The stress values follow a posteriori on element level by $\boldsymbol{\beta} = -(\boldsymbol{k}^e_{\sigma\sigma})^{-1} \boldsymbol{k}^e_{\sigma u} \boldsymbol{d}$. It should be noted that such a static condensation can be interpreted as an alternative solution strategy which in general has a huge impact on the computational efficiency. Nonetheless, this procedure does not manipulate the result for the displacements or the stresses.

Stress Interpolation Following the limitation principle by Fraeijs de Veubeke [1965], it can be shown that the following 39 parameter based interpolation is equivalent to a primal displacement formulation because the resulting stress spaces are equivalent in both elements. For this case the interpolation vectors for the stresses are given by

$$\begin{aligned}
\mathbb{L}_{\xi\xi} &= (1,\, \xi,\, \eta,\, \zeta,\, \xi\eta,\, \eta\zeta,\, \xi\zeta) \\
\mathbb{L}_{\eta\eta} &= (1,\, \xi,\, \eta,\, \zeta,\, \xi\eta,\, \eta\zeta,\, \xi\zeta) \\
\mathbb{L}_{\zeta\zeta} &= (1,\, \xi,\, \eta,\, \zeta,\, \xi\eta,\, \eta\zeta,\, \xi\zeta) \\
\mathbb{L}_{\xi\eta} &= (1,\, \xi,\, \eta,\, \zeta,\, \eta\zeta,\, \xi\zeta) \\
\mathbb{L}_{\eta\zeta} &= (1,\, \xi,\, \eta,\, \zeta,\, \xi\eta,\, \xi\zeta) \\
\mathbb{L}_{\xi\zeta} &= (1,\, \xi,\, \eta,\, \zeta,\, \xi\eta,\, \eta\zeta)
\end{aligned} \tag{5.39}$$

39 stress modes

As known from (selective) reduced integration methods, an expedient reduction of introduced stress-modes lead to a softening of the formulation. However, care must be taken not to relax the formulation too much, since this could lead to artificial deformation states. A well known and very efficient stress discretization of the proposed assumed stress formulation is the 18 parameter based interpolation scheme proposed by Pian and Tong [1986], which is a 3D extension of the element by Pian and Sumihara [1984]. Here the individual interpolation vectors are given by

$$\begin{aligned}
\mathbb{L}_{\xi\xi} &= (1,\, \eta,\, \zeta,\, \eta\zeta) \\
\mathbb{L}_{\eta\eta} &= (1,\, \xi,\, \zeta,\, \xi\zeta) \\
\mathbb{L}_{\zeta\zeta} &= (1,\, \xi,\, \eta,\, \xi\eta) \\
\mathbb{L}_{\xi\eta} &= (1,\, \zeta) \\
\mathbb{L}_{\eta\zeta} &= (1,\, \xi) \\
\mathbb{L}_{\xi\zeta} &= (1,\, \eta)
\end{aligned} \tag{5.40}$$

18 stress modes

Note, that this stress interpolation considers a minimal number of stress unknowns, since any further reduction would lead to singular system matrices due to a violation of the count condition. A further stress interpolation is based on the following 30-parameter

approach

$$\begin{aligned}
\mathbb{L}_{\xi\xi} &= (1,\, \eta,\, \zeta,\, \eta\zeta) \\
\mathbb{L}_{\eta\eta} &= (1,\, \xi,\, \zeta,\, \xi\zeta) \\
\mathbb{L}_{\zeta\zeta} &= (1,\, \xi,\, \eta,\, \xi\eta) \\
\mathbb{L}_{\xi\eta} &= (1,\, \xi,\, \eta,\, \zeta,\, \eta\zeta,\, \xi\zeta) \\
\mathbb{L}_{\eta\zeta} &= (1,\, \xi,\, \eta,\, \zeta,\, \xi\eta,\, \xi\zeta) \\
\mathbb{L}_{\xi\eta} &= (1,\, \xi,\, \eta,\, \zeta,\, \xi\eta,\, \eta\zeta)
\end{aligned} \tag{5.41}$$

30 stress modes

It can be recognized that the only difference between the interpolation schemes of Equations (5.40) and (5.41) are the additional terms for the interpolation of the shear stresses. In addition we consider the interpolation scheme which is nested in between the interpolations from Equations (5.40) and (5.41). The corresponding vectors follow by

$$\begin{aligned}
\mathbb{L}_1^{\xi} &= (1,\, \eta,\, \zeta,\, \eta\zeta) \\
\mathbb{L}_2^{\xi} &= (1,\, \xi,\, \zeta,\, \xi\zeta) \\
\mathbb{L}_3^{\xi} &= (1,\, \xi,\, \eta,\, \xi\eta) \\
\mathbb{L}_4^{\xi} &= (1,\, \zeta,\, \eta\zeta,\, \xi\zeta) \\
\mathbb{L}_5^{\xi} &= (1,\, \xi,\, \xi\eta,\, \xi\zeta) \\
\mathbb{L}_6^{\xi} &= (1,\, \eta,\, \xi\eta,\, \eta\zeta)
\end{aligned} \tag{5.42}$$

24 stress modes

5.4.2 A Tetrahedral Finite Element for Primal Hellinger-Reissner with Continuity of the Traction Vector

The *limitation principle* and the *count condition* for finite elements based on the primal Hellinger-Reissner variational formulation highly restrict the capabilities for the construction of novel low order tetrahedral shaped elements. On one side, an enlargement of the stress space leads to equivalent element formulations and on the other side a simple reduction of the stress space, as it is utilized in the framework of the assumed stress element, violates the *count condition*. A possible approach has been presented in Viebahn et al. [2018b]. The crucial point in this formulation is a restriction of the solution space of the stresses in combination with a classical conforming linear approximation for the displacements, e.g.

$$\boldsymbol{u}_h \in U_h := \{\boldsymbol{u}_h \in [\mathcal{H}_0^1(\Omega)]^3,\, \boldsymbol{u}_h \text{ cont. on } \Omega : \boldsymbol{u}_h|_{\widehat{\Omega}^e} \in T_1 \,\forall\, \Omega^e \in \Omega\}\,. \tag{5.43}$$

While in the primal Hellinger-Reissner formulation the largest conforming solution space for the stresses is the $\mathcal{L}^2(\Omega)$-space, in the proposed formulation the discrete stresses are restricted to a subset of the $\mathcal{H}(\mathrm{Div}, \Omega)$-space. This means in particular, a restriction of the stresses such that continuity of the traction vector $\boldsymbol{t}$ across interelement faces is ensured,

whereas the traction vector is approximated by a constant on each face. This leads to the confined space for the stresses

$$\boldsymbol{\sigma}_h \in \Sigma_h^{\mathrm{RT}} := \{\boldsymbol{\tau}_h \in [\mathcal{H}(\mathrm{Div}, \Omega)]^3 : \boldsymbol{\tau}_h|_{\widehat{\Omega}^e} \in [\mathrm{RT}_0]^3 \; \forall \; \Omega^e \in \Omega\}\,, \tag{5.44}$$

where RT_0 denotes the lowest order Raviart-Thomas interpolation introduced by Raviart and Thomas [1977]. It should be highlighted that this particular stress interpolation is still conforming, since $\Sigma_h^{\mathrm{RT}} \subset \mathcal{L}^2(\Omega)^3$. Furthermore it does not lead to a formulation which is equivalent to a displacement based element since $\Sigma_h^{\mathrm{RT}} \not\supseteq \Sigma(U_h)$, since $\Sigma(U_h)$ contains all piecewise constant functions and Σ_h^{RT} is restricted to continuous traction vectors. The restriction of the continuity of the traction vector can also be motivated from a physical point of view, since any jump of traction vectors across any internal surface violates the local equilibrium condition.

A well known difficulty related to the Raviart-Thomas interpolation of the stresses is associated to the requirement of stress symmetry, which ensures the balance of angular momentum. In contrast to the approaches where a weak symmetry constrain is imposed in form of an additional weak form, see e.g. Arnold et al. [1984a; 2007], Stenberg [1988], here a related approach as in Cai and Starke [2004] and Cai et al. [2005] is utilized. The symmetry of the discrete stress tensor is enforced utilizing the symmetry of $\boldsymbol{\varepsilon}(\boldsymbol{u}_h)$ and the application of a non symmetrizing constitutive tensor which fulfills the constitutive relation for isotropic linear elasticity. The description of the modified fourth order tensor is given by

$$\widehat{\mathbb{C}} := \lambda\, \boldsymbol{I} \otimes \boldsymbol{I} + 2\mu\, \boldsymbol{I} \boxtimes \boldsymbol{I}, \tag{5.45}$$

with the special dyadic product between two tensors of second order, see Halmos [1958], defined by

$$(\boldsymbol{A} \boxtimes \boldsymbol{B}) : \boldsymbol{a} \otimes \boldsymbol{b} = \boldsymbol{A}\boldsymbol{a} \otimes \boldsymbol{B}\boldsymbol{b}\,. \tag{5.46}$$

The inverse of the constitutive tensor follows by

$$\widehat{\mathbb{C}}^{-1} = -\frac{\lambda}{4\,\mu^2 + 6\,\mu\,\lambda}\, \boldsymbol{I} \otimes \boldsymbol{I} + \frac{1}{2\,\mu}\, \boldsymbol{I} \boxtimes \boldsymbol{I}\,. \tag{5.47}$$

The important property of the constitutive tensor, representing only major symmetries, becomes clear by the consideration of an additive split of the stress tensor into a symmetric and a skew symmetric part in Equation $(5.25)_1$

$$\begin{aligned} a(\boldsymbol{\sigma}_h, \delta\boldsymbol{\sigma}_h) + b(\delta\boldsymbol{\sigma}_h, \boldsymbol{u}_h) &= \int_\Omega \left(\widehat{\mathbb{C}}^{-1} : \boldsymbol{\sigma}_h - \boldsymbol{\varepsilon}(\boldsymbol{u}_h)\right) : \delta\boldsymbol{\sigma}_h \; \mathrm{d}V \\ &= \int_\Omega \left(\widehat{\mathbb{C}}^{-1} : \mathrm{sym}[\boldsymbol{\sigma}_h] + \widehat{\mathbb{C}}^{-1} : \mathrm{skew}[\boldsymbol{\sigma}_h] - \boldsymbol{\varepsilon}(\boldsymbol{u}_h)\right) : \delta\boldsymbol{\sigma}_h \; \mathrm{d}V \\ &= 0 \quad \forall\, \delta\boldsymbol{\sigma}_h \in \Sigma_h^{\mathrm{RT}}\,, \end{aligned} \tag{5.48}$$

whereas $\mathrm{sym}[\boldsymbol{\sigma}_h] := \frac{1}{2}(\boldsymbol{\sigma}_h + \boldsymbol{\sigma}_h^T)$ and $\mathrm{skew}[\boldsymbol{\sigma}_h] := \boldsymbol{\sigma}_h - \mathrm{sym}[\boldsymbol{\sigma}_h]$ denote the symmetric and skew symmetric part of the stresses. Therein, $(\widehat{\mathbb{C}}^{-1} : \mathrm{sym}[\boldsymbol{\sigma}_h] - \boldsymbol{\varepsilon}(\boldsymbol{u}_h))$ corresponds to the constitutive equation. In addition the stress symmetry is enforced in a weak sense by the second part $(\widehat{\mathbb{C}}^{-1} : \mathrm{skew}[\boldsymbol{\sigma}])$. Obviously, a constitutive tensor with minor symmetries is not able to control the skew-symmetric part of the stresses. A numerical validation of the stress symmetry condition is also shown in the numerical examples.

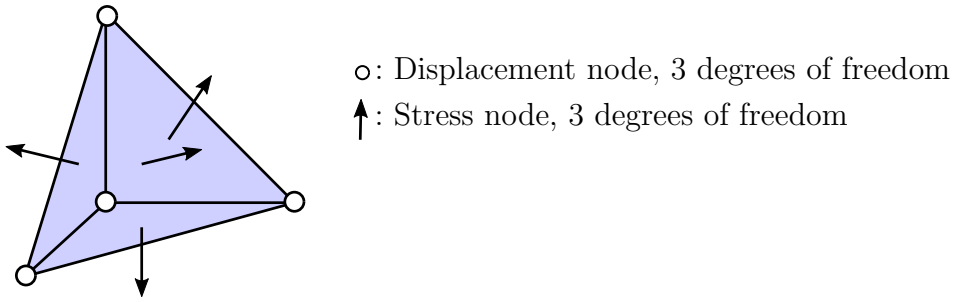

Figure 5.3: Sketch of the $\mathrm{RT}_0\mathrm{T}_1$ Hellinger-Reissner based element.

Implementation A sketch of the corresponding finite element and nodal discretization points is depicted in Figure 5.3. The circles, located at the element corners, denote the discretization points of the displacements. The arrows, associated to the faces of the element, are the discretization points of the stresses. Its degrees of freedom are the entries of the local traction vectors. Thus, for a single element the number of unknowns related to the stresses coincides with the number of unknowns related to the displacements $n_\sigma = n_u$. In addition, due to the assembling procedure, where always three displacement related nodes but only a single stress related node are merged between neighboring elements, every regular patch of elements holds $n_\sigma \geq n_u$, which represents the satisfaction of the the count condition of Chapter 5.2.2. The approximation of the geometry, displacements and its gradient and virtual counterparts are given by Equations (5.18) and (5.20). Note that for this formulation N^I is restricted to linear Lagrangian interpolation functions, related to the polynomial space T_1 in Equation (5.3). In addition the stress field and its virtual counterpart are approximated by a lowest order Raviart-Thomas type interpolation

$$\boldsymbol{\sigma}_h = \sum_{I=1}^{n_{\text{faces}}} \boldsymbol{\beta}^I \otimes \boldsymbol{\Psi}^I \,, \quad \delta\boldsymbol{\sigma}_h = \sum_{I=1}^{n_{\text{faces}}} \delta\boldsymbol{\beta}^I \otimes \boldsymbol{\Psi}^I \,, \tag{5.49}$$

where $\boldsymbol{\beta}^I$ is a vector of dimension three, containing the stress-related degrees of freedom associated to face I. The vector $\boldsymbol{\Psi}^I$ contains the Raviart-Thomas interpolation functions of the corresponding face. Note that face I is defined to be the face on the opposing side of node I. A simple construction procedure for the lowest order Raviart-Thomas interpolation has been proposed for a typical element e by Bahriawati and Carstensen [2005] as

$$\boldsymbol{\Psi}^I = \sigma_I \frac{A^I}{3V_e}(\boldsymbol{X}_h - \hat{\boldsymbol{X}}^I). \tag{5.50}$$

Here σ_I defines the positive flow direction between two elements, A^I the surface area of face I, V_e the volume of element e and $\hat{\boldsymbol{X}}^I$ the nodal coordinate vector of node I. Additional information and advices regarding the construction of Raviart-Thomas shape functions can be found in e.g. Ervin [2012], **?**, Steeger [2016] and Bentley [2017]. The discrete

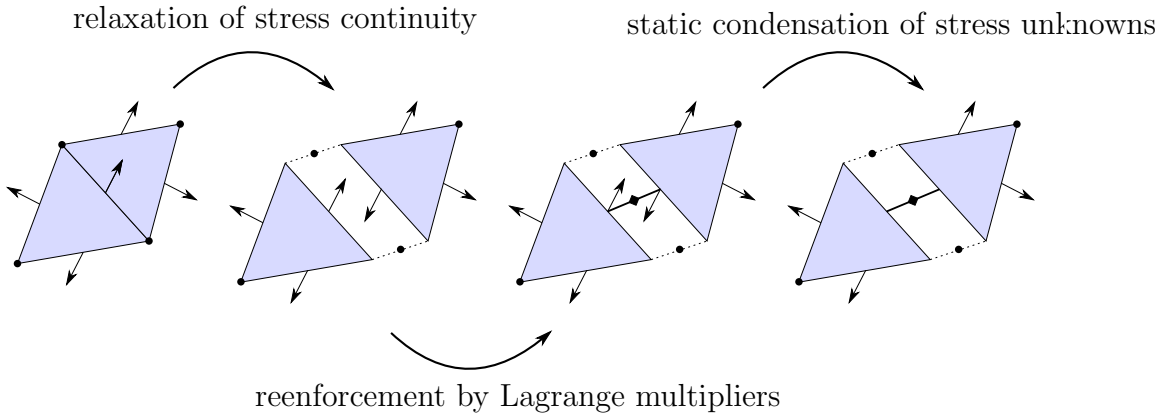

Figure 5.4: Sketch of the hybridization procedure of a two element patch, for simplicity depicted in 2D.

weak form of Equation (5.25) follows for a typical element e as

$$\begin{aligned}
&\Bigg(\underbrace{\int_{\Omega^e} \frac{\partial^2 (\frac{1}{2}\boldsymbol{\sigma}_h : \widehat{\mathbb{C}}^{-1} : \boldsymbol{\sigma}_h)}{\partial \boldsymbol{\beta}\, \partial \boldsymbol{\beta}} \, \mathrm{d}V}_{\boldsymbol{k}^e_{\sigma\sigma}} \boldsymbol{\beta} \underbrace{- \int_{\Omega^e} \frac{\partial^2 (\boldsymbol{\sigma}_h : \boldsymbol{\varepsilon}(\boldsymbol{u}_h))}{\partial \boldsymbol{\beta}\, \partial \boldsymbol{d}} \, \mathrm{d}V}_{\boldsymbol{k}^e_{\sigma u}} \boldsymbol{d} \Bigg) \cdot \delta\boldsymbol{\beta} = 0 \,, \\
&\Bigg(\underbrace{- \int_{\Omega^e} \frac{\partial^2 (\boldsymbol{\sigma}_h : \boldsymbol{\varepsilon}(\boldsymbol{u}_h))}{\partial \boldsymbol{d}\, \partial \boldsymbol{\beta}} \, \mathrm{d}V}_{\boldsymbol{k}^e_{u\sigma}} \boldsymbol{\beta} + \underbrace{\int_{\Omega^e} \frac{\partial (\boldsymbol{f} \cdot \boldsymbol{u}_h)}{\partial \boldsymbol{d}} \, \mathrm{d}V + \int_{\partial\Omega^e} \frac{\partial (\boldsymbol{t}_0 \cdot \boldsymbol{u}_h)}{\partial \boldsymbol{d}} \, \mathrm{d}A}_{\boldsymbol{r}^e_u} \Bigg) \cdot \delta\boldsymbol{d} = 0 \,.
\end{aligned} \tag{5.51}$$

Therefore, the global system of equations follows by

$$\overset{num_{ele}}{\underset{e=1}{\mathbf{A}}} \begin{bmatrix} \delta\boldsymbol{\beta} \\ \delta\boldsymbol{d} \end{bmatrix}^T \left(\begin{bmatrix} \boldsymbol{k}^e_{\sigma\sigma} & \boldsymbol{k}^e_{\sigma u} \\ \boldsymbol{k}^e_{u\sigma} & \mathbf{0} \end{bmatrix} \begin{bmatrix} \boldsymbol{\beta} \\ \boldsymbol{d} \end{bmatrix} + \begin{bmatrix} \mathbf{0} \\ \boldsymbol{r}^e_u \end{bmatrix} \right) = 0 \,, \tag{5.52}$$

which depicts again the typical saddle point structure. In contrast to the previous discussed assumed stress elements, a static condensation is not applicable in this case due to the global continuity of the traction vector. However, a positive definite system matrix can be achieved at low computational cost by a hybridization procedure. The general procedure of the hybridization technique is sketched, for simplicity in 2D, in Figure 5.4. Therein the continuity of the traction vector is first relaxed and then reinforced by the application of Lagrangian multipliers denoted as $\boldsymbol{d}_\lambda$. The resulting system of equations is obtained on element level as

$$\begin{bmatrix} \delta\boldsymbol{\eta} \\ \delta\boldsymbol{d} \\ \delta\boldsymbol{d}_\lambda \end{bmatrix}^T \left(\begin{bmatrix} \boldsymbol{k}^e_{\sigma\sigma} & \boldsymbol{k}^e_{\sigma u} & \boldsymbol{k}^e_{\sigma\lambda} \\ \boldsymbol{k}^e_{u\sigma} & \mathbf{0} & \mathbf{0} \\ \boldsymbol{k}^e_{\lambda\sigma} & \mathbf{0} & \mathbf{0} \end{bmatrix} \begin{bmatrix} \boldsymbol{\beta} \\ \boldsymbol{d} \\ \boldsymbol{d}_\lambda \end{bmatrix} + \begin{bmatrix} \mathbf{0} \\ \boldsymbol{r}^e_u \\ \mathbf{0} \end{bmatrix} \right) = 0 \,, \tag{5.53}$$

In contrast to the prior approximation, the nodal values of the stresses can now be solved already on element level with respect to the nodal displacements and the Lagrangian

multiplier. This leads to the reduced system of equations as

$$\begin{bmatrix} \delta \boldsymbol{d} \\ \delta \boldsymbol{d}_\lambda \end{bmatrix}^T \Bigg(\underbrace{\begin{bmatrix} -\boldsymbol{k}^e_{u\sigma}(\boldsymbol{k}^e_{\sigma\sigma})^{-1}\boldsymbol{k}^e_{\sigma u} & -\boldsymbol{k}^e_{u\sigma}(\boldsymbol{k}^e_{\sigma\sigma})^{-1}\boldsymbol{k}^e_{\sigma\lambda} \\ -\boldsymbol{k}^e_{\lambda\sigma}(\boldsymbol{k}^e_{\sigma\sigma})^{-1}\boldsymbol{k}^e_{\sigma u} & -\boldsymbol{k}^e_{\lambda\sigma}(\boldsymbol{k}^e_{\sigma\sigma})^{-1}\boldsymbol{k}^e_{\sigma\lambda} \end{bmatrix}}_{\boldsymbol{k}^e_{\text{red}}} \begin{bmatrix} \boldsymbol{d} \\ \boldsymbol{d}_\lambda \end{bmatrix} + \underbrace{\begin{bmatrix} \boldsymbol{r}^e_u \\ \boldsymbol{0} \end{bmatrix}}_{\boldsymbol{r}^e_{\text{red}}} \Bigg) = 0\,. \tag{5.54}$$

The global system of equations can be written as $\boldsymbol{K}_{\text{red}}\,\Delta\boldsymbol{D} = \boldsymbol{R}_{\text{red}}$ with

$$\boldsymbol{K}_{\text{red}} = \mathop{\mathbf{A}}_{e=1}^{num_{ele}} \boldsymbol{k}^e_{\text{red}}\,, \quad \boldsymbol{R}_{\text{red}} = \mathop{\mathbf{A}}_{e=1}^{num_{ele}} \boldsymbol{r}^e_{\text{red}} \tag{5.55}$$

Note, that the hybridization yields a global system of equations which has the same number of unknowns as the system of equations associated to Equation (5.52). However, due to the hybridization the system matrix is positive definite, which is beneficial for many solving procedures.

5.5 Displacement-Pressure Elements

In the framework of incompressible elasticity, one of the most common finite element formulations is the approximation of displacements and pressure. Especially if selective reduced integration procedures (see e.g. Hughes [1980]) are incorporated, which are in fact equivalent to mixed finite elements with a discontinuous approximation of the pressure as emphasized by Malkus and Hughes [1978]. Its prominence can be probably concluded by their relatively simplicity, efficiency and their close algebraic relation to the Stokes problem of incompressible fluid flow. A detailed analysis of this element family can be found in many textbook concerning the analysis of the Finite Element Method, e.g. Boffi et al. [2013], Bathe [1996] or Braess [2000]. Due to their remarkable significance in the considered field of (nearly) incompressibility they are used in the present thesis for the purpose of comparison. Conforming finite dimensional subspaces $U_h \subset [\mathcal{H}^1_0(\Omega)]^3$ and $P_h \subset \mathcal{L}^2(\Omega)$ are chosen and an approximate solution for $\boldsymbol{u}_h \in U_h$ and $p_h \in P_h$ is computed by the problem

$$\begin{aligned} a(\boldsymbol{u}_h, \delta\boldsymbol{u}_h) + b(\delta\boldsymbol{u}_h, p_h) &= F_v(\delta\boldsymbol{u}_h) \quad \forall\, \delta\boldsymbol{u}_h \in U_h \\ b(\boldsymbol{u}_h, \delta p_h) \; - \int_\Omega \frac{1}{\Lambda}\, p_h\, \delta p_h \; \mathrm{d}V &= F_w(\delta p_h) \quad \forall\, \delta p_h \in P_h\,. \end{aligned} \tag{5.56}$$

The discrete counterparts of Equation (4.39) are given by

$$\begin{aligned} a(\boldsymbol{u}_h, \delta\boldsymbol{u}_h) &= \int_\Omega 2\mu\, \boldsymbol{\varepsilon}(\boldsymbol{u}_h) : \boldsymbol{\varepsilon}(\delta\boldsymbol{u}_h)\; \mathrm{d}V\,, \\ b(\delta\boldsymbol{u}_h, p_h) &= \int_\Omega \mathrm{Div}[\delta\boldsymbol{u}_h]\, p_h\; \mathrm{d}V\,, \\ F_v(\delta\boldsymbol{u}_h) &= \int_{\partial\Omega_t} \bar{\boldsymbol{t}}_0 \cdot \delta\boldsymbol{u}_h\, \mathrm{d}A + \int_\Omega \boldsymbol{f} \cdot \delta\boldsymbol{u}_h\, \mathrm{d}V\,, \\ b(\boldsymbol{u}_h, \delta p_h) &= \int_\Omega \mathrm{Div}[\boldsymbol{u}_h]\, \delta p_h\; \mathrm{d}V\,, \\ F_w(\delta p_h) &= 0. \end{aligned} \tag{5.57}$$

A great benefit in this framework is that the bilinear form $a(\boldsymbol{u}_h, \boldsymbol{u}_h)$ is coercive for all conforming approximations of the displacements $\boldsymbol{u}_h \in U_h$. Thus, it only remains to verify the inf-sup condition in order to check the well posedness of the formulations. This is different to the previously discussed elements based on the Hellinger-Reissner formulation and tremendously simplifies the construction of stable elements. Due to the coercivity of $a(\boldsymbol{u}_h, \boldsymbol{u}_h)$ stable element approximations can always be achieved just by an adequate enrichment of U_h. However, unbalanced polynomial orders for the approximation of the displacements and pressures could lead to non optimal convergence orders.

5.5.1 Discontinuous Pressure Elements: $\mathrm{Q_1dP_0}$ and $\mathrm{T_2dP_0}$

Especially in the engineering community a common choice for the solution spaces is a continuous approximation for the displacements such that

$$\boldsymbol{u}_h \in U_h := \{\boldsymbol{u}_h \in [\mathcal{H}_0^1(\Omega)]^3,\, \boldsymbol{u}_h \text{ cont. on } \Omega : \boldsymbol{u}_h|_{\widehat{\Omega}^e} \in P \,\forall\, \Omega^e \in \Omega\}\,, \tag{5.58}$$

where $P = T_2$ in case of tetrahedral or $P = Q_1$ in case of hexahedral shaped elements, combined with a piecewise constant approximation for the pressure such that

$$p_h \in P_h := \{p_h \in \mathcal{L}^2(\Omega) : p_h|_{\widehat{\Omega}^e} \in T_0 \,\forall\, \Omega^e \in \Omega\}\,. \tag{5.59}$$

The corresponding elements, depicted in Figure 5.5, are denoted in the following as $\mathrm{T_2dP_0}$ and $\mathrm{Q_1dP_0}$, whereas the dP should emphasis the discontinuous pressure approximation. Especially the $\mathrm{Q_1dP_0}$ formulation is an omnipresent element in the framework of (nearly) incompressibility and that in defiance of the well known fact that it does not fulfill the inf-sup stability. However, it turned out that for the most engineering applications this instability does not occur and therefore this element is widely used, see Wriggers [2008]. In case of the 3D version of the $\mathrm{T_2dP_0}$ element the inf-sup condition does also not hold, as mentioned in Boffi et al. [2013], even if the plane strain complement is well posed in the incompressible limit. The consequence of the inf-sup failure is that existence and uniqueness of the pressure field cannot be guaranteed, following Equation (3.21). A main advantage of the discontinuous approximation of the pressure is that in the non incompressible case a static condensation can be performed, which leads to a generalized displacement formulation with a positive definite system matrix and a reduced number of degrees of freedom.

5.5.2 Continuous Pressure Element: $\mathrm{T_2T_1}$

The most common representatives of continuous pressure elements are related to the family proposed by Hood and Taylor [1974]. These elements are described by a continuous approximation for both, displacements and pressure, whereas the polynomial order for the displacements is one order higher than for the pressure. In this work we will focus on the lowest order tetrahedral shaped Hood-Taylor element, which will be denoted in the following as $\mathrm{T_2P_1}$, also depicted in Figure 5.5. The corresponding solution spaces for the displacements are

$$\boldsymbol{u}_h \in U_h := \{\boldsymbol{u}_h \in [\mathcal{H}_0^1(\Omega)]^3,\, \boldsymbol{u}_h \text{ cont. on } \Omega : \boldsymbol{u}_h|_{\widehat{\Omega}^e} \in T_2 \,\forall\, \Omega^e \in \Omega\}\,, \tag{5.60}$$

and for the pressure

$$p_h \in P_h := \{p_h \in \mathcal{L}^2(\Omega),\, p_h \text{ cont. on } \Omega : p_h|_{\widehat{\Omega}^e} \in T_1 \,\forall\, \Omega^e \in \Omega\}\,. \tag{5.61}$$

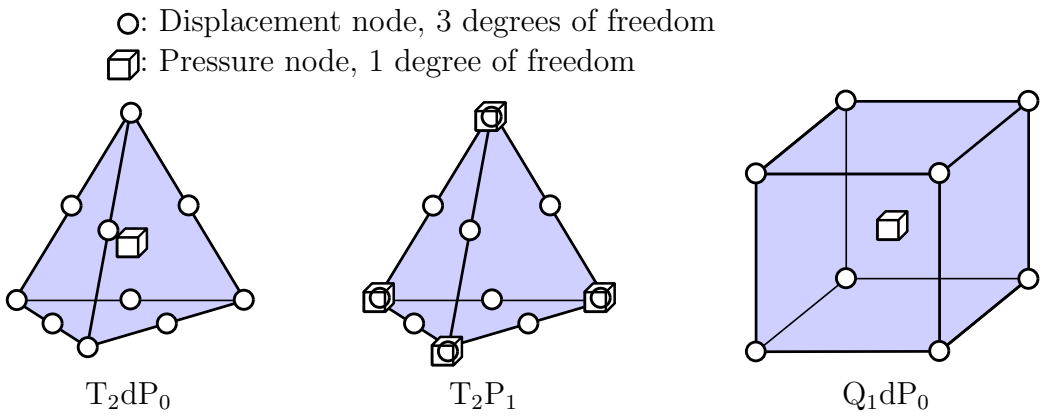

Figure 5.5: Sketch of the displacement-pressure based elements.

It has been shown in Boffi [1994; 1997], that the whole family of Hood-Taylor elements fulfills the inf-sup conditions and thus is well-posed also in the case of incompressibility. A drawback of these elements is that the resulting system matrix cannot be reduced, since the pressure is approximated continuously. Also a hybridization technique cannot be performed with a reasonable computational cost, as e.g. done in Chapter 5.4.2, since the pressure related degrees of freedom are associated to the nodes and therefore linked to too many neighboring elements. Thus, solving procedures have to be chosen which can treat indefinite system matrices.

Implementation: The approximation of the geometry, displacements, its gradient and virtual counterparts are given by Equation (5.18) and (5.20). In addition the pressure field and its virtual counterpart are approximated by

$$p_h = \sum_{I=1}^{n_{\text{p-nodes}}} \widehat{N}^I(\boldsymbol{\xi})\, \eta^I = \widehat{\mathbb{N}}\, \boldsymbol{\eta}\,, \quad \delta p_h = \sum_{I=1}^{n_{\text{p-nodes}}} \widehat{N}^I(\boldsymbol{\xi})\, \delta\eta^I = \widehat{\mathbb{N}}\, \delta\boldsymbol{\eta} \tag{5.62}$$

where η^I is the pressure related degree of freedom, $\boldsymbol{\eta}$ its related vector of element unknowns, $n_{\text{p-nodes}}$ the number of pressure related nodes and $\widehat{N}^I$ denotes the Lagrangian type interpolation function corresponding to the interpolation order of the pressure. The discrete weak form of Equation (5.56) follows for a typical element e as

$$\begin{aligned}\Big(\underbrace{\int_{\Omega^e} \mu \frac{\partial^2(\boldsymbol{\varepsilon}(\boldsymbol{u}_h) : \boldsymbol{\varepsilon}(\boldsymbol{u}_h))}{\partial \boldsymbol{d}\, \partial \boldsymbol{d}}\, \mathrm{d}V}_{\boldsymbol{k}^e_{uu}}\, \boldsymbol{d} + \underbrace{\int_{\Omega^e} \frac{\partial^2(\mathrm{Div}[\boldsymbol{u}_h]\, p_h)}{\partial \boldsymbol{d}\, \partial \boldsymbol{\eta}}\, \mathrm{d}V}_{\boldsymbol{k}^e_{up}}\, \boldsymbol{\eta} \ldots \\ \ldots \underbrace{- \int_{\Omega^e} \frac{\partial(\boldsymbol{f} \cdot \boldsymbol{u}_h)}{\partial \boldsymbol{d}}\, \mathrm{d}V - \int_{\partial\Omega^e} \frac{\partial(\boldsymbol{t}_0 \cdot \boldsymbol{u}_h)}{\partial \boldsymbol{d}}\, \mathrm{d}A}_{\boldsymbol{r}^e_u} \Big) \cdot \delta\boldsymbol{d} = 0\,, \end{aligned} \tag{5.63}$$

$$\Big(\underbrace{\int_{\Omega^e} \frac{\partial^2(\mathrm{Div}[\boldsymbol{u}_h]\, p_h)}{\partial \boldsymbol{\eta}\, \partial \boldsymbol{d}}\, \mathrm{d}V}_{\boldsymbol{k}^e_{pu}}\, \boldsymbol{d} \underbrace{- \int_{\Omega^e} \frac{1}{2\Lambda} \frac{\partial^2({p_h}^2)}{\partial \boldsymbol{\eta}\, \partial \boldsymbol{\eta}}\, \mathrm{d}V}_{\boldsymbol{k}^e_{pp}}\, \boldsymbol{\eta} \Big) \cdot \delta\boldsymbol{\eta} = 0\,.$$

	$(\widehat{\varepsilon}_{11}, \widehat{\varepsilon}_{22}, \widehat{\varepsilon}_{33})^T\|_{\widehat{\Omega}} \in$	$(\widehat{\varepsilon}_{23}, \widehat{\varepsilon}_{13}, \widehat{\varepsilon}_{12})^T\|_{\widehat{\Omega}} \in$	Reference	Equivalent AS element
$\text{EAS}_{\widetilde{9}}$	$A_0 \oplus B_1 \oplus B_2$	$\emptyset$	[81]	AS_{30}
EAS_{15}	$A_0 \oplus B_1 \oplus B_2$	$A_1 \oplus A_2$	[92]	AS_{24}
EAS_{21}	$A_0 \oplus B_1 \oplus B_2$	$A_1 \oplus A_2 \oplus B_1 \oplus B_2$	[2]	AS_{18}

Table 5.2: Considered polynomial bases for the enhanced strains in the EAS elements and the corresponding equivalent AS elements.

Assembling yields the global system of equations as

$$\overset{num_{ele}}{\underset{e=1}{\mathbf{A}}} \begin{bmatrix} \delta \boldsymbol{d} \\ \delta \boldsymbol{\eta} \end{bmatrix}^T \left(\begin{bmatrix} \boldsymbol{k}^e_{uu} & \boldsymbol{k}^e_{up} \\ \boldsymbol{k}^e_{pu} & \boldsymbol{k}^e_{pp} \end{bmatrix} \begin{bmatrix} \boldsymbol{d} \\ \boldsymbol{\eta} \end{bmatrix} + \begin{bmatrix} \boldsymbol{r}^e_u \\ \boldsymbol{0} \end{bmatrix} \right) = 0 \,, \tag{5.64}$$

whereas in the incompressible case with $\Lambda \to \infty$ the matrix $\boldsymbol{k}^e_{pp}$ approaches $\boldsymbol{0}$, resulting into a classical saddle-point structure.

5.6 Enhanced Assumed Strain Elements

The pioneering idea of the enhanced assumed strain method has been proposed in the works of Simo and Rifai [1990], Pantuso and Bathe [1995] and is used in this thesis only for comparison purposes. Therefore, the related theoretical framework is just briefly sketched and the interested reader is referred for a detailed analysis to Reddy and Simo [1995], Braess [1998] and Braess et al. [2004]. The underlying variational formulation can be embedded into the Hu-Washizu framework with the displacements $\boldsymbol{u}$, stresses $\boldsymbol{\sigma}$ and an enhanced strain field $\widehat{\boldsymbol{\varepsilon}}$ as the underlying field quantities. The enhanced strains augment the displacement-related strains additively. The essential idea is the orthogonal approximation of stresses and enhanced strains, such that the stress field can be eliminated directly on the level of the variational formulation. This results in a discrete two field problem in terms of the displacements and enhanced strains. An approximate solution $\boldsymbol{u}_h \in U_h$ and $\widehat{\boldsymbol{\varepsilon}}_h \in \widehat{E}_h$ is computed, with the conforming approximation spaces

$$\begin{aligned} U_h &:= \{\boldsymbol{u}_h \in [\mathcal{H}^1_0(\Omega)]^3,\, \boldsymbol{u}_h \text{ cont. on } \Omega : \boldsymbol{u}_h|_{\widehat{\Omega}^e} \in Q_1 \,\forall\, \Omega^e \in \Omega\} \\ \widehat{E}_h &:= \{\widehat{\boldsymbol{\varepsilon}}_h \in [\mathcal{L}^2(\Omega)]^{3\times 3}_{\text{sym}} : \widehat{\boldsymbol{\varepsilon}}_h|_{\widehat{\Omega}^e} \in E^{\square} \subset Q_1 \,\forall\, \Omega^e \in \Omega\} \,. \end{aligned} \tag{5.65}$$

We consider different discretizations schemes for the enhanced assumed strains, which are constructed by direct sums of the bases given in Equation (5.2). The considered combinations for $E^{\square} \subset Q_1$ are summarized in Table 5.2. In addition, the Table indicates the primary literature of the approximation scheme and the corresponding equivalent assumed stress element, with regard to Chapter 5.2.3. The discrete formulation follows by

$$\begin{aligned} a(\boldsymbol{u}_h, \delta\boldsymbol{u}_h) + b(\delta\boldsymbol{u}_h, \widehat{\boldsymbol{\varepsilon}}_h) &= F_v(\delta\boldsymbol{u}_h) \quad \forall\, \delta\boldsymbol{u}_h \in U_h \,, \\ b(\boldsymbol{u}_h, \delta\widehat{\boldsymbol{\varepsilon}}_h) + \int_\Omega \widehat{\boldsymbol{\varepsilon}}_h : \mathbb{C} : \delta\widehat{\boldsymbol{\varepsilon}}_h \, \mathrm{d}V &= F_w(\delta\widehat{\boldsymbol{\varepsilon}}_h) \quad \forall\, \delta\widehat{\boldsymbol{\varepsilon}}_h \in \widehat{E}_h \,. \end{aligned} \tag{5.66}$$

It should be recognized that due to the additional term in Equation $(5.66)_2$ the formulation does not fit into the proposed abstract mixed variational formulation and therefore a

discussion on the well posedness of these element formulations is omitted. However, the element characteristic of the enhanced assumed strain elements can be directly adopted from their equivalent assumed stress elements. The discrete bilinear forms and right hand sides are given by

$$\begin{aligned} a(\boldsymbol{u}_h, \delta\boldsymbol{u}_h) &:= \int_\Omega \boldsymbol{\varepsilon}(\boldsymbol{u}_h) : \mathbb{C} : \boldsymbol{\varepsilon}(\delta\boldsymbol{u}_h)\, \mathrm{d}V\,, \\ b(\delta\boldsymbol{u}_h, \widehat{\boldsymbol{\varepsilon}}_h) &:= \int_\Omega \boldsymbol{\varepsilon}(\delta\boldsymbol{u}_h) : \mathbb{C} : \widehat{\boldsymbol{\varepsilon}}_h\, \mathrm{d}V\,, \\ F_v(\delta\boldsymbol{u}_h) &:= \int_{\partial\Omega_t} \bar{\boldsymbol{t}}_0 \cdot \delta\boldsymbol{u}_h\, \mathrm{d}A + \int_\Omega \boldsymbol{f} \cdot \delta\boldsymbol{u}_h\, \mathrm{d}V\,, \\ b(\boldsymbol{u}_h, \delta\widehat{\boldsymbol{\varepsilon}}_h) &:= \int_\Omega \boldsymbol{\varepsilon}(\boldsymbol{u}_h) : \mathbb{C} : \delta\widehat{\boldsymbol{\varepsilon}}_h\, \mathrm{d}V\,, \\ G_w(\delta\widehat{\boldsymbol{\varepsilon}}_h) &:= 0. \end{aligned} \tag{5.67}$$

Implementation: The approximation of the geometry, displacements and its gradient and virtual counterparts are given by Equation (5.18) and (5.20). Note that for this formulation N^I is restricted to trilinear Lagrangian interpolation functions. In addition the enhanced assumed strain field is approximated in the parametric space in Voigt type vector notation by

$$\underline{\widehat{\boldsymbol{\varepsilon}}}_\xi = (\widehat{\boldsymbol{\varepsilon}}_{\xi\xi}, \widehat{\boldsymbol{\varepsilon}}_{\eta\eta}, \widehat{\boldsymbol{\varepsilon}}_{\zeta\zeta}, \widehat{\boldsymbol{\varepsilon}}_{\xi\eta}, \widehat{\boldsymbol{\varepsilon}}_{\eta\zeta}, \widehat{\boldsymbol{\varepsilon}}_{\xi\zeta}) = \mathbb{M}_\xi\, \boldsymbol{\alpha} \tag{5.68}$$

whereas only the six independent strain components have to be considered due to the symmetry of the strain tensor and $\boldsymbol{\alpha}$ denotes the vector of element wise unknowns related to the enhanced strain field. The interpolation matrix $\mathbb{M}_\xi$ has the general structure

$$\mathbb{M}_\xi = \mathrm{diag}(\mathbb{M}_{\xi\xi}, \mathbb{M}_{\eta\eta}, \mathbb{M}_{\zeta\zeta}, \mathbb{M}_{\xi\eta}, \mathbb{M}_{\eta\zeta}, \mathbb{M}_{\xi\zeta}) \tag{5.69}$$

and contains the corresponding interpolation functions. The explicit forms are given in the following subchapter. The transformation from the isoparametric domain to the physical space for the enhanced strains is described by

$$\widehat{\boldsymbol{\varepsilon}}_h = \frac{\det \boldsymbol{J}_0}{\det \boldsymbol{J}} \boldsymbol{J}_0^{-T}\, \widehat{\boldsymbol{\varepsilon}}_\xi\, \boldsymbol{J}_0^{-1} \quad \text{with } \widehat{\boldsymbol{\varepsilon}}_\xi = \begin{pmatrix} \widehat{\boldsymbol{\varepsilon}}_{\xi\xi} & \widehat{\boldsymbol{\varepsilon}}_{\xi\eta} & \widehat{\boldsymbol{\varepsilon}}_{\xi\zeta} \\ \widehat{\boldsymbol{\varepsilon}}_{\xi\eta} & \widehat{\boldsymbol{\varepsilon}}_{\eta\eta} & \widehat{\boldsymbol{\varepsilon}}_{\eta\zeta} \\ \widehat{\boldsymbol{\varepsilon}}_{\xi\zeta} & \widehat{\boldsymbol{\varepsilon}}_{\eta\zeta} & \widehat{\boldsymbol{\varepsilon}}_{\zeta\zeta} \end{pmatrix} \tag{5.70}$$

where the mapping between the isoparametric coordinates $\boldsymbol{\xi}$ and the reference coordinates $\boldsymbol{X}$ follows by Equation (5.34). The discretized weak form in Equation (5.66) follows a typical element e as

$$\begin{aligned} \Bigg(\underbrace{\int_{\Omega^e} \frac{\partial^2(\frac{1}{2}\boldsymbol{\varepsilon}(\boldsymbol{u}_h) : \mathbb{C} : \boldsymbol{\varepsilon}(\boldsymbol{u}_h))}{\partial \boldsymbol{d}\, \partial \boldsymbol{d}}\, \mathrm{d}V}_{\boldsymbol{k}^e_{uu}}\, \boldsymbol{d} + \underbrace{\int_{\Omega^e} \frac{\partial^2(\boldsymbol{\varepsilon}(\boldsymbol{u}_h) : \mathbb{C} : \widehat{\boldsymbol{\varepsilon}}_h)}{\partial \boldsymbol{d}\, \partial \boldsymbol{\alpha}}\, \mathrm{d}V}_{\boldsymbol{k}^e_{u\varepsilon}}\, \boldsymbol{\alpha} \ldots \\ \ldots \underbrace{- \int_{\Omega^e} \frac{\partial(\boldsymbol{f} \cdot \boldsymbol{u}_h)}{\partial \boldsymbol{d}}\, \mathrm{d}V - \int_{\partial\Omega^e} \frac{\partial(\boldsymbol{t} \cdot \boldsymbol{u}_h)}{\partial \boldsymbol{d}}\, \mathrm{d}A}_{\boldsymbol{r}^e_u} \Bigg) \cdot \delta\boldsymbol{d} = 0\,, \end{aligned} \tag{5.71}$$

$$\Bigg(\underbrace{\int_{\Omega^e} \frac{\partial^2(\boldsymbol{\varepsilon}(\boldsymbol{u}_h) : \mathbb{C} : \widehat{\boldsymbol{\varepsilon}}_h)}{\partial \boldsymbol{\alpha}\, \partial \boldsymbol{d}}\, \mathrm{d}V}_{\boldsymbol{k}^e_{\varepsilon u}}\, \boldsymbol{d} + \underbrace{\int_{\Omega^e} \frac{\partial^2(\frac{1}{2}\widehat{\boldsymbol{\varepsilon}}_h : \mathbb{C} : \widehat{\boldsymbol{\varepsilon}}_h)}{\partial \boldsymbol{\alpha}\, \partial \boldsymbol{\alpha}}\, \mathrm{d}V}_{\boldsymbol{k}^e_{\varepsilon\varepsilon}}\, \boldsymbol{\alpha} \Bigg) \cdot \delta\boldsymbol{\alpha} = 0\,.$$

Therefore the global system of equations is given by

$$\overset{num_{ele}}{\underset{e=1}{\mathbf{A}}} \begin{bmatrix} \delta \boldsymbol{d} \\ \delta \boldsymbol{\alpha} \end{bmatrix}^T \left(\begin{bmatrix} \boldsymbol{k}^e_{uu} & \boldsymbol{k}^e_{u\varepsilon} \\ \boldsymbol{k}^e_{\varepsilon u} & \boldsymbol{k}^e_{\varepsilon\varepsilon} \end{bmatrix} \begin{bmatrix} \boldsymbol{d} \\ \boldsymbol{\alpha} \end{bmatrix} + \begin{bmatrix} \boldsymbol{r}^e_u \\ \boldsymbol{0} \end{bmatrix} \right) = 0 \,. \tag{5.72}$$

In order to obtain a reduced system size, a static condensation can be applied already on element level. Therefore, the degrees of freedom associated to the enhanced strains are solved on the individual element level with respect to the displacements. This leads to a global system of equations where only the degrees of freedom associated to the displacements are the remaining unknowns. The condensed form is given for a typical element e by

$$\delta \boldsymbol{d}^T (\underbrace{\boldsymbol{k}^e_{uu} - \boldsymbol{k}^e_{u\varepsilon} \, (\boldsymbol{k}^e_{\varepsilon\varepsilon})^{-1} \, \boldsymbol{k}^e_{\varepsilon u}}_{\boldsymbol{k}^e_{\text{red}}} \boldsymbol{d} + \boldsymbol{r}^e_u) = 0 \,. \tag{5.73}$$

Assembling of all element stiffness matrices and element residual vectors yield the global stiffness matrix $\boldsymbol{K}_{\text{red}}$ and residual vector $\boldsymbol{R}_{\text{red}}$ as

$$\boldsymbol{K}_{\text{red}} = \overset{num_{ele}}{\underset{e=1}{\mathbf{A}}} \boldsymbol{k}^e_{\text{red}} \,, \quad \boldsymbol{R}_{\text{red}} = \overset{num_{ele}}{\underset{e=1}{\mathbf{A}}} \boldsymbol{r}^e_u \,. \tag{5.74}$$

Thus the global nodal displacements can be computed by $\boldsymbol{D} = -\boldsymbol{K}^{-1}_{\text{red}} \boldsymbol{R}_{\text{red}}$.

Enhanced Assumed Strain Interpolation: As already annotated in Table 5.2, three different discretization schemes for the enhanced assumed strains are considered. In particular they are chosen such that the resulting elements are equivalent to the already discussed assumed stress elements if in addition the condition of a constant Jacobian is fulfilled, see Chapter 5.2.3. The counterpart of the AS_{30} element is given by an interpolation scheme which has been proposed recently in the large strain framework by Krischok and Linder [2016]. It contains 9 enhanced parameters and the interpolation matrices follow by

$$\begin{aligned} \mathbb{M}_{\xi\xi} &= (\xi, \, \xi\eta, \, \xi\zeta) \\ \mathbb{M}_{\eta\eta} &= (\eta, \, \eta\zeta, \, \eta\xi) \\ \mathbb{M}_{\zeta\zeta} &= (\zeta, \, \zeta\xi, \, \zeta\eta) \\ \mathbb{M}_{\xi\eta} &= \emptyset \\ \mathbb{M}_{\eta\zeta} &= \emptyset \\ \mathbb{M}_{\xi\zeta} &= \emptyset \end{aligned} \tag{5.75}$$

9 enhanced strain modes

In order to avoid confusion, it should be highlighted that this formulation differs from the originally EAS element, proposed by Simo and Rifai [1990], which also contains 9 enhanced modes. The formulation containing 15 enhanced modes for the strains is the counterpart to the AS_{24} element. The EAS_{15} discretization scheme goes back to the work

of PANTUSO AND BATHE [1995] and is given in detail by

$$\boxed{\begin{aligned}
\mathbb{M}_{\xi\xi} &= (\xi,\, \xi\eta,\, \xi\zeta) \\
\mathbb{M}_{\eta\eta} &= (\eta,\, \eta\zeta,\, \eta\xi) \\
\mathbb{M}_{\zeta\zeta} &= (\zeta,\, \zeta\xi,\, \zeta\eta) \\
\mathbb{M}_{\xi\eta} &= (\xi,\, \eta) \\
\mathbb{M}_{\eta\zeta} &= (\eta,\, \zeta) \\
\mathbb{M}_{\xi\zeta} &= (\xi,\, \zeta)
\end{aligned}} \qquad (5.76)$$

15 enhanced strain modes

The third considered formulation, which contains 21-enhanced strain parameters, is equivalent to the element AS_{18} whereas the interpolation matrix corresponds to

$$\boxed{\begin{aligned}
\mathbb{M}_{\xi\xi} &= (\xi,\, \xi\eta,\, \xi\zeta) \\
\mathbb{M}_{\eta\eta} &= (\eta,\, \eta\zeta,\, \eta\xi) \\
\mathbb{M}_{\zeta\zeta} &= (\zeta,\, \zeta\xi,\, \zeta\eta) \\
\mathbb{M}_{\xi\eta} &= (\xi,\, \eta,\, \xi\zeta,\, \eta\zeta) \\
\mathbb{M}_{\eta\zeta} &= (\eta,\, \zeta,\, \xi\eta,\, \xi\zeta) \\
\mathbb{M}_{\xi\zeta} &= (\xi,\, \zeta,\, \xi\eta,\, \zeta\eta)
\end{aligned}} \qquad (5.77)$$

21 enhanced strain modes

Displacement based elements:	
T_1	Tetrahedral shaped element with linear interpolation
T_2	Tetrahedral shaped element with quadratic interpolation
Q_1	Hexahedral shaped element with trilinear interpolation
Hellinger-Reissner based elements:	
AS_{39}	Hexahedral shaped element with trilinear interpolation for the displacements and 39 parameters for the stress interpolation (equivalent to Q_1).
AS_{30}	Hexahedral shaped element with trilinear interpolation for the displacements and 30 parameters for the stress interpolation.
AS_{24}	Hexahedral shaped element with trilinear interpolation for the displacements and 24 parameters for the stress interpolation.
AS_{18}	Hexahedral shaped element with trilinear interpolation for the displacements and 18 parameters for the stress interpolation.
RT_0T_1	Tetrahedral shaped element with linear interpolation for the displacements and lowest order Raviart-Thomas interpolation for the stresses.
Displacement pressure elements:	
Q_1dP_0	Hexahedral shaped element with trilinear interpolation of the displacements and piecewise constant pressure approximation.
T_2dP_0	Tetrahedral shaped element with quadratic interpolation of the displacements and piecewise constant pressure approximation.
T_2P_1	Tetrahedral shaped element with quadratic interpolation of the displacements and continuous linear pressure approximation.
Enhanced assumed strain elements:	
$EAS_{\widetilde{9}}$	Hexahedral shaped element with trilinear interpolation for the displacements and 9 enhanced strain parameters (equivalent to AS_{30}).
EAS_{15}	Hexahedral shaped element with trilinear interpolation for the displacements and 15 enhanced strain parameters (equivalent to AS_{24}).
EAS_{21}	Hexahedral shaped element with trilinear interpolation for the displacements and 21 enhanced strain parameters (equivalent to AS_{18}).

Table 5.3: Summary of the proposed elements and their abbreviations

5.7 Numerical Examples

In the following chapter different meaningful examples are considered in order to investigate the numerical behavior of the proposed finite elements for linear elasticity. Despite some of these results are already known from the analysis on the well posedness of the element formulation, the numerical effects are additionally shown and discussed. Each test is constructed such that a special characteristic of the finite element discretizations is examined. They comprise in detail the inf-sup test, a regular boundary value problem and a pure bending problem. Throughout these numerical examples the different characteristics of the elements are discussed and the results of the displacements and also the stresses are compared to each other and if available to the analytical solution. Table 5.3 summarizes the proposed elements. For sake of brevity, only meshes with hexahedral shaped elements will be depicted in the following. The corresponding tetrahedral meshes are constructed by a subdivision of the hexahedral element into five tetrahedral elements, as exemplary depicted in Figure 5.6.

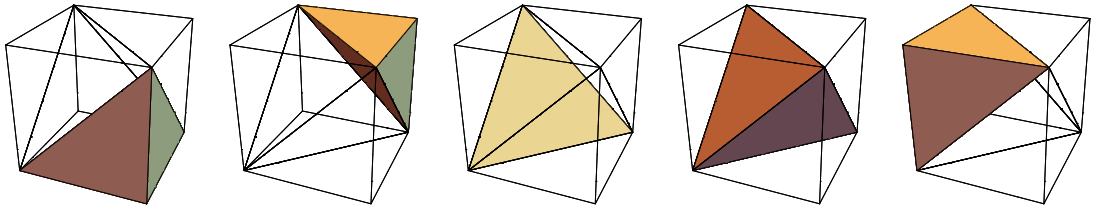

Figure 5.6: Exemplary subdivision of a hexahedral element into five tetrahedral elements.

5.7.1 Inf-Sup Test

As extensively discussed, the satisfaction of the discrete inf-sup condition is a necessary condition in order to guarantee existence and uniqueness of the solution in the framework of mixed finite elements. Unfortunately, in many cases the analytical proof of it is cumbersome. Also a direct numerical evaluation of the analytical expression is impossible because an infinite number of problems must be taken into account. For the engineering praxis, a numerical inf-sup test has been proposed in Chapelle and Bathe [1993] and Bathe [1996; 2001]. The objective of this test is to verify numerically the inf-sup condition. For the proposed Hellinger-Reissner based formulations the discrete inf-sup condition is satisfied if there exists a positive value $c_{b,1}$, which is independent of the mesh, such that

$$\sup_{\boldsymbol{\sigma}_h \in \Sigma_h} \frac{\left| \int_\Omega \boldsymbol{\sigma}_h : \boldsymbol{\varepsilon}(\boldsymbol{u}_h) \, \mathrm{d}V \right|}{\|\boldsymbol{\sigma}_h\|_{\mathcal{L}^2}} \geq c_{b,1} \, \|\boldsymbol{\varepsilon}(\boldsymbol{u}_h)\|_{\mathcal{L}^2} \quad \forall \, \boldsymbol{u}_h \in U_h, \tag{5.78}$$

whereas Korn's inequality has been exploited on the right hand side in order to use the $\mathcal{L}^2$-norm of $\boldsymbol{\varepsilon}(\boldsymbol{u}_h)$ instead of the $\mathcal{H}^1$-norm of $\boldsymbol{u}_h$. It has been shown, e.g in Brezzi and Fortin [1991], that the square root of the smallest non zero eigenvalue, denoted by λ_p, of the following eigenvalue problem

$$\boldsymbol{B}^T \boldsymbol{T}^{-1} \boldsymbol{B} \, \boldsymbol{d} = \lambda_p \, \boldsymbol{A} \, \boldsymbol{d} \tag{5.79}$$

is equivalent to the inf-sup constant $c_{b,1}$, where the matrices are computed by

$$\begin{aligned} \int_\Omega \boldsymbol{\sigma}_h : \boldsymbol{\varepsilon}(\boldsymbol{u}_h)\,\mathrm{d}V &= \boldsymbol{\beta}^T \boldsymbol{B}\,\boldsymbol{d}\,, \\ \int_\Omega \boldsymbol{\sigma}_h : \boldsymbol{\sigma}_h\,\mathrm{d}V &= \boldsymbol{\beta}^T \boldsymbol{T}\,\boldsymbol{\beta}\,, \\ \int_\Omega \boldsymbol{\varepsilon}(\boldsymbol{u}_h) : \boldsymbol{\varepsilon}(\boldsymbol{u}_h)\,\mathrm{d}V &= \boldsymbol{d}^T \boldsymbol{A}\,\boldsymbol{d}\,. \end{aligned} \tag{5.80}$$

In case of the displacement pressure formulations the discrete inf-sup conditions reads as

$$\sup_{\boldsymbol{u}_h \in U_h} \frac{\left|\int_\Omega \mathrm{Div}[\boldsymbol{u}_h]\, p_h\,\mathrm{d}V\right|}{\|\boldsymbol{\varepsilon}(\boldsymbol{u}_h)\|_{\mathcal{L}^2}} \geq c_{b,1}\,\|p_h\|_{\mathcal{L}^2} \quad \forall\, p_h \in P_h. \tag{5.81}$$

Therefore the corresponding eigenvalue problem follows as

$$\boldsymbol{B}^T\,\boldsymbol{T}^{-1}\,\boldsymbol{B}\,\boldsymbol{\eta} = \lambda_p\,\boldsymbol{A}\,\boldsymbol{\eta} \tag{5.82}$$

where the matrices are given by

$$\begin{aligned} \int_\Omega \mathrm{Div}[\boldsymbol{u}_h]\, p_h\,\mathrm{d}V &= \boldsymbol{d}^T \boldsymbol{B}\,\boldsymbol{\eta}\,, \\ \int_\Omega \boldsymbol{\varepsilon}(\boldsymbol{u}_h) : \boldsymbol{\varepsilon}(\boldsymbol{u}_h)\,\mathrm{d}V &= \boldsymbol{d}^T \boldsymbol{T}\,\boldsymbol{d}\,, \\ \int_\Omega p_h^2\,\mathrm{d}V &= \boldsymbol{\eta}^T \boldsymbol{A}\,\boldsymbol{\eta}\,. \end{aligned} \tag{5.83}$$

In order to evaluate the inf-sup constant in a numerical test, a simple supported rectangle in 2D with a consecutive number of uniform mesh refinements has been investigated in Chapelle and Bathe [1993] for different mixed finite elements. In this fashion a simple supported unit cube $\Omega = (0,1)^3$ is considered where the proposed Hellinger-Reissner

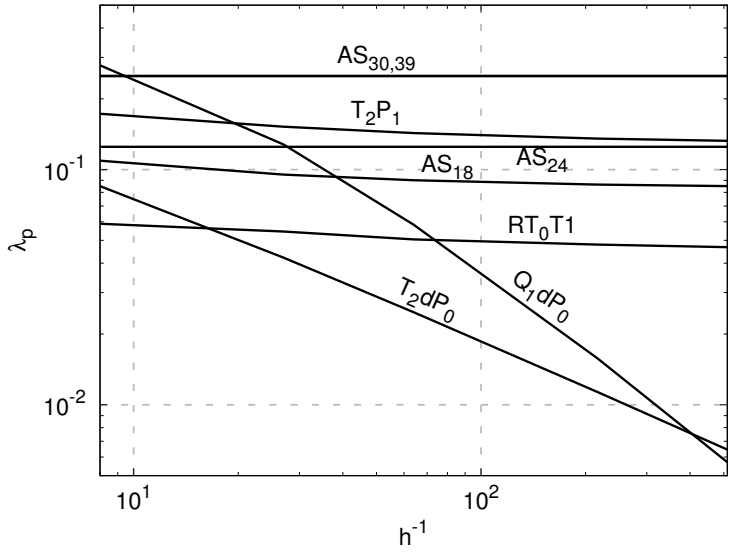

Figure 5.7: Inf-Sup test; λ_p over the inverse element size h.

based elements and displacement-pressure elements are investigated. The corresponding eigenvalue problems of Equations (5.79) and (5.82) are solved for a consecutive refinement of a regular mesh. The smallest non zero eigenvalue is depicted over the inverse of the element size h in Figure 5.7. The elements satisfy the inf-sup test if λ_p is bounded away from zero, independent of the mesh density. For a couple of the considered element formulations an analytical statement on the discrete inf-sup criterium has already been discussed in the previous chapters. The analytical outcomes are approved by the numerical results. It is shown that all proposed Hellinger-Reissner based formulations and the Hood Taylor element $\mathrm{T_2P_1}$ satisfy the inf-sup test, whereas the $\mathrm{T_2dP_0}$ and the $\mathrm{Q_1dP_0}$ fail [1.)].

5.7.2 Volumetric Locking: A Regular Problem

The following numerical example is a regular problem consisting of a unit cube $\Omega = (0,1)^3$ with homogeneous displacement boundary conditions, i.e. $\boldsymbol{u}_h = \boldsymbol{0}$ on $\partial\Omega$, and a non-trivial body force $\boldsymbol{f}$. The analytical solution for this boundary value problem has been proposed by Qi et al. [2005]. The body force is given by the fourth order polynomial function

$$\boldsymbol{f} = \begin{bmatrix} -400\mu(2x_2-1)(2x_3-1)(3(x_1^2-x_1)^2(x_2^2-x_2+x_3^2-x_3)+ \\ \quad 200\mu(2x_3-1)(2x_1-1)(3(x_2^2-x_2)^2(x_3^2-x_3+x_1^2-x_1)+ \quad \dots \\ \quad 200\mu(2x_1-1)(2x_2-1)(3(x_3^2-x_3)^2(x_1^2-x_1+x_2^2-x_2)+ \end{bmatrix}$$

$$\begin{bmatrix} (1-6x_1+6x_1^2)(x_2^2-x_2)(x_3^2-x_3)) \\ \dots \quad (1-6x_2+6x_2^2)(x_3^2-x_3)(x_1^2-x_1)) \\ (1-6x_3+6x_3^2)(x_1^2-x_1)(x_2^2-x_2)) \end{bmatrix}. \tag{5.84}$$

The numerical example will be solved in a compressible framework, defined by the Lamé constants $\mu = 1$ and $\Lambda = 1$ and in a nearly incompressible setup $\mu = 1$ and $\Lambda = 10^6$. Thus this problem exposes the Λ-dependency of the discrete solution for the different element formulations. Furthermore it is distinguished between a regular mesh where each hexahedral element is a cuboid and a slightly perturbed mesh. The perturbation, exemplary depicted for the coarsest meshes in Figure 5.8, leads to non affine mappings from the isoparametric space to the physical space in case of the hexahedral elements and tetrahedral elements with quadratic interpolation of the displacements. Note that the perturbation is so small that the resulting mesh quality is still very good.

Results of the displacements: The analytical solution for the displacements is given by

$$\boldsymbol{u} = \begin{bmatrix} 200\mu(x_1-x_1^2)^2(2x_3^3-3x_3^2+x_3)(2x_2^3-3x_2^2+x_2) \\ -100\mu(x_2-x_2^2)^2(2x_1^3-3x_1^2+x_1)(2x_3^3-3x_3^2+x_3) \\ -100\mu(x_3-x_3^2)^2(2x_2^3-3x_2^2+x_2)(2x_1^3-3x_1^2+x_1) \end{bmatrix}. \tag{5.85}$$

We consider the mesh convergence of the $\mathcal{L}_2$-error of the displacements defined as

$$\|\boldsymbol{u}-\boldsymbol{u}_h\|_{\mathcal{L}_2} = \left(\int_\Omega (\boldsymbol{u}-\boldsymbol{u}_h)\cdot(\boldsymbol{u}-\boldsymbol{u}_h)\,\mathrm{d}V \right)^{1/2}. \tag{5.86}$$

[1.)] Note that the $\mathrm{T_2dP_0}$ is inf-sup stable in the plane strain setting, whereas the $\mathrm{Q_1dP_0}$ is not, see Boffi et al. [2013]

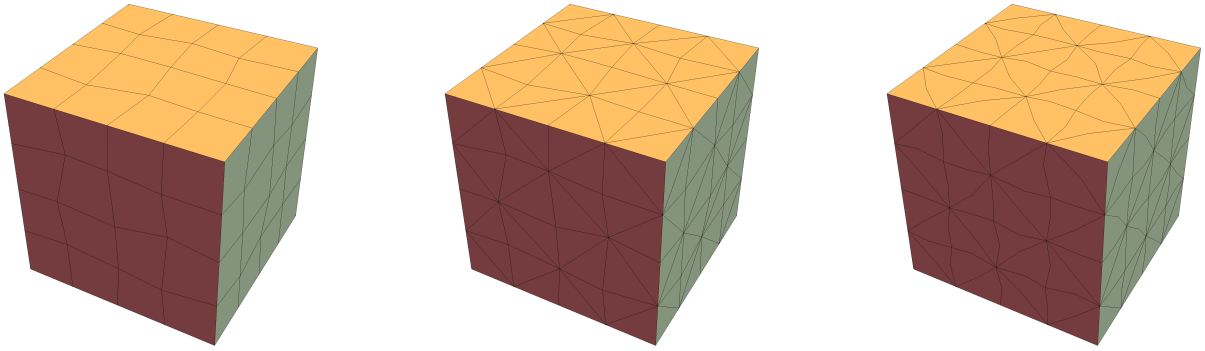

Q_1 T_1 T_2

Figure 5.8: Exemplary perturbed meshes.

Due to the regularity of the problem the error is uniformly distributed over the domain Ω and thus a regular mesh refinement is optimal and yields to the best possible convergence rate. Figure 5.9 depicts the error convergence of the displacements for the compressible case. It can be noted, that for both meshing strategies the convergence rate $\frac{k+1}{d}$ of all lowest order elements is close to the theoretically optimal value of

$$\|\boldsymbol{u} - \boldsymbol{u}_h\|_{\mathcal{L}_2} \leq c\, n_{\text{dof}}{}^{-\frac{k+1}{d}}, \tag{5.87}$$

where d denotes the spatial dimension and k the polynomial order of the displacement approximation. In fact, the convergence rate for the RT_0T_1 is even slightly superior, which is likely to be boundary value dependent and not the general case. In contrast, the elements with a nonlinear approximation of the displacements (T_2, T_2dP_0 and T_2P_1) suffer in the case of the perturbed mesh, which leads to a decrease of the convergence rate. In case of the computations with the regular structured meshes, the results of the assumed stress elements are identical (up to computer precision) as for their equivalent enhanced assumed strain counterparts, see Table 5.2, and correspond to a optimal order of convergence. The mesh perturbation leads to a marginal difference between those formulations, which is reasonable since the condition of a constant Jacobian is violated, compare Equation (5.8).

The results for the nearly incompressible case are considered in the Figures 5.10 a) and b). A strong locking behavior is observed for the T_1, Q_1 and AS_{39} already for the regular structured meshes. A decrease of the convergence rate is also recognized in case of the T_2, which evolves to be substantial for the perturbed meshes. These locking effects have already been predicted by the analysis on the well posedness in the previous chapter. For the regular structured meshes the remaining elements depict similar characteristics as in the compressible case, including the equivalence between the assumed stress and enhanced assumed strain elements. The mesh perturbation decreases the convergence rates for the T_2dP_0, the T_2P_1 and all EAS-elements. Thus, only the RT_0T_1, Q_1dP_0 and the assumed stress elements yield optimal results (in sense of Equation (5.87)) for the displacements regardless of the compressibility and mesh regularity.

a) Regular mesh:

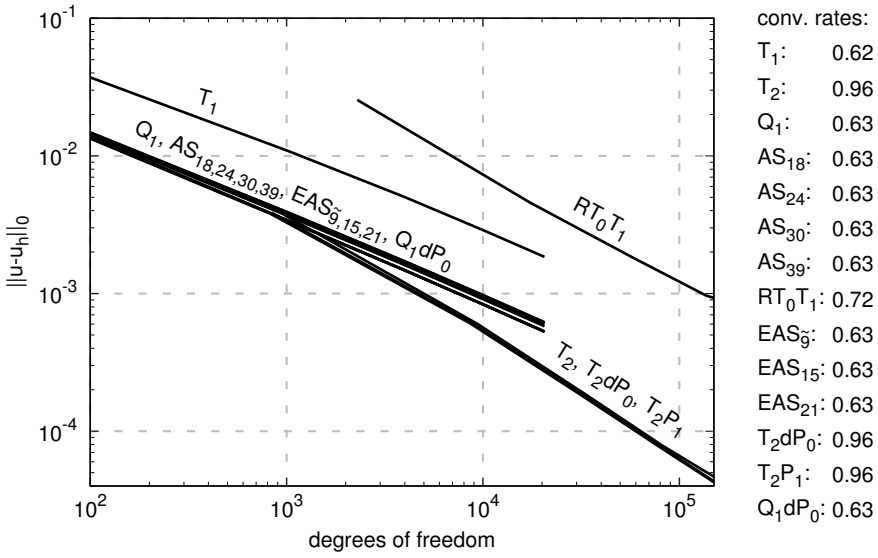

b) Perturbed mesh:

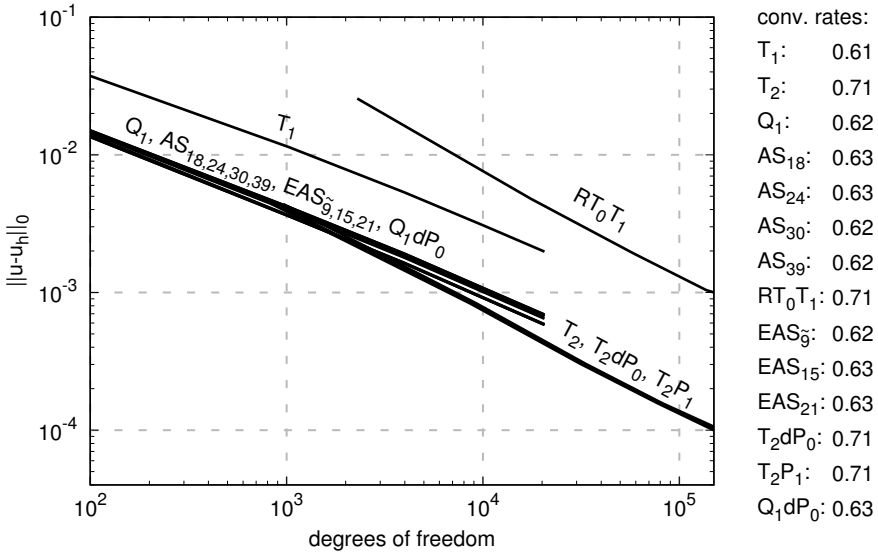

Figure 5.9: Regular problem with compressible material $\mu = 1$, $\Lambda = 1$; Convergence plot and corresponding rates of the displacement error over the degrees of freedom for regular structured meshes a) and perturbed meshes b).

a) Regular mesh:

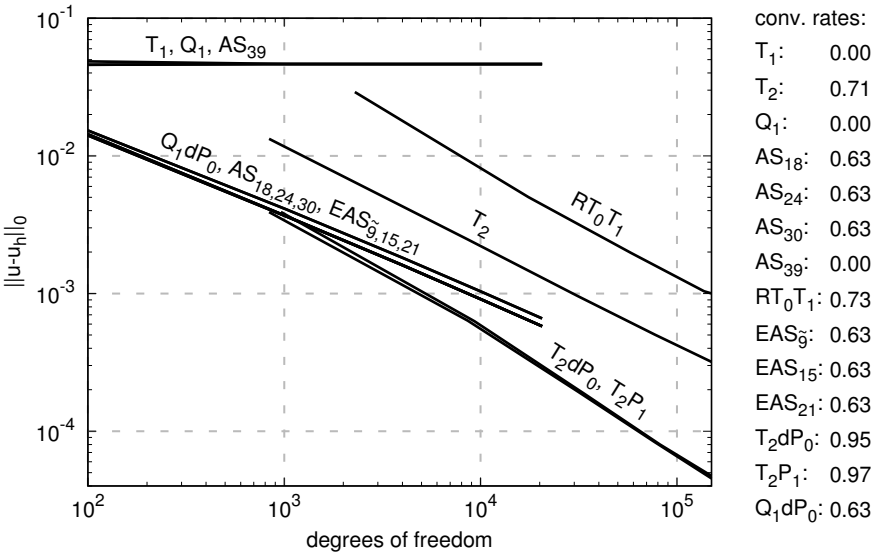

b) Perturbed mesh:

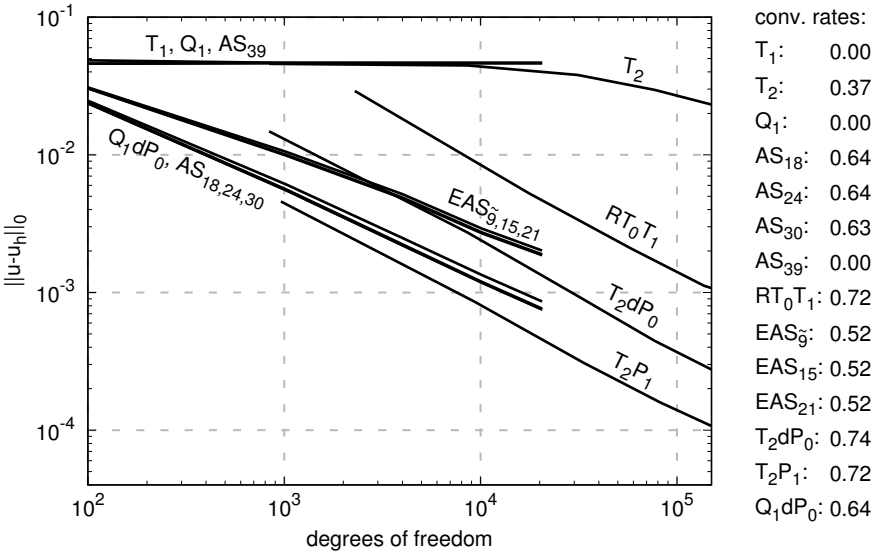

Figure 5.10: Regular problem with nearly incompressible material $\mu = 1, \Lambda = 10^6$; Convergence plot and corresponding rates of the displacement error over the degrees of freedom for regular structured meshes a) and perturbed meshes b).

Results of the stresses: The stresses, which are independent of the Lamé constant Λ result analytical into

$$\begin{bmatrix} \sigma_{11} \\ \sigma_{22} \\ \sigma_{33} \\ \sigma_{12} \\ \sigma_{23} \\ \sigma_{13} \end{bmatrix} = \begin{bmatrix} 800c_1(-1+2x_1)c_2(-1+2x_2)c_3(-1+2x_3)\mu^2 \\ -400c_1(-1+2x_1)c_2(-1+2x_2)c_3(-1+2x_3)\mu^2 \\ -400c_1(-1+2x_1)c_2(-1+2x_2)c_3(-1+2x_3)\mu^2 \\ 100(-(1+6c_1)c_2^2+2c_1^2(1+6c_2))c_3(-1+2x_3)\mu^2 \\ 100c_1(-1+2x_1)(-(1+6c_2)c_3^2-c_2^2(1+6c_3))\mu^2 \\ 100c_2(-1+2x_2)(-(1+6c_1)c_3^2+2c_1^2(1+6c_3))\mu^2 \end{bmatrix} \tag{5.88}$$

with $c_i = (x_i - 1)\, x_i$ (no summation). The convergence of the stress-error, defined as

$$\|\boldsymbol{\sigma} - \boldsymbol{\sigma}_h\|_{\mathcal{L}_2} = \left(\int_\Omega (\boldsymbol{\sigma} - \boldsymbol{\sigma}_h) : (\boldsymbol{\sigma} - \boldsymbol{\sigma}_h)\, \mathrm{d}V \right)^{1/2}, \tag{5.89}$$

is depicted in Figure 5.11 for the compressible case and Figure 5.12 for the nearly incompressible case. In the compressible case the results are closely related to the behavior of the displacement error. All elements show its optimal rate of convergence also for the perturbed mesh, with the exception of the second order tetrahedral elements T_2, $\mathrm{T}_2\mathrm{dP}_0$ and $\mathrm{T}_2\mathrm{P}_1$. However, in the framework of nearly incompressibility the resulting picture is different. In case of the regular mesh, all displacement based elements and the AS_{39} do not show convergence of the stresses at all. In addition also the $\mathrm{T}_2\mathrm{dP}_0$ depicts locking behavior. Optimal rate of convergences are still obtained by the $\mathrm{T}_2\mathrm{P}_1$, $\mathrm{Q}_1\mathrm{dP}_0$, $\mathrm{T}_2\mathrm{dP}_0$, $\mathrm{RT}_0\mathrm{T}_1$ and the remaining assumed stress and enhanced assumed strain elements. Consideration of Figure 5.12 b) shows that the enhanced assumed strain elements respond more sensitive to the mesh perturbation resulting in an error one order of magnitude larger compared to the $\mathrm{Q}_1\mathrm{dP}_0$ and assumed stress elements. In addition the convergence of the $\mathrm{T}_2\mathrm{P}_1$ is not uniform anymore due to the perturbed meshes. A reason for that can be found in the point that the finer mesh does not embed the coarse mesh in case of the perturbed meshes.

a) Regular mesh:

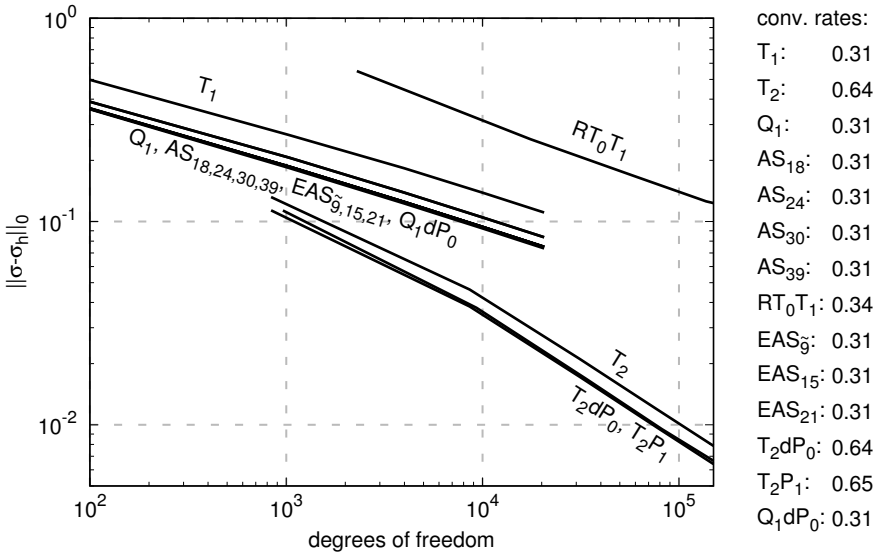

b) Perturbed mesh:

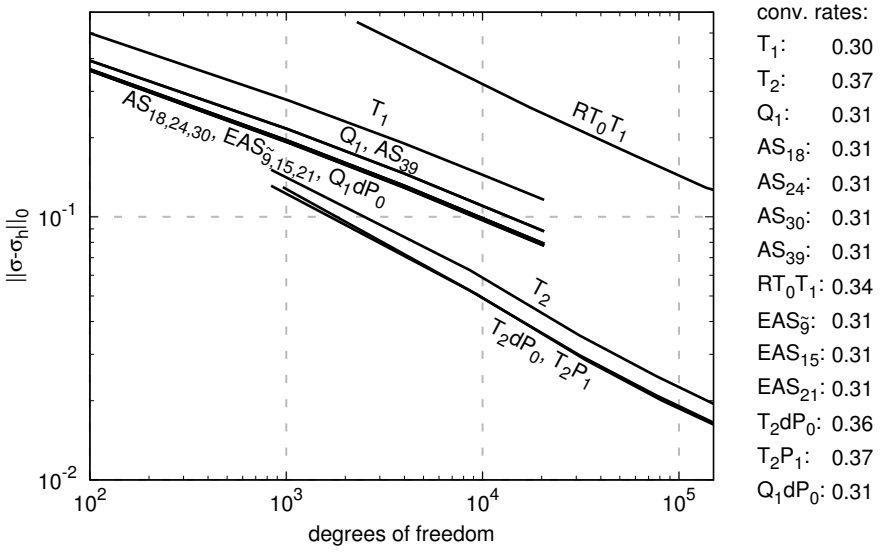

Figure 5.11: Regular problem with compressible material $\mu = 1$, $\Lambda = 1$; Convergence plot and corresponding rates of the stress error over the degrees of freedom for regular structured meshes a) and perturbed meshes b).

a) Regular mesh:

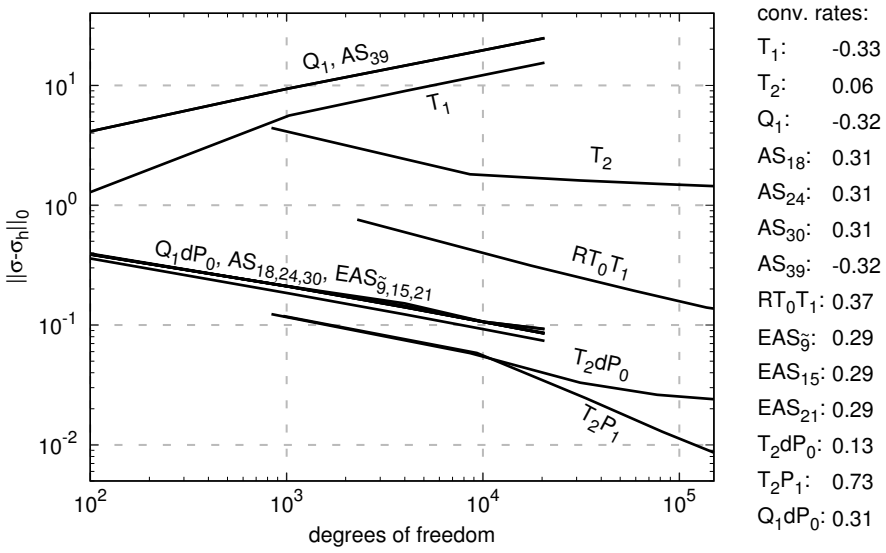

b) Perturbed mesh:

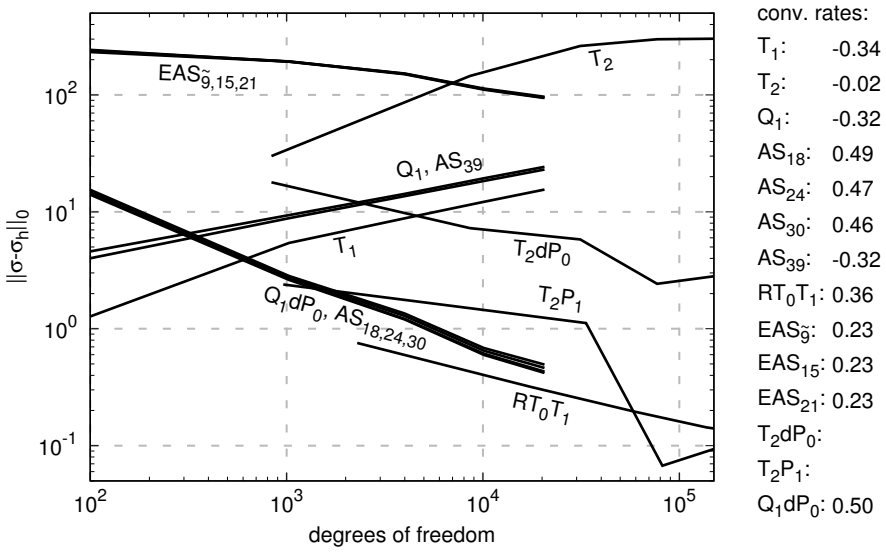

Figure 5.12: Regular problem with nearly incompressible material $\mu = 1, \Lambda = 10^6$; Convergence plot and corresponding rates of the stress error over the degrees of freedom for regular structured meshes a) and perturbed meshes b).

5.7.3 Shear locking: Bending Beam

The previous numerical example depicted the well or ill posedness of the element formulations approaching the incompressible regime $\Lambda \to \infty$. In case of the ill posed elements, non optimal convergence appeared for the displacements as well as the stresses, often denoted as volumetric locking. The following example targets for the problem of shear locking. This phenomena may appear in bending dominated problems, where the aspect ratio of the considered body deteriorates. Therefore a thin beam with a square shaped cross section in a pure bending mode is considered. The beam is simply supported at one end, such that lateral strains are permitted. At the opposing end a moment M_0 is applied. In addition the displacements perpendicular to the bending direction are constrained on the corresponding faces, imitating a plane strain setting. The geometry and the boundary conditions are depicted in Figure 5.13. The analytical solution for the displacements of the problem are given by the bi-quadratic polynomial function

$$\boldsymbol{u} = \begin{bmatrix} \alpha\, x_1\, x_2 \\ -\frac{1}{2}\alpha\, x_1^2 + \beta\, x_2^2 \\ 0 \end{bmatrix} \quad \text{with} \quad \begin{aligned} \alpha &= \frac{(1-\nu)^2}{E}\frac{3M_0}{2\,(t/2)^3} \\ \beta &= -\frac{1}{2}\frac{\nu(1+\nu)}{E}\frac{3M_0}{2\,(t/2)^3} \end{aligned} \tag{5.90}$$

where M_0 is the applied moment, t the thickness of the beam, $E = \frac{\mu(3\Lambda+2\mu)}{\Lambda+\mu}$ the Young's modulus and $\nu = \frac{\Lambda}{2(\Lambda+\mu)}$ the Poisson's ratio. Figure 5.14 depicts the normalized displacement error with respect to a regular mesh refinement considering the different finite element formulations for different thicknesses t. Since in this boundary value problem the error is not uniform over the domain, a regular mesh refinement is not expected to lead to an optimal convergence rate. Therefore the rate of the convergence itself is neglected in the following discussion.

Considering first the elements of second order, it can be noticed that the T_2 and T_2P_1 yield accurate results independent of the ratio of length and thickness, already for the coarsest mesh. For decreasing t, the quality of the solution increases. This superior and unlikely behavior is explained by the fact that for $t \to 0$ the bi-quadratic part of the solution for u_2 reduces to a quadratic polynomial which is included in the approximation spaces of these elements. In contrast, the error of the T_2dP_0 is almost constant for the different ratios. This is due to the piecewise constant approximation of the pressure, such that also in the limit case of $t \to 0$ the approximation does not include the analytical solution.

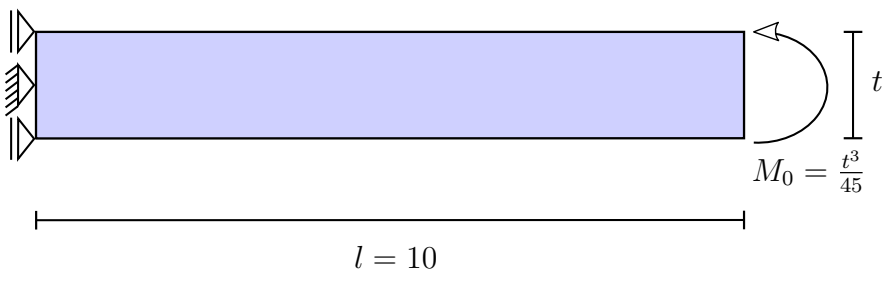

Figure 5.13: Bending of a beam; Boundary value problem.

a) t=10:

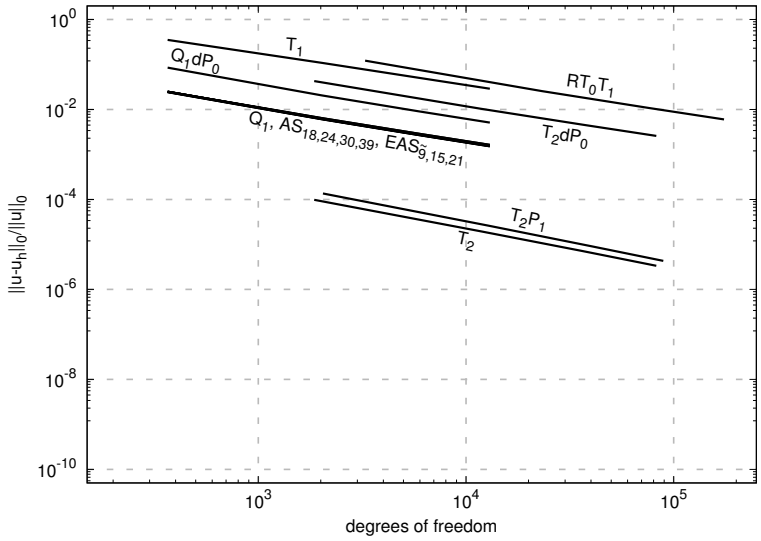

b) t=1:

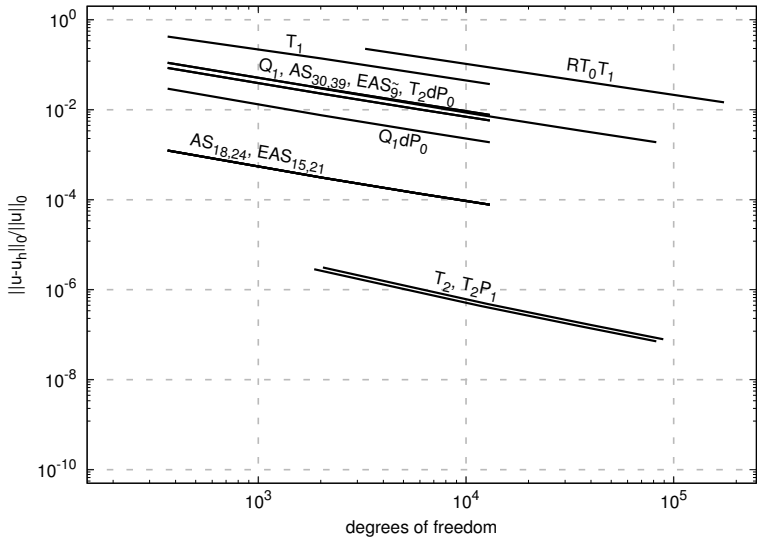

c) t=0.1:

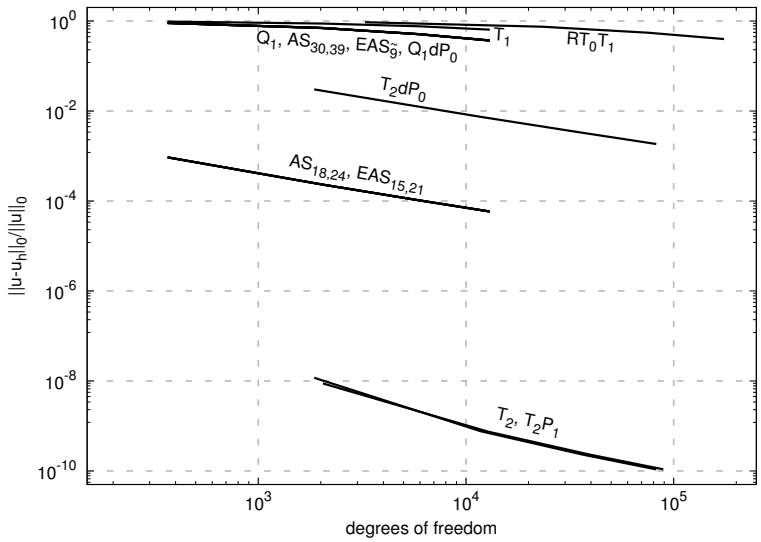

Figure 5.14: Bending of a beam with compressible material $\mu = 1$, $\Lambda = 1$; Convergence plot of the displacement error over the degrees of freedom.

Comparing the first order elements, the poor bending behavior of the tetrahedral based elements (T_1 and RT_0T_1) can be noticed. Already for well posed ratios of length and thickness the initial error is very large. In addition in the case of $t = 0.1$, convergence in general is only obtained for fine meshes. It is interesting to note, that the result of the RT_0T_1 differs to the the element behavior in the two dimensional case, published in VIEBAHN ET AL. [2018b]. In case of $t = 10$ the results for the Q_1, all AS and EAS elements are equivalent. But increasing the ratio of length to thickness, the shear locking phenomena can be recognized for the Q_1, AS_{39}, AS_{30} and $EAS_{\tilde{9}}$ elements. In contrast, the AS_{18}, AS_{24}, EAS_{15} and EAS_{21} seem to be free of shear locking. A shear locking effect can also be recognized in the case of the Q_1dP_0 formulation.

5.8 Summary of FEM for Linear Elasticity

In this chapter the different proposed discretization schemes for the problem of linear elasticity have been introduced, discussed and investigated. In particular, their properties in the incompressible regime and in the framework of deteriorated aspect ratios of the physical body have been of special interest, since these represent the limit cases of the classical primal finite element method. The presented numerical examples illustrated the capability that the mixed finite element method is able to overcome these drawbacks, if suitable discretization schemes are adopted. In detail it has been shown that elements of the family of assumed stresses, enhanced assumed strains and Hood-Taylor formulations can be constructed such that they are stable by means of the inf-sup test and do not suffer due to locking phenomena in the considered numerical examples. In case of the Hood-Taylor element, the well posedness for incompressibility has already been shown by the analysis discussed in Chapter 5.5. Considering the family of assumed stress elements, then volumetric locking is avoided if the trace related stress approximation satisfies

$$(\tau_{11},\, \tau_{22},\, \tau_{33})^T|_{\widehat{\Omega}^e} \not\supset A_0 \otimes B_1 \otimes B_2\,. \tag{5.91}$$

This is the case for the AS_{30}, AS_{24} and AS_{18} compare with Table 5.1. The corresponding volumetric locking free EAS elements are related to the discretization of type

$$(\widehat{\boldsymbol{\varepsilon}}_{11},\, \widehat{\boldsymbol{\varepsilon}}_{22},\, \widehat{\boldsymbol{\varepsilon}}_{33})^T|_{\widehat{\Omega}^e} \supseteq A_0 \otimes B_1 \otimes B_2\,, \tag{5.92}$$

which is satisfied for all considered EAS elements, compare Table 5.2. The shear locking phenomena is highly related to the approximation of shear related quantities. Thus, the assumed stress elements seem to be shear locking free if the discretization satisfies

$$(\tau_{23},\, \tau_{13},\, \tau_{12})^T|_{\widehat{\Omega}^e} \not\supset A_1 \otimes A_2\,. \tag{5.93}$$

The related shear locking free EAS elements are based on

$$(\widehat{\boldsymbol{\varepsilon}}_{23},\, \widehat{\boldsymbol{\varepsilon}}_{13},\, \widehat{\boldsymbol{\varepsilon}}_{12})^T|_{\widehat{\Omega}^e} \supseteq A_1 \otimes A_2\,. \tag{5.94}$$

The corresponding elements are the AS_{24}, AS_{18}, EAS_{21} and EAS_{15}. Especially the proposed elements based on the family of assumed stresses seem be a superior choice. With a suitable stress approximation, they do not suffer due to volumetric or shear locking, they are robust to mesh perturbations and they fulfill the numerical inf-sup test. In addition a lowest order interpolation for the displacements is utilized and the size of the system of equations can

be reduced to the size of unknowns related to the displacements by a static condensation. In comparison, the T_2P_1 is also free of locking behavior and its tetrahedral shape is of huge advantage considering automatic mesh generation. However it has the drawbacks of a higher order interpolation which may lead to larger computational costs and an indefinite global system of equations which is problematic in case of non direct solving strategies.

6 Isotropic Hyperelasticity

In the previous chapters small displacements, small strains and a linear stress strain relationship have been assumed. This led to formulations which could be analyzed well from a mathematical point of view. However, in many engineering applications these assumptions are not valid. As mentioned in the pioneering work of Truesdell and Noll [1965]:

> Rubber, glass and steel are all linearly elastic in small strain but their several responses to large strain or to repeated strain differ from one another.

Therefore the following chapter extends the previously discussed variational frameworks to the case of large deformations. Therein the displacements, rotations and strains can be of arbitrary magnitude and also the stress strain relation can be nonlinear. The remaining assumptions are the restriction to isothermal processes and that the dissipation is assumed to be zero. This means that only reversible, isothermal processes are considered. In addition, the existence of a so-called Helmholtz free energy function $\psi = \psi(\boldsymbol{C})$ depending solely on the on the right Cauchy Green tensor $\boldsymbol{C} = \boldsymbol{F}^T\boldsymbol{F}$ and material parameter is postulated. In the geometrically nonlinear framework different settings of the variational formulation can be considered. On the one hand, the governing equations may be constructed with respect to the reference or current configuration. In addition various choices of work conjugated quantities can be chosen. The reader is referred to the textbook of Wriggers [2008] for an excellent overview on this topic and its consequences for the finite element formulation. The scope of this thesis is focused on a representation based on the so called material setting, where the internal work is given in terms of the second Piola-Kirchhoff stress tensor $\boldsymbol{S}$ and the right Cauchy-Green tensor $\boldsymbol{C}$. In addition, the boundary conditions are restricted to be conservative, i.e. related to the reference configuration, and do not change during the loading. In this framework the following equations describe the fundamental boundary value problem

$$\begin{aligned}
&\mathrm{Div}[\boldsymbol{F}\boldsymbol{S}] + \boldsymbol{f} = \boldsymbol{0} && \text{on } \mathcal{B}_0 \\
&2\partial_C \psi = \boldsymbol{S} && \text{on } \mathcal{B}_0 \\
&\boldsymbol{F} = \boldsymbol{I} + \nabla \boldsymbol{u} && \text{on } \mathcal{B}_0 \\
&\boldsymbol{S} = \boldsymbol{S}^T && \text{on } \mathcal{B}_0 \\
&(\boldsymbol{F}\boldsymbol{S})\boldsymbol{N} = \bar{\boldsymbol{t}}_0 && \text{on } \partial\mathcal{B}_{0,t} \\
&\boldsymbol{u} = \overline{\boldsymbol{u}} && \text{on } \partial\mathcal{B}_{0,u}
\end{aligned} \tag{6.1}$$

which are the balance of linear momentum, constitutive equation, compatibility equation, balance of angular momentum and boundary conditions, compare their derivations in Chapter 2. In contrast to the linear elastic case, an analysis on the well posedness of the solution is rather difficult. For example the demanded requirement on the uniqueness of a solution contradicts the physics, keeping in mind for example the physical resonable presence of bifurcation points. Therefore, it is much more complicated to decide if the obtained solution is physically valid or an artifact arising from the discretization method. This is of course in particular the case if already the linear elastic counterpart of the discretization method is not well posed. Therefore it is advisable to use only finite element

formulations which fulfill the requirements on existence and uniqueness of a solution in the linear elastic setting. However, this does not guarantee physically meaningful results of the simulation as it is depicted in the numerical example in Chapter 7.5.5.

The nonlinearity of the boundary value problem leads to the necessity of iterative solution procedures. In the framework of the Finite Element Method the Newton-Raphson procedure has been established as a very powerful solution algorithm and is utilized also in this thesis. Since this procedure solves a linearized system of equations, the linearizations of the weak forms are required and are additionally given in the following chapter.

6.1 Pure Displacement Formulation

Considering the boundary value problem for hyperelasticity (6.1), the compatibility and constitutive condition may be inserted into the balance of linear momentum. In this case the balance of angular momentum is, similarly as in the linear elastic setup, a priori fulfilled due to the constitutive condition and the inherent symmetry of the strain tensor. This leads to a formulation where the displacements are the sole unknown field and the boundary value problem reduces to: find $\boldsymbol{u}$ such that

$$\begin{aligned} &\mathrm{Div}[\boldsymbol{F}\boldsymbol{S}] + \boldsymbol{f} = \boldsymbol{0} && \text{on } \mathcal{B}_0, \\ &(\boldsymbol{F}\boldsymbol{S})\boldsymbol{N} = \bar{\boldsymbol{t}}_0 && \text{on } \partial\mathcal{B}_{0,t}, \\ &\boldsymbol{u} = \boldsymbol{0} && \text{on } \partial\mathcal{B}_{0,u}\,, \end{aligned} \tag{6.2}$$

whereas, similar to the discussion in Chapter 4, only the case of trivial Dirichlet boundary conditions is considered without loss of generality. Note that in this formulation the second Piola-Kirchhoff stress is a function of the gradient of the displacement field $\boldsymbol{S} := \boldsymbol{S}(\nabla\boldsymbol{u})$. The weak form G is obtained as usual by the standard Galerkin approach as: find $\boldsymbol{u} \in [\mathcal{W}_0^{1,p}(\mathcal{B}_0)]^3$ such that

$$G := \int_{\mathcal{B}_0} \left(2\frac{\partial\psi(\boldsymbol{C})}{\partial\boldsymbol{C}} : \frac{1}{2}\delta\boldsymbol{C} - \boldsymbol{f}\cdot\delta\boldsymbol{u} \right) \mathrm{d}V - \int_{\partial\mathcal{B}_{0,t}} \bar{\boldsymbol{t}}\cdot\delta\boldsymbol{u}\ \mathrm{d}A = 0 \quad \forall\,\delta\boldsymbol{u} \in [\mathcal{W}_0^{1,p}(\mathcal{B})]^3\,, \tag{6.3}$$

with $\delta\boldsymbol{C} = \delta\boldsymbol{F}^T\boldsymbol{F} + \boldsymbol{F}^T\delta\boldsymbol{F}$, $\delta\boldsymbol{F} = \boldsymbol{I} + \nabla_X\delta\boldsymbol{u}$ and p being sufficiently large. It should be denoted that in the general hyperelastic framework p depends directly on the choice of ψ, which is in contrast to the case of linear elasticity, where $p = 2$ due to the quadratic structure of the equations. In order to solve this problem the linearization, $\mathrm{Lin}G = G(\boldsymbol{u}) + \Delta G(\Delta\boldsymbol{u})$, is needed whereas the increment appears as

$$\Delta G = \int_{\mathcal{B}_0} \left(\left(4\frac{\partial^2\psi}{\partial\boldsymbol{C}\partial\boldsymbol{C}} : \frac{1}{2}\Delta\boldsymbol{C} \right) : \frac{1}{2}\delta\boldsymbol{C} + 2\frac{\partial\psi(\boldsymbol{C})}{\partial\boldsymbol{C}} : \frac{1}{2}\Delta\delta\boldsymbol{C} \right) \mathrm{d}V \tag{6.4}$$

with the increment of the right Cauchy-Green tensor as $\Delta\delta\boldsymbol{C} = \delta\boldsymbol{F}^T\Delta\boldsymbol{F} + \Delta\boldsymbol{F}^T\delta\boldsymbol{F}$ and the increment of the deformation tensor as $\Delta\boldsymbol{F} = \Delta\nabla_X\boldsymbol{u}$.

6.2 Mixed Variational Formulation

In the following the different mixed variational formulations, which have already been discussed in the framework of linear elasticity, are considered with regard to the large

deformation case. In contrast to the Hu-Washizu based formulations which can be extended to the nonlinear framework in a straight forward manner, an extension of the Hellinger-Reissner formulation is rather difficult and discussed in detail. Furthermore, a series of publications Auricchio et al. [2005a; 2010; 2013] have reported numerical instabilities in the large strain framework of displacement-pressure formulations. Therefore, this framework is first discussed in the classical formulation and then extended to a consistent stabilized formulation proposed in Schröder et al. [2017].

6.2.1 Hellinger-Reissner Formulation

The underlying field quantities in the Hellinger-Reissner formulation are the stresses and displacements. In the large deformation setup, different stress quantities occur and it is not obvious which one is the optimal choice to be the unknown field. It seems to be reasonable to choose the second Piola-Kirchhoff stresses $\boldsymbol{S}$ since it is beneficial to work in the reference configuration and because of its symmetric character which leads to a simple consideration of the balance of angular momentum. However, it could also be argued for the choice of the first Piola-Kirchhoff stresses $\boldsymbol{P}$ or also a stress measure which is related to the actual configuration like the Kirchhoff stresses $\boldsymbol{\tau}$ or Cauchy stresses $\boldsymbol{\sigma}$.

The extension of the Hellinger-Reissner formulation to hyperelasticity is first focused on the case where the constitute relation can be described in form of an explicit complementary stored energy function $\chi(\boldsymbol{S})$. In a following step this formulation is extended to general hyperelasticity. Note that such an explicit complementary energy only exists in very special cases, e.g. in the framework of St. Venant-Kirchhoff type nonlinear elasticity, compare Chapter 2.4.4. In this framework the strong form of the boundary value problem reads as: find $\boldsymbol{S}$ and $\boldsymbol{u}$ such that

$$\begin{aligned} &\mathrm{Div}[\boldsymbol{F}\boldsymbol{S}] + \boldsymbol{f} = \boldsymbol{0} && \text{on } \mathcal{B}_0 \\ &\partial_S \chi(\boldsymbol{S}) = \boldsymbol{E} && \text{on } \mathcal{B}_0 \\ &(\boldsymbol{F}\boldsymbol{S})\boldsymbol{N} = \bar{\boldsymbol{t}}_0 && \text{on } \partial\mathcal{B}_{0,t} \\ &\boldsymbol{u} = \boldsymbol{0} && \text{on } \partial\mathcal{B}_{0,u}\,. \end{aligned} \tag{6.5}$$

The corresponding weak forms follow after the multiplication with the test functions $\delta\boldsymbol{S}$ and $\delta\boldsymbol{u}$ and the usual mathematical steps as: find $\boldsymbol{S} \in [\mathcal{L}^p(\mathcal{B}_0)]^{3\times3}_{\mathrm{sym}}$ and $\boldsymbol{u} \in [\mathcal{W}_0^{1,p}(\mathcal{B}_0)]^3$

$$\begin{aligned} G_S &:= \int_{\mathcal{B}} \left(\boldsymbol{E} - \frac{\partial \chi(\boldsymbol{S})}{\partial \boldsymbol{S}} \right) : \delta\boldsymbol{S}\, \mathrm{d}V = 0 \quad \forall\, \delta\boldsymbol{S} \in [\mathcal{L}^p(\mathcal{B})]^{3\times3}_{\mathrm{sym}}\,, \\ G_u &:= \int_{\mathcal{B}} \boldsymbol{S} : \delta\boldsymbol{E}\, \mathrm{d}V - \int_{\mathcal{B}} \boldsymbol{f} \cdot \delta\boldsymbol{u}\, \mathrm{d}V - \int_{\partial\mathcal{B}_t} \bar{\boldsymbol{t}}_0 \cdot \delta\boldsymbol{u}\, \mathrm{d}A = 0 \quad \forall\, \delta\boldsymbol{u} \in [\mathcal{W}_0^{1,p}(\mathcal{B})]^3\,, \end{aligned} \tag{6.6}$$

with $\delta\boldsymbol{E} = \frac{1}{2}\delta\boldsymbol{C}$ and p being sufficiently large. The corresponding increments follow as

$$\begin{aligned} \Delta G_S(\boldsymbol{S}, \boldsymbol{u}) &= \int_{\mathcal{B}} \left(\Delta\boldsymbol{E} - \frac{\partial^2 \chi(\boldsymbol{S})}{\partial \boldsymbol{S} \partial \boldsymbol{S}} : \Delta\boldsymbol{S} \right) : \delta\boldsymbol{S}\, \mathrm{d}V\,, \\ \Delta G_u(\boldsymbol{S}, \boldsymbol{u}) &= \int_{\mathcal{B}} (\boldsymbol{S} : \Delta\delta\boldsymbol{E} + \Delta\boldsymbol{S} : \delta\boldsymbol{E})\, \mathrm{d}V\,, \end{aligned} \tag{6.7}$$

with $\Delta\boldsymbol{E} = \frac{1}{2}\Delta\boldsymbol{C}$. A problem arises if an explicit form of the complementary stored energy function $\chi(\boldsymbol{S})$ is not defined, as it is generally the case for a nonlinear description of the

constitutive equation, as discussed in OGDEN [1984]. A generalization to hyperelasticity has been proposed by VIEBAHN ET AL. [2019]. The basic idea is, that the partial derivative of the complementary stored energy function $\partial_S \chi(\boldsymbol{S})$ which appears in the weak form, is substituted by a second-order tensor valued function $\boldsymbol{E}^S(\boldsymbol{S})$ which fulfills the nonlinear relationship

$$\boldsymbol{r}(\boldsymbol{E}^S, \boldsymbol{S}) = \boldsymbol{S} - \left.\frac{\partial \psi(\widetilde{\boldsymbol{E}})}{\partial \widetilde{\boldsymbol{E}}}\right|_{\widetilde{\boldsymbol{E}}=\boldsymbol{E}^S} = \boldsymbol{0}\,. \tag{6.8}$$

In this context, $\boldsymbol{E}^S$ can be interpreted as a Green-Lagrange strain related quantity, which implicitly fulfills the constitutive relation defined by a suitable Helmholtz free energy function ψ. The residual in Equation (6.8) can be solved with a Newton scheme at fixed $\boldsymbol{S}$, by the update algorithm

$$\boldsymbol{E}^S_{n+1} = \boldsymbol{E}^S_n + \left(\left.\frac{\partial^2 \psi(\widetilde{\boldsymbol{E}})}{\partial \widetilde{\boldsymbol{E}} \partial \widetilde{\boldsymbol{E}}}\right|_{\widetilde{\boldsymbol{E}}=\boldsymbol{E}^S_n}\right)^{-1} : \boldsymbol{r}(\boldsymbol{E}^S_n, \boldsymbol{S}) \tag{6.9}$$

until $\|\boldsymbol{r}(\boldsymbol{E}^S_n, \boldsymbol{S})\| \approx 0$ is obtained. The corresponding linearization of the weak form with respect to $\boldsymbol{S}$ is than given by

$$\Delta G_S = \int_{\mathcal{B}_0} \left(\Delta \boldsymbol{E} - \left(\left.\frac{\partial^2 \psi(\widetilde{\boldsymbol{E}})}{\partial \widetilde{\boldsymbol{E}} \partial \widetilde{\boldsymbol{E}}}\right|_{\widetilde{\boldsymbol{E}}=\boldsymbol{E}^S}\right)^{-1} : \Delta \boldsymbol{S} \right) : \delta \boldsymbol{S}\, \mathrm{d}V. \tag{6.10}$$

6.2.2 Hu-Washizu Formulation

In the Hu-Washizu variational framework, the displacements $\boldsymbol{u}$, the Green-Lagrangian strains $\widehat{\boldsymbol{E}}$ and the second Piola-Kirchhoff stresses $\boldsymbol{S}$ are chosen as the independent field quantities. This leads to the strong form of the boundary value problem as

$$\begin{aligned}
&\mathrm{Div}[\boldsymbol{F}\boldsymbol{S}] + \boldsymbol{f} = \boldsymbol{0} && \text{on } \mathcal{B}_0 \\
&\boldsymbol{S} = \partial_{\widehat{\boldsymbol{E}}} \psi(\widehat{\boldsymbol{E}}) && \text{on } \mathcal{B}_0 \\
&\widehat{\boldsymbol{E}} = \boldsymbol{E} && \text{on } \mathcal{B}_0 \\
&(\boldsymbol{F}\boldsymbol{S})\boldsymbol{N} = \bar{\boldsymbol{t}}_0 && \text{on } \partial\mathcal{B}_{0,t} \\
&\boldsymbol{u} = \boldsymbol{0} && \text{on } \partial\mathcal{B}_{0,u}\,,
\end{aligned} \tag{6.11}$$

whereas $\boldsymbol{E} := \boldsymbol{E}(\boldsymbol{u})$ remains a function of the displacements. The corresponding weak forms follow as: find $\boldsymbol{u} \in [\mathcal{W}^{1,p}_0(\mathcal{B}_0)]^3$, $\widehat{\boldsymbol{E}} \in [\mathcal{L}^p(\mathcal{B}_0)]^{3\times 3}_{\mathrm{sym}}$ and $\boldsymbol{S} \in [\mathcal{L}^p(\mathcal{B}_0)]^{3\times 3}_{\mathrm{sym}}$ such that

$$\begin{aligned}
G_u &:= \int_{\mathcal{B}_0} (\boldsymbol{S} : \delta \boldsymbol{E} - \boldsymbol{f} \cdot \delta \boldsymbol{u})\, \mathrm{d}V - \int_{\partial\mathcal{B}_{0,t}} \bar{\boldsymbol{t}}_0 \cdot \delta \boldsymbol{u}\, \mathrm{d}A = 0 \quad \forall\, \delta \boldsymbol{u} \in [\mathcal{W}^{1,p}_0(\mathcal{B}_0)]^3, \\
G_{\widehat{E}} &:= \int_{\mathcal{B}_0} (\partial_{\widehat{E}} \psi(\widehat{\boldsymbol{E}}) - \boldsymbol{S}) : \delta \widehat{\boldsymbol{E}}\, \mathrm{d}V = 0 \quad \forall\, \delta \widehat{\boldsymbol{E}} \in [\mathcal{L}^p(\mathcal{B}_0)]^{3\times 3}_{\mathrm{sym}}, \\
G_S &:= \int_{\mathcal{B}_0} \left(\boldsymbol{E} - \widehat{\boldsymbol{E}}\right) : \delta \boldsymbol{S}\, \mathrm{d}V = 0 \quad \forall\, \delta \boldsymbol{S} \in [\mathcal{L}^p(\mathcal{B}_0)]^{3\times 3}_{\mathrm{sym}},
\end{aligned} \tag{6.12}$$

and the increments follow as

$$\begin{aligned} \Delta G_u &= \int_{\mathcal{B}_0} (\Delta \boldsymbol{S} : \delta \boldsymbol{E} + \boldsymbol{S} : \Delta\delta \boldsymbol{E}) \mathrm{d}V \,, \\ \Delta G_E &= \int_{\mathcal{B}_0} \left(\frac{\partial^2 \psi(\widehat{\boldsymbol{E}})}{\partial \widehat{\boldsymbol{E}} \, \partial \widehat{\boldsymbol{E}}} : \Delta \widehat{\boldsymbol{E}} - \Delta \boldsymbol{S} \right) : \delta \widehat{\boldsymbol{E}} \, \mathrm{d}V \,, \\ \Delta G_S &= \int_{\mathcal{B}_0} \left(\Delta \boldsymbol{E} - \Delta \widehat{\boldsymbol{E}} \right) : \delta \boldsymbol{S} \, \mathrm{d}V \,. \end{aligned} \tag{6.13}$$

6.2.3 Displacement-Pressure Formulation

The introduction of a pressure related field quantity is a widely used approach in order to overcome the locking associated to incompressibility also in the framework of large deformations. However, investigations by Auricchio et al. [2005b; 2013] have shown that the ad-hoc extension of the variational form discussed in Chapter 4.3.3 to hyperelasticity could lead to instabilities and must be treated with care. Even discretizations that provide in the linear case stable and unique finite element approximations and are optimal in the small strain regime suffer in some situations due to unphysical modes undergoing finite strains. An alternative consistent variational approach, appropriate for displacement and pressure discretization, has been proposed by Schröder et al. [2017]. In this approach the volume dilatation is computed based on the pressure field with help of an iterative solution procedure. This novel formulation yields physical meaningful solutions for the numerical examples, where the classical approach suffers due to instabilities.

For the investigation of both variational formulations we assume that the underlying Helmholtz free energy function is split additively into a compressible part ψ^{comp} and an additional part related to the volumetric deformation. This second part may be interpreted as a penalty formulation such that we obtain

$$\psi = \psi^{\mathrm{comp}}(\boldsymbol{C}) + \frac{\Lambda}{2} \vartheta(J)^2 \,. \tag{6.14}$$

Therein, $\vartheta(J)$ is an arbitrary function depending on J such that

$$\begin{aligned} &\vartheta(J) = 0 \quad \text{if and only if} \quad J = 1 \,, \\ &\vartheta'(1) \neq 0 \quad \text{with} \quad \vartheta'(J) = \tfrac{\partial \vartheta}{\partial J} \,. \end{aligned} \tag{6.15}$$

In this framework the second Piola-Kirchhoff stress tensor follows with the derivative $\partial_C \vartheta(J) = \vartheta'(J) \, J \, \boldsymbol{C}^{-1}$ as

$$\boldsymbol{S}(\boldsymbol{C}) = 2 \frac{\partial \psi^{\mathrm{comp}}(\boldsymbol{C})}{\partial \boldsymbol{C}} + \Lambda \, \vartheta(J) \, \vartheta'(J) \, J \, \boldsymbol{C}^{-1} \,. \tag{6.16}$$

The main difference between the classical displacement pressure formulation and the consistent complementary formulation is based on a different substitution for the pressure field as compared in the following.

Classical approach In order to eliminate the Λ-dependency of the formulation, the pressure p is introduced as an additional field quantity by the substitution of $p = \Lambda \, \vartheta(J)$ such that the second Piola-Kirchhoff stresses appear as

$$\boldsymbol{S}(\boldsymbol{C}, p) = 2 \frac{\partial \psi^{\mathrm{comp}}(\boldsymbol{C})}{\partial \boldsymbol{C}} + p \, \vartheta'(J) \, J \, \boldsymbol{C}^{-1} \,. \tag{6.17}$$

Therefore the strong form of the related boundary value problem is given as

$$\begin{aligned} &\mathrm{Div}[\boldsymbol{F}\boldsymbol{S}] + \boldsymbol{f} = \boldsymbol{0} && \text{on } \mathcal{B}_0 \\ &\vartheta(J) - \frac{1}{\Lambda}\, p = 0 && \text{on } \mathcal{B}_0 \\ &(\boldsymbol{F}\boldsymbol{S})\boldsymbol{N} = \bar{\boldsymbol{t}}_0 && \text{on } \partial\mathcal{B}_{0,t} \\ &\boldsymbol{u} = \boldsymbol{0} && \text{on } \partial\mathcal{B}_{0,u}\,. \end{aligned} \tag{6.18}$$

The related weak forms follow with the usual mathematical steps as: find $\boldsymbol{u} \in [\mathcal{W}_0^{1,p}(\mathcal{B}_0)]^3$ and $p \in \mathcal{L}^p(\mathcal{B}_0)$

$$\begin{aligned} G_u &:= \int_{\mathcal{B}_0} \boldsymbol{S} : \frac{1}{2}\delta\boldsymbol{C}\ \mathrm{d}V - \int_{\mathcal{B}_0} \boldsymbol{f}\cdot\delta\boldsymbol{u}\,\mathrm{d}V - \int_{\partial\mathcal{B}_{0,t}} \bar{\boldsymbol{t}}_0\cdot\delta\boldsymbol{u}\,\mathrm{d}A = 0 \quad \forall\,\delta\boldsymbol{u} \in [\mathcal{W}_0^{1,p}(\mathcal{B}_0)]^3, \\ G_p &:= \int_{\mathcal{B}_0} \left(\vartheta(J) - \frac{1}{\Lambda}\,p\right)\delta p\ \mathrm{d}V = 0 \qquad\qquad \forall\,\delta p \in \mathcal{L}^p(\mathcal{B}), \end{aligned} \tag{6.19}$$

with the corresponding increments

$$\begin{aligned} \Delta G_u &= \int_{\mathcal{B}} \left(\boldsymbol{S} : \frac{1}{2}\Delta\delta\boldsymbol{C} + \left(\frac{\partial \boldsymbol{S}}{\partial \boldsymbol{C}} : \Delta\boldsymbol{C} + \frac{\partial \boldsymbol{S}}{\partial p}\Delta p\right) : \frac{1}{2}\delta\boldsymbol{C}\right)\ \mathrm{d}V \\ \Delta G_p &= \int_{\mathcal{B}} \left(\vartheta'(J)\, J\, \boldsymbol{C}^{-1} : \Delta\boldsymbol{C} - \frac{1}{\Lambda}\,\Delta p\right)\delta p\ \mathrm{d}V\,. \end{aligned} \tag{6.20}$$

Consistent complementary approach The fundamental idea is based on the modified substitution of the pressure as $p := \Lambda\,\vartheta(J)\,\vartheta'(J)$. In this full complementary form the pressure is given as a function of the volumetric deformation $J := \varphi(p)$. Therefore, the second Piola-Kirchhoff stresses follow as

$$\boldsymbol{S}(\boldsymbol{C}, p) = 2\,\frac{\partial \psi^{\mathrm{comp}}(\boldsymbol{C})}{\partial \boldsymbol{C}} + p\, J\, \boldsymbol{C}^{-1}\,. \tag{6.21}$$

The idea is closely related to the approach of the hyperelastic extension of the Hellinger-Reissner formulation, discussed in Chapter 6.2.1. In case of a linear relation between p and J the complementary function $J = \varphi(p)$ can be computed a priori in an explicit form. However if $\vartheta(J)$ is a nonlinear function, the complementary form has to be computed implicitly using and iterative procedure. The strong form of the related boundary value problem is given by

$$\begin{aligned} &\mathrm{Div}[\boldsymbol{F}\boldsymbol{S}] + \boldsymbol{f} = \boldsymbol{0} && \text{on } \mathcal{B}_0\,, \\ &J = \varphi(p) && \text{on } \mathcal{B}_0\,, \\ &(\boldsymbol{F}\boldsymbol{S})\boldsymbol{N} = \bar{\boldsymbol{t}}_0 && \text{on } \partial\mathcal{B}_{0,t}\,, \\ &\boldsymbol{u} = \boldsymbol{0} && \text{on } \partial\mathcal{B}_{0,u}\,. \end{aligned} \tag{6.22}$$

In case of a nonlinear function $\vartheta(J)$ the complementary form $J = \varphi(p)$ is computed iteratively with the introduction of the internal variable $\theta := \varphi(p)$ and the residual

$$r(\theta, p) := \Lambda\,\vartheta(\theta)\,\vartheta'(\theta) - p = 0\,. \tag{6.23}$$

From the linearization with a fixed pressure

$$\mathrm{Lin}[r(\theta,p)] = r(\theta_n,p) + \Lambda\big(\vartheta'(\theta_n)\vartheta'(\theta_n) + \vartheta(\theta_n)\vartheta''(\theta_n)\big)\Delta\theta = 0 \tag{6.24}$$

we obtain the increment of θ as

$$\Delta\theta = -(\Lambda(\vartheta'(\theta_n)\vartheta'(\theta_n) + \vartheta(\theta_n)\vartheta''(\theta_n)))^{-1}\, r(\theta_n,p)\,. \tag{6.25}$$

This yields by means of the Newton-Raphson scheme the update as

$$\theta_{n+1} = \theta_n - \frac{\vartheta(\theta_n)\vartheta'(\theta_n)}{(\vartheta'(\theta_n)\vartheta'(\theta_n) + \vartheta''(\theta_n)\vartheta(\theta_n))} + \frac{p}{\Lambda(\vartheta'(\theta_n)\vartheta'(\theta_n) + \vartheta''(\theta_n)\vartheta(\theta_n))}\,. \tag{6.26}$$

With the introduction of the following abbreviations

$$\begin{aligned} c_1 &:= \theta_n - \frac{\vartheta(\theta_n)\vartheta'(\theta_n)}{(\vartheta'(\theta_n)\vartheta'(\theta_n) + \vartheta''(\theta_n)\vartheta(\theta_n))} \\ c_2 &:= \frac{1}{\Lambda(\vartheta'(\theta_n)\vartheta'(\theta_n) + \vartheta''(\theta_n)\vartheta(\theta_n))} \end{aligned}$$

the related weak forms appear as: find $\boldsymbol{u} \in [\mathcal{W}_0^{1,p}(\mathcal{B}_0)]^3$ and $p \in \mathcal{L}^p(\mathcal{B}_0)$

$$\begin{aligned} G_u &:= \int_{\mathcal{B}_0} \boldsymbol{S} : \frac{1}{2}\delta\boldsymbol{C}\,\mathrm{d}V - \int_{\mathcal{B}_0} \boldsymbol{f}\cdot\delta\boldsymbol{u}\,\mathrm{d}V - \int_{\partial\mathcal{B}_{0,t}} \bar{\boldsymbol{t}}_0\cdot\delta\boldsymbol{u}\,\mathrm{d}A = 0 \quad \forall\,\delta\boldsymbol{u} \in [\mathcal{W}_0^{1,p}(\mathcal{B}_0)]^3, \\ G_p &:= \int_{\mathcal{B}_0} (J - c_1 - c_2\,p)\,\delta p\;\mathrm{d}V = 0 \quad \forall\,\delta p \in \mathcal{L}^p(\mathcal{B}_0), \end{aligned} \tag{6.27}$$

with the corresponding increments

$$\begin{aligned} \Delta G_u &= \int_{\mathcal{B}_0} \left(\boldsymbol{S} : \frac{1}{2}\Delta\delta\boldsymbol{C} + \left(\frac{\partial \boldsymbol{S}}{\partial \boldsymbol{C}} : \Delta\boldsymbol{C} + \Delta p\, J\, \boldsymbol{C}^{-1} \right) : \frac{1}{2}\delta\boldsymbol{C} \right)\,\mathrm{d}V\,, \\ \Delta G_p &= \int_{\mathcal{B}_0} \left(J\,\boldsymbol{C}^{-1} : \frac{1}{2}\Delta\boldsymbol{C} - c_2\,\Delta p \right)\delta p\;\mathrm{d}V\,. \end{aligned} \tag{6.28}$$

7 Finite Element Method for Isotropic Hyperelasticity

In the following chapter, conforming finite element discretizations for the introduced variational formulations for hyperelasticity are discussed. As in the FE framework for linear elasticity discussed in Chapter 5, a shape regular triangulation of the body in the initial configuration $\Omega = \cup_e \Omega^e \approx \mathcal{B}_0$ into a finite number of elements Ω^e is considered. An isoparametric mapping from the element in parameter space $\widehat{\Omega}_e$ is used for the generation of a typical element in the physical space. In order to avoid repetitions, the following discrete subspaces are not given explicitly. The unknown field quantities are approximated using the same finite dimensional subspaces as proposed in the appropriate subchapter of the finite elements for linear elasticity. A conforming interpolation is ensured also for the hyperelastic case, since the chosen polynomial approximation functions are trivially p-integrable for all $p \geq 1$.

Remark on the Newton Raphson procedure In contrast to the system of equations discussed for linear elasticity, an iterative Newton-Raphson procedure is applied in order to calculate the equilibrated state of deformation. In detail we would like to solve a residuum of the form

$$\boldsymbol{R}(\boldsymbol{D}) = \boldsymbol{0} \tag{7.1}$$

being a system of n_{dof} nonlinear equations for n_{dof} unknowns. Due to the nonlinear structure of the system, we cannot directly solve for the unknowns $\boldsymbol{D}$. The introduction of an approximated solution denoted as $\boldsymbol{D}^*$ yields

$$\boldsymbol{D} = \boldsymbol{D}^* + \Delta\boldsymbol{D}\,. \tag{7.2}$$

Now a Taylor expansion of $\boldsymbol{R}(\boldsymbol{D})$ around $\boldsymbol{D}^*$ can be applied leading to

$$\boldsymbol{R}(\boldsymbol{D}) = \boldsymbol{R}(\boldsymbol{D}^*) + \left.\frac{\partial \boldsymbol{R}}{\partial \boldsymbol{D}}\right|_{\boldsymbol{D}=\boldsymbol{D}^*} \Delta\boldsymbol{D} + O(\Delta\boldsymbol{D}^2). \tag{7.3}$$

With the requirement that the approximated solution $\boldsymbol{D}^*$ is close enough to the true solution $\boldsymbol{D}$, $\Delta\boldsymbol{D}$ is sufficiently small such that

$$\boldsymbol{R}(\boldsymbol{D}^*) = -\left.\frac{\partial \boldsymbol{R}}{\partial \boldsymbol{D}}\right|_{\boldsymbol{D}=\boldsymbol{D}^*} \Delta\boldsymbol{D}\,. \tag{7.4}$$

This can be written in an iterative algorithm

$$\boldsymbol{R}(\boldsymbol{D}_i) = -\left.\frac{\partial \boldsymbol{R}}{\partial \boldsymbol{D}}\right|_{\boldsymbol{D}=\boldsymbol{D}_i} (\boldsymbol{D}_{i+1} - \boldsymbol{D}_i) \tag{7.5}$$

and thus

$$\begin{aligned} \boldsymbol{D}_{i+1} &= \boldsymbol{D}_i - \left(\left.\frac{\partial \boldsymbol{R}}{\partial \boldsymbol{D}}\right|_{\boldsymbol{D}=\boldsymbol{D}_i}\right)^{-1} \boldsymbol{R}(\boldsymbol{D}_i) \\ &= \boldsymbol{D}_i - \boldsymbol{K}^{-1}\boldsymbol{R}(\boldsymbol{D}_i) \end{aligned} \tag{7.6}$$

where $\boldsymbol{K}$ is the tangent matrix of the system of equations and $\boldsymbol{D}_i$ is the known solution of the last iteration. The solution procedure is typically written as

$$\begin{aligned} \Delta\boldsymbol{D} &= -\boldsymbol{K}^{-1}\,\boldsymbol{R}(\boldsymbol{D}_i), \\ \boldsymbol{D}_{i+1} &= \boldsymbol{D} + \Delta\boldsymbol{D}\,. \end{aligned} \tag{7.7}$$

The resulting system of equations is solved until a convergent solution is obtained, i.e. $\|\Delta \boldsymbol{D}\| < \text{tol}$ or $\|\boldsymbol{R}(\boldsymbol{D}_i)\| < \text{tol}$ where tol is typically a small number in the range of $\text{tol} = 10^{-8}$. The Newton-Raphson procedure yields asymptotically a quadratic rate of convergence, but only if the initial vector $\boldsymbol{D}_0$ is close enough to the final solution. Then $\boldsymbol{D}_0$ is called to be in the convergence radius. If $\boldsymbol{D}_0$ is not in the convergence radius, then an incremental loading procedure has to be adopted. Therein the load is applied in a number of n_{steps} load-steps, whereas each increment has to be chosen such that the solution of the previous load step is within the convergence range of the solution for the actual load step. This iterative solution procedure and incremental load stepping highly affects the computational efficiency. Therefore finite element formulations which are more robust against larger load increments, i.e. facilitate a larger convergence radius, are preferable. Thus not only the number of unknowns are highly responsible for the computational efficiency of the method but also the number of necessary load steps. Since for the proposed formulations this number differs considerably it is additionally compared in the numerical examples.

7.1 Pure Displacement Finite Elements

In order to obtain the discrete counterpart of the weak form and the increment of the pure displacement formulation in large strains given by Equations (6.3) and (6.4) the geometries in the reference and actual configuration are approximated by

$$\boldsymbol{X}_h = \sum_{I=1}^{n_{\text{u-nodes}}} N^I(\boldsymbol{\xi})\, \hat{\boldsymbol{X}}^I = \mathbb{N}\, \hat{\boldsymbol{X}}\,, \quad \boldsymbol{x}_h = \sum_{I=1}^{n_{\text{u-nodes}}} N^I(\boldsymbol{\xi})\, \hat{\boldsymbol{x}}^I = \mathbb{N}\, \hat{\boldsymbol{x}}, \tag{7.8}$$

whereas $N^I(\boldsymbol{\xi})$ denote the appropriate ansatz functions defined in the parametric space $\boldsymbol{\xi} = \{\xi, \eta, \zeta\}$. In addition $\hat{\boldsymbol{X}}^I$ and $\hat{\boldsymbol{x}}^I$ are the nodal coordinates related to the corresponding configuration. The alternative representation considers the nodal coordinate vector $\hat{\boldsymbol{X}}$ with the nodal wise ordered, nested set of all coordinates of all element nodes

$$\hat{\boldsymbol{X}} = \{X_1^I, X_2^I, X_3^I, \dots\}^T \quad \text{for } I = 1, \dots, n_{\text{nodes}}\,. \tag{7.9}$$

Thus $\mathbb{N}$ represents a suitable matrix containing the ansatz functions in appropriate order. The vector of all nodal displacements of the element $\boldsymbol{d}$ follows by

$$\hat{\boldsymbol{x}} = \hat{\boldsymbol{X}} + \boldsymbol{d}\,. \tag{7.10}$$

Within the utilized isoparametric concept the displacements and its variation and increment are approximated by the same ansatz as the geometry such that

$$\boldsymbol{u}_h = \mathbb{N}\, \boldsymbol{d}\,, \quad \delta \boldsymbol{u}_h = \mathbb{N}\, \delta \boldsymbol{d}\,, \quad \Delta \boldsymbol{u}_h = \mathbb{N}\, \Delta \boldsymbol{d}\,. \tag{7.11}$$

The approximation of the right Cauchy-Green tensor follows simply by $\boldsymbol{C}_h = \boldsymbol{F}_h^T \boldsymbol{F}_h$. The deformation gradient is constructed with aid of the chain rule as

$$\boldsymbol{F}_h = \frac{\partial \boldsymbol{x}_h}{\partial \boldsymbol{X}_h} = \boldsymbol{I} + \frac{\partial \boldsymbol{u}_h}{\partial \boldsymbol{X}_h} = \boldsymbol{I} + \frac{\partial \boldsymbol{u}_h}{\partial \boldsymbol{\xi}} \left(\frac{\partial \boldsymbol{X}_h}{\partial \boldsymbol{\xi}} \right)^{-1}, \tag{7.12}$$

where $\boldsymbol{I}$ denotes the second order identity tensor. With this in hands the discrete counterpart of the weak form and its linearization related to Equations (6.3) and (6.4) are obtained for a typical element e as

$$\begin{aligned} G_h^e &= \underbrace{\left(\int_{\Omega^e} \frac{\partial(\psi(\boldsymbol{C}_h) - \boldsymbol{u}_h \cdot \boldsymbol{f})}{\partial \boldsymbol{d}} \, \mathrm{d}V - \int_{\partial\Omega^e} \frac{\partial(\boldsymbol{u}_h \cdot \boldsymbol{t})}{\partial \boldsymbol{d}} \, \mathrm{d}A \right)}_{\boldsymbol{r}^e} \cdot \delta \boldsymbol{d} = 0 \,, \\ \Delta G_h^e &= \left(\underbrace{\int_{\Omega^e} \frac{\partial^2 \psi(\boldsymbol{C}_h)}{\partial \boldsymbol{d} \, \partial \boldsymbol{d}} \, \mathrm{d}V}_{\boldsymbol{k}^e} \, \Delta \boldsymbol{d} \right) \cdot \delta \boldsymbol{d} \,, \end{aligned} \tag{7.13}$$

whereas $\boldsymbol{k}^e$ and $\boldsymbol{r}^e$ denote the element stiffness matrix and element residual vector. Assembling of all element stiffness matrices and element residual vectors yield the global stiffness matrix $\boldsymbol{K}$ and residual vector $\boldsymbol{R}$ as

$$\boldsymbol{K} = \mathop{\mathsf{A}}_{e=1}^{num_{ele}} \boldsymbol{k}^e \,, \quad \boldsymbol{R} = \mathop{\mathsf{A}}_{e=1}^{num_{ele}} \boldsymbol{r}^e \,. \tag{7.14}$$

The global discrete linearized system of equations follows by

$$\delta \boldsymbol{D}^T \left(\boldsymbol{K} \, \Delta \boldsymbol{D} + \boldsymbol{R} \right) = 0 \quad \forall \, \delta \boldsymbol{D} \neq \boldsymbol{0} \,, \tag{7.15}$$

whereas $\delta \boldsymbol{D}$, $\Delta \boldsymbol{D}$ denote the vectors of variation and increment of the global nodal displacements. Thus the increment of the nodal displacements is computed iteratively by $\Delta \boldsymbol{D} = -\boldsymbol{K}^{-1} \boldsymbol{R}$ until $|\boldsymbol{R}|$ approaches zero.

7.2 A Family of Assumed Stress Finite Elements for Hyperelasticity

The geometry, displacements and its variations and increments are approximated as in Equations (7.8) and (7.11), using lowest order Lagrange type interpolations functions for hexahedra. Also the approximation of the deformation gradient and the right Cauchy-Green tensor follows the same approach as in the pure displacement based element given by Equation (7.12). The interpolation of the assumed stress field in the parametric space is given in Voigt type vector notation by

$$\underline{\boldsymbol{S}}_\xi = (S_{\xi\xi}, S_{\eta\eta}, S_{\zeta\zeta}, S_{\xi\eta}, S_{\eta\zeta}, S_{\xi\zeta})^T = \mathbb{L}_\xi \, \boldsymbol{\beta} \,, \tag{7.16}$$

where due to the symmetry of the second Piola Kirchhoff stress only the six independent components are considered and $\boldsymbol{\beta}$ denotes the vector of element-wise unknowns. The interpolation matrix $\mathbb{L}_\xi$ has the general structure

$$\mathbb{L}_\xi = \mathrm{diag} \left(\mathbb{L}_{\xi\xi}, \mathbb{L}_{\eta\eta}, \mathbb{L}_{\zeta\zeta}, \mathbb{L}_{\xi\eta}, \mathbb{L}_{\eta\zeta}, \mathbb{L}_{\xi\zeta} \right) \,, \tag{7.17}$$

containing the corresponding interpolation functions. A variety of suitable interpolation functions have already been discussed in chapter 5.4.1 regarding the linearized theory and is accordingly omitted here. The transformation from the isoparametric domain to the reference configuration for the second Piola-Kirchhoff stresses is described by

$$\boldsymbol{S}_h = \boldsymbol{J}_0 \, \boldsymbol{S}_\xi \, \boldsymbol{J}_0^T \quad \text{with} \quad \boldsymbol{S}_\xi = \begin{pmatrix} S_{\xi\xi} & S_{\xi\eta} & S_{\xi\zeta} \\ S_{\xi\eta} & S_{\eta\eta} & S_{\eta\zeta} \\ S_{\xi\zeta} & S_{\eta\zeta} & S_{\zeta\zeta} \end{pmatrix} \,, \tag{7.18}$$

where the Jacobian matrix $\boldsymbol{J}$, which maps from the isoparametric coordinates $\boldsymbol{\xi}$ to reference coordinates $\boldsymbol{X}$, follows as

$$\boldsymbol{J} = \frac{\partial \boldsymbol{X}(\boldsymbol{\xi})}{\partial \boldsymbol{\xi}} \quad \text{and} \quad \boldsymbol{J}_0 = \left.\frac{\partial \boldsymbol{X}(\boldsymbol{\xi})}{\partial \boldsymbol{\xi}}\right|_{\boldsymbol{\xi}=0} . \tag{7.19}$$

In order to pass the patch test, which is discussed in Chapter 7.5.1, it is necessary to use the values of the Jacobian at the origin $\{\xi, \eta, \zeta\} = \{0, 0, 0\}$ as it is discussed in Pian and Sumihara [1984] and Pian and Tong [1986]. In general cases, where an explicit form of the complementary stored energy function is not known, the constitutive relation has to be computed iteratively. Therefore $\boldsymbol{E}^S$ is considered as a Gauss point based history dependent variable, which implicitly evaluates the constitutive relation. Therefore $\boldsymbol{E}^S$ is computed iteratively at each integration point $\boldsymbol{E}^S$ from the discrete counterpart of the residual given in Equation (6.8)

$$\boldsymbol{r}(\boldsymbol{E}^S, \boldsymbol{S}_h) = \boldsymbol{S}_h - \left.\frac{\partial \psi(\widehat{\boldsymbol{E}})}{\partial \widehat{\boldsymbol{E}}}\right|_{\widehat{\boldsymbol{E}}=\boldsymbol{E}^S} = \boldsymbol{0} . \tag{7.20}$$

The application of a Newton-Raphson scheme, compare Equation (6.9), leads to the discrete update algorithm

$$\boldsymbol{E}^S_{n+1} = \boldsymbol{E}^S_n + \underbrace{\left[\left.\frac{\partial^2 \psi(\widehat{\boldsymbol{E}})}{\partial \widehat{\boldsymbol{E}}\, \partial \widehat{\boldsymbol{E}}}\right|_{\widehat{\boldsymbol{E}}=\boldsymbol{E}^S_n}\right]^{-1}}_{=:\,\mathbb{D}} : \boldsymbol{r}(\boldsymbol{E}^S_n,\, \boldsymbol{S}_h) \tag{7.21}$$

until $\|\boldsymbol{r}(\boldsymbol{E}^S_n, \boldsymbol{S}_h)\| \approx 0$. Here, $\mathbb{D}$ represents a fourth order complementary constitutive tensor. Table 7.1 sketches the nested algorithmic treatment for a typical element for the case of an unknown explicit complementary stored energy. Note that in the numerical implementation the calculation of $\boldsymbol{E}^s$ is realized in Voigt notation which enables a simple inversion of the constitutive tensor $\mathbb{D}$, assuming nonsingularity. The discrete counterparts of the weak forms related to Equation (6.6) for a typical element e are given by

$$\begin{aligned} G^e_{h,u} &= \underbrace{\left(\int_{\Omega^e} \frac{\partial (\boldsymbol{E}_h : \boldsymbol{S}_h - \boldsymbol{u}_h \cdot \boldsymbol{f})}{\partial \boldsymbol{d}} \,\mathrm{d}V - \int_{\partial\Omega^e} \frac{\partial (\boldsymbol{u}_h \cdot \boldsymbol{t}_0)}{\partial \boldsymbol{d}} \mathrm{d}A \right)}_{\boldsymbol{r}^e_u} \cdot \delta \boldsymbol{d} = 0 , \\ G^e_{h,S} &= \underbrace{\left(\int_{\Omega^e} \frac{\partial (\boldsymbol{S}_h : (\boldsymbol{E}_h - \boldsymbol{E}^S))}{\partial \boldsymbol{\beta}} \,\mathrm{d}V \right)}_{\boldsymbol{r}^e_S} \cdot \delta \boldsymbol{\beta} = 0 , \end{aligned} \tag{7.22}$$

whereas the discrete Green-Lagrange strain tensor follows simply as $\boldsymbol{E}_h = \frac{1}{2}(\boldsymbol{C}_h - \boldsymbol{I})$.

ELEMENT LOOP

(1) Update displacements and stresses (Newton iteration k+1)

$\boldsymbol{d} = \boldsymbol{d}_n^{(k)} + \Delta\boldsymbol{d}$, $\boldsymbol{\beta} = \boldsymbol{\beta}_n^{(k)} + \Delta\boldsymbol{\beta}$

INTEGRATION LOOP

(2) Compute stresses $\boldsymbol{S}_h$ and Green-Lagrange strain tensor $\boldsymbol{E}_h$ in each Gauss Point:

$\underline{\boldsymbol{S}}_\xi = \boldsymbol{L}\,\boldsymbol{\beta}$, $\boldsymbol{S}_h = \boldsymbol{J}_0 \boldsymbol{S}_\xi \boldsymbol{J}_0^T$,

$\boldsymbol{u}_h = \mathbb{N}\,\boldsymbol{d}$, $\boldsymbol{F}_h = \boldsymbol{I} + \frac{\partial \boldsymbol{u}_h}{\partial \boldsymbol{X}_h}$, $\boldsymbol{C}_h = \boldsymbol{F}_h^T \boldsymbol{F}_h$, $\boldsymbol{E}_h = \frac{1}{2}(\boldsymbol{C}_h - \boldsymbol{I})$

Read from history: $\boldsymbol{E}^S$

CONSTITUTIVE LOOP

(3) Compute residuum: $\boldsymbol{r}(\boldsymbol{E}^S, \boldsymbol{S}_h) = \boldsymbol{S}_h - \boldsymbol{S}^E$

with $\boldsymbol{S}^E = \partial_{\widehat{\boldsymbol{E}}} \psi(\widehat{\boldsymbol{E}})|_{\widehat{\boldsymbol{E}}=\boldsymbol{E}^S}$

(4) Update: $\boldsymbol{E}^S = \boldsymbol{E}^S + \mathbb{D} : \boldsymbol{r}(\boldsymbol{E}^S, \boldsymbol{S}_h)$

with $\mathbb{D} = (\partial_{\widehat{\boldsymbol{E}}} \boldsymbol{S}^E|_{\widehat{\boldsymbol{E}}=\boldsymbol{E}^S})^{-1}$

(5) Check convergence

IF $\|\mathbb{D} : \boldsymbol{r}(\boldsymbol{\phi}, \boldsymbol{S}_h)\|^2 \leq tol$

THEN Update History $\boldsymbol{E}^S$ and exit CONSTITUTIVE LOOP

(6) Check divergence

IF $n_{\text{iter}} > n_{\text{tol}}$ THEN Stop Calculation

(7) Determine and export element stiffness and rhs-vector

Table 7.1: Nested algorithmic treatment for a single element

The discrete increments for a typical element e related to Equation (6.10) follow as

$$\begin{aligned}
\Delta G^e_{h,u} &= \Bigg(\underbrace{\int_{\Omega^e} \frac{\partial^2 (\boldsymbol{E}_h : \boldsymbol{S}_h)}{\partial \boldsymbol{d}\, \partial \boldsymbol{d}} \, \mathrm{d}V}_{\boldsymbol{k}^e_{uu}} \Delta \boldsymbol{d} + \underbrace{\int_{\Omega^e} \frac{\partial^2 (\boldsymbol{E}_h : \boldsymbol{S}_h)}{\partial \boldsymbol{d}\, \partial \boldsymbol{\beta}} \, \mathrm{d}V}_{\boldsymbol{k}^e_{uS}} \Delta \boldsymbol{\beta} \Bigg) \cdot \delta \boldsymbol{d} \,, \\
\Delta G^e_{h,S} &= \Bigg(\underbrace{\int_{\Omega^e} \frac{\partial^2 (\boldsymbol{E}_h : \boldsymbol{S}_h)}{\partial \boldsymbol{\beta}\, \partial \boldsymbol{d}} \, \mathrm{d}V}_{\boldsymbol{k}^e_{Su}} \Delta \boldsymbol{d} - \underbrace{\int_{\Omega^e} \frac{\partial^2 (\frac{1}{2} \boldsymbol{S}_h : \mathbb{D} : \boldsymbol{S}_h)}{\partial \boldsymbol{\beta}\, \partial \boldsymbol{\beta}} \, \mathrm{d}V}_{\boldsymbol{k}^e_{SS}} \Delta \boldsymbol{\beta} \Bigg) \cdot \delta \boldsymbol{\beta} \,.
\end{aligned} \tag{7.23}$$

Assembling over the number of elements n_{ele} leads to the global system of equations

$$\mathop{\mathsf{A}}_{e=1}^{num_{ele}} \begin{bmatrix} \delta \boldsymbol{d}^T \\ \delta \boldsymbol{\beta}^T \end{bmatrix} \left(\begin{bmatrix} \boldsymbol{k}^e_{uu} & \boldsymbol{k}^e_{uS} \\ \boldsymbol{k}^e_{Su} & \boldsymbol{k}^e_{SS} \end{bmatrix} \begin{bmatrix} \Delta \boldsymbol{d} \\ \Delta \boldsymbol{\beta} \end{bmatrix} + \begin{bmatrix} \boldsymbol{r}^e_u \\ \boldsymbol{r}^e_S \end{bmatrix} \right) = \delta \boldsymbol{D}^T (\boldsymbol{K}\, \Delta \boldsymbol{D} + \boldsymbol{R}) = 0 \tag{7.24}$$

and therefore the nodal unknowns are computed via

$$\Delta \boldsymbol{D} = -\boldsymbol{K}^{-1} \boldsymbol{R} \,. \tag{7.25}$$

Due to the element-wise discontinuous interpolation of the stresses, the unknowns $\Delta \boldsymbol{\beta}$ may already be eliminated at element level. This leads to a global system of equations with the same number of unknowns, and almost the same computational cost, as a displacement based trilinear element.

7.3 Displacement-Pressure Finite Elements

In both discussed formulations, regarding the displacement pressure approach the same approximation as for the displacement based approach is considered for the geometry, displacements its variations and its increments, following Equations (7.8) and (7.11). Also the approximation of the deformation gradient and right Cauchy-Green tensor is the same as in the pure displacement based approach. In addition the pressure field, its virtual counterpart and increment are approximated by

$$\begin{aligned}
p_h &= \sum_{I=1}^{n_{\text{p-nodes}}} \widehat{N}^I(\boldsymbol{\xi})\, \eta^I &&= \widehat{\mathbb{N}}\, \boldsymbol{\eta} \,, \\
\delta p_h &= \sum_{I=1}^{n_{\text{p-nodes}}} \widehat{N}^I(\boldsymbol{\xi})\, \delta \eta^I &&= \widehat{\mathbb{N}}\, \delta \boldsymbol{\eta} \,, \\
\Delta p_h &= \sum_{I=1}^{n_{\text{p-nodes}}} \widehat{N}^I(\boldsymbol{\xi})\, \Delta \eta^I &&= \widehat{\mathbb{N}}\, \Delta \boldsymbol{\eta}
\end{aligned} \tag{7.26}$$

where η^I is the pressure related degree of freedom, $n_{\text{p-nodes}}$ the number of pressure related nodes and $\widehat{N}^I$ denotes the Lagrangian type interpolation function corresponding to the interpolation order of the pressure.

7.3.1 Classical Approach

In the classical discrete version of the displacement pressure formulation the approximated second Piola-Kirchhoff stresses appear with $J_h = \det \boldsymbol{F}_h$ as

$$\boldsymbol{S}_h(\boldsymbol{C}_h, p_h) = 2\,\frac{\partial \psi^{\text{comp}}(\boldsymbol{C}_h)}{\partial \boldsymbol{C}_h} + p_h \vartheta'(J_h)\, J_h\, \boldsymbol{C}_h^{-1}\,, \tag{7.27}$$

compare Equation (6.17). Therefore the discrete counterparts of the weak forms in Equation (6.19) follow for a typical element e as

$$\begin{aligned} G^e_{h,u} &= \Bigg(\underbrace{\int_{\Omega^e} \frac{\partial(\psi^{\text{comp}}(\boldsymbol{C}_h) + p_h\,\vartheta(J_h) - \boldsymbol{u}_h \cdot \boldsymbol{f})}{\partial \boldsymbol{d}}\,\mathrm{d}V - \int_{\partial\Omega^e} \frac{\partial(\boldsymbol{u}_h \cdot \boldsymbol{t}_0)}{\partial \boldsymbol{d}}\,\mathrm{d}A}_{\boldsymbol{r}^e_u} \Bigg) \cdot \delta\boldsymbol{d} = 0\,, \\ G^e_{h,p} &= \underbrace{\int_{\Omega^e} \frac{\partial((\vartheta(J_h) - \frac{1}{2\Lambda}\,p_h)\,p_h)}{\partial \boldsymbol{\eta}}\,\mathrm{d}V}_{\boldsymbol{r}^e_p} \cdot \delta\boldsymbol{\eta} = 0\,. \end{aligned} \tag{7.28}$$

The discrete counterparts of the increments in Equation (6.20) are given by

$$\begin{aligned} \Delta G^e_{h,u} &= \Bigg(\underbrace{\int_{\Omega^e} \frac{\partial^2(\psi^{\text{comp}}(\boldsymbol{C}_h) + p_h\,\vartheta(J_h))}{\partial \boldsymbol{d}\,\partial \boldsymbol{d}}\,\mathrm{d}V}_{\boldsymbol{k}^e_{uu}}\,\Delta\boldsymbol{d} + \underbrace{\int_{\Omega^e} \frac{\partial^2(p_h\,\vartheta(J_h))}{\partial \boldsymbol{d}\,\partial \boldsymbol{\eta}}\,\mathrm{d}V}_{\boldsymbol{k}^e_{up}}\,\Delta\boldsymbol{\eta} \Bigg) \cdot \delta\boldsymbol{d}\,, \\ \Delta G^e_{h,p} &= \Bigg(\underbrace{\int_{\Omega^e} \frac{\partial^2(p_h\,\vartheta(J_h))}{\partial \boldsymbol{\eta}\,\partial \boldsymbol{d}}\,\mathrm{d}V}_{\boldsymbol{k}^e_{pu}}\,\Delta\boldsymbol{d} - \underbrace{\int_{\Omega^e} \frac{\partial^2(\frac{1}{2\Lambda}\,{p_h}^2)}{\partial \boldsymbol{\eta}\,\partial \boldsymbol{\eta}}\,\mathrm{d}V}_{\boldsymbol{k}^e_{pp}}\,\Delta\boldsymbol{\beta} \Bigg) \cdot \delta\boldsymbol{\eta}\,. \end{aligned} \tag{7.29}$$

Assembling over the number of elements n_{ele} leads to the global system of equations

$$\overset{num_{ele}}{\underset{e\,=\,1}{\mathbf{A}}} \begin{bmatrix} \delta\boldsymbol{d}^T \\ \delta\boldsymbol{\eta}^T \end{bmatrix} \left(\begin{bmatrix} \boldsymbol{k}^e_{uu} & \boldsymbol{k}^e_{up} \\ \boldsymbol{k}^e_{pu} & \boldsymbol{k}^e_{pp} \end{bmatrix} \begin{bmatrix} \Delta\boldsymbol{d} \\ \Delta\boldsymbol{\eta} \end{bmatrix} + \begin{bmatrix} \boldsymbol{r}^e_u \\ \boldsymbol{r}^e_p \end{bmatrix} \right) = \delta\boldsymbol{D}(\boldsymbol{K}\,\Delta\boldsymbol{D} + \boldsymbol{R}) = 0 \tag{7.30}$$

and therefore the nodal unknowns are computed via

$$\Delta\boldsymbol{D} = -\boldsymbol{K}^{-1}\boldsymbol{R}\,. \tag{7.31}$$

In case of a discontinuous interpolation of the pressure field and compressibility, the unknowns $\Delta\boldsymbol{\eta}$ in can be eliminated at element level resulting in a formulation with the system size depending only on the displacement approximation.

7.3.2 Consistent Complementary Approach

Considering the consistent complementary approach, the discrete second Piola-Kirchhoff stresses appear following Equation (6.16) as

$$\boldsymbol{S}_h(\boldsymbol{C}_h, p_h) = 2\,\frac{\partial \psi^{\text{comp}}(\boldsymbol{C}_h)}{\partial \boldsymbol{C}_h} + p_h\, J_h\, \boldsymbol{C}_h^{-1}\,. \tag{7.32}$$

In accordance to the derivation in Chapter 6.2.3, the volume dilation is computed as a function of the pressure. Therefore, we introduce the Gauss point based history variable θ which fulfills the residual at fixed p_h

$$r(\theta, p_h) := \Lambda\, \vartheta(\theta)\, \vartheta'(\theta) - p_h = 0\,. \tag{7.33}$$

The linearization of this residual is obtained by

$$\mathrm{Lin}[r(\theta, p_h)] = r(\theta_n, p_h) + \left.\frac{\partial r(\theta, p_h)}{\partial \theta}\right|_{\theta=\theta_n} \Delta\theta\,. \tag{7.34}$$

From $\mathrm{Lin}[r(\theta, p_h)] = 0$ the increment of θ is computed as

$$\Delta\theta = -\left(\left.\frac{\partial r(\theta, p_h)}{\partial \theta}\right|_{\theta=\theta_n}\right)^{-1} r(\theta, p_h)\,, \tag{7.35}$$

which yields for the final Newton step

$$\theta_{n+1} = c_1 + p_h c_2\,, \tag{7.36}$$

where the following abbreviations have been utilized

$$\begin{aligned} c_1 &:= \theta_n - \frac{\vartheta(\theta_n)\vartheta'(\theta_n)}{(\vartheta'(\theta_n)\vartheta'(\theta_n) + \vartheta''(\theta_n)\vartheta(\theta_n))}\,, \\ c_2 &:= \frac{1}{\Lambda(\vartheta'(\theta_n)\vartheta'(\theta_n) + \vartheta''(\theta_n)\vartheta(\theta_n))}\,. \end{aligned}$$

For a typical element e the discrete weak form follows as

$$\begin{aligned} G^e_{h,u} &= \underbrace{\left(\int_{\Omega^e} \frac{\partial(\psi^{\mathrm{comp}} + p_h\, J_h - \boldsymbol{u}_h \cdot \boldsymbol{f})}{\partial \boldsymbol{d}}\, \mathrm{d}V - \int_{\partial\Omega^e} \frac{\partial(\boldsymbol{u}_h \cdot \boldsymbol{t}_0)}{\partial \boldsymbol{d}}\, \mathrm{d}A\right)}_{\boldsymbol{r}^e_u} \cdot \delta\boldsymbol{d} = 0\,, \\ G^e_{h,p} &= \underbrace{\int_{\Omega^e} \frac{\partial((J_h - c_1 - \frac{1}{2}c_2\, p_h)p_h)}{\partial \boldsymbol{\eta}} \mathrm{d}V}_{\boldsymbol{r}^e_p} \cdot \delta\boldsymbol{\eta} = 0\,, \end{aligned} \tag{7.37}$$

with the corresponding increments as

$$\begin{aligned} \Delta G^e_{h,u} &= \left(\underbrace{\int_{\Omega^e} \frac{\partial^2(\psi^{\mathrm{comp}} + p_h\, J_h)}{\partial \boldsymbol{d}\, \partial \boldsymbol{d}} \mathrm{d}V}_{\boldsymbol{k}^e_{uu}} \Delta\boldsymbol{d} + \underbrace{\int_{\Omega^e} \frac{\partial^2(p_h\, J_h)}{\partial \boldsymbol{d}\, \partial \boldsymbol{\eta}}\, \mathrm{d}V}_{\boldsymbol{k}^e_{up}} \Delta\boldsymbol{\eta}\right) \cdot \delta\boldsymbol{d}\,, \\ \Delta G^e_{h,p} &= \left(\underbrace{\int_{\Omega^e} \frac{\partial^2(p_h\, J_h)}{\partial \boldsymbol{\eta}\, \partial \boldsymbol{d}}\, \mathrm{d}V}_{\boldsymbol{k}^e_{pu}} \Delta\boldsymbol{d} - \underbrace{\int_{\Omega^e} \frac{\partial^2(\frac{1}{2}c_2\, {p_h}^2)}{\partial \boldsymbol{\eta}\, \partial \boldsymbol{\eta}}\, \mathrm{d}V}_{\boldsymbol{k}^e_{pp}} \Delta\boldsymbol{\beta}\right) \cdot \delta\boldsymbol{\eta}\,. \end{aligned} \tag{7.38}$$

Assembling over the number of elements n_{ele} leads to the global system of equations

$$\overset{num_{ele}}{\underset{e=1}{\mathbf{A}}} \begin{bmatrix} \delta \boldsymbol{d}^T \\ \delta \boldsymbol{\eta}^T \end{bmatrix} \left(\begin{bmatrix} \boldsymbol{k}^e_{uu} & \boldsymbol{k}^e_{up} \\ \boldsymbol{k}^e_{pu} & \boldsymbol{k}^e_{pp} \end{bmatrix} \begin{bmatrix} \Delta \boldsymbol{d} \\ \Delta \boldsymbol{\eta} \end{bmatrix} + \begin{bmatrix} \boldsymbol{r}^e_u \\ \boldsymbol{r}^e_p \end{bmatrix} \right) = \delta \boldsymbol{D} (\boldsymbol{K} \, \Delta \boldsymbol{D} + \boldsymbol{R}) = 0 \tag{7.39}$$

and therefore the nodal unknowns are computed via

$$\Delta \boldsymbol{D} = -\boldsymbol{K}^{-1} \boldsymbol{R} \, . \tag{7.40}$$

In case of elementwise discontinuous interpolation of the pressure field and compressibility, the unknowns $\Delta \boldsymbol{\eta}$ in can be eliminated at element level resulting in a formulation with the system size depending only on the displacement approximation. In the following numerical examples the stabilized elements will be denoted as ${}^*\mathrm{T}_2\mathrm{dP}_0$, ${}^*\mathrm{T}_2\mathrm{P}_1$ and ${}^*\mathrm{Q}_1\mathrm{dP}_0$.

7.4 Enhanced Assumed Strain Elements

The basic idea of the enhanced assumed strain formulation for hyperelasticity is the enhancement of the deformation gradient by a piecewise continuous function. The approximation of the geometry, displacements and its gradient and virtual counterparts are given by Equation (7.8) and (7.11). Note that for this formulation N^I is restricted to trilinear Lagrangian interpolation functions. The enhanced assumed displacement gradient in the parametric space is approximated in Voigt type vector notation according to

$$\underline{\boldsymbol{F}}^{\text{enh}}_{\xi} = (F^{\text{enh}}_{\xi\xi}, F^{\text{enh}}_{\eta\eta}, F^{\text{enh}}_{\zeta\zeta}, F^{\text{enh}}_{\xi\eta}, F^{\text{enh}}_{\eta\zeta}, F^{\text{enh}}_{\xi\zeta}, F^{\text{enh}}_{\eta\xi}, F^{\text{enh}}_{\zeta\eta}, F^{\text{enh}}_{\zeta\xi}) = \mathbb{M}_{\xi} \, \boldsymbol{\alpha} \tag{7.41}$$

whereas $\boldsymbol{\alpha}$ denotes the vector of element wise unknowns related to the enhanced strain field. The interpolation matrix $\mathbb{M}_{\xi}$ has the general structure

$$\mathbb{M}_{\xi} = \mathrm{diag}(\mathbb{M}_{\xi\xi}, \mathbb{M}_{\eta\eta}, \mathbb{M}_{\zeta\zeta}, \mathbb{M}_{\xi\eta}, \mathbb{M}_{\eta\zeta}, \mathbb{M}_{\xi\zeta}, \mathbb{M}_{\eta\xi}, \mathbb{M}_{\zeta\eta}, \mathbb{M}_{\zeta\xi}) \tag{7.42}$$

and contains the corresponding interpolation functions. The explicit forms of the considered approximations are summarized by

$\mathbb{M}_{\xi\xi} = (\xi, \xi\eta, \xi\zeta)$	$\mathbb{M}_{\xi\xi} = (\xi, \xi\eta, \xi\zeta)$	$\mathbb{M}_{\xi\xi} = (\xi, \xi\eta, \xi\zeta)$
$\mathbb{M}_{\eta\eta} = (\eta, \eta\zeta, \eta\xi)$	$\mathbb{M}_{\eta\eta} = (\eta, \eta\zeta, \eta\xi)$	$\mathbb{M}_{\eta\eta} = (\eta, \eta\zeta, \eta\xi)$
$\mathbb{M}_{\zeta\zeta} = (\zeta, \zeta\xi, \zeta\eta)$	$\mathbb{M}_{\zeta\zeta} = (\zeta, \zeta\xi, \zeta\eta)$	$\mathbb{M}_{\zeta\zeta} = (\zeta, \zeta\xi, \zeta\eta)$
$\mathbb{M}_{\xi\eta} = \emptyset$	$\mathbb{M}_{\xi\eta} = (\eta)$	$\mathbb{M}_{\xi\eta} = (\eta, \eta\zeta)$
$\mathbb{M}_{\eta\xi} = \emptyset$	$\mathbb{M}_{\eta\xi} = (\xi)$	$\mathbb{M}_{\eta\xi} = (\xi, \xi\zeta)$
$\mathbb{M}_{\eta\zeta} = \emptyset$	$\mathbb{M}_{\eta\zeta} = (\zeta)$	$\mathbb{M}_{\eta\zeta} = (\zeta, \xi\zeta)$
$\mathbb{M}_{\zeta\eta} = \emptyset$	$\mathbb{M}_{\zeta\eta} = (\eta)$	$\mathbb{M}_{\zeta\eta} = (\eta, \xi\eta)$
$\mathbb{M}_{\xi\zeta} = \emptyset$	$\mathbb{M}_{\xi\zeta} = (\zeta)$	$\mathbb{M}_{\xi\zeta} = (\zeta, \zeta\eta)$
$\mathbb{M}_{\zeta\xi} = \emptyset$	$\mathbb{M}_{\zeta\xi} = (\xi)$	$\mathbb{M}_{\zeta\xi} = (\xi, \xi\eta)$
9 enhanced strain modes	15 enhanced strain modes	21 enhanced strain modes

(7.43)

Following the remarks of Glaser and Armero [1997], the transformation from the isoparametric domain to the physical space is described by

$$\boldsymbol{F}_h^{\text{enh}} = \frac{\det \boldsymbol{J}_0}{\det \boldsymbol{J}} \boldsymbol{F}_0 \, \boldsymbol{J}_0^{-T} \, \boldsymbol{F}_\xi^{\text{enh}} \, \boldsymbol{J}_0^{-1} \quad \text{with } \boldsymbol{F}_\xi^{\text{enh}} = \begin{pmatrix} F_{\xi\xi}^{\text{enh}} & F_{\xi\eta}^{\text{enh}} & F_{\xi\zeta}^{\text{enh}} \\ F_{\eta\xi}^{\text{enh}} & F_{\eta\eta}^{\text{enh}} & F_{\eta\zeta}^{\text{enh}} \\ F_{\zeta\xi}^{\text{enh}} & F_{\zeta\eta}^{\text{enh}} & F_{\zeta\zeta}^{\text{enh}} \end{pmatrix} . \tag{7.44}$$

The multiplication with the constant part of the deformation gradient $\boldsymbol{F}_0$ is necessary in order to ensure objectivity of the formulation. Note that the interpolation matrix is chosen in such a way, that for $\boldsymbol{F} = \boldsymbol{I}$ $\text{sym}[\boldsymbol{F}_\xi^{\text{enh}}]$ is equivalent to the enhanced assumed strain field $\widehat{\boldsymbol{\varepsilon}}_\xi$ in the linear theory, compare Equation (5.68). In a next step the deformation gradient and the enhanced counterpart are summed to the underlying kinematic quantity $\widehat{\boldsymbol{F}}_h$. In this framework different enhancement techniques have been applied in the literature

$$\begin{aligned} &\text{Classical EAS (Simo and Armero [1992]):} && \widehat{\boldsymbol{F}}_h = \boldsymbol{F}_h + \boldsymbol{F}_h^{\text{enh}} , \\ &\text{Transposed EAS (Korelc and Wriggers [1996]):} && \widehat{\boldsymbol{F}}_h = \boldsymbol{F}_h + \boldsymbol{F}_h^{\text{enh}^T} . \\ &\text{Symmetric EAS (Glaser and Armero [1997]):} && \widehat{\boldsymbol{F}}_h = \boldsymbol{F}_h + \text{sym}[\boldsymbol{F}_h^{\text{enh}}] , \end{aligned} \tag{7.45}$$

It should be noted that for the reduction to linear elasticity all three formulations are consistent with the proposed enhanced assumed strain approximation discussed in Chapter 5.6. In the scope of this thesis we consider only the classical discretization approach of Equation $(7.45)_1$. The enriched right Cauchy-Green tensor, which is the basis for the constitutive relation, follows simply by $\widehat{\boldsymbol{C}}_h = \widehat{\boldsymbol{F}}_h^T \widehat{\boldsymbol{F}}_h$. With this in hand, the discretized weak form follows for a typical element e as

$$\begin{aligned} G_{h,u}^e &= \underbrace{\left(\int_{\Omega^e} \frac{\partial (\psi(\widehat{\boldsymbol{C}}_h) - \boldsymbol{u}_h \cdot \boldsymbol{f})}{\partial \boldsymbol{d}} \, \mathrm{d}V - \int_{\partial\Omega^e} \frac{\partial (\boldsymbol{u}_h \cdot \boldsymbol{t})}{\partial \boldsymbol{d}} \, \mathrm{d}A \right)}_{\boldsymbol{r}_u^e} \cdot \delta \boldsymbol{d} = 0 , \\ G_{h,F}^e &= \underbrace{\left(\int_{\Omega^e} \frac{\partial \psi(\widehat{\boldsymbol{C}}_h)}{\partial \boldsymbol{\alpha}} \mathrm{d}V \right)}_{\boldsymbol{r}_F^e} \cdot \delta \boldsymbol{\alpha} = 0 . \end{aligned} \tag{7.46}$$

with the corresponding increments as

$$\begin{aligned} \Delta G_{h,u}^e &= \left(\underbrace{\int_{\Omega^e} \frac{\partial^2 \psi(\widehat{\boldsymbol{C}}_h)}{\partial \boldsymbol{d} \, \partial \boldsymbol{d}} \mathrm{d}V}_{\boldsymbol{k}_{uu}^e} \Delta \boldsymbol{d} + \underbrace{\int_{\Omega^e} \frac{\partial^2 \psi(\widehat{\boldsymbol{C}}_h)}{\partial \boldsymbol{d} \, \partial \boldsymbol{\alpha}} \, \mathrm{d}V}_{\boldsymbol{k}_{uF}^e} \Delta \boldsymbol{\alpha} \right) \cdot \delta \boldsymbol{d} , \\ \Delta G_{h,F}^e &= \left(\underbrace{\int_{\Omega^e} \frac{\partial^2 \psi(\widehat{\boldsymbol{C}}_h)}{\partial \boldsymbol{\alpha} \, \partial \boldsymbol{d}} \, \mathrm{d}V}_{\boldsymbol{k}_{Fu}^e} \Delta \boldsymbol{d} + \underbrace{\int_{\Omega^e} \frac{\partial^2 \psi(\widehat{\boldsymbol{C}})}{\partial \boldsymbol{\alpha} \, \partial \boldsymbol{\alpha}} \mathrm{d}V}_{\boldsymbol{k}_{FF}^e} \Delta \boldsymbol{\alpha} \right) \cdot \delta \boldsymbol{\alpha} , \end{aligned} \tag{7.47}$$

Assembling over the number of elements n_{ele} leads to the global system of equations

$$\mathop{\mathsf{A}}_{e=1}^{num_{ele}} \begin{bmatrix} \delta \boldsymbol{d}^T \\ \delta \boldsymbol{\alpha}^T \end{bmatrix} \left(\begin{bmatrix} \boldsymbol{k}_{uu}^e & \boldsymbol{k}_{uF}^e \\ \boldsymbol{k}_{Fu}^e & \boldsymbol{k}_{FF}^e \end{bmatrix} \begin{bmatrix} \Delta \boldsymbol{d} \\ \Delta \boldsymbol{\alpha} \end{bmatrix} + \begin{bmatrix} \boldsymbol{r}_u^e \\ \boldsymbol{r}_F^e \end{bmatrix} \right) = \delta \boldsymbol{D} (\boldsymbol{K} \, \Delta \boldsymbol{D} + \boldsymbol{R}) = 0 \tag{7.48}$$

and therefore the nodal unknowns are computed via

$$\Delta \boldsymbol{D} = -\boldsymbol{K}^{-1}\boldsymbol{R}\,. \tag{7.49}$$

Since the enhanced field is approximated discontinuous the unknowns $\Delta\boldsymbol{\alpha}$ can be eliminated on element level resulting in a formulation with the system depending only on the displacement approximation.

7.5 Numerical Examples

In the following chapter the proposed finite elements for isotropic hyperelasticity are compared in a set of numerical benchmarks. Since in most cases no analytical solution exists for nontrivially boundary value problems in the framework of large deformations, the approximation error cannot be computed. Therefore, the convergence of nodal values, e.g. the displacements, at specific points and also the quality of the stress distributions is analyzed. In addition stability investigations are explored, where the occurrence of spurious bifurcation modes (known as hourglassing) are investigated. Unless explicitly specified the underlying constitutive relation is defined by the Neo-Hookean type strain energy function given by the additive split

$$\begin{aligned}
&\psi(\boldsymbol{C}) = \psi^{\mathrm{comp}}(\boldsymbol{C}) + \frac{\Lambda}{2}\vartheta(J)^2 \quad \text{with} \\
&\psi^{\mathrm{comp}}(\boldsymbol{C}) = \frac{\mu}{2}(\mathrm{tr}\boldsymbol{C} - 3) - \mu \ln J \quad \text{and} \\
&\vartheta(J) = J - 1\,.
\end{aligned} \tag{7.50}$$

Note that for this case both discussed formulations related to the displacement-pressure approach presented in Chapter 6.2.3 coincide, since $\vartheta(J)$ is a linear function in J. A list of the element abbreviations is given in Table 5.3.

7.5.1 Patch Test

The patch test is a necessary condition for the convergence of finite elements. It demands that an arbitrary patch of assembled elements is able to reproduce a constant state of stress and strain if subjected to boundary displacements consistent with constant straining. This condition is necessary since with respect to mesh refinement, where $h \to 0$, all boundary value problems tend to constant stress and strains in each element. This test is mainly attributed to the work of Bruce Iron, first presented in Bazeley et al. [1966]. A summary on its theory, practice and possible conclusions on its satisfaction can be found in Taylor et al. [1986]. Following Korelc et al. [2010], two different load scenarios are considered, described in Figures 7.1 and 7.2. Load case (A) prescribes a pure rigid body motion by a rotation around the z-axis. All proposed elements are free of resulting stresses and strains and thus fulfill the first patch test. Load case (B) prescribes a combined deformation of shear and uniaxial strain, which analytical solution leads to a constant strain and stress over the whole domain. All proposed elements result in the expected constant stress and strain field and therefore fulfill the second patch test.

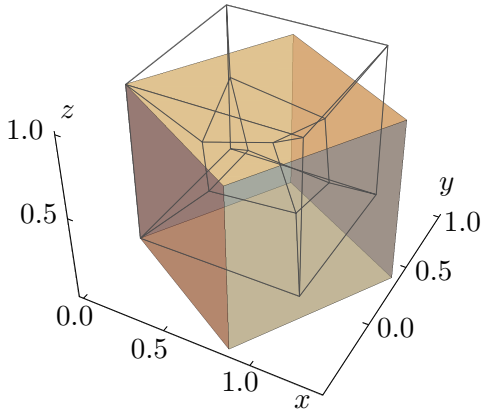

Load case (A):

$x = 0 \wedge y = 0$:
$u_1 = 0$
$u_2 = 0$
$u_3 = 0$

$x = 0 \wedge y = 1 \wedge z = 1$:
$u_1 = 0.5$

Figure 7.1: Patch test 1; Reference mesh depicted by the grid, deformed body depicted by the solid figure.

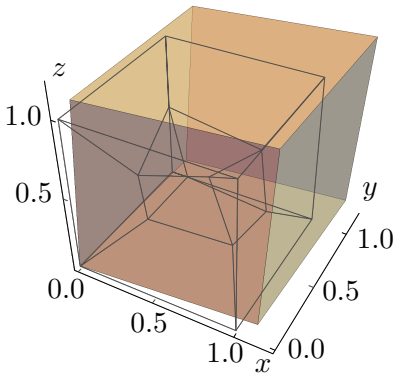

Load case (B):

$x = 0 \vee x = 1 \vee$
$y = 0 \vee y = 1 \vee z = 0 \vee z = 1$:
$u_1 = 0.1x + 0.05y + 0.05z$
$u_2 = 0.05x + 0.1y + 0.05z$
$u_3 = 0.05x + 0.05y + 0.1z$

Figure 7.2: Patch test 2; Reference mesh depicted by the grid, deformed body depicted by the solid figure.

7.5.2 Bending of a Clamped Plate

The following numerical example constitutes a bending dominated problem and is related to the already discussed difficulty of shear locking in the framework of linear elasticity in Chapter 5.7.3. In detail a thin rectangular plate is considered which is clamped at one side and nodal forces which are equivalent to a moment M_0 are applied at the opposing side. The moment is assumed to be a dead-load, i.e. it is referred to the reference configuration of the plate. A sketch of the geometry in the reference and deformed configuration, the boundary conditions and essential parameter are summarized in Figure 7.3. The dimensions of the plate are $10 \times 0.1 \times 10$ and the material parameter are assumed to be compressible with $\Lambda = 1$ and $\mu = 1$. We consider in Figure 7.4 a) the convergence of the nodal displacements $u_2(10, 0.05, 5)$ with respect to mesh refinement. In this example the mesh is uniformly refined with respect to its in-plane direction whereas in thickness direction only a single finite element is considered. Similar to the numerical investigation in case of linear elasticity

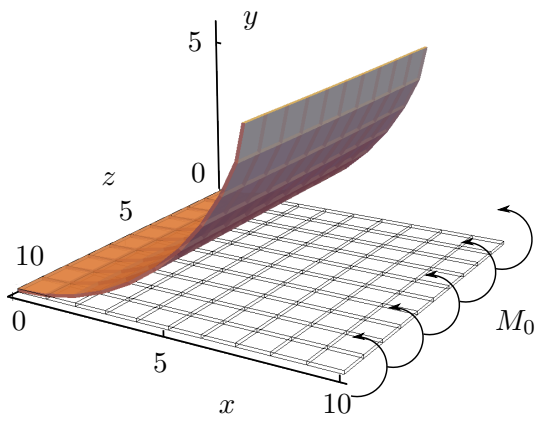

Boundary Conditions:

$x = 0$:
$u_1 = 0$
$u_2 = 0$
$u_3 = 0$

$x = 10$:
$M_0 = 0.001$

Parameter:

$\Lambda = 1$
$\mu = 1$

$l = 10$
$t = 0.1$

Figure 7.3: Bending of a clamped plate; An exemplary reference mesh depicted by the grid and the deformed body depicted by the solid figure.

in Chapter 5.7.3, the elements indicate again the categorization into shear locking free and shear locking formulations. The convergence of the nodal displacements of the Q_1, Q_1dP_0, $AS_{30,39}$, $EAS_{\widetilde{9}}$ and T_1 is distinctly poor due to the shear locking effect. Better convergence is obtained by the shear locking free formulations $AS_{18,24}$, $EAS_{15,21}$, T_2, T_2dP_0 and T_2P_1. These results are consent to the results from the bending analysis in the linear elastic framework, discussed in Chapter 5.7.3. It is remarkable that the primal T_2 element performs slightly better compared to the formulations with an additional approximation of the pressure which is likely due to the low ratio of Λ/μ.

Additional to the characterization of the elements with respect to shear locking, Figure 7.4 b) gives the opportunity to classify them by their robustness considering the load step size. It is remarkable that all assumed stress elements need a maximal number of only three load steps. In contrast all other elements require for the finer meshes a division of the load into 13-20 increments [2.)]. A reason for that superior behavior of the assumed stress elements might be the element-based iteration of the constitutive relation, such that on the global level less constraints have to be taken into account.

[2.)] Here, the results of the T_1 have been ignored by purpose, since due to the intense locking of the nodal displacements the results are incomparable

a) Nodal Displacements:

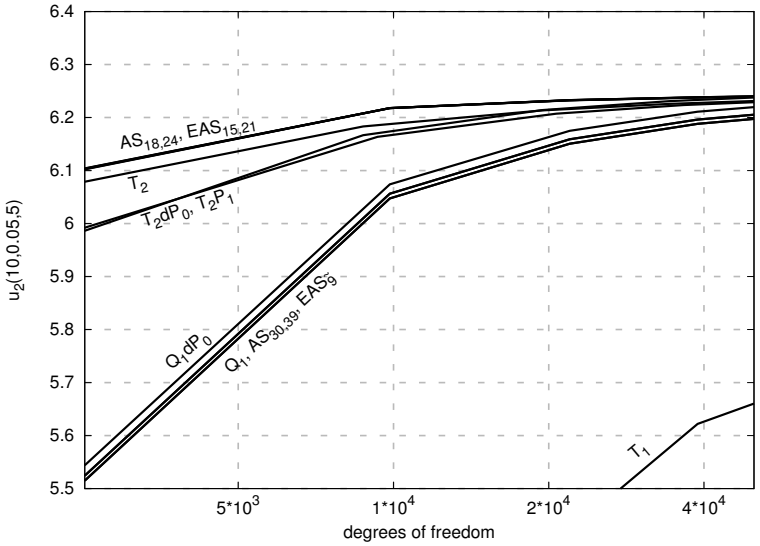

b) Necessary load steps:

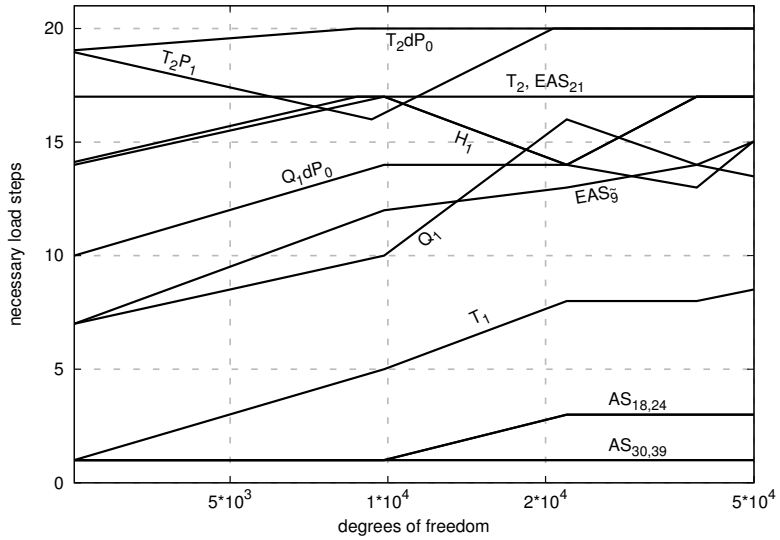

Figure 7.4: Bending of a clamped plate; a) Convergence of nodal displacements $u_2(10, 0.05, 5)$ with respect to the degrees of freedom. b) Number of necessary load steps over the degrees of freedom.

7.5.3 Cook's Membrane

A tapered cantilever beam known as the Cook's membrane problem is considered, representing a bulk related boundary value problem with nearly incompressible material. The geometry, boundary conditions and material parameter are summarized in Figure 7.5. The cantilever, with a thickness of $t = 10$ is clamped on the left and a constant shear stress is applied on the right face. Furthermore, the material parameters are chosen to be nearly incompressible whereas the Lamé parameters are given by $\Lambda = 33288.9$ and $\mu = 66.711$. This corresponds to a Young's modulus of $E = 200$ and a Poisson's ratio of $\nu = 0.499$.

The convergence of the tip displacement for a regular mesh refinement are shown in Figure 7.6 a). In accordance to the discussion of the elements in the linear elastic framework, the suffering due to volumetric locking can be recognized for the displacement based elements T_1, T_2 and Q_1. Note that in the depicted plot, the results for the Q_1 are not shown because the locking leads to such a huge under estimation of the displacements, that even for the finest considered mesh the tip displacements are out of the considered plot range. In detail the resulting displacements for the Q_1 is $u_2(48, 60, 0) = 14.52$ for the case of the finest mesh with 44280 degrees of freedom. In contrast all mixed finite elements achieve a comparably good convergence behavior of the tip displacements, since they do not suffer due to volumetric locking. However, due to the moderate bending of the domain, the group of shear locking free elements still acquires slightly better results.

Consideration of the necessary load steps, depicted in Figure 7.6 b), indicate that the displacement pressure formulations and the assumed stress elements are able to deal with large load steps in case of nearly incompressibility. For this boundary value problem

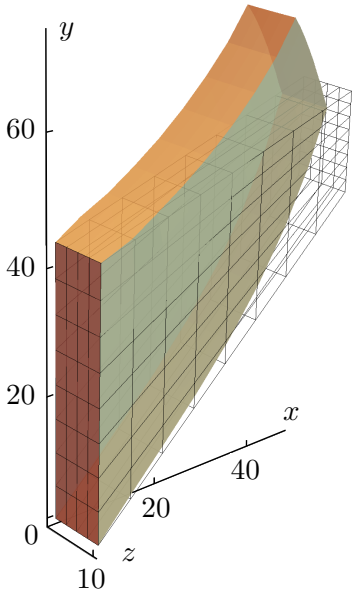

Boundary Conditions:

$x = 0$:
$u_1 = 0$
$u_2 = 0$
$u_3 = 0$

$x = 48$:
$\bar{\boldsymbol{t}} = (0, 15, 0)^T$

Parameters:

$E = 200$
$\nu = 0.499$

$t = 10$

Figure 7.5: Cook's membrane problem; An exemplary reference mesh depicted by the grid and the deformed body depicted by the solid figure on the left and boundary conditions and parameters on the right.

especially the displacement-pressure based elements seem to be superior, since they are able to compute the full deformation in a single load step. In contrast all enhanced assumed strain elements and the second order displacement based element need a much higher number of load increments, leading to a substantially larger computation time. The level of necessary load steps in case of the lowest order displacement based elements is moderate but it should kept in mind that their performance by means of mesh convergence is insufficient. Note that for this boundary value problem the AS_{39} did not converge.

a) Nodal Displacements:

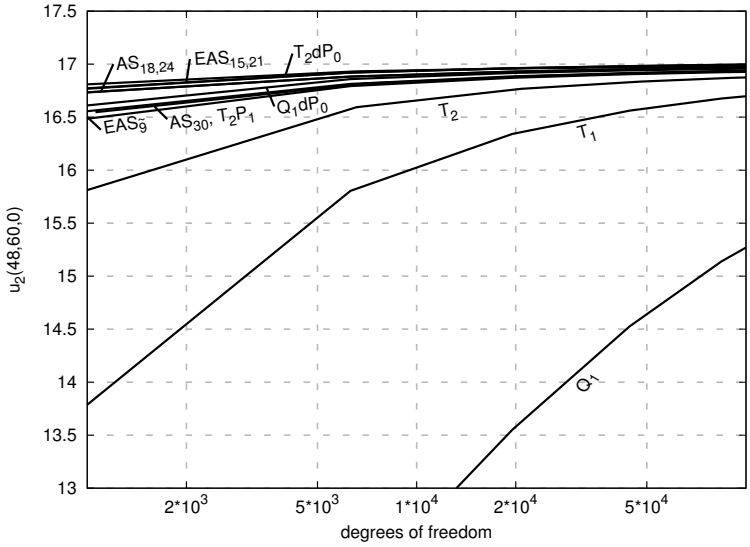

b) Necessary load steps:

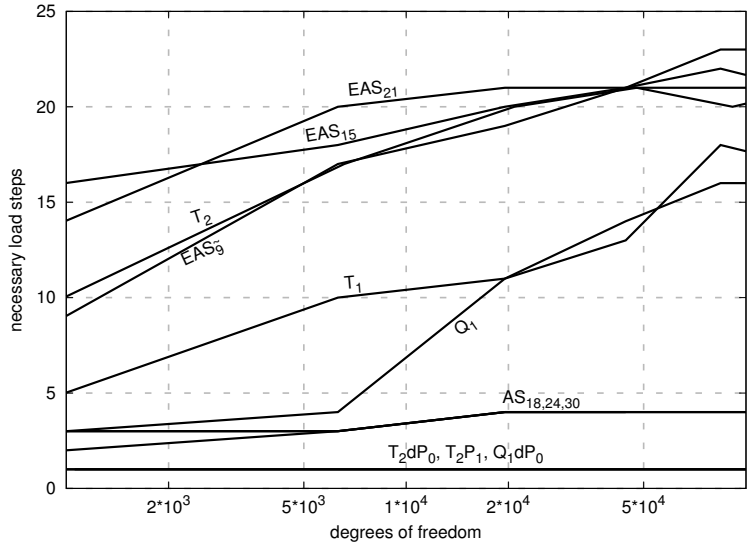

Figure 7.6: Cook's membrane problem; a) Convergence of nodal displacements $u_2(48, 60, 0)$ with respect to the degrees of freedom. b) Number of necessary load steps over the degrees of freedom.

7.5.4 Plate with Circular Hole

In many engineering finite element applications the most important quantities are not the displacements but the stresses. Thus, the quality of the approximation of the Cauchy stresses is investigated by means of the example of a nearly incompressible plate with a circular hole. This boundary value problem is related to the benchmark problem proposed by Stein et al. [2002], where it has been used in the framework of linear elasticity and elasto-plasticity. In detail, a rectangular plate with a side length of $l = 20$ and a thickness of $t = 2$ is considered. The circular hole, which's midpoint coincides with the center of the plate, has a radius of $r = 5$. The plate is elongated in y-direction using non-homogeneous boundary conditions for the displacements by a total magnitude of $\Delta l = 4$. Due to the symmetry with respect to all three coordinate axes only an octant of the geometry is discretized and additional boundary conditions take care of the symmetric deformation response. The geometry, a representative discretization, boundary conditions and the material parameters are summarized in Figure 7.7.

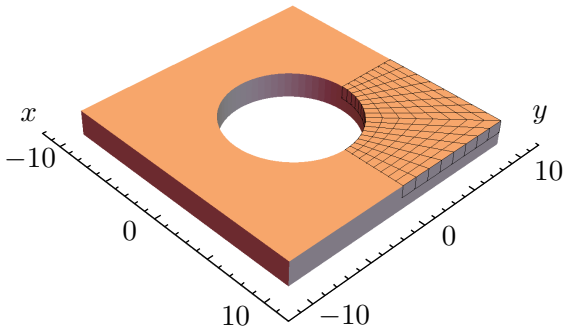

Boundary Conditions:

$x = 0$:
$u_1 = 0$

$y = 0$:
$u_2 = 0$

$z = 0$:
$u_3 = 0$

$y = 10$:
$u_2 = 2$

Material Parameter:

$E = 200$

$\nu = 0.49$

Figure 7.7: Plate with hole; Geometry, representative mesh and the boundary conditions.

The first considered result is the distribution of the approximation of the hydrostatic pressure, defined as $\hat{p}_h = \frac{1}{3}\mathrm{tr}\boldsymbol{\sigma}_h$, depicted in Figure 7.8. In addition the norm of the deviatoric part of the Cauchy's stresses $\boldsymbol{\sigma}_h^{\mathrm{dev}} = \boldsymbol{\sigma}_h - \frac{1}{3}\mathrm{tr}\boldsymbol{\sigma}_h \boldsymbol{I}$ is depicted in Figure 7.9. The plots permit jumping values between neighboring elements and thus do not smear out oscillating effects. In case of an equivalent value of the postprocessing quantity for the different element formulations the corresponding plots are condensed. Equivalence in this sense is determined by a deviation of less than one percent of the sum of all post-processed nodal values.

Considering the results for the hydrostatic pressure such an equivalence appears for the AS_{30}, AS_{24} and AS_{18} and also for all considered enhanced assumed strain elements. This observation is explained by the circumstance that for the corresponding elements the discretization of the trace related parts of the stresses are equivalent, compare Tables 5.1 and 5.2. The ill-posedness of the Q_1, T_2 and AS_{39} in the nearly incompressible regime is demonstrated by high unphysical oscillating values of the pressure. In contrast, the pressure distribution for the remaining mixed element formulations is reasonable smooth whereas the results of the $\mathrm{T}_2\mathrm{P}_1$ are superior. This is due to the continuous interpolation of the pressure within this finite element formulation.

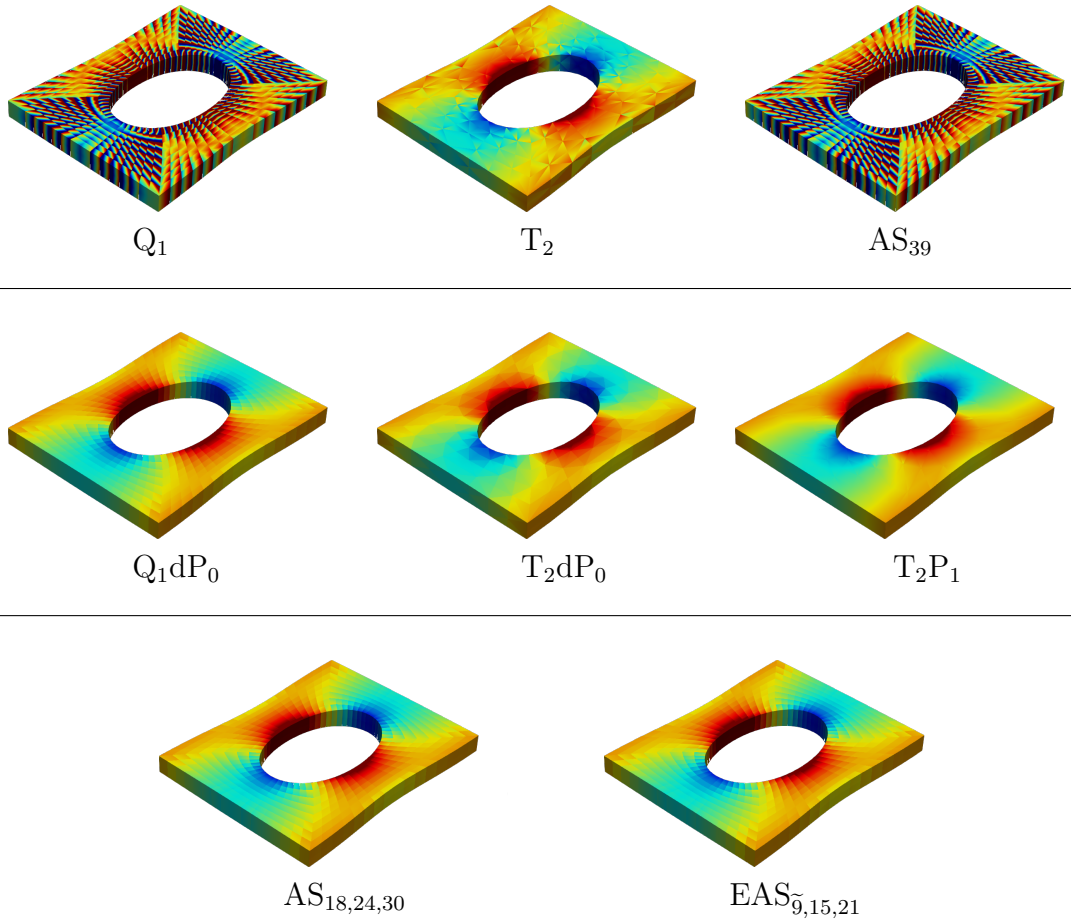

Figure 7.8: Plate with hole; Plot of the hydrostatic pressure $\hat{p}_h = \frac{1}{3}\mathrm{tr}\boldsymbol{\sigma}_h$.

Considering the norm of the deviatoric part of the stresses an equivalence appears for the following elements: Q_1 and AS_{39}; T_2 and T_2P_1; AS_{30} and $EAS_{\tilde{9}}$; and also for the AS_{18}, AS_{24}, EAS_{15} and EAS_{21}. However all finite element formulations yield reasonable smooth results and do not show high oscillating values. However it can be stated, that the elements with a higher order interpolation of the displacements (T_2, T_2P_1 and T_2dP_0) produce a slightly smoother distribution of the deviatoric stresses.

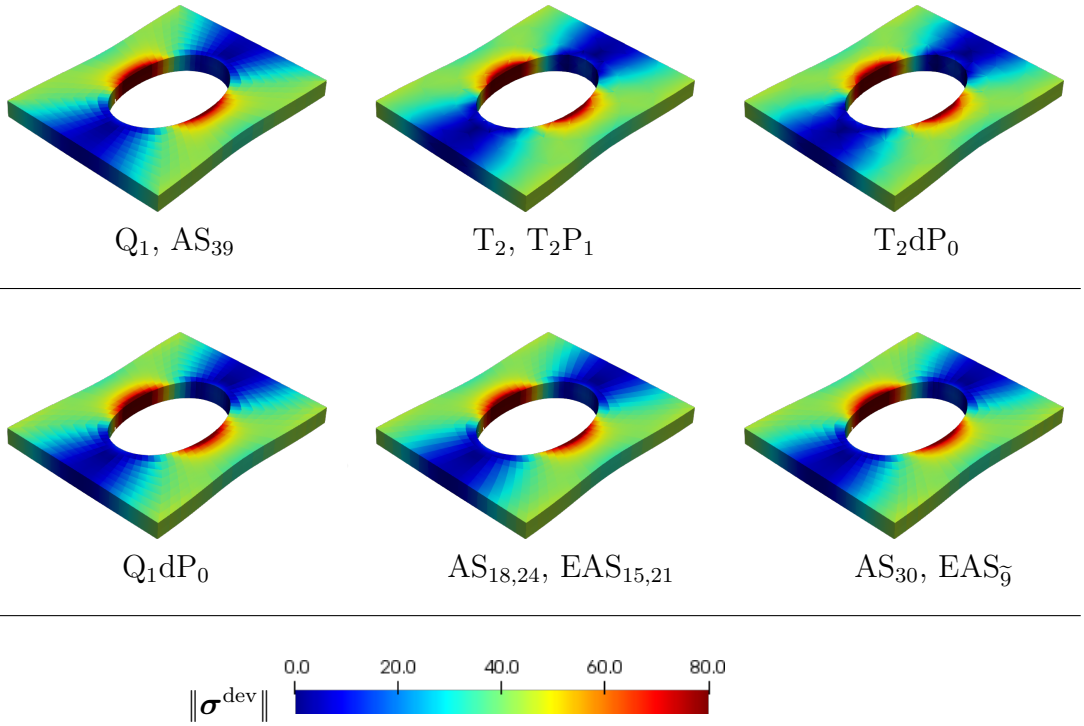

Figure 7.9: Plate with hole; Plot of the norm of the deviatoric part of the Cauchy stress $\|\boldsymbol{\sigma}_h^{\mathrm{dev}}\| = \|\boldsymbol{\sigma}_h - \frac{1}{3}\mathrm{tr}\boldsymbol{\sigma}_h\, \boldsymbol{I}\|$.

7.5.5 Investigation of Stability Range

The deficiency of some mixed element formulations in the large deformation framework to artificial free energy modes have first been detected by Wriggers and Reese [1996]. These unphysical mechanisms which can be summarized as rank deficiency problems are often denoted as hourglassing and preferably appear in case of homogeneous stress states. Further studies on this numerical phenomena have been done e.g. by Glaser and Armero [1997] and de Souza Neto et al. [1995]. These instabilities all refer to the family of enhanced assumed strain techniques. However, rank deficiency problems in the large de-

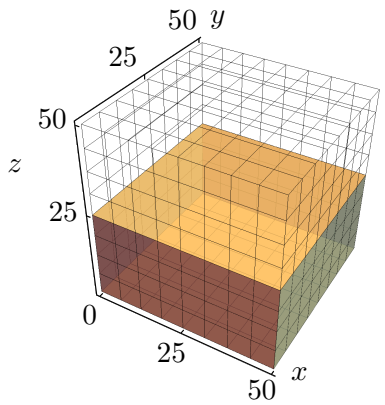

Boundary Conditions:

$x = 0 \vee x = 50$:
$u_1 = 0$

$y = 0 \vee y = 50$:
$u_2 = 0$

$z = 0$:
$u_3 = 0$

Case 1: Compression

$z = 50$:
$u_3 = -25$

Case 2: Tension

$z = 50$:
$u_3 = 25$

Material Parameter:

$E = 5$

$\nu = 0.49$

Figure 7.10: Hourglassing test; Geometry, representative mesh, deformed configuration (case 1) and the boundary conditions.

formation case have also been observed for other mixed finite element formulations, see Lovadina and Auricchio [2003], Auricchio et al. [2010; 2013]. Interestingly, these unrealistic instabilities are not confined to elements which do not pass the inf-sup condition in the linear elastic regime. In fact also inf-sup stable finite element discretizations are affected. The artificial modes appear in relatively unsophisticated states of deformation, thus that a simple model problem can be investigated in order to demonstrate the stability behavior of the proposed finite element formulations. Therefore, a nearly incompressible cube with a side length of $l = 50$ is considered first in a homogeneous compression and second in a homogeneous tension state. Displacement boundary conditions are applied such that all faces of the cube are constrained to be straight and no deformation is permitted perpendicular to the axis of elongation. Due to this choice of boundary conditions any form of surface buckling is precluded and no corresponding bifurcation point is expected. Thus each numerical detected point of bifurcation, identified by a singular stiffness matrix, is introduced by the discretization scheme and can be considered as artificial. Details of the considered boundary value problem are depicted in Figure 7.10. In order to be able to illustrate also the rank deficiency problems of the displacement pressure formulations, we consider a slightly modified strain energy function of the form

$$\begin{aligned} \psi(\boldsymbol{C}) &= \psi^{\text{comp}}(\boldsymbol{C}) + \frac{\Lambda}{2}\vartheta(J)^2 \quad \text{with} \\ \psi^{\text{comp}}(\boldsymbol{C}) &= \frac{\mu}{2}(\text{tr}\boldsymbol{C} - 3) - \mu \ln J \quad \text{and} \\ \vartheta(J) &= \ln J \,. \end{aligned} \tag{7.51}$$

The important difference is the nonlinear condition in the penalization of the incompressibility, such that $\ln J \to 0$ for $\Lambda \to \infty$. It should be emphasized, that in case of a linear penalization (e.g. $\vartheta(J) = (J-1)$) no instabilities have been found in case of the classical displacement pressure elements, which is consent with the observations proposed by Lovadina and Auricchio [2003], Auricchio et al. [2010; 2013].

Case 1: Compression test The first test can be classified as a classical hourglass test, where a state of homogeneous compression is applied, similarly to the examples reported in the literature (e.g. Wriggers and Reese [1996]). In order to detect possible artificial modes, Figure 7.11 shows the development of the smallest eigenvalues of $\boldsymbol{K}^2$, where $\boldsymbol{K}$ is the global stiffness matrix, over the level of compression. A point of bifurcation is determined by a zero eigenvalue of $\boldsymbol{K}$. Since the mixed element formulations lead to indefinite global stiffness matrices, we consider the squared matrix which naturally constitutes a positive semidefinite matrix and therefore enables a simple comparison between the different formulations. It can be noted, that the correct physical behavior is not captured by all considered element formulations. In detail the AS_{18}, EAS_{21}, AS_{24} and EAS_{15} suffer due to an unphysical rank deficiency. The related eigenmodes, which determine the nontrivial solution paths, corresponding to the points of bifurcation are depicted in Figure 7.12. Here, the typical hourglass patterns can be identified. The ill-posed elements are exactly the shear locking free assumed stress and enhanced assumed strain elements. The introduced softening, related to the shear deformation or stress terms apparently lead to the existence of artificial zero energy modes. A deeper discussion and a geometrical interpretation of this instability phenomenon in the framework of two dimensional EAS elements has been proposed by Wall et al. [2000].

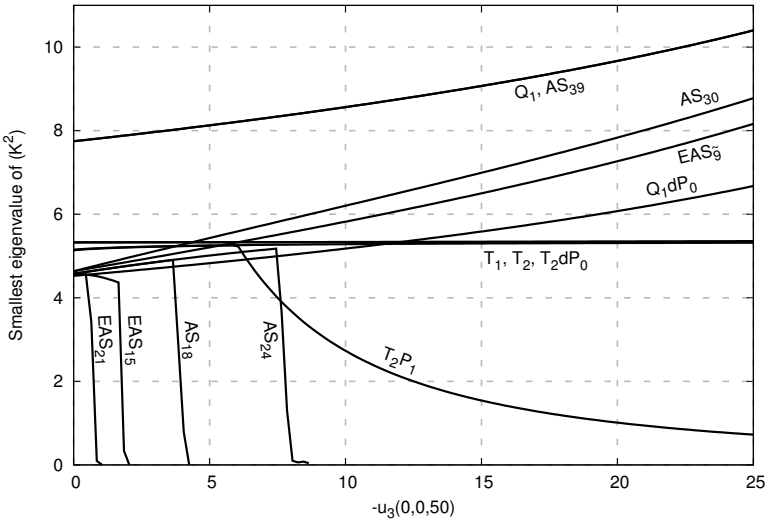

Figure 7.11: Stability investigation, compression; Development of the smallest eigenvalue of $\boldsymbol{K}^2$, where $\boldsymbol{K}$ is the stiffness matrix, over the loading.

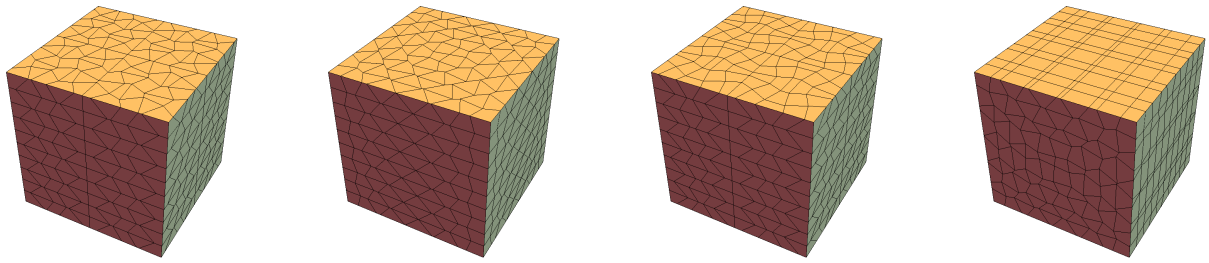

AS_{18} EAS_{21} AS_{24} EAS_{15}

Figure 7.12: Stability investigation, compression; Artificial modes.

Case 2: Tension test Hourglass patterns in case of enhanced assumed strain elements in the state of large tension deformations states have already been reported e.g. by Glaser and Armero [1997] and Lovadina and Auricchio [2003]. In ensuing publications (Auricchio et al. [2010; 2013]) unphysical modes have also been detected in the framework of displacement pressure finite elements, even for the case of inf-sup stable interpolation pairs. The considered model problem in tension state is closely connected to the 2D examples given in the prior mentioned literature. Similar to the case of compression, no point of bifurcation is expected from a physical point of view. However, considering Figure 7.13, where the development of the smallest eigenvalue of $\boldsymbol{K}^2$ is depicted, it can be noted that only the primal displacement based elements and the AS_{39} are able to capture the correct range of stability. All remaining proposed formulations lead to artificial free energy modes. The corresponding relevant eigenmodes are shown in Figure 7.14. The hexahedral shaped elements show again the typical hourglass pattern, whereas the mode of failure for the tetrahedral based elements differs. Considering that the AS_{39} is able to reproduce the correct stability range, it can be concluded that the assumed stress technique itself or its numerical implementation is not the cause of the insufficient behavior. However, the confinement of the stress interpolation polynomials seems to be crucial.

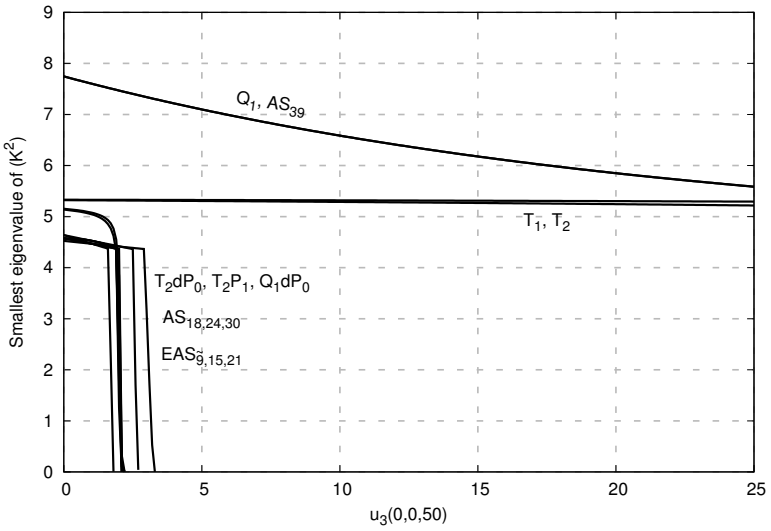

Figure 7.13: Stability investigation, tension; Development of the smallest eigenvalue of $\boldsymbol{K}^2$, where $\boldsymbol{K}$ is the stiffness matrix, over the loading.

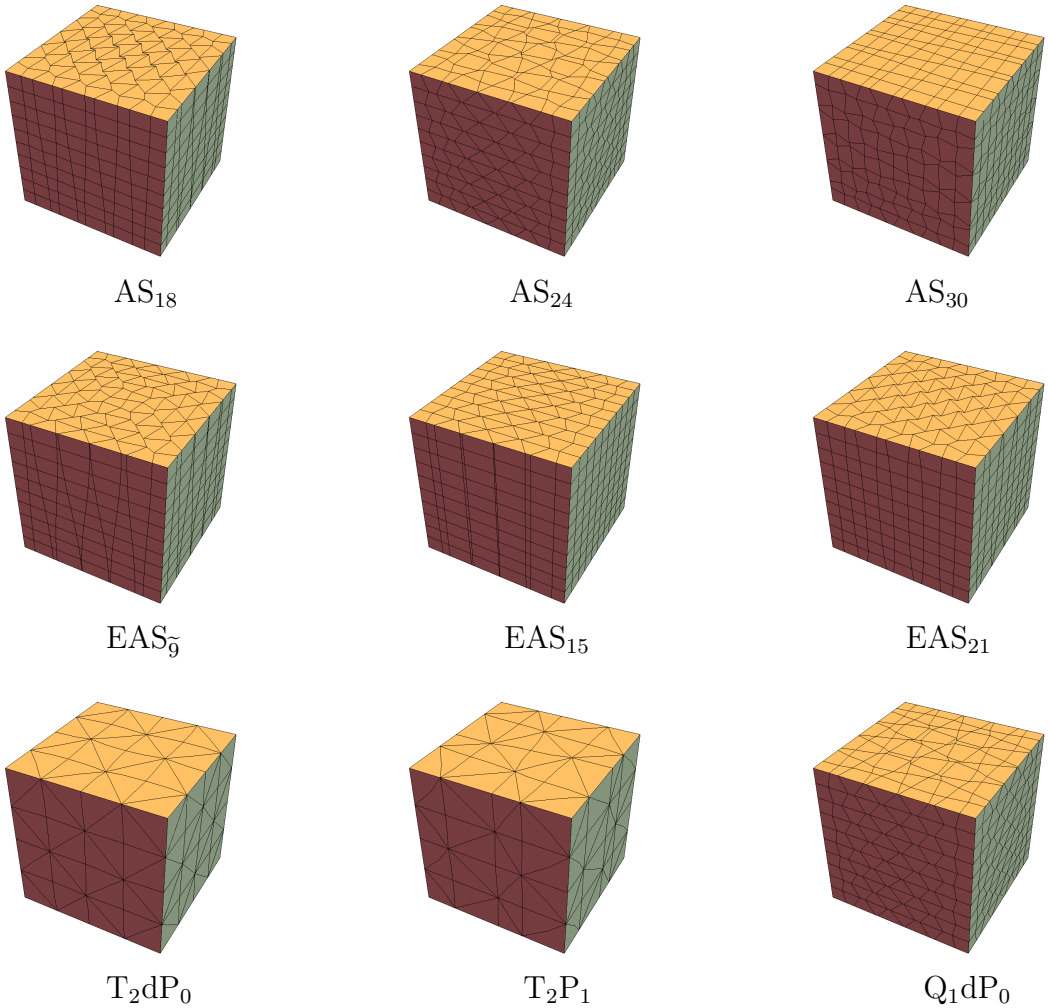

Figure 7.14: Stability investigation, tension; Artificial modes.

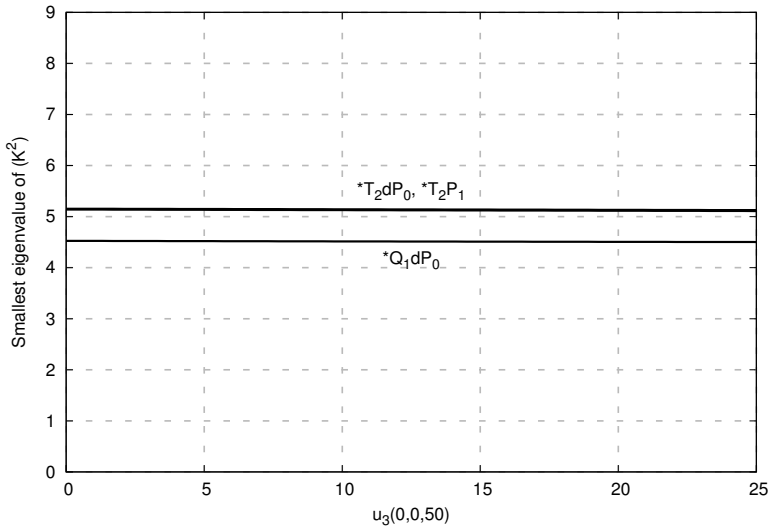

Figure 7.15: Stability investigation, tension; consistent stabilized approach for displacement pressure elements. Development of the smallest eigenvalue of $\boldsymbol{K}^2$ over the loading.

In the framework of the displacement pressure based element formulations a variational consistent stabilization has been discussed in Chapter 6.2.3. Its application leads to sufficient results for this numerical example, as depicted in Figure 7.15. It can be noted that the use of the consistent complementary approach enables a correct reproduction of the stability range for this boundary value problem.

7.6 Summary FEM for Isotropic Hyperelasticity

In the latter chapter different finite elements discretizations have been discussed and numerically verified. Generally speaking, the conclusions made for finite elements in the linear elastic framework in Chapter 5.8 are confirmed. This implies that all formulations which already suffer due to locking phenomena in the linear regime show similar defects in the hyperelastic extension. However, the numerical example concerning the investigation of the stability range (see Chapter 7.5.4) and the lack of robustness of many elements with respect to efficiently large load steps depict significantly the need of additional care in the construction of efficient and reliable finite element discretizations for large deformations. Especially two families of finite element formulations seem to be promising for the application in hyperelastic boundary value problems.
On the one hand side, the $\mathrm{T_2P_1}$ element fulfills the necessity of well posedness in the incompressible regime and does not suffer due to unphysical zero energy modes if the proposed consistent complementary approach is considered. In addition its higher order interpolation of the displacements and continuous discretization of the pressure yield a superior stress distribution even in the (nearly) incompressible framework. Its tetrahedral shape is of huge advantage for the mesh construction since it can be fully automatized, which is yet not possible for hexahedral shaped elements. On the downside of this formulation is its lack of robustness regarding large load steps in bending dominated situations. In addition, due to the continuous interpolation of the pressure, the inherent saddle point problem cannot be omitted and therefore the choice of solving techniques is highly reduced, due to the related non definite system matrix.

On the other hand side the hyperelastic extension of the assumed stress elements shows promising behavior for the discussed numerical examples. Especially its robustness for large load steps seems to be superior, compared to other finite element techniques. This is in particular of importance in the nearly incompressible regime taking in mind that in many engineering applications rubberlike materials are used in situations where large deformations are expected. However, care must be taken considering the correct choice of the interpolation scheme for the stresses. In situations where large homogeneous compression states may occur the AS_{18} and AS_{24} formulations suffer due to unphysical zero energy modes. However in this case the AS_{30} seems to be an appropriate choice. In contrast, in bending dominated problems, homogeneous stress states are unlikely and the performance of the AS_{18} and AS_{24} are superior, taking into account as well the efficiency with respect to the number of unknowns as well as the robustness for large load steps. Unfortunately, in case of large homogeneous tension states none of the investigated assumed stress discretization yield satisfying results concerning its stability. Therefore it is not advisable to use these elements in such situation unless a special stabilization scheme takes care of the zero energy modes. However, comparing these results with the widely accepted enhanced assumed strain elements, it can be noticed that also the EAS formulations show the same lack of instability and in addition suffer due to the need of much smaller load increments.

8 Finite Elements for (Nearly) Inextensible Materials

Until this point, the discussion of the finite elements has been restricted to isotropic materials. However, also in the field of anisotropic materials limiting values appear, which are from an algebraic point of view comparable to the restriction of incompressibility. A special case of recent interest is the finite element approximation of (nearly-)inextensible transversely isotropic bodies. In this framework, a locking phenomenon is observed due to the high stiffness ratios between the preferred and its transverse directions. One of the reasons for the special interest on the modeling of such materials is its high occurrence in the field of biomechanics. For example many soft biological tissues are characterized as fiber-reinforced composites of a non-collagenous matrix and collagen fibers, where the growth of the fiber stiffness is often exponentially. In addition, due to the high amount of stored water, such materials are in many cases also in the nearly incompressible regime. See for example Balzani et al. [2006] and the references therein, for an overview on the material modeling for soft biological tissues. A detailed theoretical and computational study on the well posedness of finite elements for such nearly-incompressible and near-inextensible transversely isotropic bodies in the linearized framework has been proposed recently by Rasolofoson et al. [2018]. Therein, the effects of under-integration of the terms related to volumetric deformation and extension in fiber direction are analyzed and relations to a mixed finite element formulation are discussed.

In the nonlinear regime, many classical finite element formulations show non-physical behavior in the class of fiber-reinforced materials, see Weiss et al. [1996], Holzapfel et al. [2000], Sansour [2008] and Helfenstein et al. [2010]. These authors outlined that all fiber-related terms in the energy should be formulated with respect to the complete deformation tensor and not just with respect to its isochoric part in order to avoid unphysical material expansion. A first idea for special mixed finite elements, treating the locking effects of nearly-inextensibility, has been proposed by Schröder et al. [2015] and was later elaborated in Schröder et al. [2016]. This novel approach is based on a Hu-Washizu like variational framework and considers a separation of the deformation measures associated to the isotropic and anisotropic material response. The crucial point is the relaxation of the constraints emerging from the nearly inextensibility by a reduced interpolation order of the deformation measure related to the anisotropic material response. Analogous Hu-Washizu based approaches have been published recently by Zdunek and Rachowicz [2017a] and Dal [2018]. Here, instead of a relaxation of the complete deformation measure, only the fiber stretch and its work conjugated stress-like variable are considered as additional scalar valued fields. The prior formulation has been additionally extended to a higher order approach in Zdunek and Rachowicz [2017b]. In contrast to these three field formulations, a two field formulation proposed by Wriggers et al. [2016] includes also the limit case of inextensibility utilizing the method of Lagrange multipliers. For the case of extensible fibers a perturbed Lagrangian formulation is discussed therein as well. These approaches have been analyzed in an ensuing work in the linearized setup by Auricchio et al. [2017].

In this chapter, the approach presented in Schröder et al. [2016] is presented and numerically analyzed.

8.1 Simplified Kinematics for Anisotropy (SKA)

In order to relax the emerging constraints associated to the anisotropy, the strain energy is additively split into its isotropic and anisotropic parts and an additional deformation measure $\widehat{\boldsymbol{C}}$, related to the right Cauchy-Green tensor $\boldsymbol{C}$, is introduced. This novel variable controls the stored energy related to the anisotropic material response. In addition, different well-established discretization schemes may be applied to the isotropic related deformation. As already discussed, this is in particular of interest in the framework of nearly incompressibility, where it is advisable to pay special attention to the terms related to volumetric deformation. A possible approach is the application of the displacement-pressure formulation as discussed in the isotropic case in Chapter 7.3, which will also be used in the following numerical examples. However, in order to bring the proposed simplified kinematics for anisotropy into focus the ensuing discussion will consider only a primal displacement approach for the isotropic part of the deformation. Therefore the strain energy is given by means of the split

$$\psi(\boldsymbol{C}, \widehat{\boldsymbol{C}}) = \psi^{\text{i-p}}(\boldsymbol{C}) + \psi^{\text{a-p}}(\widehat{\boldsymbol{C}})\,. \tag{8.1}$$

The second-order tensorial Lagrange-multiplier $\widehat{\boldsymbol{S}}$ is introduced in order to connect the additional deformation tensor $\widehat{\boldsymbol{C}}$ with its variational counterpart $\boldsymbol{C}(\boldsymbol{u})$. For the resulting three-field formulation the boundary value problem reads: find $\boldsymbol{u}$, $\widehat{\boldsymbol{C}}$, and $\widehat{\boldsymbol{S}}$ such that

$$\begin{aligned}
&\text{Div}[\boldsymbol{F}\boldsymbol{S}] + \boldsymbol{f} = \boldsymbol{0} && \text{on } \mathcal{B}_0\,,\\
&\widehat{\boldsymbol{C}} = \boldsymbol{C} && \text{on } \mathcal{B}_0\,,\\
&\widehat{\boldsymbol{S}} = 2\,\partial_{\widehat{\boldsymbol{C}}}\psi^{\text{a-p}}(\widehat{\boldsymbol{C}}) && \text{on } \mathcal{B}_0\,,\\
&(\boldsymbol{F}\boldsymbol{S})\boldsymbol{n}_0 = \overline{\boldsymbol{t}}_0 && \text{on } \partial\mathcal{B}_{0,t}\,,\\
&\boldsymbol{u} = \overline{\boldsymbol{u}} && \text{on } \partial\mathcal{B}0,_u\,,
\end{aligned} \tag{8.2}$$

whereas the second Piola-Kirchhoff stress is computed by $\boldsymbol{S} = 2\,\partial_{\boldsymbol{C}}\psi^{\text{i-p}} + \widehat{\boldsymbol{S}}$. In terms of energy minimization a functional can be constructed, which stationary points are equivalent to the solutions of the boundary value problem as

$$\begin{aligned}
\Pi(\boldsymbol{u}, \widehat{\boldsymbol{C}}, \widehat{\boldsymbol{S}}) = \int_{\mathcal{B}_0} \psi^{\text{i-p}}(\boldsymbol{C})\;\mathrm{d}V + \int_{\mathcal{B}_0} \psi^{\text{a-p}}(\widehat{\boldsymbol{C}})\;\mathrm{d}V + \int_{\mathcal{B}_0} \tfrac{1}{2}\widehat{\boldsymbol{S}} : (\boldsymbol{C} - \widehat{\boldsymbol{C}})\;\mathrm{d}V \ldots\\
\cdots - \int_{\mathcal{B}_0} \boldsymbol{u}\cdot\boldsymbol{f}\;\mathrm{d}V - \int_{\partial\mathcal{B}_{0,t}} \boldsymbol{u}\cdot\boldsymbol{t}_0\;\mathrm{d}A\,.
\end{aligned} \tag{8.3}$$

The corresponding weak forms appear as

$$\begin{aligned}
G_u &= \delta_u\Pi = \int_{\mathcal{B}_0} \boldsymbol{S} : \tfrac{1}{2}\delta\boldsymbol{C}\,\mathrm{d}V - \int_{\mathcal{B}_0} \boldsymbol{f}\cdot\delta\boldsymbol{u}\,\mathrm{d}V - \int_{\partial\mathcal{B}_{0,t}} \overline{\boldsymbol{t}}_0\cdot\delta\boldsymbol{u}\,\mathrm{d}A = 0\,,\\
G_{\widehat{C}} &= \delta_{\widehat{C}}\Pi = \int_{\mathcal{B}_0} (\partial_{\widehat{\boldsymbol{C}}}\psi^{\text{a-p}} - \tfrac{1}{2}\widehat{\boldsymbol{S}}) : \delta\widehat{\boldsymbol{C}}\;\mathrm{d}V = 0\,,\\
G_{\widehat{S}} &= \delta_{\widehat{S}}\Pi = \int_{\mathcal{B}_0} (\boldsymbol{C} - \widehat{\boldsymbol{C}}) : \tfrac{1}{2}\delta\widehat{\boldsymbol{S}}\;\mathrm{d}V = 0\,,
\end{aligned} \tag{8.4}$$

and the increments as

$$\begin{aligned}
\Delta G_u &= \int_{\mathcal{B}_0} \left(\Delta \boldsymbol{S} : \tfrac{1}{2}\delta \boldsymbol{C} + \boldsymbol{S} : \frac{1}{2}\Delta\delta \boldsymbol{C} \right) \mathrm{d}V \\
\Delta G_{\widehat{C}} &= \int_{\mathcal{B}_0} \left(\frac{\partial^2 \psi^{\text{a-p}}}{\partial \widehat{\boldsymbol{C}} \partial \widehat{\boldsymbol{C}}} : \Delta \widehat{\boldsymbol{C}} - \frac{1}{2}\Delta \widehat{\boldsymbol{S}} \right) : \delta \widehat{\boldsymbol{C}} \, \mathrm{d}V \,, \\
\Delta G_{\widehat{S}} &= \int_{\mathcal{B}_0} (\Delta \boldsymbol{C} - \Delta \widehat{\boldsymbol{C}}) : \frac{1}{2}\delta \widehat{\boldsymbol{S}} \, \mathrm{d}V \,,
\end{aligned} \tag{8.5}$$

with

$$\Delta \boldsymbol{S} = \left(4 \frac{\partial^2 \psi^{i\text{-}p}}{\partial \boldsymbol{C} \partial \boldsymbol{C}} \right) : \frac{1}{2}\Delta \boldsymbol{C} + \Delta \widehat{\boldsymbol{S}} \,. \tag{8.6}$$

8.2 Finite Element Discretization

The discrete counterparts of the unknown fields are interpolated with quadratic Lagrangian shape functions in case of the displacements, and piecewise constant functions for the remaining fields. This piecewise constant approximation for $\widehat{\boldsymbol{C}}$ results in the simplified kinematic for the anisotropic response. Thus the displacements, its gradient and virtual counterparts are given by the Equations (7.8) and (7.11). In accordance with the right Cauchy-Green tensor $\boldsymbol{C}$, the introduced deformation measure $\widehat{\boldsymbol{C}}$ is assumed to be symmetric, such that only six components have to be discretized. With the introduction of $\boldsymbol{\Phi}$ as the vector containing the related degrees of freedom, the discretization of the individual components of $\widehat{\boldsymbol{C}}$, its virtual and incremental counterparts are described by

$$\begin{bmatrix} \widehat{C}_{h,11} \\ \widehat{C}_{h,22} \\ \widehat{C}_{h,33} \\ \widehat{C}_{h,12} \\ \widehat{C}_{h,23} \\ \widehat{C}_{h,13} \end{bmatrix} = \begin{bmatrix} \Phi_1 \\ \Phi_2 \\ \Phi_3 \\ \Phi_4 \\ \Phi_5 \\ \Phi_6 \end{bmatrix} = \boldsymbol{\Phi}, \quad \begin{bmatrix} \delta\widehat{C}_{h,11} \\ \delta\widehat{C}_{h,22} \\ \delta\widehat{C}_{h,33} \\ \delta\widehat{C}_{h,12} \\ \delta\widehat{C}_{h,23} \\ \delta\widehat{C}_{h,13} \end{bmatrix} = \begin{bmatrix} \delta\Phi_1 \\ \delta\Phi_2 \\ \delta\Phi_3 \\ \delta\Phi_4 \\ \delta\Phi_5 \\ \delta\Phi_6 \end{bmatrix} = \delta\boldsymbol{\Phi}, \quad \begin{bmatrix} \Delta\widehat{C}_{h,11} \\ \Delta\widehat{C}_{h,22} \\ \Delta\widehat{C}_{h,33} \\ \Delta\widehat{C}_{h,12} \\ \Delta\widehat{C}_{h,23} \\ \Delta\widehat{C}_{h,13} \end{bmatrix} = \begin{bmatrix} \Delta\Phi_1 \\ \Delta\Phi_2 \\ \Delta\Phi_3 \\ \Delta\Phi_4 \\ \Delta\Phi_5 \\ \Delta\Phi_6 \end{bmatrix} = \Delta\boldsymbol{\Phi} \,. \tag{8.7}$$

In the same manner the Lagrangian multiplier $\widehat{\boldsymbol{S}}$ is discretized

$$\begin{bmatrix} \widehat{S}_{h,11} \\ \widehat{S}_{h,22} \\ \widehat{S}_{h,33} \\ \widehat{S}_{h,12} \\ \widehat{S}_{h,23} \\ \widehat{S}_{h,13} \end{bmatrix} = \begin{bmatrix} \beta_1 \\ \beta_2 \\ \beta_3 \\ \beta_4 \\ \beta_5 \\ \beta_6 \end{bmatrix} = \boldsymbol{\beta}, \quad \begin{bmatrix} \delta\widehat{S}_{h,11} \\ \delta\widehat{S}_{h,22} \\ \delta\widehat{S}_{h,33} \\ \delta\widehat{S}_{h,12} \\ \delta\widehat{S}_{h,23} \\ \delta\widehat{S}_{h,13} \end{bmatrix} = \begin{bmatrix} \delta\beta_1 \\ \delta\beta_2 \\ \delta\beta_3 \\ \delta\beta_4 \\ \delta\beta_5 \\ \delta\beta_6 \end{bmatrix} = \delta\boldsymbol{\beta}, \quad \begin{bmatrix} \Delta\widehat{S}_{h,11} \\ \Delta\widehat{S}_{h,22} \\ \Delta\widehat{S}_{h,33} \\ \Delta\widehat{S}_{h,12} \\ \Delta\widehat{S}_{h,23} \\ \Delta\widehat{S}_{h,13} \end{bmatrix} = \begin{bmatrix} \Delta\beta_1 \\ \Delta\beta_2 \\ \Delta\beta_3 \\ \Delta\beta_4 \\ \Delta\beta_5 \\ \Delta\beta_6 \end{bmatrix} = \Delta\boldsymbol{\beta} \,, \tag{8.8}$$

whereas $\boldsymbol{\beta}$ denotes the vector of the element wise unknowns of $\widehat{\boldsymbol{S}}$. In order to avoid the construction of the complete system of equations, related to Equations (8.4) and (8.5) the discrete counterparts of $(8.4)_{2-3}$ are solved a priori on element level, which is possible due to the discontinuous approximation of the related unknown fields. Taking into account the constant interpolation, we obtain for the discrete counterpart of the weak forms $(8.4)_{2-3}$

for a typical element Ω^e

$$\begin{aligned} \widehat{\boldsymbol{C}}_h &= \frac{1}{V_{\Omega^e}} \int_{\Omega^e} \boldsymbol{C}_h \, \mathrm{d}V \quad \forall\, \delta\widehat{\boldsymbol{S}} \\ \widehat{\boldsymbol{S}}_h &= 2\, \partial_{\widehat{C}_h} \psi^{\text{a-p}}(\widehat{C}_h) \quad \forall\, \delta\widehat{\boldsymbol{C}}_h \,. \end{aligned} \tag{8.9}$$

A linearization leads to the increments as

$$\begin{aligned} \Delta\widehat{\boldsymbol{C}}_h &= \frac{1}{V_{\Omega^e}} \int_{\Omega^e} \Delta\boldsymbol{C}_h \, \mathrm{d}V \\ \Delta\widehat{\boldsymbol{S}}_h &= 2\, \frac{\partial^2 \psi^{\text{a-p}}(\widehat{\boldsymbol{C}}_h)}{\partial\widehat{\boldsymbol{C}}_h \partial\widehat{\boldsymbol{C}}_h} \, \Delta\widehat{\boldsymbol{C}}_h \,. \end{aligned} \tag{8.10}$$

This can now be inserted into the remaining weak form $(8.4)_1$ and increment $(8.5)_1$, which yields the problem in form of a generalized displacement formulation

$$G^e_{h,u} = \underbrace{\left(\int_{\Omega^e} \frac{1}{2} \frac{\partial(\boldsymbol{C}_h : \boldsymbol{S}_h)}{\partial \boldsymbol{d}} \, \mathrm{d}V - \frac{\partial(\boldsymbol{u}_h \cdot \boldsymbol{f})}{\partial \boldsymbol{d}} \, \mathrm{d}V - \int_{\partial\Omega^e} \frac{\partial(\boldsymbol{u}_h \cdot \boldsymbol{t}_0)}{\partial \boldsymbol{d}} \, \mathrm{d}A \right)}_{\boldsymbol{r}^e} \cdot \delta\boldsymbol{d} \,, \tag{8.11}$$

with the associated increment

$$\Delta G^e_{h,u} = \Big(\underbrace{\int_{\Omega^e} \frac{1}{2} \frac{\partial^2(\boldsymbol{C}_h : \boldsymbol{S}_h)}{\partial \boldsymbol{d}\, \partial \boldsymbol{d}} \, \mathrm{d}V}_{\boldsymbol{k}^e} \Delta\boldsymbol{d} \Big) \cdot \delta\boldsymbol{d} \,. \tag{8.12}$$

Assembling of all element stiffness matrices and element residual vectors yield the global stiffness matrix $\boldsymbol{K}$ and residual vector $\boldsymbol{R}$ as

$$\boldsymbol{K} = \mathop{\mathsf{A}}_{e=1}^{num_{ele}} \boldsymbol{k}^e \,, \quad \boldsymbol{R} = \mathop{\mathsf{A}}_{e=1}^{num_{ele}} \boldsymbol{r}^e \,. \tag{8.13}$$

The global discrete linearized system of equations is given by

$$\delta\boldsymbol{D}^T \left(\boldsymbol{K}\, \Delta\boldsymbol{D} + \boldsymbol{R} \right) = 0 \quad \forall\, \delta\boldsymbol{D} \neq \boldsymbol{0} \,, \tag{8.14}$$

whereas $\delta\boldsymbol{D}$, $\Delta\boldsymbol{D}$ denote the vectors of variation and increment of the global nodal displacements. The evaluation of Equations $(8.9)_1$ and $(8.10)_1$ requires the implementation of an additional integration loop which leads to a small lack of efficiency. Alternatively the concept of selective reduced integration may be applied. This concept was first employed in order to obtain improved bending behavior for a Q_1 in linear elasticity by Doherty et al. [1969]. Further studies in this field, see e.g. Fried [1974], Nagtegaal et al. [1974] and Malkus [1976], have led to a better understanding of the improved performance of these elements resulting into a unification of the selective reduced integration concept and mixed finite elements, proposed by Malkus and Hughes [1978]. Later on, this approach, which is also often denoted as B-bar or F-bar method, has been extended to nonlinear phenomena, see e.g. Hughes [1980] and Simo et al. [1985]. Following this concept the integrals on the right hand side of Equations $(8.9)_1$ and $(8.10)_1$ are be approximated by the corresponding value in the barycenter of the element. However, due to the quadratic interpolation of the displacement field, the discrete right Cauchy-Green tensor $\boldsymbol{C}_h$ appears as a nonlinear quantity and therefore the reduced integration technique might lead to additional integration errors. Therefore, we consider in the proposed model the application of an additional full integration loop.

8.3 Numerical Examples

In the following we validate the introduced finite element in two different numerical examples. The proposed formulation containing Simplified Kinematics for Anisotropy (SKA) is abbreviated by "SKA-T_2A_0", whereas the A_0 should indicate the constant approximation for the additional deformation measure and stress-like field. In addition, we consider the "SKA-$T_2P_0A_0$" which combines the displacement pressure formulation discussed in Chapter 7.3 for the isotropic part of the deformation and the simplified kinematics for the anisotropic part. The results will be compared with a standard displacement-based element as discussed in Chapter 7.1 labeled as T_2, with a mixed displacement pressure approach as discussed in Chapter 7.3 labeled as T_2P_0. Note that the following results have been previously published in Schröder et al. [2016].

8.3.1 Dual Clamped Plate

The first numerical example examines a highly constrained benchmark for compressible and nearly incompressible anisotropic material under plane strain conditions. As sketched in Figure 8.1(a) the quadratic Plate of unit length is clamped on the upper and lower boundaries and a constant normal load $q_0 = 30$ is applied on the left boundary. A transversal isotropic material, with a single family of fibers in the direction $\boldsymbol{a}_0 = (1/2, \sqrt{3}/2, 0)^T$ is considered. An exemplary mesh for the boundary value problem is depicted in Figure 8.1(b). The considered strain energy function is given by the sum of Equations (2.69) and (2.70).

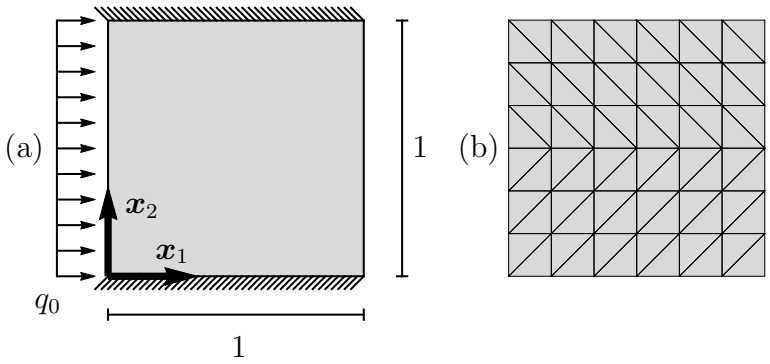

Figure 8.1: Dual clamped ; Boundary conditions (a), regular mesh (b).

Convergence study with increasing fiber stiffness. In this numerical example we examine the influence of an increasing stiffening of the fiber and therefore different choices of the material parameter $\alpha_1 = \{10^2, 10^4, 10^6, 10^8\}$ are investigated. In order to compare the obtained solution the displacements in the $\boldsymbol{x}_1$-direction at the point with the coordinates $\boldsymbol{X} = (0, 0.5)^T$ are plotted in a convergence study over the elements per edge. Additionally the computational efficiency is analyzed by comparing the total number of iterations until convergence occurs. For the convergence studies an adaptive load stepping scheme is used. As an initial load increment the full load is applied $\Delta\lambda_1 = 1$, whereas λ denotes the load factor. If the Newton method does not find a converged solution within 10 iterations the increment $\Delta\lambda$ is halved. This procedure is repeated until an applicable load increment is found. After every successful Newton iteration, the initial load increment

of the following step is the complete remaining load $\Delta\lambda_{i+1} = 1 - (\sum_i \Delta\lambda_i)$. This load increment is again halved until the Newton method converges. As a termination criterion a minimal load step of $\Delta\lambda = 10^{-8}$ is chosen. For the results in Figures 8.2 and 8.3 the iteration steps of all successful load steps are summed up. All results are plotted using a logarithmic scale on the x-axis.

This numerical example is investigated once for compressible material behavior (Poisson ratio $\nu = 0.3$), see Figure 8.2 and once for nearly incompressibility ($\nu = 0.49$) see Figure 8.3. The remaining material parameters are $E = 200$ for the Young's modulus and $\alpha_2 = 2$. The corresponding Lamé parameters follow for the compressible case as $\Lambda = 115.39$ and $\mu = 76.92$ and for the nearly incompressible case as $\Lambda = 3288.59$ and $\mu = 67.11$.

In case of a less higher stiffness in the preferred direction it can be noticed that the results of the investigated element formulations do not differ significantly, independently from the material setup. But in case of a higher difference of the stiffnesses the SKA-T_2A_0 and the SKA-$T_2A_0P_0$ clearly outperform the T_2 and T_2P_0 elements. The classical element formulations exhibit significant problems in finding a converged solution and even if they are able to find a solution they need up to 50 times more iterations. On the other side the novel formulations always present a good convergence behavior independently from the material setup. Also the number of iterations remain on the same level for increasing mesh density.

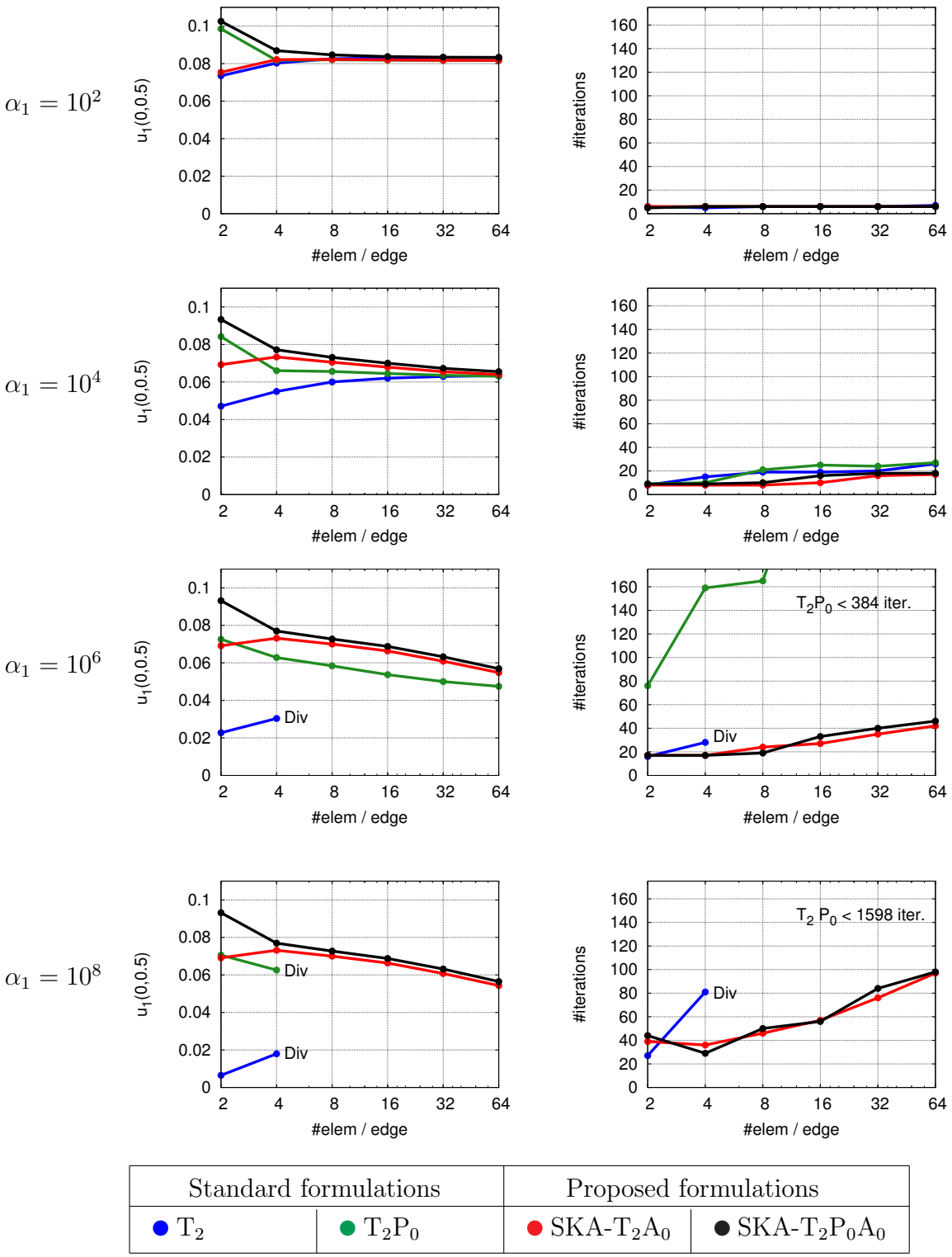

Figure 8.2: Dual clamped with $\nu = 0.3$; Displacement convergence on the left, necessary iteration on the left.

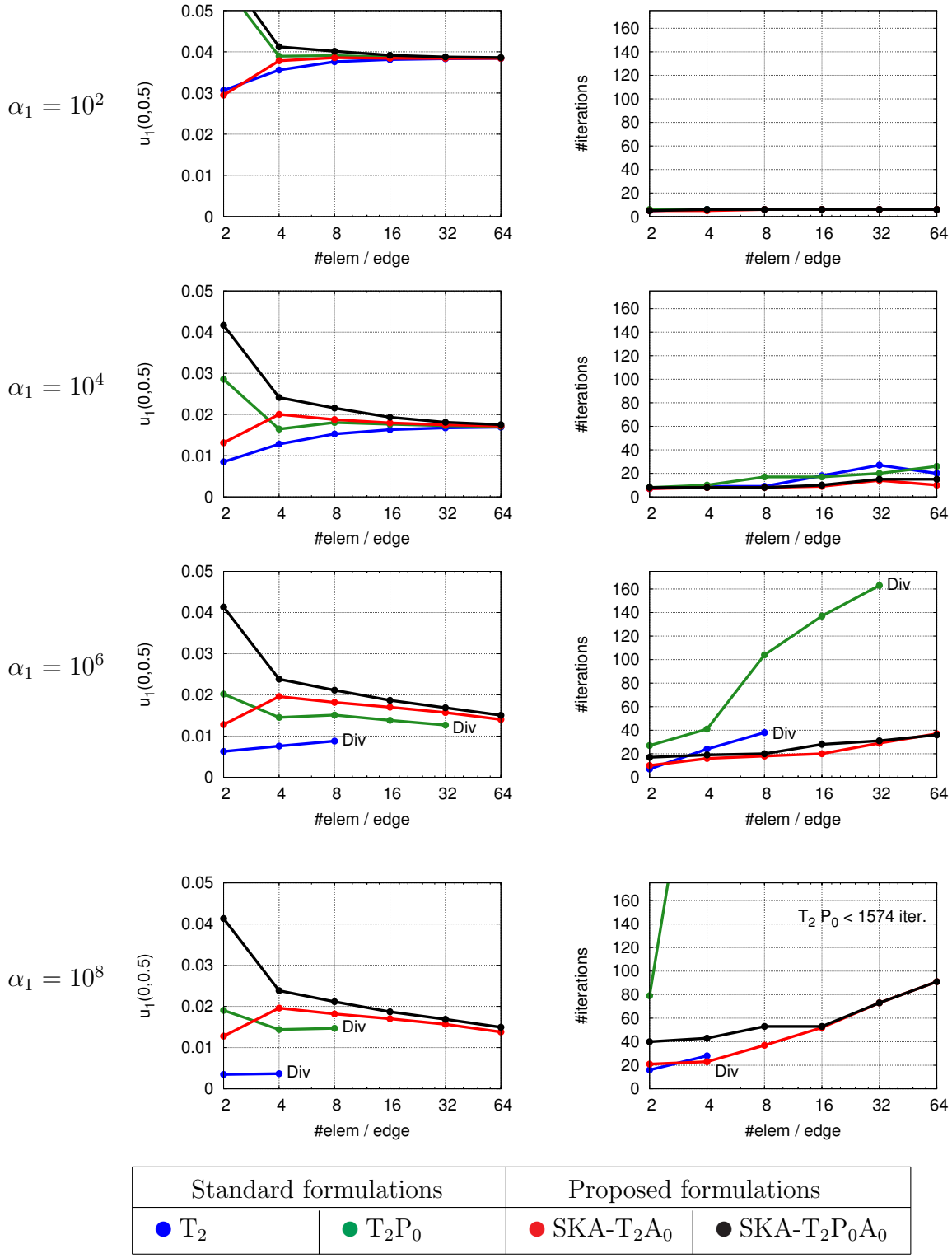

Figure 8.3: Dual clamped with $\nu = 0.49$; Displacement convergence on the left, necessary iteration on the left.

Convergence of the Newton Scheme for the Load Step from $0.9\mathbf{q_0}$ to $1.0\mathbf{q_0}$ In order to demonstrate the convergence behavior of the Newton scheme we present the residuals of one load step. For this we choose the parameters $E = 200$, $\nu = 0.3$, $\alpha_1 = \{10^2, 10^4\}$, $\alpha_2 = 2$ and 16 elements per edge. For the parameter $\alpha_1 = 10^2$ we observe

T_2	T_2P_0	SKA-T_2A_0	SKA-$T_2P_0A_0$
2.36891e-3	2.34672e-3	2.34964e-3	2.38265e-3
1.11729e-5	1.16430e-5	1.19195e-5	1.12253e-5
1.72709e-8	5.23261e-8	2.77721e-8	9.40961e-8
8.45366e-13	1.67429e-11	1.41550e-12	3.63150e-12
6.91370e-18	4.78360e-18	9.46073e-18	6.15925e-18

Table 8.1: Exemplary residuals for dual clamped ($\alpha_1 = 10^2$).

T_2	T_2P_0	SKA-T_2A_0	SKA-$T_2P_0A_0$
1.40914e-3	1.45028e-3	1.54207e-3	1.58698e-3
2.88268e-5	2.96782e-5	3.03282e-5	3.03303e-5
4.06429e-7	6.53144e-7	6.63708e-7	6.65458e-7
1.93893e-7	5.68163e-8	2.66509e-9	3.46107e-10
2.49160e-10	3.18832e-10	6.68922e-13	3.74633e-15

Table 8.2: Exemplary residuals for dual clamped ($\alpha_1 = 10^4$).

a good convergence behavior for all analyzed elements, see Table 8.1. In case of $\alpha_1 = 10^4$, see Table 8.2, the convergence rate of the Newton scheme is not optimal for all elements, but especially for the T_2 and T_2P_0 formulations ill-posedness can be recognized. The proposed SKA elements still behave more robust. Beyond a value of approximately 10^5 for α_1 the situation becomes peremptory, i.e. we observe no convergence for the T_2 and T_2P_0 elements even for very small load steps. In contrast to this the proposed SKA formulations still converge for $\alpha_1 = 10^8$, compare Figure 8.2 and 8.3.

Evaluation of the Stress Distributions In order to get an idea about the quality of the distributions of the Cauchy-stresses $\boldsymbol{\sigma} = \boldsymbol{F}\boldsymbol{S}\boldsymbol{F}^T/J$ we plot the component

$$\sigma_{aa}^{\text{a-p}} = \boldsymbol{\sigma}^{\text{a-p}} : \boldsymbol{a} \otimes \boldsymbol{a} \quad \text{with} \quad \boldsymbol{a} = \frac{\boldsymbol{F}\boldsymbol{A}}{\|\boldsymbol{F}\boldsymbol{A}\|} \tag{8.15}$$

where $\boldsymbol{\sigma}^{\text{a-p}}$ are the Cauchy stresses resulting only from the anisotropic part of the free energy $\psi^{\text{a-p}}$. The stresses are plotted discontinuously over element edges, with a linear distribution on each element. For the stress plots the material parameters are chosen as $E = 200$, $\nu = 0.3$, $\alpha_1 = 10^4$, $\alpha_2 = 2$ and 32 elements per edge are used. In case of the pure displacement element, compare Figure 8.4(a), a stiffening effect can be observed, which results in high stresses. In addition to that, strong oscillations are present. These oscillations exist also in case of the T_2P_0 element, see Figure 8.4(b). Taking into account the SKA formulation in (Figure 8.4(c/d)), the oscillations vanish and we observe a smooth stress distribution.

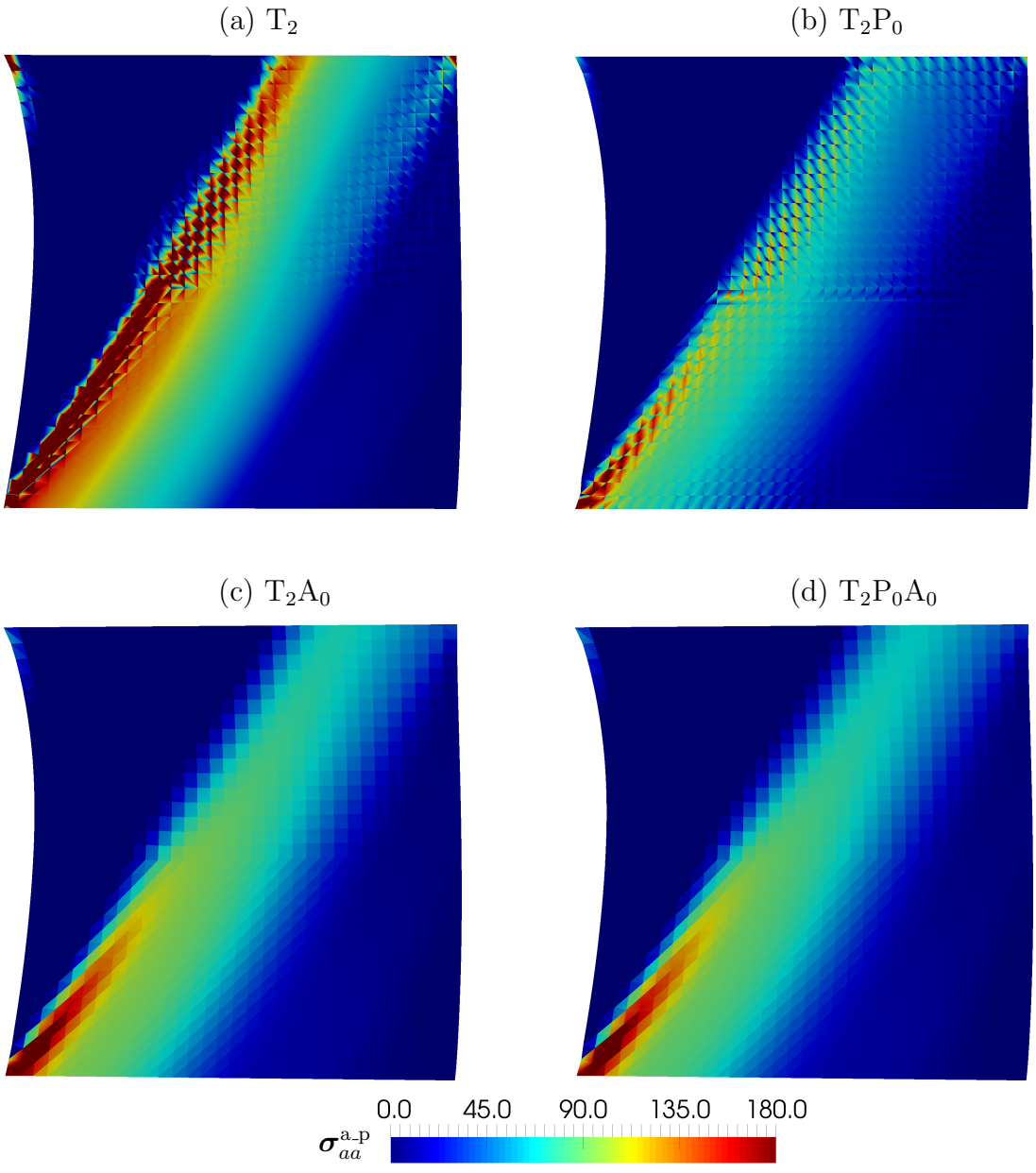

Figure 8.4: Dual clamped ; Cauchy stress components $\boldsymbol{\sigma}_{aa}^{\text{a\_p}}$.

8.3.2 3D Artery

In the next section we consider a simulation of a 3D arterial wall. An arterial wall can be decomposed into three distinct tissue layers, the intima, the media and the adventitia. In FE simulations it is common to take only the media and adventitia into account since the influence of the intima on the mechanical properties of the arterial wall may be considered negligible. The material is approximated by two superimposed transversely isotropic models, whereas the two fiber families of the adventitia and media are arranged crosswise helically. The angle between the fiber and the circumferential direction is denoted as β. The interested reader is referred to Holzapfel et al. [2000] and Balzani et al. [2012]. The chosen polyconvex material model goes back to Balzani et al. [2006] using a least-square fitted material parameter set from Brands et al. [2008], summarized in Table 8.3. The corresponding isotropic and anisotropic parts of the polyconvex strain energy function

Layer	Figure	c_1 (kPa)	ϵ_1 (kPa)	ϵ_2 (-)	α_1 (kPa)	α_2 (-)	β
Adventitia	a	6.6	23.9	10.0	1503.0	6.3	49.0
Media	b	17.5	499.8	2.4	30001.9	5.1	43.39

Table 8.3: Material parameter set for adventitia and media.

read as

$$\psi^{\text{i-p}} = c_1 \left(\frac{I_1}{I_1^{1/3}} - 3 \right) + \varepsilon_1 \left(I_3^{\varepsilon_2} + \frac{1}{I_3^{\varepsilon_2}} - 2 \right) \tag{8.16}$$

and

$$\psi^{\text{a-p}} = \sum_{a=1}^{2} \alpha_1 \langle I_1 + I_4^{(a)} - I_5^{(a)} - 2 \rangle^{\alpha_2}. \tag{8.17}$$

Uniaxial Tension Test In order to depict the main characteristics of the materials, the stress response of the media and adventitia is depicted in Figure 8.5 in an uniaxial tension test in longitudinal and circumferential direction. Here the Cauchy stress σ_{11} is plotted over the strains $\lambda = l_0/l$ with l_0 as the initial length. The high nonlinearity of

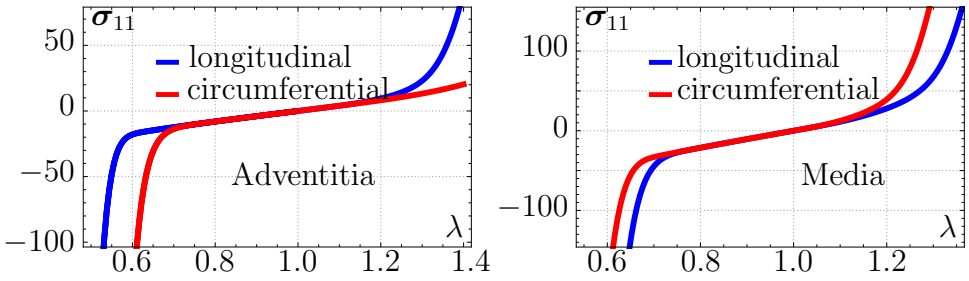

Figure 8.5: Uniaxial tension tests for adventitia and media.

the constitutive description can be recognized here. Especially the enormous increase of the stress-strain rate in the large tensile regime ($\lambda \geq 1.2$) leads to the near inextensible material behavior causing locking effects for classical discretization schemes.

Artery under physiological pressure In this numerical example the stresses of healthy arterial walls under a physiological blood pressure are investigated. The discretized arterial wall, consisting of the media and the adventitia, is depicted on Figure 8.6. The geometry is gathered by an intravascular ultrasound (IVUS) as described in Balzani et al. [2012]. As boundary conditions the front- and end-side are fixed in

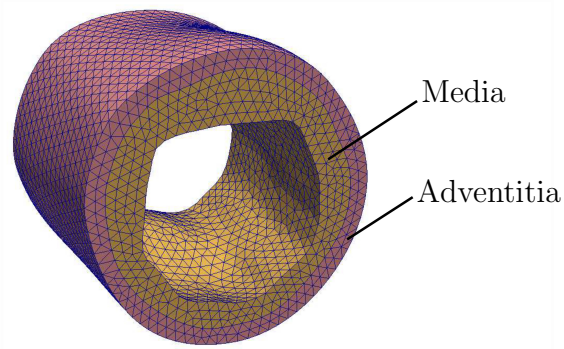

Figure 8.6: Arterial wall; Illustration of discretized tissue components.

longitudinal direction. Furthermore, an internal pressure of 24 kPa, corresponding to a blood pressure of approximately 180 mmHg, is applied. The von Mises stresses are considered for the comparison of the different finite element formulations. The Figures 8.7 illustrates the distribution of the von Mises stress in the artery. In order to display the stresses, the calculated stresses at the Gauss points are projected to the neighboring nodes and then plotted discontinuously over element edges. It can be noticed, that all four formulations lead to comparable stress distributions.

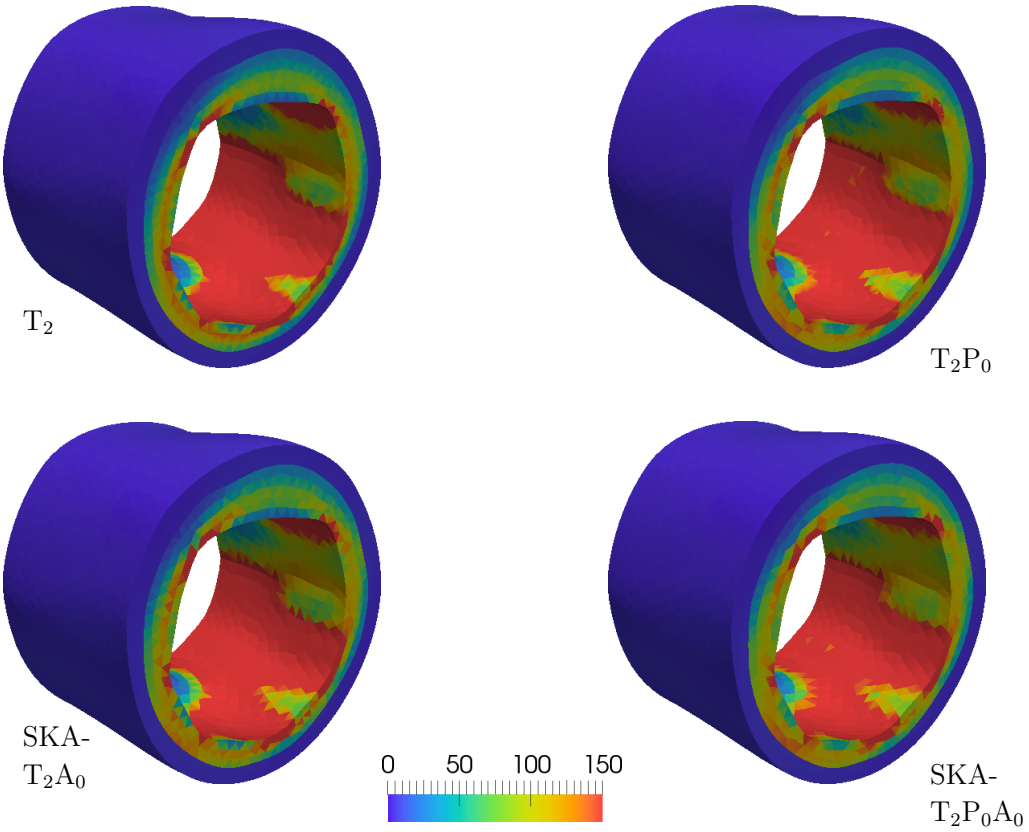

Figure 8.7: Arterial wall; Distribution of von Mises stresses

Comparison of robustness In addition to the simulation under physiological blood pressure we use the same geometry and mesh for an examination of the robustness of the finite element formulations applying a supra-physiological pressure. In order to compare the elements, the displacements of the node corresponding to the reference coordinates of $\boldsymbol{X} = (1.411, -0.828, 0.165)^T$, highlighted on the left in Figure 8.8, are investigated. The norm of the displacements $|\boldsymbol{u}|$ at this point is plotted over the applied pressure p in Figure 8.8. A bullet in the plot depicts the point of the last converged solution for the specified elements. In the case that no bullet is depicted, the simulation converges even for the highest applied pressure. Considering displacement and convergence behavior, similar

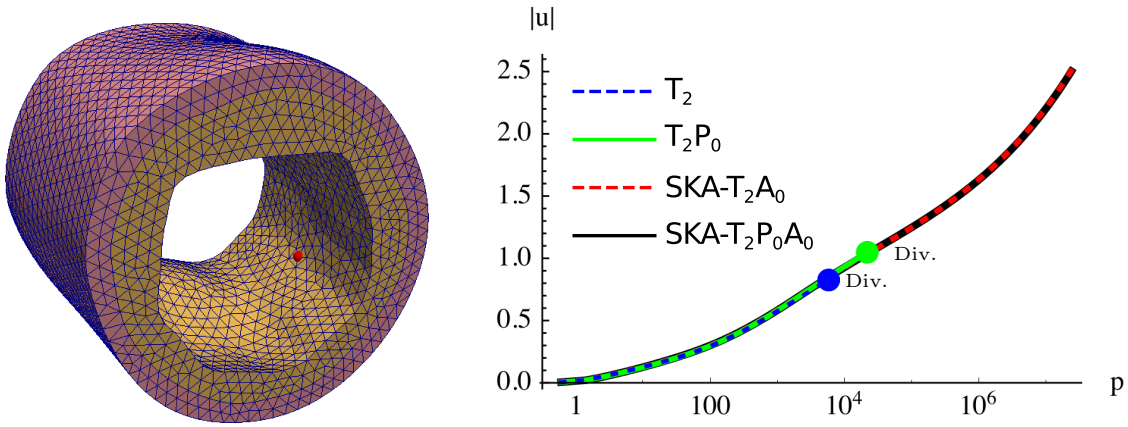

Figure 8.8: Arterial wall; study of robustness.

results are obtained as in the numerical example in Chapter 8.3.1. The displacements are nearly identical for all element formulations if a solution is obtained. But in case of the classical element formulations the converging solutions suddenly terminate at a specific value of the pressure. In case of the T_2 formulation the maximally applicable pressure constitutes $p_{max} = 5808$ and in case of the T_2P_0 we obtain $p_{max} = 21888$. In contrast to these results, we have not been able to find a maximal pressure for the novel formulations. A pressure of $p = 24 \cdot 10^7$ has been applied and we still observed good convergence rates of the Newton scheme. In order to visualize the significant differences, the final deformed configurations with the undeformed inner boundary (blue) are depicted in Figure 8.9.

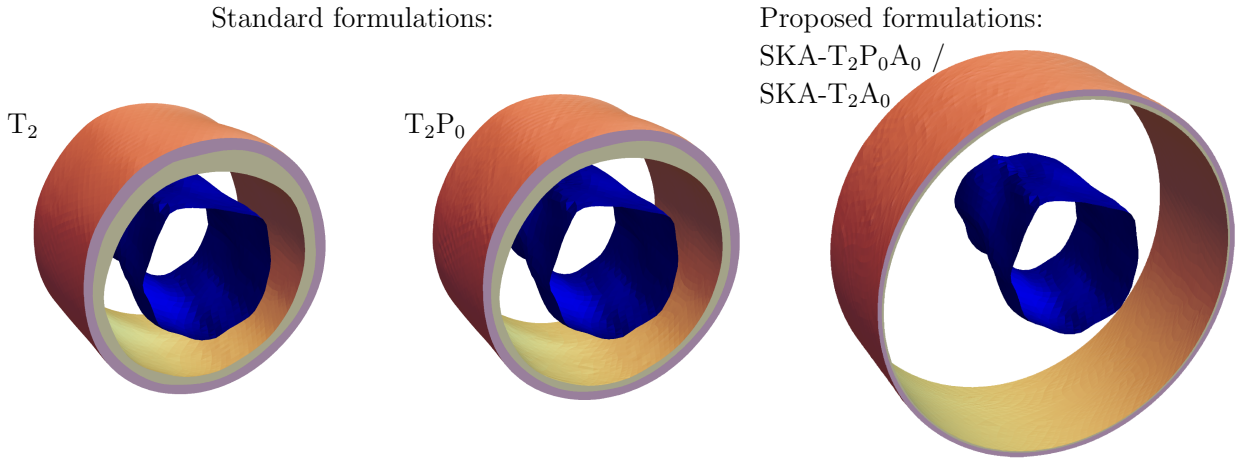

Figure 8.9: Arterial wall; maximal computed deformation for the different elements.

9 Summary, Conclusion and Outlook

The present thesis dealt with the construction of stable and reliable finite element formulations for hyperelasticity enable to incorporate additional constraints like incompressibility or inextensibility. After a brief review on the state of the art and previous milestones in the considered context, the fundamental equations for the problem of elasticity was consistently derived based on the framework of continuum mechanics. This chapter was followed by the introduction of abstract variational formulations, to construct a suitable environment for the analysis and investigation of finite element formulations in a linearized context. This analysis implicated the proof of existence and uniqueness of the solution. It was discussed that the related requirements, which guarantee stability and reliability of the formulation, have to be carried out for the continuous variational problem as well as for the discrete finite element counterpart. The restriction to the framework of linear problems was required since no comparable analysis exists for the generalized nonlinear framework. In detail, it was shown that the corresponding analysis consists on a boundedness and a coercivity condition in case of a primal formulation, whereas in case of a mixed formulation a boundedness, a kernel coercivity, and an inf-sup condition are necessary. The ensuing chapter reviewed a set of primal and mixed variational approaches for the problem of linear elasticity, where the particular focus was set on the investigation of their well-posedness based on the previously introduced abstract analysis. The crucial point was the satisfaction of the necessary conditions for the whole range of the material parameter, including the limit of incompressibility. It was shown that, in contrast to the primal displacement based approach which fails in the regime of incompressibility, most discussed mixed approaches are well posed also in the limit case. Several finite element discretizations, restricted to conforming approximations, were introduced for the considered variational problems. In addition to implementational notes, the analysis on the well-posedness was carried out for each considered element. A set of significant numerical examples closed the chapter related to linear elasticity, which reveal the performance of the finite elements in limit situations. It was concluded that mixed finite elements seem to be a promising candidate for the extension to large deformations if they satisfy the conditions on the well-posedness. The corresponding extension to hyperelasticity was carried out in the following two chapters. First, for the continuous variational framework and subsequently for discrete element formulations. Therein, the Hellinger-Reissner approach was considered in detail since its application to the hyperelastic regime is non-trivial. In addition, a novel variational consistent approach for the framework of displacement-pressure based formulations was introduced, necessary due to the observation of numerical instabilities for the classical method. A set of meaningful numerical examples closed the chapter, emphasizing the benefits of the novel elements. These were in detail the outstanding robustness to large load increments for the Hellinger-Reissner based discretizations and the additional stability for the novel displacement-pressure formulations. The last chapter investigated a special mixed finite element discretization constructed for the framework of nearly inextensible and nearly incompressible materials. This kind of materials are especially of interest in the numerical simulations of arterial walls. In this chapter, the consistent variational approach was presented, ensued by the corresponding finite element discretization. The fundamental idea for the incorporation of nearly inextensibility was the relaxation of the deformation measure related to the anisotropic material response. In particular, a piecewise constant approximation was applied for the right Cauchy-Green tensor concerning for the fiber

related strain energy. As demonstrated by the numerical examples, the proposed mixed finite element is characterized by its excellent robustness to large deformations.

In summary, this thesis introduced and investigated different finite element formulations in the framework of constrained hyperelasticity. The novel proposed elements, which are based on the Hellinger-Reissner and displacement-pressure formulation, and also the novel discretization scheme for nearly inextensibility depict clear advantages compared to the classical non-mixed and mixed formulations. The benefits are expressed in terms of significantly larger load steps, increased stability and increased robustness to large deformations.

A prospect of future research should be the extension to non-reversible material descriptions of the novel proposed formulations. A first step into this direction has already been made by Schröder et al. [2017], where the Pian-Sumihara element was extended to small strain elasto-plasticity. The related algorithm could be connected to the proposed extension to the large deformation case in order to achieve a formulation applicable for a wider range of problems. Besides, a further promising approach constitutes the application of the nonlinear extension of the Hellinger-Reissner formulation to tetrahedral shaped elements. For example a possible approach is presented by a reasonable choice of additional bubble shape functions for the approximation of the displacements, such that count condition and the limitation principle are satisfied. The huge benefit of tetrahedral shaped elements is connected to the meshing procedure. Nowadays, meshing algorithms can be applied to generate automatically tetrahedral based approximations for arbitrary complex domains. In contrast the generation of hexahedral based meshes is to a great extent a manual operation and still very time consuming. From the mathematical point of view, a consistent analysis on the well-posedness of nonlinear finite elements is still a missing tool and would fill an important gap for the proper construction of finite elements.

List of Figures

List of Tables

References

S. Adams and B. Cockburn. A mixed finite element method for elasticity in three dimensions. *Journal of Scientific Computing*, 25(3):515–521, 2005.

U. Andelfinger and E. Ramm. EAS-elements for two-dimensional, three-dimensional, plate and shell structures and their equivalence to HR-elements. *International Journal for Numerical Methods in Engineering*, 36:1311–1337, 1993.

D. N. Arnold. Mixed finite element methods for elliptic problems. *Computer Methods in Applied Mechanics and Engineering*, 82:291–300, 1990.

D. N. Arnold and F. Brezzi. Mixed and nonconforming finite element methods: implementation, postprocessing and error estimates. *Mathematical Modelling and Numerical Analysis*, 19:7–32, 1985.

D. N. Arnold and R. Winther. Mixed finite elements for elasticity. *Numerische Mathematik*, 92:401–419, 2002.

D. N. Arnold, F. Brezzi, and J. Douglas. PEERS: A new mixed finite element for plane elasticity. *Japan J. Appl. Math.*, 1:347–367, 1984a.

D. N. Arnold, F. Brezzi, and M. Fortin. A stable finite element for the stokes equations. *CALCOLO*, 21:337–344, 1984b.

D. N. Arnold, J. Douglas, and C. Gupta. A family of higher order mixed finite element methods for plane elasticity. *Numerische Mathematik*, 45:1–22, 1984c.

D. N. Arnold, R. S. Falk, and R. Winther. Mixed finite element methods for linear elasticity with weakly imposed symmetry. *Math. Comp.*, 76:1699–1723, 2007.

D. N. Arnold, G. Awanou, and R. Winther. Finite elements for symmetric tensors in three dimensions. *Mathematics of Computation*, 263:1229–1251, 2008.

S. N. Atluri. On the hybrid stress finite element model in incremental analysis of large deflection problems. *International Journal of Solids and Structures*, 9:1188–1191, 1973.

F. Auricchio, L. Beirão da Veiga, C. Lovadina, and A. Reali. An analysis of some mixed-enhanced finite element for plane linear elasticity. *Computer Methods in Applied Mechanics and Engineering*, 194:2947–2968, 2005a.

F. Auricchio, L. Beirão da Veiga, C. Lovadina, and A. Reali. A stability study of some mixed finite elements for large deformation elasticity problems. *Computer Methods in Applied Mechanics and Engineering*, 194:1075–1092, 2005b.

F. Auricchio, L. Beirao da Veiga, C. Lovadina, and A. Reali. The importance of the exact satisfaction of the incompressibility constraint in nonlinear elasticity: Mixed FEMs versus NURBS-based approximations. *Computer Methods in Applied Mechanics and Engineering*, 199:314–323, 2010.

F. Auricchio, L. Beirão da Veiga, C. Lovadina, A. Reali, R. Taylor, and P. Wriggers. Approximation of incompressible large deformation elastic problems: some unresolved issues. *Computational Mechanics*, 52(5):1153–1167, 2013.

F. Auricchio, G. Scalet, and P. Wriggers. Fiber-reinforced materials: finite elements for the treatment of the inextensibility constraint. *Computational Mechanics*, 60(6):905–922, 2017.

I. Babuška. The finite element method with Lagrangian multipliers. *Numerische Mathematik*, 20(3):179–192, 1973.

I. Babuška and M. Suri. Locking effects in the finite element approximation of elasticity problems. *Numerische Mathematik*, 62(1):439–463, 1992.

C. Bahriawati and C. Carstensen. Three matlab implementations of the lowest-order Raviart-Thomas MFEM with a posteriori error control. *Computational Methods in Applied Mathematics*, 4:333–361, 2005.

D. Balzani, P. Neff, J. Schröder, and G. A. Holzapfel. A polyconvex framework for soft biological tissues. Adjustment to experimental data. *International Journal of Solids and Structures*, 43(20):6052–6070, 2006.

D. Balzani, D. Böse, D. Brands, R. Erbel, A. Klawonn, O. Rheinbach, and J. Schröder. Parallel simulation of patient-specific atherosclerotic arteries for the enhancement of intravascular ultrasound diagnostics. *Engineering Computations*, 29(8):888–906, 2012.

K. J. Bathe. *Finite Element Procedures*. Prentice Hall, New Jersey, 1996.

K. J. Bathe. The inf-sup condition and its evaluation for mixed finite element methods. *Computers and Structures*, 79:243–252, 2001.

H. R. Bayat, J. Krämer, L. Wunderlich, S. Wulfinghoff, S. Reese, B. Wohlmuth, and C. Wieners. Numerical evaluation of discontinuous and nonconforming finite element methods in nonlinear solid mechanics. *Computational Mechanics*, 62(6):1413–1427, 2018.

G. P. Bazeley, Y. K. Cheung, B. M. Irons, and O. C. Zienkiewicz. Triangular elements in plate bending. conforming and nonconforming solutions. In *1st Conf. Matrix Methods in Structural Mechanics*, pages 547–576, 1966.

A. Bentley. Explicit construction of computational bases for RT_k and BDM_k spaces in R^3. *Computers and Mathematics with Applications*, 73:1421–1432, 2017.

M. Bischoff, E. Ramm, and D. Braess. A class of equivalent enhanced assumed strain and hybrid stress finite elements. *Computational Mechanics*, 22:443–449, 1999.

P. B. Bochev and M. D. Gunzburger. *Least-Squares Finite Element Methods*. Springer-Verlag, New York, 1st edition, 2009.

J. P. Boehler. Lois de comportement anisotrope des milieux continus. *Journal de Mécanique*, 17(2):153–190, 1978.

J. P. Boehler. A simple derivation of respresentations for non-polynomial constitutive equations in some cases of anisotropy. *Zeitschrift für angewandte Mathematik und Mechanik*, 59:157–167, 1979.

J. P. Boehler. Introduction to the invariant formulation of anisotropic constitutive equations. In J. P. Boehler, editor, *Applications of Tensor Functions in Solid Mechanics*, volume 292 of *CISM Courses and Lectures*, pages 13–30. Springer, 1987.

D. Boffi. Stability of higher order triangular Hood–Taylor methods for the stationary Stokes equations. *Mathematical Models and Methods in Applied Sciences*, 04(02):223–235, 1994.

D. Boffi. Three-dimensional finite element methods for the Stokes problem. *SIAM Journal on Numerical Analysis*, 34(2):664–670, 1997.

D. Boffi and R. Stenberg. A remark on finite element schemes for nearly incompressible elasticity. *Computers and Mathematics with Applications*, 2017. https://doi.org/10.1016/j.camwa.2017.06.006.

D. Boffi, F. Brezzi, and M. Fortin. Reduced symmetry elements in linear elasticity. *Commun. Pure Appl. Anal.*, 8:95–121, 2009.

D. Boffi, F. Brezzi, and M. Fortin. *Mixed Finite Element Methods and Applications*. Springer, Heidelberg, 2013.

J. Bonet, A. J. Gil, and R. Ortigosa. On a tensor cross product based formulation of large strain solid mechanics. *International Journal of Solids and Structures*, 84:49–63, 2016.

D. Braess. Enhanced assumed strain elements and locking in membrane problems. *Computer Methods in Applied Mechanics and Engineering*, 165:155–174, 1998.

D. Braess. *Finite Elemente, Theorie, schnelle Löser und Anwendungen in der Elastizitätstheorie*. Springer, 2000.

D. Braess, C. Carstensen, and B. D. Reddy. Uniform convergence and a posteriori error estimators for the enhanced strain finite element method. *Numerische Mathematik*, 96 (3):461–479, 2004.

D. Brands, A. Klawonn, O. Rheinbach, and J. Schröder. Modelling and convergence in arterial wall simulations using a parallel FETI solution strategy. *Computer Methods in Biomechanics and Biomedical Engineering*, 11(5):569–583, 2008.

S. C. Brenner and L. R. Scott. *The mathematical theory of finite element methods*. Springer, 1994.

F. Brezzi. On the existence, uniqueness and approximation of saddle-point problems arising from Lagrangian multipliers. *Revue française d'automatique, informatique, recherche opérationnelle. Analyse numérique*, 8(2):129–151, 1974.

F. Brezzi and M. Fortin. *Mixed and Hybrid Finite Element Methods*. Springer-Verlag, NewYork, 1991.

Z. Cai and G. Starke. First-order system least squares for the stress-displacement formulation: Linear elasticity. *SIAM Journal on Numerical Analysis*, 41:715–730, 2003.

Z. Cai and G. Starke. Least-squares methods for linear elasticity. *SIAM Journal on Numerical Analysis*, 42:826–842, 2004.

Z. Cai, J. Korsawe, and G. Starke. An adaptive least squares mixed finite element method for the stress-displacement formulation of linear elasticity. *Numerical Methods for Partial Differential Equations*, 21:132–148, 2005.

C. Carstensen and F. Hellwig. Low-order discontinuous petrov–galerkin finite element methods for linear elasticity. *SIAM Journal on Numerical Analysis*, 54(6):3388–3410, 2016.

C. Carstensen, P. Bringmann, F. Hellwig, and P. Wriggers. Nonlinear discontinuous petrov–galerkin methods. *Numerische Mathematik*, 139(3):529–561, 2018.

J. Cea. Approximation variationnelle des problèmes aux limites. *Annales de l'institut Fourier*, 14(2):345–444, 1964.

D. Chapelle and K. Bathe. The inf-sup test. *Computers and Structures*, 47:537–545, 1993.

L. B. da Veiga, F. Brezzi, A. Cangiani, G. Manzini, L. D. Marini, and A. Russo. Basic principles of Virtual Element Methods. *Mathematical Models and Methods in Applied Sciences*, 23(01):199–214, 2013.

H. Dal. A quasi-incompressible and quasi-inextensible element formulation for transversely isotropic materials. *International Journal for Numerical Methods in Engineering*, 117: 118–140, 2018.

E. A. de Souza Neto, D. Peric, G. C. Huang, and D. R. J. Owen. Remarks on the stability of enhanced strain elements in finite elasticity and elastoplasticity. *Communications in Numerical Methods in Engineering*, 11(11):951–961, 1995.

L. Demkowicz and J. Gopalakrishnan. A class of discontinuous petrov–galerkin methods. part i: The transport equation. *Computer Methods in Applied Mechanics and Engineering*, 199(23-24):1558–1572, 2010a.

L. Demkowicz and J. Gopalakrishnan. A class of discontinuous petrov-galerkin methods. II. optimal test functions. *Numerical Methods for Partial Differential Equations*, 27(1): 70–105, 2010b.

J. K. Djoko and B. D. Reddy. An extended Hu-Washizu formulation for elasticity. *Comput. Meth. Appl. Mech. Engrg.*, 195:44–47, 2006.

J. K. Djoko, B. P. Lamichhane, B. P. Reddy, and B. I. Wohlmuth. Conditions for equivalence between the Hu-Washizu and related formulations, and computational behavior in the incompressible limit. *Computer Methods in Applied Mechanics and Engineering*, 195: 4161–4178, 2006.

W. P. Doherty, E. L. Wilson, and R. L. Taylor. Stress analysis of axisymmetric solids utilizing higher-order quadrilateral finite elements, 1969.

V. J. Ervin. Computational bases for RT_k and BDM_k on triangles. *Computers and Mathematics with Applications*, 64:2765–2774, 2012.

B. Fraeijs de Veubeke. Displacement and equilibrium models in the finite element method. In O. Zienkiewicz and G. Holister, editors, *Stress Analysis*. Wiley, 1965.

L. P. Franca and T. J. R. Hughes. Two classes of mixed finite element methods. *Computer Methods in Applied Mechanics and Engineering*, 69:89–129, 1988.

L. P. Franca, T. J. R. Hughes, A. F. D. Loula, and I. Miranda. A new family of stable elements for nearly incompressible elasticity based on a mixed petrov-galerkin finite element formulation. *Numerische Mathematik*, 53:123–141, 1988.

I. Fried. Finite element analysis of incompressible material by residual energy balancing. *International Journal of Solids and Structures*, 10(9):993–1002, 1974.

S. Glaser and F. Armero. On the formulation of enhanced strain finite elements in finite deformations. *Engineering Computations*, 14:759–791, 1997.

P. R. Halmos. *Finite-dimensional Vector Spaces.* Van Nostrand, New York, 1958.

J. Helfenstein, M. Jabareen, E. Mazza, and S. Govindjee. On non-physical response in models for fiber-reinforced hyperelastic materials. *International Journal of Solids and Structures*, 47(16):2056–2061, 2010.

E. Hellinger. Encyklopädie der mathematischen Wissenschaften mit Einschluss ihrer Anwendungen. In *Encyklopädie der mathematischen Wissenschaften mit Einschluss ihrer Anwendungen*, volume 4, 1913.

G. A. Holzapfel. *Nonlinear solid mechanics, a continuum approach for engineering.* Wiley, 2000.

G. A. Holzapfel, T. C. Gasser, and R. W. Ogden. A new constitutive framework for arterial wall mechanics and a comparative study of material models. *Journal of Elasticity*, 61 (1/3):1–48, 2000.

P. Hood and C. Taylor. Navier-stokes equations using mixed interpolation. In J. T. Oden, O. C. Zienkiewicz, R. H. Gallagher, and C. Taylor, editors, *Finite Element Methods in Flow Problems*, pages 121–132. UAH Press, 1974.

H. C. Hu. On some variational principles in the theory of elasticity and the theory of plasticity. *Science Sinica*, 4:33–54, 1955.

T. J. R. Hughes. Generalization of selective integration procedures to anisotropic and nonlinear media. *International Journal for Numerical Methods in Engineering*, 15: 1413–1418, 1980.

Human Brain Project. visited on 6th March, 2019. URL `http://www.humanbrainproject.eu`.

B.-N. Jiang. *The Least-Squares Finite Element Method.* Springer-Verlag, Berlin, 1998.

C. Johnson and B. Mercier. Some equilibrium finite element methods for two-dimensional elasticity problems. *Numerische Mathematik*, 30:85–99, 1978.

O. Klaas, J. Schröder, E. Stein, and C. Miehe. A Regularized Dual Mixed Element for Plane Elasticity – Implementation and Performance of the BDM Element. *Computer Methods in Applied Mechanics and Engineering*, 121:201–209, 1995.

J. Korelc and P. Wriggers. Consistent gradient formulation for a stable enhanced strain method for large deformations. *Engineering Computations*, 13:103–123, 1996.

J. Korelc, U. Solinc, and P. Wriggers. An improved EAS brick element for finite deformation. *Computational Mechanics*, 46:641–659, 2010.

A. Kraus, P. Wriggers, N. Viebahn, and J. Schröder. Low order locking-free mixed finite element formulation with approximation of the minors of the deformation gradient. *International Journal for Numerical Methods in Engineering*, 2019.

A. Krischok and C. Linder. On the enhancement of low-order mixed finite element methods for the large deformation analysis of diffusion in solids. *International Journal for Numerical Methods in Engineering*, 106:278–297, 2016.

O. Ladyzhenskaya. *The mathematical theory of viscous incompressible flow*, volume 76. Gordon and Breach New York, 1969.

P. Lax and A. Milgram. Parabolic equations. In *Contributions to the theory of partial differential equations*, number 33 in Annals of Mathematics Studies, pages 167–190, 1954.

B. Li, X. Xie, and S. Zhang. New convergence analysis for assumed stress hybrid quadrilateral finite element method. *Discrete and Continuous Dynamical Systems Series B*, 22 (7):2831–2856, 2017.

C. Lovadina and F. Auricchio. On the enhanced strain technique for elasticity problems. *Computers and Structures*, 81(8):777–787, 2003.

D. S. Malkus. A finite element displacement model valid for any value of the compressibility. *International Journal of Solids and Structures*, 12(11):731–738, 1976.

S. Malkus and T. J. R. Hughes. Mixed finite element methods - reduced and selective integration techniques: A unification of concepts. *Computer Methods in Applied Mechanics and Engineering*, 15:63–81, 1978.

L. E. Malver. *Introduction to the Mechanics of a Continuous Medium*. Prentice-Hall, 1969.

J. C. Nagtegaal, D. M. Parks, and J. R. Rice. On numerically accurate finite element solutions in the fully plastic range. *Computer Methods in Applied Mechanics and Engineering*, 4:152–177, 1974.

W. Noll. *The foundations of mechanics and thermodynamics*. Springer, 1974.

R. W. Ogden. *Non-linear elastic deformations*. Dover Publications, 1984.

D. Pantuso and K. J. Bathe. A four-node quadrilateral mixed-interpolated element for solids and fluids. *Mathematical Models and Methods in Applied Sciences (M3AS)*, 5(8): 1113–1128, 1995.

A. Pechstein and J. Schöberl. Tangential-displacement and normal-normal-stress continuous mixed finite elements for elasticity. *Mathematical Models and Methods in Applied Sciences*, 21(8):1761–1782, 2011.

T. H. H. Pian. Derivation of element stiffness matrices by assumed stress distribution. *AIAA Journal*, 20:1333–1336, 1964.

T. H. H. Pian and D.-P. Chen. Alternative ways for formulation of hybrid stress elements. *International Journal for Numerical Methods in Engineering*, 18:1679–1684, 1982.

T. H. H. Pian and K. Sumihara. A rational approach for assumed stress finite elements. *International Journal for Numerical Methods in Engineering*, 20:1685–1695, 1984.

T. H. H. Pian and P. Tong. Relations between incompatible displacement model and hybrid stress model. *International Journal for Numerical Methods in Engineering*, 22: 173–181, 1986.

G. Prange. *Das Extremum der Formänderungsarbeit.* Habilitationsschrift, Technische Hochschule Hannover, 1916.

H. Qi, L.-H. Wang, and W.-Y. Zheng. On locking-free finite element schemes for three dimensional elasticity. *Journal of Computational Mathematics*, 23(1):101–112, 2005.

F. Rasolofoson, B. J. Grieshaber, and B. D. Reddy. Finite element approximations for near-incompressible and near-inextensible transversely isotropic bodies. *International Journal for Numerical Methods in Engineering*, 117(6):693–712, nov 2018.

P. A. Raviart and J. M. Thomas. A mixed finite element method for 2-nd order elliptic problems. Mathematical aspects of finite element methods. *Lecture Notes in Mathematics, Springer-Verlag New York*, pages 292–315, 1977.

B. D. Reddy and J. C. Simo. Stability and convergence of a class of enhanced strain finite element methods. *SIAM Journal on Numerical Analysis*, 32(6):17051728, 1995.

W. H. Reed and T. R. Hill. Triangular mesh methods for the neutron transport equation. *Los Alamos Report*, (LA-UR-73-479), 1973.

S. Reese, H. R. Bayat, and S. Wulfinghoff. On an equivalence between a discontinuous galerkin method and reduced integration with hourglass stabilization for finite elasticity. *Computer Methods in Applied Mechanics and Engineering*, 325:175–197, 2017.

E. Reissner. On a variational theorem in elasticity. *Journal of Mathematical Physics*, 29: 90–95, 1950.

R. S. Rivlin. Large elastic deformations of isotropic materials II. Some uniqueness theorems for pure homogeneous deformation. *Philosophical Transactions of the Royal Society of London*, 240:491–508, 1948.

C. Sansour. On the physical assumptions underlying the volumetric-isochoric split and the case of anisotropy. *European Journal of Mechanics, A/Solids*, 27:28–39, 2008.

J. Schröder. Anisotropic polyconvex energies. In J. Schröder and P. Wriggers, editors, *Poly-, Quasi- and Rank-One Convexity in Applied Mechanics*, volume 566 of *CISM International Centre for Mechanical Sciences*, pages 131–175. Springer, 2014.

J. Schröder and P. Neff. Invariant formulation of hyperelastic transverse isotropy based on polyconvex free energy functions. *International Journal of Solids and Structures*, 40: 401–445, 2003.

J. Schröder, O. Klaas, E. Stein, and C. Miehe. A physically nonlinear dual mixed finite element formulation. *Computer Methods in Applied Mechanics and Engineering*, 144: 77–92, 1997.

J. Schröder, P. Wriggers, and D. Balzani. A new mixed finite element based on different approximations of the minors of deformation tensors. *Computer Methods in Applied Mechanics and Engineering*, 200(49):3583–3600, 2011.

J. Schröder, N. Viebahn, P. Wriggers, and D. Balzani. A novel mixed finite element for anisotropy - basic ideas. In *Report of the Workshop 43 at the "Mathematisches Forschungsinstitut Oberwolfach" entitled "Computational Engineering", organized by S. Brenner, C. Carstensen, L. Demkowicz, P. Wriggers*, Oberwolfach, September, 27$^{\text{th}}$ – October, 03$^{\text{rd}}$ 2015.

J. Schröder, N. Viebahn, D. Balzani, and P. Wriggers. A novel mixed finite element for finite anisotropic elasticity; the SKA-element. *Computer Methods in Applied Mechanics and Engineering*, 310:475–494, 2016.

J. Schröder, M. Igelbüscher, A. Schwarz, and G. Starke. A Prange-Hellinger-Reissner type finite element formulation for small strain elasto-plasticity. *Computer Methods in Applied Mechanics and Engineering*, 317:400–418, 2017.

J. Schröder, N. Viebahn, P. Wriggers, F. Auricchio, and K. Steeger. On the stability analysis of hyperelastic boundary value problems using three- and two-field mixed finite element formulations. *Computational Mechanics*, 60(3):479–492, 2017.

A. Schwarz, K. Steeger, I. M., and J. Schröder. Different approaches for mixed LSFEMs in hyperelasticity: Application of logarithmic deformation measures. *International Journal for Numerical Methods in Engineering*, 115:1138–1153, 2018.

J. C. Simo and F. Armero. Geometrically non-linear enhanced strain mixed methods and the method of incompatible modes. *International Journal for Numerical Methods in Engineering*, 33:1413–1449, 1992.

J. C. Simo and M. S. Rifai. A class of mixed assumed strain methods and the method of incompatible modes. *International Journal for Numerical Methods in Engineering*, 29: 1595–1638, 1990.

J. C. Simo, R. L. Taylor, and K. S. Pister. Variational and projection methods for the volume constraint in finite deformation elasto-plasticity. *Computer Methods in Applied Mechanics and Engineering*, 51:177–208, 1985.

J. C. Simo, J. G. Kennedy, and R. L. Taylor. Complementary mixed finite element formulations for elastoplasticity. *Computer Methods in Applied Mechanics and Engineering*, 74:177–206, 1989.

G. F. Smith. On a fundamental error in two papers of C.-C. Wang "On representations for isotropic functions, Parts I and II". *Archive for Rational Mechanics and Analysis*, 36:161–165, 1970.

G. F. Smith. On isotropic functions of symmetric tensors, skew-symmetric tensors and vectors. *International Journal of Engineering Science*, 9:899–916, 1971.

A. J. M. Spencer. Theory of invariants. In A. C. Eringen, editor, *Continuum Physics*, volume 1, pages 239–353. Academic Press, New York, 1971.

K. Steeger. *Least-squares mixed finite elements for geometrically nonlinear solid mechanics*. PhD thesis, University Duisburg-Essen, Institute of Mechanics, 2016.

E. Stein and F.-J. Barthold. Elastizitätstheorie. In G. Mehlhorn, editor, *Der Ingenieurbau: Grundwissen*, number 4. Ernst and Sohn, 1996.

E. Stein, P. Wriggers, A. Rieger, and M. Schmidt. Benchmarks. In E. Stein, editor, *Error-controlled Adaptive Finite Elements in Solid Mechanics*. John Wiley & Sons, Ltd New York, 2002.

R. Stenberg. On the construction of optimal mixed finite element methods for the linear elasticity problem. *Numerische Mathematik*, 42:447–462, 1986.

R. Stenberg. A family of mixed finite elements for the elastic problem. *Numerische Mathematik*, 53:513–538, 1988.

H. Stolarski and T. Belytschko. Limitation principles for mixed finite elements based on the Hu-Washizu variational formulation. *Computer Methods in Applied Mechanics and Engineering*, 60:195–216, 1987.

C. Taylor and P. Hood. A numerical solution of the Navier-Stokes equations using the finite element technique. *Computers and Fluids*, 1:73–100, 1973.

R. L. Taylor, J. C. Simo, O. C. Zienkiewicz, and A. C. H. Chan. The patch test - a condition for assessing FEM convergence. *International Journal for Numerical Methods in Engineering*, 1986.

C. Truesdell. *Rational Thermodynamics*. McGraw-Hill, New York, 1969.

C. Truesdell and W. Noll. The nonlinear field theories of mechanics. In S. Flügge, editor, *Encyclopedia of Physics*, volume III/3. Springer, 1965.

C. Truesdell and R. Toupin. The classical field theories. In S. Flügge, editor, *Encyclopedia of Physics*, number III/1. Springer, 1960.

N. Viebahn, J. Schröder, and P. Wriggers. Application of assumed stress finite elements in hyperelasticity. In *Report of the Workshop 1843 at the "Mathematisches Forschungsinstitut Oberwolfach" entitled "Computational Engineering", organized by O. Allix, A. Buffa C. Carstensen and J. Schröder*, 2018a.

N. Viebahn, K. Steeger, and J. Schröder. A simple and efficient Hellinger-Reissner type mixed finite element for nearly incompressible elasticity. *Computer Methods in Applied Mechanics and Engineering*, 340:278–295, 2018b.

N. Viebahn, J. Schröder, and P. Wriggers. An extension of assumed stress finite elements to a general hyperelastic framework. *Advanced Modeling and Simulation in Engineering Sciences*, 2019.

W. A. Wall, M. Bischoff, and E. Ramm. A deformation dependent stabilization technique, exemplified by eas elements at large strains. *Computer Methods in Applied Mechanics and Engineering*, 188:859–871, 2000.

C. C. Wang. On representations for isotropic functions. Part I. Isotropic functions of symmetric tensors and vectors. *Archive for Rational Mechanics and Analysis*, 33:249–267, 1969a.

C. C. Wang. On representations for isotropic functions. Part II. Isotropic functions of skew-symmetric tensors, symmetric tensors, and vectors. *Archive of Rational Mechanics and Analysis*, 33:268–287, 1969b.

C. C. Wang. A new representation theorem for isotropic functions: An answer to professor G. F. Smith's Criticism of my papers on representations for isotropic functions. Part 2. Vector-valued isotropic functions, symmetric tensor-valued isotropic functions, and skew-symmetric tensor-valued isotropic functions. *Archive for Rational Mechanics and Analysis*, 36:198–223, 1970.

C. C. Wang. Corrigendum to my recent papers on: wallerepresentations for isotropic functions. *Archive of Rational Mechanics and Analysis*, 43:392–395, 1971.

K. Washizu. On the variational principles of elasticity and plasticity. Technical Report 2518, Aeroelastic and Structures Research Laboratory, Massachusetts Institute of Technology, Cambridge, March 1955.

J. A. Weiss, B. N. Maker, and S. Govindjee. Finite element implementation of incompressible, transversely isotropic hyperelasticity. *Computer Methods in Applied Mechanics and Engineering*, 135:107–128, 1996.

P. Wriggers. *Nonlinear finite element methods*. Springer, 2008.

P. Wriggers. Mixed finite element methods - theory and discretization. In C. Carstensen and P. Wriggers, editors, *Mixed Finite Element Technologies*, volume 509 of *CISM International Centre for Mechanical Sciences*. Springer, 2009.

P. Wriggers and S. Reese. A note on enhanced strain methods for large deformations. *Computer Methods in Applied Mechanics and Engineering*, 135:201–209, 1996.

P. Wriggers, J. Schröder, and F. Auricchio. Finite element formulations for large strain anisotropic material with inextensible fibers. *Advanced Modeling and Simulation in Engineering Sciences*, 3, 2016.

P. Wriggers, B. D. Reddy, W. Rust, and B. Hudobivnik. Efficient virtual element formulations for compressible and incompressible finite deformations. *Computational Mechanics*, 60(2):253–268, 2017.

S. T. Yeo and B. C. Lee. Equivalence between enhanced assumed strain method and assumed stress hybrid method based on the Hellinger-Reissner principle. *International Journal for Numerical Methods in Engineering*, 39:3083–3099, 1996.

G. Yu, X. Xie, and C. Carstensen. Uniform convergence and a posteriori error estimation for assumed stress hybrid finite element methods. *Computer Methods in Applied Mechanics and Engineering*, 200:2421–2433, 2011.

A. Zdunek and W. Rachowicz. A 3-field formulation for strongly transversely isotropic compressible finite hyperelasticity. *Computer Methods in Applied Mechanics and Engineering*, 315:478–500, 2017a.

A. Zdunek and W. Rachowicz. A mixed higher order FEM for fully coupled compressible transversely isotropic finite hyperelasticity. *Computers & Mathematics with Applications*, 74(7):1727–1750, oct 2017b.

O. C. Zienkiewicz, S. Qu, R. L. Taylor, and S. Nakazawa. The patch test for mixed formulations. *International Journal for Numerical Methods in Engineering*, 23:1873–1883, 1986.

Der Lebenslauf ist in der Online-Version aus Gründen des Datenschutzes nicht enthalten.

In dieser Schriftenreihe bisher erschienene Berichte:

Nr. 1 (2004) *Ein Modell zur Beschreibung finiter anisotroper elasto-plastischer Deformationen unter Berücksichtigung diskreter Rissausbreitung*, J. Löblein, Dissertation, 2004.

Nr. 2 (2006) *Polyconvex Anisotropic Energies and Modeling of Damage applied to Arterial Walls*, D. Balzani, Dissertation, 2006.

Nr. 3 (2006) *Kontinuumsmechanische Modellierung ferroelektrischer Materialien im Rahmen der Invariatentheorie*, H. Romanowski, Dissertation, 2006.

Nr. 4 (2007) *Mehrskalen-Modellierung polykristalliner Ferroelektrika basierend auf diskreten Orientierungsverteilungsfunktionen*, I. Kurzhöfer, Dissertation, 2007.

Nr. 5 (2007) *Proceedings of the First Seminar on the Mechanics of Multifunctional Materials*, J. Schröder, D.C. Lupascu, D. Balzani (Ed.), Tagungsband, 2007.

Nr. 6 (2008) *Zur Modellierung und Simulation diskreter Rissausbreitungsvorgänge*, O. Hilgert, Dissertation, 2008.

Nr. 7 (2009) *Least-Squares Mixed Finite Elements for Solid Mechanics*, A. Schwarz, Dissertation, 2009.

Nr. 8 (2010) *Design of Polyconvex Energy Functions for All Anisotropy Classes*, V. Ebbing, Dissertation, 2010.

Nr. 9 (2012) *Modeling of Electro-Mechanically Coupled Materials on Multiple Scales*, M.-A. Keip, Dissertation, 2012.

Nr. 10 (2012) *Geometrical Modeling and Numerical Simulation of Heterogeneous Materials*, D. Brands, Dissertation, 2012.

Nr. 11 (2012) *Modeling and simulation of arterial walls with focus on damage and residual stresses*, S. Brinkhues, Dissertation, 2012.

Nr. 12 (2014) *Proceedings of the Second Seminar on the Mechanics of Multifunctional Materials*, J. Schröder, D.C. Lupascu, M.-A. Keip, D. Brands (Ed.), Tagungsband, 2014.

Nr. 13 (2016) *Mixed least squares finite element methods based on inverse stress-strain relations in hyperelasticity*, B. Müller, Dissertation, 2016.

Nr. 14 (2016) *Electromechanical Modeling and Simulation of Thin Cardiac Tissue Constructs*, R. Frotscher, Dissertation, 2016.

Nr. 15 (2017) *Least-squares mixed finite elements for geometrically nonlinear solid mechanics*, K. Steeger, Dissertation, 2017.

Nr. 16 (2017) *Scale-Bridging of Elasto-Plastic Microstructures using Statistically Similar Representative Volume Elements*, L. Scheunemann, Dissertation, 2017.

Nr. 17 (2018) *Modeling of Self-healing Polymers and Polymeric Composite Systems*, S. Specht, Dissertation, 2017.

Nr. 18 (2018) *Proceedings of the Third Seminar on the Mechanics of Multifunctional Materials*, J. Schröder, D.C. Lupascu, H. Wende, D. Brands (Ed.), Tagungsband, 2018.

Nr. 19 (2018) *Least-squares finite element methods with applications in fluid and solid mechanics*, C. Nisters, Dissertation, 2018.

Nr. 20 (2018) *A two-scale homogenization scheme for the prediction of magneto-electric product properties*, M. Labusch, Dissertation, 2018.

Nr. 21 (2019) *Modeling the passive mechanical response of soft tissues: constitutive modeling approaches, efficient parameter selection and subsequent adjustments due to residual stresses*, M. von Hoegen, Dissertation, 2019

Nr. 22 (2019) *Constitutive modeling of female pelvic floor dysfunctions and reconstructive surgeries using prosthetic mesh implants*, A. Bhattarai, Dissertation, 2019